Role of the (Pro)renin Receptor [(P)RR/ATP6ap2] in Osteoclast and Macrophage Physiology

Dissertation

Zur Erlangung des akademischen Grades
Doctor rerum naturalium (Dr. rer. nat.)
Im Fach Biologie

eingereicht an der Lebenswissenschaftlichen Fakultät
der Humboldt-Universität zu Berlin

Von
Anthony Rousselle, M.Sc.

Präsident Der Humboldt-Universität zu Berlin
Prof. Dr. Jan-Hendrik Olbertz

Dekan der Lebenswissenschaftlichen Fakultät
Prof. Dr. Richard Lucius

Gutachter: 1. Prof. Michael Bader
2. Prof. Achim Leutz
3. Prof. Uwe Kornak

Tag der mündlichen Prufung: 10/02/2017

Role of the (Pro)renin Receptor [(P)RR/ATP6ap2] in Osteoclast and Macrophage Physiology

Dissertation

Zur Erlangung des akademischen Grades
Doctor rerum naturalium (Dr. rer. nat.)
Im Fach Biologie

eingereicht an der Lebenswissenschaftlichen Fakultät
der Humboldt-Universität zu Berlin

Von
Anthony Rousselle, M.Sc.

Work performed between 2010 and 2015 in the group of
Prof. Dr. Michael Bader at the Max-Delbrück Center in Berlin

"Les véritables splendeurs de la science ne sont pas dans les réponses -éphémères- qu'elle procure mais dans le questionnement permanent qu'elle fait naître".

"The real magnificences of science are not in the -ephemeral- answers provided, but in the permanent questions being raised".

Jean Claude Ameisen
La sculpture du vivant
Editions du Seuil (2003)

Acknowledgements

First and foremost, I very much like to thank Prof. Dr. Michael Bader for the supervision of my PhD project at the MDC. Michael gave me the opportunity to work in his lab even after a round of PhD selection which was not successful for me. I have to thank him for his trust and confidence. Along the years, Michael has had always time to answer questions, solve problems or simply to share opinions about the latest interesting paper.

I would like to thank Dr. Uwe Kornak, Sabine Stumpp and Claire Schlack (University of Medicine, Charité, Berlin) for their help with micro-CT, bone histology and for their devotion to share knowledge about bone and osteoclast physiology. I also thank Prof. Klaus von der Mark (University of Erlangen) for his advices in December 2011 when we faced unexpected phenotype with our animal model.

For all meetings and discussions about the (pro)renin receptor, I would like to thank Prof. Geneviève Nguyen, Prof. Dominik Mueller and their respective group members.

Five years at the MDC have given the opportunity to meet incredible people coming from all around the world (many Russians and Brazilians among others) and to chat about topics beyond science such as sports, traditions and cultures.
There are too many people to thank individually here, but several deserve particular words:

First, Dr. Gabin Sihn and Dr. Johan Duchêne, the two other members of the French mafia; an appellation affectionately attributed by some people in the lab. I learned scientific rigor and time distortion (5 min can last actually 45 min…) with Gabin trying to decipher new roles of the (pro)renin receptor. I wish him good luck for his new professional orientation either in France or in any other exotic country. Johan introduced me to the mysterious world of chemokines and immune cells associated to inflammation. He was also a precious help in several aspects of my project. I wish him all the best in his professional career and personal life in Munich.

I am grateful to Dr. Fatimunnisa Qadri (aka Sayeeda) for performing the vast majority of the immunohistological work on various tissues such as bone and penis (sorry about this). Her generosity and kindness paved our discussions along these 4-5 years and sharing Indian food (she is a fantastic cooker) with her was sensational. I wish her all the best for her future scientific career.

Sabine Grüger, for our weekly meeting (almost every Tuesday morning) in the animal house facility to take care of my animal colonies and sharing some gossips. I also thank Manfred Ströhmann, Annegret Dahlke, Mihail Todiras and Lena Popova for their help with mice, rats and *in vivo* experiments.

Andrea Müller, Lisa Mallis, Susanne da Costa Goncalves, Tanja Schalow and Thorsten Riepenhausen for all the technical help and the good atmosphere they bring every morning. All students and trainees who closely worked with me are greatly thanked.
Our secretary, Iris Apostel-Krause, for her generous help with MDC bureaucracy and our hilarious French lessons.

All members and guests of the lab who were around to discuss, share advices, change my mood or simply go to the mensa with a special mention to Dr. Daniel Beis, Dr. Susann Matthes and Dr. Ashish Ranjan (I am the last one to get this title…).

And last but certainly not least, I would like to thank my family in France for their constant and lovely support the last thirty two years. Of course, my last thanks go to my "German family": my wife and my three daughters (including the last one born during the writing) for their love and support.

Abstract

A decade ago, the (pro)renin receptor [(P)RR] was discovered and depicted as a new component of the renin-angiotensin system. In tissues, the receptor was found to bind renin and its inactive precursor prorenin, leading simultaneously to the generation of local angiotensin II and to the initiation of intracellular signalling pathways. For these reasons, the (P)RR has been extensively studied for its potential contribution to end-organ damage in cardiovascular diseases and diabetes. However, recent studies have opened a new field of investigation on the potential role of (P)RR in cell homeostasis. Indeed, the (P)RR has been shown to associate with the vacuolar H^+-ATPase (V-ATPAse), hence its other name ATP6ap2 (vacuolar H^+-ATPase associated protein 2). Accordingly, several animal models have confirmed that this association is important for the acidification of intracellular compartments and cell survival.

Osteoclasts are multinucleated cells resulting from the fusion of myeloid progenitors (monocytes/macrophages) with the unique ability to degrade extracellular bone matrix. In those cells, V-ATPases are mainly located at the plasma membrane facing the bone surface and extrude protons into the extracellular space. The generation of an acidic environment is crucial for the enzymatic degradation of the bone matrix. In consequence, mice with genetic deletion of various V-ATPase subunits are characterized by an increase of bone mass (osteopetrosis) as a consequence of absent or dysfunctional osteoclasts.
In this work, we found that (P)RR is highly expressed in mature osteoclasts *in vitro* and *in vivo* suggesting that (P)RR might be important for osteoclast differentiation and/or functions. In order to clarify the role of (P)RR in osteoclast physiology and activity, we used mice with a floxed (P)RR allele and Cre recombinase transgenic mice to delete (P)RR either in mature osteoclasts (Cathepsin K-Cre, CtsK-Cre) or in osteoclast progenitors (Lysozyme M-Cre, LysM-Cre). In contrast to our hypothesis, micro-computed tomography and histological analysis demonstrated an absence of osteopetrosis in both mouse models and rather revealed a complex bone phenotype characterized by a reduction of bone density. Several lines of evidence suggested that osteoclasts in both models display increased differentiation and/or activity *in vitro* and *in vivo*. We therefore suggest that (P)RR does not directly regulate V-ATPases located at the plasma membrane but interferes with osteoclast physiology through other mechanisms. In terms of morphology, mice with CtsK-Cre-mediated (P)RR deletion displayed growth retardation whereas mice with LysM-Cre-mediated (P)RR deletion had a normal growth. Using R26-YFP reporter mice, we found that the CtsK-Cre expression was not restricted to osteoclasts in bone but also characterized some cells located in the groove of Ranvier. The role of this new cell population remains elusive but might explain the growth retardation observed in this animal model.

Macrophages are professionalized phagocytes crucial for immune response. Phagocytosis is an essential cellular process which is initiated by the engulfment of a pathogen into a structure termed phagosome. Maturation of the phagosome is a multistep process involving interactions with several organelles and ends with the destruction of the engulfed material after fusion with lysosomes. To circumvent the defective autophagy and the cellular death observed in (P)RR knockout mice generated via the Cre/Lox system, the generation of a new transgenic animal model was required. Therefore, we generated transgenic rats with a conditional depletion of (P)RR with the use of a doxycycline-induced shRNA expression system. Efficient (P)RR depletion in macrophages was accomplished by doxycycline treatment *in vivo* in drinking water and *in vitro* in culture medium. (P)RR deletion in mouse tissues has been associated with cell death due to an alkalization of intracellular vesicles and subsequent accumulation of autophagic vacuoles. In this work, we found that the impairment of vesicular pH is not an early event but rather a late consequence after (P)RR deletion. Indeed, despite efficient (P)RR knockdown after 24h of doxycycline treatment, the pH of intracellular vesicles remained normal during few more days.
We found that (P)RR deletion did not impair neither phagocytosis nor endocytosis but rather perturbed the recycling of the transferrin receptor to the plasma membrane. This effect occurred quickly after (P)RR depletion and was not associated with a defective pH. In conclusion, our findings suggest that (P)RR might be important for receptor recycling in macrophages.

Keywords: (pro)renin receptor, V-ATPase, acidification, trafficking, osteoclast, macrophage

Zusammenfassung

Vor zehn Jahren wurde der (Pro)Renin-Rezeptor [(P)RR] entdeckt und als neuer Bestandteil des Renin-Angiotensin-Systems beschrieben. In Geweben bindet dieser Rezeptor Renin und seinen inaktiven Vorläufer Prorenin, was gleichzeitig zur lokalen Bildung von Angiotensin II und zur Aktivierung intrazellulärer Signalkaskaden führt. Aus diesem Grund wurde der potentielle Beitrag des (P)RR zu Endorganschäden bei Herz-Kreislauf-Erkrankungen und Diabetes ausgiebig untersucht. Neuere Studien ergaben jedoch einen neuen Forschungsansatz für die potentielle Rolle von (P)RR in der Zell-Homöostase: es konnte gezeigt werden, dass der (P)RR mit der vakuolären H^+-ATPase (V-ATPAse) assoziiert sein kann, weshalb er auch ATP6ap2 (vacuolar H^+-ATPase associated protein 2) genannt wird. Übereinstimmend haben mehrere Tiermodelle diese Assoziation und ihre Bedeutung für die Ansäuerung intrazellulärer Kompartimente und das Überleben von Zellen bestätigt.

Bei Osteoklasten handelt es sich um mehrkernige Zellen. Sie entstehen bei der Verschmelzung von myeloiden Vorläuferzellen (Monozyten/Makrophagen) und besitzen die einzigartige Fähigkeit extrazelluläre Knochenmatrix zu degradieren. In diesen Zellen befinden sich V-ATPasen hauptsächlich an der zur Knochenoberfläche gerichteten Plasmamembran und transportieren Protonen in den extrazellulären Raum. Die Generierung einer sauren Umgebung ist wesentlich für die enzymatische Degradierung der Knochenmatrix. Dementsprechend sind Mäuse mit genetischer Deletion verschiedener V-ATPase- Untereinheiten charakterisiert durch einen Anstieg von Knochenmasse (Osteopetrose) als Folge abwesender oder dysfunktionaler Osteoklasten.
In der vorliegenden Arbeit fanden wir heraus, dass (P)RR stark in reifen Osteoklasten *in vitro* und *in vivo* exprimiert wird, was nahelegt, dass der (P)RR für die Osteoklastendifferenzierung und/oder -funktion wichtig ist. Um die Rolle des (P)RR in der Osteoklastenphysiologie und –aktivität zu klären, wurden Mäusen untersucht, die ein „floxed“ (P)RR-Allel aufwiesen und transgene Cre-Rekombinase Mäuse (P)RR. Damit wurde gezielt der (P)RR entweder in reifen Osteoklasten (Cathepsin K-Cre, CtsK-Cre) oder in Osteoklasten-Vorläuferzellen (Lysozyme M-Cre, LysM-Cre) deletiert. Im Gegensatz zu unserer Hypothese konnte mit Hilfe der Mikro-Computertomographie und der histologischen Analyse keine Osteopetrose in beiden Mausmodellen nachgewiesen werden, sondern ein komplexer Knochen-Phänotyp mit reduzierter Knochendichte. Ergebnisse aus verschiedenen Experimenten weisen darauf hin, dass die Osteoklasten in beiden Modellen vermehrte Differenzierung und/oder Aktivität *in vitro* und *in vivo* aufweisen. Wir postulieren deshalb, dass der (P)RR die in der Plasmamembran lokalisierten V-ATPasen nicht direkt reguliert, sondern mit der physiologischen Aktivität der Osteoklasten durch andere Mechanismen interferiert.

Morphologisch zeigten Mäuse mit CtsK-Cre-vermittelter (P)RR-Deletion eine Wachstumsverzögerung, während die Tiere mit LysM-Cre-vermittelter (P)RR-Deletion normal wuchsen. Durch R26-YFP Reportermäuse konnten wir zeigen, dass die Expression von CtsK-Cre nicht auf Osteoklasten in Knochen beschränkt ist, sondern auch in Zellen der Ranvier-Rinne. auftritt Die Rolle dieser neuen Zellpopulation ist unklar, könnte aber die beobachtete Wachstumsverzögerung in diesem Tiermodell erklären.

Macrophagen sind speziell auf die Immunabwehr ausgerichtete Fresszellen (Phagozyten). Phagozytose ist ein wesentlicher Zellprozess der durch das Einschließen eines Pathogens in eine spezialisierte zelluläre Struktur, das Phagosom, eingeleitet wird. Die Reifung des Phagosoms ist ein mehrstufiger Prozess, der Interaktionen mit mehreren Organellen involviert und, nach dem Zusammenschluß mit Lysosomen, mit der Zerstörung des eingeschlossenen Pathogens endet. Um die fehlerhafte Autophagie und den Zelltod zu vermeiden, der in den via Cre/Lox-System generierten (P)RR- knockout-Mäusen zu beobachten war, bedurfte es eines neuen transgenen Tiermodells. Deshalb generierten wir transgene Ratten mit konditionellen knockdown von (P)RR unter Nutzung eines Doxyzyclin-induzierten shRNA-Expressionssystems. Eine effiziente (P)RR-Depletion in Makrophagen wurde durch Behandlung mit Doxyzyclin *in vivo* im Trinkwasser und *in vitro* im Kulturmedium erreicht. Die Deletion von (P)RR in Mausgeweben wurde mit dem Zelltod durch Alkalisierung intrazellulärer Vesikel und anschließende Akkumulation autophagischer Vakuolen assoziiert. Die vorliegende Arbeit zeigt, dass die Verschiebung des vesikulären pHs nicht frühzeitig sondern erst ziemlich spät nach (P)RR-Deletion auftritt. Tatsächlich blieb der pH intrazellulärer Vesikel trotz effizientem Knockdown des (P)RR nach 24h Doxyzyclin-Behandlung normal.
Wir fanden heraus, dass (P)RR-Depletion weder Phagozytose noch Endozytose beeinträchtigte sondern vielmehr für das Recycling des Transferrin-Rezeptors zur Plasmamembran wichtig ist. Dieser Effekt trat schnell nach der Depletion von (P)RR auf und stand nicht im Zusammenhang mit einem veränderten pH. Zusammenfassend deuten unsere Ergebnisse darauf hin, dass (P)RR wichtig für Rezeptor Recycling in Makrophagen ist.

Stichworte: (Pro)Renin-Rezeptor, V-ATPase, Ansäuerung, vesikulärer Transport, Osteoklast, Makrophage

Table of Contents

CHAPTER 1 INTRODUCTION

A decade ago, the (pro)renin receptor [(P)RR] was discovered and described as a potential activator of the tissue renin-angiotensin system by binding renin and prorenin. For this reason, the role of the (P)RR in cardiovascular pathologies has been extensively studied. However, the discovery of embryonic lethality after (P)RR gene deletion in zebrafish and mouse suggested additional roles of (P)RR in cell homeostasis. Indeed, the (P)RR has been shown to associate with the vacuolar H^+-ATPase (V-ATPase), hence its other name ATP6ap2. Developmental studies in *Xenopus* and *Drosophila* have revealed an essential role of this association to promote the canonical and non-canonical Wnt signaling pathways, whereas studies with tissue-specific gene deletion have pointed out a role in autophagy. However, the precise regulation and function of this association is still unclear and requires further animal models and investigations.

1.1 (P)RR as a member of the renin-angiotensin system

1.1.1 Renin-angiotensin system

The renin-angiotensin system (RAS) is the principal volume-regulatory system of cardiovascular, renal and adrenal functions in mammals. It is the major hormonal system regulating blood pressure, fluid volume and electrolytes balance. Chronic activation of the RAS is a major factor in the development of various cardiovascular and renal diseases including hypertension and diabetes. The classical RAS is depicted as a circulating endocrine system ending with the generation of angiotensin II (Ang II) as final effector hormone. The first and rate-limiting step of this cascade is the conversion of angiotensinogen to a decapeptide, Ang I, by the proteolytic enzyme renin. Angiotensinogen is mainly synthetized in liver whereas active renin is produced in the juxtaglomerular apparatus (JGA) of the kidney. Ang I is further cleaved into the highly active octapeptide Ang II by the angiotensin converting enzyme (ACE) which is mainly present at the cell surface of endothelial cells. Additional peptides can be generated but Ang II is the main effector molecule of the RAS. Ang II binds to two major G protein-coupled receptors, the angiotensin type 1 (AT1) and angiotensin type 2 (AT2) receptor (reviewed in Bader 2010, Fournier et al. 2012). Ang II stimulates vasoconstriction, renal sodium retention, water intake, sympathetic activity, vasopressin release from brain and aldosterone secretion from adrenal cortex. All these effects are mediated through binding to the AT1 receptor and result in an increase of blood pressure. Stimulation of the AT2 receptor has been described to have protective actions by mostly counteracting the AT1 receptor.

1.1.2 Renin and prorenin

Renin is an aspartyl protease which regulates a crucial step within the RAS due to its unique ability to cleave angiotensinogen into Ang I. Prorenin is the inactive precursor of renin and does not exhibit any enzymatic activity due to an additional 43-amino acid prosegment which covers the active site cleft and prevents angiotensinogen binding. Prorenin can be activated either by a proteolytic or a non-proteolytic mechanism. Proteolytic activation occurs in the JGA in the kidney and is characterized by the cleavage and the removal of the prosegment. This activation is irreversible and was thought to involve one or more proteases commonly referred to as the prorenin-processing enzyme (PPE). Proconvertase I and cathepsin B have been described as potential PPEs *in vitro* (Derkx et al. 1992, Reudelhuber et al. 1994). However, recent studies have demonstrated that circulating active renin was still present in cathepsin B-deficient mice and that this activation was most likely achieved by hydrolysis in lysosome-like granules and do not require a specific PPE (Mercure et al. 2010, Xa et al. 2014). Non-proteolytic activation is characterized by a change in the conformation of the prosegment without being cleaved. This process has been described *in vitro* under non physiological conditions such as low pH or cold temperature (Sealy et al. 1976, Lumbers et al. 1971) but is still not yet defined *in vivo*.
In physiological conditions, the human plasma prorenin/renin ratio is around 10/1 (Danser et al. 1998) whereas chronic stimulation of the JGA is associated with more prorenin conversion and decreases this ratio (Danser et al. 2005). This is the consequence of prorenin being constitutively secreted whereas renin is stored in secretory vesicles within the JGA in the kidney until stimulus-dependent release. After bilateral nephrectomy, renin disappears but prorenin is still detectable in blood (Krop et al. 2008a). Thus, the kidney is the only renin-producing organ as expected. In contrast, this study showed that prorenin has additional origins and is also secreted by extrarenal sources. Organs such as reproductive tract, eye, placenta, adrenal and submandibular glands have been described to secrete prorenin (Krop et al. 2008b).
The common view was that renin was biologically active after activation in the JGA and secretion in the bloodstream. Prorenin was believed to have no functional relevance. The emergence of a tissue RAS with the local production of Ang II and the discovery of several new components with unexpected functions have challenged these dogma (Bader 2010). Local generation of Ang II in tissues such as heart and vascular wall in the absence of local renin expression (Müller et al. 1998, Van Kasteren et al. 1999) has raised the idea that renin and/or prorenin [(pro)renin] might bind a receptor and be enzymatically active.

1.1.3 The quest for a receptor for (pro)renin

The quest for a (pro)renin receptor lasted almost 20 years and was accompanied by intensive research. During this period, three different proteins were successively described as potential binding partners (pro)renin. First, the intracellular renin-binding protein (RnBP) emerged 30 years ago in pigs, rats and humans (Takahashi et al. 1983, Tada et al. 1992, Takahashi et al. 1992). However, mice with a genetic deletion of the RnBP had normal cardiovascular parameters (Schmitz et al. 2000) and thus, RnBP was no longer considered as “the” (pro)renin

receptor. Then, the mannose-6-phosphate/insulin-like growth factor II receptor got particular attention as it was described to bind (pro)renin with a high affinity and both are rapidly internalized (Van Kasteren et al. 1997, Saris et al. 2001a and 2001b). However, after intracellular activation, both ligands are quickly degraded in lysosomes without generating Ang I (Van den Eijnden et al. 2001, Saris et al. 2002). This receptor was therefore considered as a clearance receptor for (pro)renin. Finally, a third binding partner was discovered and appeared to be the most promising candidate to be a receptor for (pro)renin with important functions in cardiovascular homeostasis, the (pro)renin receptor.

1.1.4 The (pro)renin receptor

In 2002, Nguyen et al. provided confirmatory evidence for the concept of tissue RAS with the discovery that renin could bind to a high affinity membrane receptor on human mesangial cells in culture (Nguyen et al. 1996 and 1998). The full-length receptor was further characterized and the name (P)RR [(pro)renin receptor] was attributed after its cloning in 2002 (Nguyen et al. 2002).

1.1.4.1 Structure and localization

The gene coding for (P)RR is located on the X chromosome and codes for a protein with a length of 350 amino acids and an approximate mass of 37 kDa. Structural analysis of (P)RR has shown that it contains two hydrophobic domains predicted to be a signal peptide and a transmembrane domain, suggesting a type I transmembrane protein (Sihn et al. 2013). Thus, (P)RR can be divided into four different domains: an N-terminal signal peptide, an extracellular domain binding (pro)renin, a single transmembrane domain and a short cytoplasmic domain (Fig. 1) (Nguyen et al. 2008). In addition, shedding by proteases such as furin or ADAM19 (a disintegrin and metalloprotease 19) allows the generation of a long soluble fragment of 28-29 kDa composed of the (pro)renin binding domain (s(P)RR) and a short fragment composed of the transmembrane and intracellular parts (Cousin et al. 2009, Yoshikawa et al. 2011).

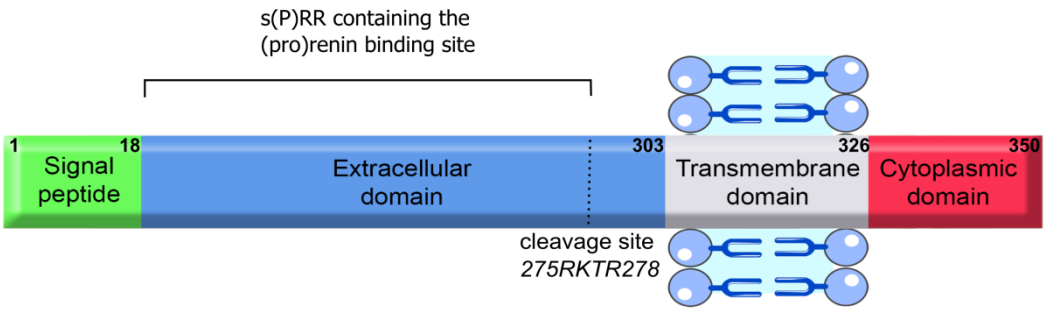

Fig. 1: Schematic structure of (P)RR.
The full length (P)RR is characterized by 4 domains: a signal peptide, an extracellular (with binding properties), a transmembrane and an intracellular domain. The presence of a cleavage site in the extracellular domain allows the generation of the soluble (s(P)RR) which can be excreted out of the cell. Numbers represent amino acids.

(P)RR shows no homology to any known membrane protein (Nguyen et al. 2002). So far, only a small part of the cytoplasmic domain was successfully crystallized (Zhang et al. 2011) but it did not yield significant information about the structure of the full-length (P)RR.
Although prominently expressed in the brain and the heart, (P)RR was also reported in other organs such as lung, liver, kidney, muscle and pancreas (Nguyen et al. 2002). Additional microarray suggests an ubiquitous expression of its mRNA (Su et al. 2004). As a receptor for (pro)renin, the (P)RR was initially described at the plasma membrane but several reports suggest a subcellular localization within intracellular compartments. This discrepancy will be developed in details in the following sections. It was described that s(P)RR can be secreted by cells into the bloodstream (Cousin et al. 2009), and this aspect initiated the development of enzyme-linked immunosorbent assays (ELISAs) to detect and quantify s(P)RR in various biological fluids (Ichihara et al. 2010, Maruyama et al. 2010). However, the exact role and regulation of the s(P)RR *in vivo* is still unclear.

1.1.4.2 Role as a receptor

Initially, both renin and prorenin were reported to bind equally (P)RR *in vitro* without internalization. After binding to (P)RR at the cell surface of mesangial cells, renin activity was increased by a factor 5 and prorenin was also non-proteolytically activated resulting in the generation of Ang I (Nguyen et al. 1996 and 2002). However, analysis of binding properties *in vitro* revealed a K_d of 7 and 20 nM for prorenin and renin respectively, arguing that prorenin may be the main endogenous ligand *in vivo* (Batenburg et al. 2007). The binding of prorenin to the (P)RR has two important functional consequences. First, as above mentioned prorenin undergoes non-proteolytic activation (ie without cleavage), displays enzymatic activity and cleaves angiotensinogen to generate Ang I (Nguyen et al. 2002, Nabi et al. 2006, Batenburg et al. 2007). The subsequent generation of Ang II by tissue ACE leads to Ang II-dependent effects via AT1 receptors. Unexpectedly, using AT1 blockers, several studies showed that (P)RR activation triggers intracellular pathways independently of the Ang II generated (Fig. 2). Indeed, signal transduction induced by (pro)renin binding activates the mitogen-activated protein kinase (MAPK) ERK1/2 in cardiomyocytes (Saris et al. 2006), vascular smooth muscle cells (Sakoda et al. 2007, Liu et al. 2011), mesangial cells (Nguyen et al. 2002, Huang et al. 2007, Melnyk et al. 2009), fibroblasts (Montes et al. 2012) and monocytes (Feldt et al. 2008). This led to the upregulation of transforming growth factor β1 (Huang et al. 2006 and 2007, Kaneshiro et al. 2006, Melnyk et al. 2009, Clavreul et al. 2011, Huang et al. 2011, Montes et al. 2012, Zhang et al. 2012) which in turn increases the expression of pro-fibrotic genes such as plasminogen-activator inhibitor-1 (Nguyen et al. 1996, Huang et al. 2006 and 2007, Zhang et al. 2008 and 2012, Melnyk et al. 2009, Clavreul et al. 2011), collagen-1 (Huang et al. 2006, Montes et al. 2012), fibronectin (Huang et al. 2006, Clavreul et al. 2011, Zhang et al. 2012) and connective tissue growth factor (Huang et al. 2011). In renal tissues, (P)RR activation upregulates inflammatory mediators such as cyclooxygenase-2 (Kaneshiro et al. 2006, Huang et al. 2009, Gonzalez et al. 2012), interleukin-1 (Huang et al. 2009, Matavelli et al. 2009) and tumor necrosis factor α (Matavelli et al. 2009). In addition to ERK1/2, JNK and p38 MAPKs have also been described to

be activated by (P)RR activation in cardiomyocytes (Saris et al. 2006) and kidney glomeruli (Kaneshiro et al. 2007). (P)RR activation has also been associated with the induction of cell proliferation and chemotaxis (Huang et al. 2007, Liu et al. 2011, Greco et al. 2012). In endothelial cells and in the retinal pigment epithelium, prorenin-dependent ERK1/2 activation was associated to an increased expression of monocyte chemotactic protein 1, vascular endothelial growth factor and again collagen-1 (Satofuka et al. 2008 and 2009, Alcazar et al. 2009, Uraoka et al. 2009, Kanda et al. 2012).

The physiological relevance of the activation of these signalling pathways has yet to be confirmed *in vivo* since they have often been described *in vitro* with supraphysiological concentration of prorenin and without adequate (P)RR loss of function.

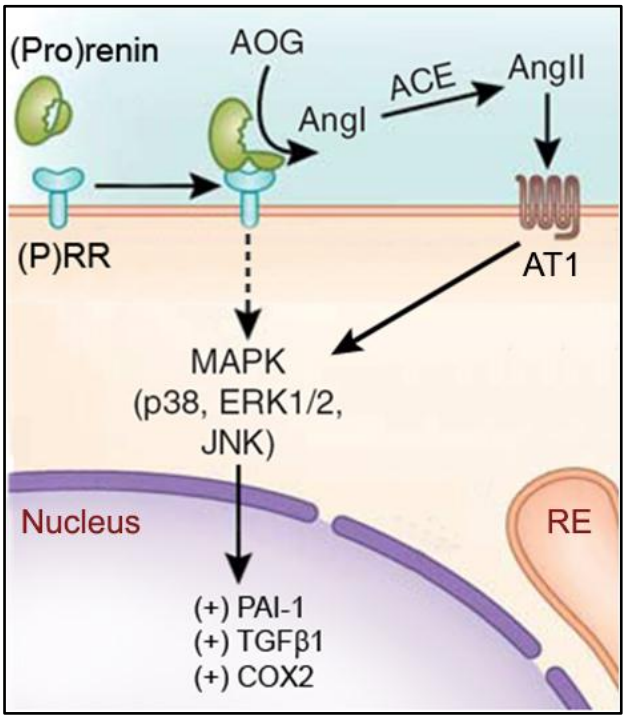

Fig. 2: Functions of (P)RR as a receptor for (pro)renin.
(Pro)renin binding to the (P)RR triggers intracellular cascade via Ang II-dependent and –independent signaling. Both signaling converge to the activation of MAPKs and the subsequent upregulation of pro-fibrotic and inflammatory genes (modified from Sihn et al. 2010). ACE, angiotensin-converting enzyme; AOG, angiotensinogen; COX2, cyclooxygenase 2; ER, endoplasmic reticulum; MAPK, mitogen-activated protein kinase; PAI-1, plasminogen-activator inhibitor-1; TGFβ1, transforming growth factor β1.

A yeast two-hybrid screen identified the promyelotic leukemia zinc finger transcription factor (PLZF) as a potential binding partner of (P)RR in cardiac tissue (Schefe et al. 2006 and 2008). Following (pro)renin-dependent (P)RR activation, PLZF was described to translocate to the nucleus and repress (P)RR expression, thereby generating a negative feedback loop which might prevent excessive (P)RR activation in high prorenin conditions. However, this mechanism described *in vitro* has to be taken with caution since a recent study described a positive feedback loop *in vivo*, as high (pro)renin levels in the kidney resulted in (P)RR upregulation (Krebs et al. 2007).

1.1.5 High prorenin levels and (P)RR expression in pathology

The consequences of the activation of (P)RR by (pro)renin have raised the hypothesis that (P)RR might play a pivotal role in pathologies associated with high prorenin conditions.
A potential role of prorenin in pathology initially appeared with the description that diabetic patients display an up to 7-fold higher prorenin/renin ratio in the blood (Luetscher et al. 1985, Deinum et al. 1999, Stankovic et al. 2006). Experimental evidence arose from transgenic rats with a constitutive prorenin expression in the liver. These animals displayed a 400-fold increased circulating prorenin level and developed cardiac hypertrophy and glomerulosclerosis but were devoid of any hypertension (Veniant et al. 1996). This absence of activated circulating RAS (no modification of circulating Ang II levels) was also observed in mice with prorenin overexpression (Prescott et al. 2002). These data suggested that non-proteolytic activation of prorenin at the tissue level through potential binding to (P)RR is a contributing factor for tissue damage. However, subsequent studies contradicted these findings. In fact, high prorenin levels are also found during pregnancy in the maternal plasma (up to 10-fold increased) but is not associated with any tissue damage (Skinner et al. 1975, Hsueh et al. 1982, Sealey et al. 1982). Also, the use of various RAS blockers such as ACE, renin and AT1 inhibitors is associated with increased circulating prorenin levels but these compounds are the prime treatment for a multitude of cardiovascular diseases in order to avoid tissue damage (Bader et al. 2000). Three different groups generated transgenic animals with high prorenin levels (rats and mice) and all reported the absence of renal damage and cardiac fibrosis in their respective models (Campbell et al. 2009, Peters et al. 2008 and 2009, Mercure et al. 2009).
All together, these controversial results suggest that neither high prorenin levels alone nor potential binding to (P)RR are conditions associated with tissue damage.

A modulation of (P)RR expression under pathologic conditions has been widely described *in vitro* and *in vivo* and suggested its direct involvement in tissue damage. Briefly, increased (P)RR expression was described *in vitro* in renal cells treated with high glucose (Huang et al. 2009 and 2010, Pereira et al. 2011) as well as in heart, kidney and retina of diabetic animals (Siragy et al. 2008, Matavelli et al. 2009, Satofuka et al. 2009, Connelly et al. 2011). Also, (P)RR has been shown to be upregulated in the remnant kidney of nephrectomized rats (Freundlich et al. 2008, Hirose et al. 2010), in atherosclerotic aorta (Kaschina et al. 2009), in the heart and kidney of rodents after myocardial infarction (Hirose et al. 2009a, Mahmud et al. 2012), in the heart of spontaneously hypertensive rats (Ichihara et al. 2006) and in the placenta of rats with preeclampsia (Thomason et al. 2015). All these studies observed an increased (P)RR expression in various pathologies but did not conclude on a detrimental role of (P)RR in the development of the symptoms as this upregulation might be a consequence and not the cause. For this reason, transgenic animals overexpressing (P)RR were expected to provide important hints. Rats with a targeted (P)RR overexpression in smooth muscle cells developed a chronic hypertension without renal complications (Burckle et al. 2006a). In contrast, rats with ubiquitous (P)RR overexpression developed renal nephropathy but displayed a normal blood pressure (Kaneshiro

et al. 2007). It is important to note that these pathologies in both models were quite mild and appearing late in life.
Recently, another group generated a new transgenic mouse line with an ubiquitous (P)RR overexpression and reported an absence of all symptoms described above (Rosendahl et al. 2014). Finally, heart-specific (P)RR overexpression in mice did not affect the cardiac remodeling process in response to stress and injury (Mahmud et al. 2014).
Therefore, based on the weak or absent phenotypes in these different models and despite a drastic overexpression of (P)RR, it is likely that (P)RR plays a marginal role in local prorenin activation and development of cardiovascular pathologies.

In humans, (P)RR has been described to be upregulated in the kidneys of patients with diabetic nephropathy (Takahashi et al. 2010), in hearts of patients with dilated cardiomyopathy (Mahmud et al. 2012) and in vitreous fluids of patients with proliferative diabetic retinopathy (Kanda et al. 2012). However, clinical data involving a direct role of (P)RR in pathology are still lacking despite some studies. Genome-wide association studies with Japanese cohorts have revealed various polymorphisms in the *(P)RR/ATP6ap2* gene associated with increased cardiovascular risks in humans (Krop et al. 2013). Firstly, the 5+169C>T polymorphism was significantly associated with blood pressure in Japanese men (Hirose et al. 2009b) and more recently in Caucasian men (Ott et al. 2011). Secondly, the +1513A>G polymorphism was significantly associated with the risk of lacunar infarction and left ventricular hypertrophy in Japanese women (Hirose et al. 2011). Finally, two additional polymorphisms were significantly associated with hypertension in additional populations with vascular diseases (Brugts et al. 2011). However, none of these reports provided evidence of an impact of these polymorphisms on (P)RR expression or function.

1.1.6 Blockade of (P)RR as a therapeutic option

After its discovery and characterization, (P)RR quickly became an interesting target to decrease end-organ damage associated with hypertension and diabetes and to complement the arsenal of anti-hypertensive drugs, which do not fully prevent tissue damage.
In 2004, Ichihara et al. designed a short peptide named Handle Region Peptide (HRP) able to interfere with prorenin/(P)RR binding (Ichihara et al. 2004). This decapeptide mimics a part (amino acids 10 to 19) of the prorenin prosegment called “handle region” previously described to be important for the non-proteolytic activation of prorenin and for the interaction with (P)RR (Suzuki et al. 2003). Thus, HRP was proposed to act as a decoy peptide inhibiting the interaction of prorenin with (P)RR. Administration of HRP to diabetic mice and rats not only prevented the development of cardiac fibrosis, proteinuria and glomerulosclerosis but also reversed established diabetic nephropathy (Ichihara et al. 2004, 2006a and 2006b, Takahashi et al. 2007, Matavelli et al. 2009). These results were obtained by concomitant administration of ACE inhibitor and AT1 receptor blocker, or using AT1 receptor KO mice. Thereby, it is suggested that deleterious actions of (P)RR take place in an Ang II-independent manner. Beneficial effects of HRP were further described in several pathologies including cardiac fibrosis in spontaneously

hypertensive rats (Ichihara et al. 2006b), retinal neovascularization and ocular inflammation (Satofuka et al. 2006, 2007 and 2009). Recently, (P)RR antagonism resulted in cardiovascular and renal benefits in experimental heart failure (Rademaker et al. 2012). Despite these encouraging results, conflicting data were obtained *in vitro* and in various animal models, generating a controversy about the efficiency, binding ability and properties of this blocker.
Feldt et al. showed *in vitro* in monocytes and smooth muscle cells that prorenin was able to bind (P)RR and activate ERK1/2 in the presence of HRP (Feldt et al. 2008a and 2008b). They also reported unspecific binding of HRP to cells lacking (P)RR (Feldt et al. 2008a). This is in agreement with a recent study showing that HRP does not bind specifically (P)RR with a high affinity (Leckie et al. 2011). In spontaneously hypertensive rats, Susic et al. could not reproduce the beneficial effect of HRP in cardiac hypertrophy (Susic et al. 2008) described by Ichihara et al. (Ichihara et al. 2006b). Also, HRP treatment in double-transgenic rats overexpressing angiotensinogen and renin (Feldt et al. 2008b) as well as in Goldblatt hypertensive rats (Krebs et al. 2008, Müller et al. 2008) ameliorated neither cardiovascular nor renal damage. In addition, HRP has been described *in vivo* to be rapidly degraded in the circulation with unpredictable beneficial effects (Wilkinson-Berka et al. 2010) and *in vitro* to act as a partial agonist of (P)RR (Lu et al. 2013). Finally, a new inhibitory peptide called PRO20 corresponding to the first 20 amino acids of the mouse prorenin prosegment has been recently synthetized and has shown beneficial effects when injected into the brain of hypertensive mice (Li et al. 2015). Although the specificity has been confirmed in (P)RR knock-out tissues, the exact mechanism of action is still pending. Thus, confirming the specificity and the efficiency of HRP and PRO20 is a fundamental aspect to ascertain a role of (P)RR in cardiovascular pathologies and to reach clinical applications.

1.2 (P)RR as a potential modulator of the V-ATPase functions

Few years after (P)RR was discovered, and in parallel to its characterization as a member of the RAS, new evidence emerged, which drastically changed the vision on this protein and its function. In the paper by Nguyen et al. (Nguyen et al. 2002), (P)RR had been described to be partially identical to a protein identified as early as 1998. In chromaffin cells of the adrenal medulla, Ludwig et al. (Ludwig et al. 1998) had described a truncated form (called M8-9) of the (P)RR corresponding roughly to the short fragment (transmembrane domain and C-terminal part) generated after shedding (L'Huillier et al. 2005, Burckle et al. 2006b). This M8-9 portion was found to co-immunoprecipitate with the V-ATPase which would later urge the scientific community to rename (P)RR as V-ATPase-associated protein 2 (ATP6ap2). They erroneously considered that an in-frame ATG upstream of this short fragment served as a start codon for the protein and did not consider the possibility of a longer protein which could be cleaved. When Nguyen et al. discovered the full-length (P)RR in 2002, the homology of the two proteins was not obvious leading to two different denominations for the same protein (Fig. 3). It took few years to realize the homology and to unite them under a common name, (P)RR/ATP6ap2.

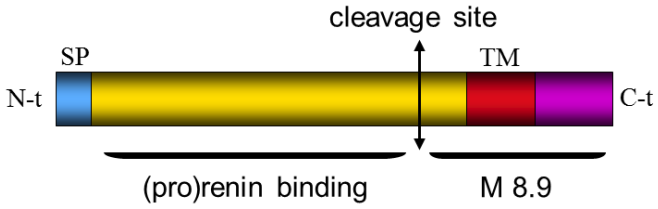

Fig. 3: (P)RR and the M8-9 fragment. Initially described as two different protein, the M8-9 fragment which co-immunoprecipitated with the V-ATPase was actually identical to the small fragment of the (P)RR after proteolytic cleavage.

1.2.1 V-ATPase: an essential proton pump for cell physiology

1.2.1.1 V-ATPase structure and proton transport

The V-ATPase is a large, multi-subunit complex divided into two domains. The peripheral (or cytoplasmic) V1 domain is responsible for ATP hydrolysis and is composed of 8 subunits (A-H) with the following stoichiometry: A_3 B_3 C D E_3 F G_3 H (Muench et al. 2009). The membrane-embedded V0 domain is involved in proton translocation and is composed of 5 subunits (a, c, c'', d and e in mammals) with the following stoichiometry: a c_5 c'' d (Forgac et al. 2007, Toei et al. 2010). In addition, accessory subunits have been described, Ac45 (ATP6ap1) and –hence– ATP6ap2, although this denomination has yet to be proven at the functional level (Fig. 4). The V-ATPase is a rotary proton pump with a high complexity. Indeed, some subunits have several isoforms which can be expressed in a tissue-specific manner and are involved in the intracellular location and function of the pump (Marshansky et al. 2014).

The V0 domain is assembled in the ER and requires a set of chaperone proteins such as VMA (vacuolar membrane ATPase activity) 12, VMA21, VMA22 and Pkr1 (Graham et al. 2003, Malkus

et al. 2004, Davis-Kaplan et al. 2006). This mechanism is well described in yeast but its description in mammals remains pending. In contrast, the V1 domain self-assembles in the cytoplasm where all V1 subunits are present. Once bound together, the V0 and V1 domains can dissociate reversibly in response to stimuli. Although the exact mechanism is still unknown, this reversible association/dissociation might be a regulatory mechanism of V-ATPase activity (Maxson et al. 2014).

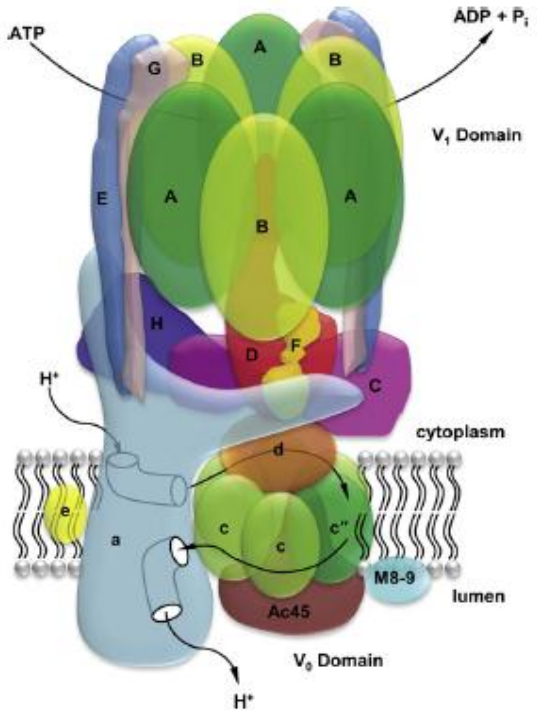

Fig. 4: Schematic structure of the mammalian V-ATPase.
The V-ATPase is a multi-subunit complex composed of a peripheral V1 domain (subunits A-H), a membrane-embedded V0 domain (subunits a-e) and 2 additional accessory subunits (Ac45 and M8-9/(P)RR). The V1 domain is responsible for ATP hydrolysis and the V0 domain is involved in proton translocation. (Picture from Qin et al. 2012).

After association of both domains, the proton pump activity is activated. The A and B subunits of the V1 domain form a hexameric structure in which three ATP catalytic sites are located at each A/B interface (Liu et al. 1996 and 1997). After hydrolysis of the ATP nucleotide, the hexamer undergoes a conformational change inducing the rotation of a central stalk composed of subunits D, F and d (Xu et al. 1999 and 2000). The a subunit of the V0 domain and two peripheral stalks composed of C, E, G and H subunits of the V1 domain play the role of a stator (ie. stay static) and prevent the rotation of the hexamer (Fethiere et al. 2005, Venzke et al. 2005, Ohira et al. 2006). The rotation of the central stalk couples the energy of ATP hydrolysis to the rotation of a proteolipid ring composed of c and c'' subunits which allow H^+ translocation through the membrane via a complex transport. Briefly, cytosolic protons pass through a first hemichannel to join the proteolipid ring whose rotation translocate protons to the lumen space through the a subunit and a second hemichannel involving crucial residues of the subunit a (Nishi et al. 2000, Guillard et al. 2009) (Fig. 4).
It is accepted that hydrolysis of one ATP nucleotide provides sufficient energy for one 360° rotation of the V0 proteolipid ring and the translocation of 2-4 protons across the membrane

(Kettner et al. 2003). Specific V-ATPase inhibitors such as Bafilomycin and Concanamycin have been described to bind to and inhibit the rotation of the V0 proteolipid ring (Huss et al. 2009).

1.2.1.2 Localization and housekeeping functions of V-ATPases

V-ATPases are ubiquitous in eukaryotes and perform essential housekeeping functions through their proton pumping activity. In most cells, V-ATPases are mainly located in intracellular compartments such as endosomes, lysosomes, autophagosomes, Golgi-derived vesicles, synaptic vesicles and melanosomes among others. These proton pumps provide an acidic environment in the lumen of these vesicles essential for protein trafficking (endocytosis, recycling and exocytosis), degradation and maturation through pH-dependent enzymes (Forgac et al. 2007, Marchansky et al. 2008).

For instance, after endocytosis, receptor-ligand complexes traffic via early endosomes where a low pH induces the dissociation of the ligand from its receptor. At this stage, the receptor can shuttle back to the membrane via recycle endosomes whereas the ligand is targeted to the lysosome via late endosomes. In some cases, a receptor can be recycled to the Golgi apparatus via late endosomes. Each of these vesicles contains a specific pH between 7 and 4.5 provided by the V-ATPase (Huotari et al. 2011). In lysosomes, V-ATPases are also essential to generate a unique low pH around 4.5 which is crucial for the activity of several proteases such as cathepsin B (Saftig et al. 2009) and subsequent protein degradation. Proteases are also important for protein maturation. Several secreted hormones including insulin and thyroxin are released as pro-hormone in secretory vesicles from the Golgi apparatus. Acidification of these vesicles (pH 5) by V-ATPases activates proteases which in turn cleave the pro-hormones into their active forms (Fisher et al. 1988). The acidification of the Golgi lumen to pH 6.3 is important for protein sorting and involves V-ATPases (Schoonderwoert et al. 2001). Inhibition of the pump neutralizes the pH and leads to protein mistrafficking (Nelson et al. 1999). In addition, the uptake and secretion of neurotransmitters in synaptic vesicles are dependent of a pH gradient generated by V-ATPase (Maxson et al. 2014). To provide such fine-tuned pH in all these compartments, it is hypothesized that the pump density and the coupling efficiency (number of H+ translocated/ATP hydrolyzed) may be specific for each organelle (Maxson et al. 2014).

In some specialized cells, V-ATPases are targeted to the plasma membrane and extrude protons to the extracellular space (Forgac et al. 2007). This occurs in intercalated cells of the renal collecting duct to acidify urine (Brown et al. 2000), in osteoclasts to resorb bone (Toyomura et al. 2003) and in epididymal clear cells for proper sperm maturation and stockage (Brown et al. 2000). Activated phagocytes such as neutrophils and macrophages also target V-ATPases to the plasma membrane to maintain a neutral cytoplasmic pH after contact with pathogens (Brisseau et al. 1996).

As previously stated, some subunits have several isoforms which can be expressed in a tissue-specific manner and involved in the intracellular localization of the V-ATPase (Marshansky et al. 2014). For instance, mammalian cells contain four isoforms of subunit a. The a1 isoform is present in synaptic vesicles and at the plasma membrane of presynaptic nerves (Morel et al. 2003). The a2 isoform is found exclusively in early endosomes at the apical surface of renal

tubule cells (Hurtado-Lorenzo et al. 2006). In contrast, the a3 isoform is found at the ruffled border of osteoclasts (Toyomura et al. 2003) and the a4 isoforms localizes to the plasma membrane of renal intercalated cells and epididymal cells (Wagner et al. 2004, Pietrement et al. 2006). In addition, 3 isoforms of subunits C and G and 2 isoforms of subunits B, E, H and d are found in mammals (Forgac et al. 2007). These isoforms are expressed in different cell types and their respective roles are unknown. Nevertheless, it suggests that all V-ATPase localizations are likely associated to a particular combination of these multiple isoforms.

1.2.1.3 Non-canonical functions of V-ATPases

In addition to the well-described acidification of vesicles and extracellular space provided by the proton pump, recent data suggest that V-ATPases contribute to additional physiological functions independently of their pumping activity. These aspects are briefly described below as they remain either not well-described or controversial. These new functions are considered as non-canonical in opposition to the housekeeping functions associated to the proton transport.
For instance, the V0 domain has been described to be important for the fusion of synaptic and secretory vesicles with the plasma membrane for exocytosis (Hiesinger et al. 2005, Sun-Wada et al. 2006). V-ATPases have also been described to act as a sensor of luminal pH and to recruit proteins through the subunit a2 after a conformational change (Hurtado-Lorenzo et al. 2006, Merkulova et al. 2010). In addition to the luminal pH, V-ATPases at the lysosomal membrane were described to sense the amino acid levels (cytoplasmic or luminal) and to recruit and activate mammalian target of rapamycin complex 1 (mTORC1), an important regulator of cell growth and autophagy (Zoncu et al. 2011, Bar-Peled et al. 2014). Finally, V-ATPases might also serve as a scaffold for proteins important for the regulation of the cytoskeleton and cellular metabolism (Lu et al. 2001, Su et al. 2003, Vitavska et al. 2003, Carnell et al. 2011).

1.2.1.4 V-ATPases in physiopathology

Experimental and clinical studies have highlighted the critical roles of V-ATPases in physiology and pathophysiology. Deletion or mutation of V-ATPase subunits in animal models and humans are associated to a wide range of phenotypes (Beyenbach et al. 2006, Sihn et al. 2010). In mice for instance, gene deletions of subunit c (Inoue et al. 1999, Sun-Wada et al. 2000), d (Miura et al. 2003) and the accessory protein Ac45 (Schoonderwoert et al. 2002) are associated with embryonic lethality. In contrast, gene deletion of subunits B1, a3 and d2 are associated with renal acidosis (Finberg et al. 2005) and osteopetrosis (Scimeca et al. 2000, Lee et al. 2006), respectively. Mutations in subunit a1 have been shown to block the secretion of exosomes in *Caenorhabditis elegans* (Liegeois et al. 2006) and synaptic vesicles in *Drosophila* (Hiesinger et al. 2005). Chemical inhibition of the proton pump activity revealed that V-ATPases are important for early *Xenopus* embryo left-right axis determination (Adams et al. 2006).
To date, genetic mutations in four V-ATPase genes have been associated with human pathologies. Diverse genetic mutations in the a3 subunit (*ATP6V0A3, TCIRG1*) are associated with autosomal recessive osteopetrosis (Frattini et al. 2000, Kornak et al. 2000), a heritable

disorder of the cytoskeleton characterized by increased bone mass and severe complications (Stark et al. 2009). Mutations in the a2 subunit gene (*ATP6V0A2*) were recently associated with cutis laxa syndrome (loose skin) due to protein glycosylation defects (Kornak et al. 2008). Finally, genetic mutations in the B1 and a4 subunits (*ATP6V1B1, ATP6V0A4*) are associated with distal renal tubular acidosis with and without hearing loss (Karet et al. 1999, Smith et al. 2000, Stover et al. 2002).

V-ATPases are also suspected to be involved in cancer metastasis through increased activity at the plasma membrane of tumor cells and subsequent acidification of the extracellular matrix (Torigoe et al. 2000, Sennoune et al. 2004). Through acidification of endosomal compartments, V-ATPases are not only responsible for the entry of bacterial toxins and viruses within cells but also for their propagation via release of viral mRNA and toxins in the cytoplasm (Abrami et al. 2004, Gruenberg et al. 2006, Forgac et al. 2007).

Altogether, V-ATPases are associated with various severe pathologies and this aspect raised a strong interest to develop specific inhibitors of the proton pump for therapeutic purposes. However, probably due to the essential housekeeping functions of V-ATPases, no inhibitor of this pump has reached the step of clinical studies.

1.2.2 Early hints for a connection between (P)RR and the V-ATPase

Nguyen et al. initially characterized (P)RR as a receptor at the cell surface where its binding to (pro)renin occurs (Nguyen et al. 2002). Therefore, all subsequent studies deciphering the consequences of this binding and trying to block it with the HRP were based on this conceptual localization. However, in parallel to these studies, several reports raised the possibility that (P)RR might have different localizations and likely resides mainly within intracellular compartments.

The description of (P)RR (as the M8-9 fragment) in membranes of cytoplasmic granules in chromaffin cells (Ludwig et al. 1998) and later in synaptic vesicle (Takamori et al. 2006) paved the way for potential intracellular locations. The full length (P)RR also appeared to be identical to an additional, but yet unpublished protein named CAPER (Genbank entry AY038990) or endoplasmic reticulum localized type I transmembrane adaptator precursor C suggesting a possible location in the endoplasmic reticulum (ER). Examination of the amino acid sequence revealed two theoretical sorting motifs within the short cytoplasmic domain compatible with such locations (Burckle et al. 2006b, Sihn et al. 2013). The first motif Y^{335}DSI is identical to a tyrosine-based sorting signal YxxØ (in which Ø is a large hydrophobic amino acid and x any amino acids). This short sequence targets a protein to the endosomal and lysosomal compartments through its interaction with adaptor protein (AP) complexes (Bonifacino et al. 2003). These localizations are still a matter of debate as we found (P)RR mainly located in endosomes and absent in lysosomes (Sihn et al. 2013) whereas others described the lysosomal compartment as the main subcellular localization (Schefe et al. 2006). The second C-terminal motif K^{346}IRMD is reminiscent to two conventional dibasic sequences K(x)Rxx and R(x)Rxx in which x is any amino acids. These motifs play a role as ER retention/retrieval signals but are uncommon and not well described in vertebrates. Mutations of the sequence in tagged-(P)RR

modified the localization from the ER to the lysosomal compartment and suggested that this motif is indeed functional (Schefe et al. 2006). Using tagged-(P)RR and specific (P)RR antibodies, we and others were able to demonstrate that ER was the main intracellular localization (Yoshikawa et al. 2011, Sihn et al. 2013). Unrelated to these sorting motifs, additional localizations have been reported by several groups. For instance, (P)RR was described *in vitro* within the Golgi apparatus where its cleavage by proteases was taking place (Cousin et al. 2009, Yoshikawa et al. 2011). Also, in A-type intercalated cells of the kidney collecting duct, Advani et al. detected (P)RR in the Golgi apparatus where it colocalized with the B1/2 subunit of the V-ATPase V1 domain (Advani et al. 2009). Such localizations in the ER/Golgi network were demonstrated recently in retinal cells of mice (Kanda et al. 2013). It is important to note that these discrepancies in the subcellular localizations of (P)RR might also have technical reasons. Indeed, most studies used tagged-(P)RR (potential misfolding), overexpressed constructs (potential missorting), different antibodies (potential unspecificity) and cell types. Thus, all these possible localizations were taken with caution at the time but already raised the idea that (P)RR was not only located at the plasma membrane.

(P)RR is not only found in vertebrates but also in lower organisms such as *C elegans* (worm) and *Drosophila melanogaster* (insect) which do not possess genes for angiotensinogen, renin and angiotensin receptors and are thus devoid of a functional RAS (Fournier et al. 2012). Interestingly, the amino acid sequence of the transmembrane and cytoplasmic domains corresponding to the V-ATPase associated M8-9 segment is conserved in both vertebrates and invertebrates. In contrast, only vertebrates share a conserved sequence of the extracellular domain, important for (pro)renin binding and corresponding to the RAS related function (Burckle et al. 2006b). From these findings, our lab postulated that (P)RR resulted from the fusion of two genes with different functions in vertebrates and corresponding to the 2 domains described above. A second hypothesis was that (P)RR had an ancestral function related to the V-ATPase and acquired its ability to bind (pro)renin during evolution later (Burckle et al. 2006b, Fournier et al. 2012). Thus, a few years after its discovery as receptor for (pro)renin, it was suggested that (P)RR might play an additional role in association with the V-ATPase. But at that time, direct evidence was lacking and the research field was focused on the ability of (P)RR to stimulate the tissue RAS. Studies with mutant zebrafish and the apparent lethality of (P)RR knockout (KO) mice (Sihn et al. 2009) suggested a more essential role of this protein than the RAS, thus engendering a progressive, yet irresistible, shift of the (P)RR research towards critical intracellular functions. However, additional years were necessary to conduct developmental studies and generate mice with tissue-specific deletion of (P)RR in order to unravel such functions.

1.2.3 (P)RR and V-ATPase in genetic models and humans

1.2.3.1 Zebrafish: first indirect in vivo link between (P)RR and the V-ATPase

Studies with zebrafish provided early hints for a potential role of (P)RR as a V-ATPase accessory subunit. Indeed, zebrafish with insertional mutagenesis of (P)RR shared a common embryonic

phenotype with mutants for several V-ATPase subunits. All mutants displayed abnormal pigmentation, multiple organ defects and necrosis in the central nervous system, finally resulting in lethality after 5 days of development (Amsterdam et al. 2004, Nuckels et al. 2009, http://zfin.org). We obtained the same results using morpholino antisense oligonucleotide injections against (P)RR in zebrafish (Sihn et al., manuscript in preparation). These results suggested that (P)RR is important for embryonic development probably linked to V-ATPase activity but no direct evidence was provided by this animal model for years. Recently, Eauclaire et al. performed a chemical mutagenesis screen to identify proteins important for biliary development (EauClaire et al. 2012). Among all mutants with abnormalities in hepatic development, one mutant called *pekin (pn)* was particularly studied. It turned out that the causative mutation in *pn* was located at the end of exon 8 of the *(P)RR/atp6ap2* gene and led to a read-through and premature stop codon. Ultrastructural examination of bile duct cells revealed accumulation of electron dense bodies at the periphery of the cells. In addition, typical features of ER stress were also present. Thus, it was suggested that decreased (P)RR levels altered protein trafficking and degradation probably by affecting V-ATPase function and altering vesicular pH. The presence of skin and eye hypopigmentation in *pn* provided further evidence as this phenotype was previously associated with inhibition of the V-ATPase (Amsterdam et al. 2004, Gross et al. 2005, Wang et al. 2008, Nuckels et al. 2009). In the skin, melanoblast markers decreased with time which suggests that melanocytes developed normally but underwent degeneration (EauClaire et al. 2012). In the eye, striking degradation of various cell layers was also observed. The fact that mutants for ATP6V0D1 and ATP6ap1 displayed defects in intrahepatic ducts similar to *pn*, and that renin morphant displayed minor defects suggested that (P)RR is important for V-ATPase activity independently of its (pro)renin receptor ability. Further studies are necessary to reveal the exact mechanism for which (P)RR is essential in biliary development.

1.2.3.2 *Xenopus*: (P)RR, V-ATPase and canonical Wnt signaling pathway

In 2010, the group of C. Niehrs carried out a genome-wide small inhibitory RNA screen in order to identify new members of the Wnt/β-catenin signaling pathway (Cruciat et al. 2010). Wnts are a superfamily of secreted glycoproteins which signal through various receptors and co-receptors. The so-called canonical Wnt signaling involves β-catenin as a major downstream effector and is essential for embryonic development and cellular growth. Impaired Wnt signaling is associated with various human diseases including carcinogenesis (Clevers et al. 2012). The initiation of the Wnt/β-catenin signaling requires the formation of a tertiary complex composed of a soluble Wnt ligand, the receptor Frizzled (Fz) and low-density lipoprotein receptor-related protein 6 (LRP6) as a co-receptor. This leads to the stabilization of β-catenin, which translocates into the nucleus and induces transcription of downstream genes (Niehrs, 2012). An important step in this cascade is the aggregation of LRP6 and the formation of a signalosome at the plasma membrane (Bilic et al. 2007). Following LRP6 phosphorylation, the complex is internalized in vesicles and subsequent endocytosis is essential to transduce the signal (Niehrs, 2012, Blitzer et al. 2006, Yamamoto et al. 2006).

From their screen, Cruciat et al. revealed that (P)RR is important to initiate the canonical Wnt signaling pathway (Cruciat et al. 2010). Absence of (P)RR resulted in abnormal frog embryos with small heads, shortened tails and hypopigmentation as described in (P)RR mutant zebrafish embryos (Amsterdam et al. 2004, Nuckels et al. 2009, http://zfin.org). In addition, a loss of anterior-posterior neural patterning was also observed. They showed that (P)RR was required for V-ATPase-mediated signalosome acidification and subsequent LRP6 phosphorylation (Cruciat et al. 2010). Indeed, decreased acidification following inhibition of V-ATPase with antisense RNA and pharmacological treatment, impaired LRP6 phosphorylation and Wnt signaling in two different cell lines, and mimicked results obtained after deletion of (P)RR. At the molecular level, (P)RR was described to provide a bridge between the Wnt receptor complex and the V-ATPase (Fig. 5). Interestingly, the extracellular domain of the (P)RR was sufficient to bind Fz8 and LRP6 but the transmembrane domain was necessary to transduce the signal. On the contrary, both domains were required to bind (directly or indirectly) ATP6V0C and ATP6V0D1. Thus, the cytoplasmic part of (P)RR which is important for signal transduction after (pro)renin binding does not seem to play a role here. Also, it is important to stress that prorenin is absent at early stages of development and addition of renin did not influence the Wnt reporter assay. Altogether, this study was the first to provide an explanation for the essential role of (P)RR for normal embryonic development, independently of its ability to bind (pro)renin.

1.2.3.3 *Drosophila*: (P)RR, V-ATPase, non-canonical Wnt signaling pathway and endolysosomal sorting

In addition to the canonical Wnt signaling described above, two additional noncanonical pathways are also existing and known as Wnt/Ca2+ and the planar cell polarity (PCP) pathways. The latter involves Fz receptors and the downstream activation of small GTPases inducing expression of their target genes and changes in cytoskeleton dynamics (Niehrs 2012). The PCP is a highly conserved pathway essential to orientate and polarize cells in the plane of a tissue. In *Drosophila*, PCP is important for the orientation of hairs and bristles of the wing among other structures. Two independent genome-wide RNA interference (RNAi) screens in *Drosophila* revealed an important role of the gene *CG8444* in the canonical Wnt signaling (Bartscherer et al. 2006) and the PCP pathway (Mummery-Widmer et al. 2009). This gene codes for a transmembrane protein which was originally named VhaM8-9 due to its sequence homology to ATP6ap2 but whose function was not fully characterized (Allan et al. 2005). In two novel studies, the gene was renamed to refer to its homology to (P)RR. Buechling et al. used dPRR (*Drosophila* homolog of prorenin receptor) whereas Hermle et al. used VhaPRR (vacuolar-type H^+-ATPase prorenin receptor) (Buechling et al. 2010, Hermle et al. 2010). These two studies in *Drosophila* concordantly described a role of (P)RR in the PCP pathway. (P)RR interference with antisense RNAs against (P)RR resulted in severe PCP defects, characterized by abnormal anterior-posterior orientation and hair mispolarization. Interestingly, the phenotype could be rescued by injection of the full-length human (P)RR mRNA but not with a N-terminally truncated form (Buechling et al. 2010, Hermle et al. 2010). This suggested an essential role of the extracellular domain to transduce the noncanonical Wnt signaling, in a fashion similar to what has been

described for the canonical signaling (Cruciat et al. 2010). In addition, (P)RR was shown to interact with Fz, and the lack of (P)RR impaired targeting of Fz to the plasma membrane, thus disrupting its asymmetric localization necessary for normal pupal wings (Buechling et al. 2010, Hermle et al. 2010). In contrast, components of the canonical signaling (Fz2 receptor and coreceptor arrow) displayed a normal localization (Hermle et al. 2010). Thus, it was suggested that (P)RR, through potential regulation of V-ATPase, was important for PCP initiation by trafficking specifically Fz to the plasma membrane (Fig. 5). To study this functional association, RNAi against 12 V-ATPase subunits were tested. Surprisingly, only the deletion of the subunit B (*Vha55*) mimicked the severe defects observed after (P)RR ablation (Hermle et al. 2010). Thus, the exact mechanism remains obscure and requires further analysis. The absence of a renin/prorenin system in *Drosophila* suggests that this mechanism does not involve the ability of (P)RR to bind (pro)renin.

In an effort to better understand the role of (P)RR within the PCP pathway, the group of M. Simons generated mutant flies with clonal deletion of (P)RR in the pupal wing (Hermle et al. 2013). In epithelial cells, an important feature of the PCP signaling is the formation of asymmetric PCP domains at apical junctions. To date, six proteins including Fz and Flamingo (Fmi) were described to form these structures and are termed PCP core proteins. This study showed that clonal elimination of (P)RR led to strong PCP defects consistent with the previous reports (Buechling et al. 2010, Hermle et al. 2010) but it also provided new molecular mechanisms for (P)RR. Indeed, (P)RR was shown to co-localize with PCP core proteins during all stages of pupal wing development (Hermle et al. 2013). Absence of (P)RR reduced the presence of PCP proteins such as Fz and Fmi at apical junctions of cells. Instead, these proteins were seen to localize in vesicular compartments. Previously described to bind Fz, the extracellular domain of (P)RR interacted also with Fmi in this model and thus, was important for normal targeting of both proteins. Interestingly, the cleavage site and hence the soluble (P)RR were not required for normal PCP signaling as rescue of mutant flies with a construct expressing a non-cleavable (P)RR restored all aspects of the phenotype. A reciprocal association was also revealed with an essential role of Fmi to recruit (P)RR to the PCP domain and for subsequent apical trafficking. Altogether, these results suggested that (P)RR possessed all the characteristics of a PCP core protein and may be considered as such. It is important to note that genetic manipulation of some V-ATPase subunits did not impair significantly the PCP, illustrating that the V-ATPase seemed to have no direct role in this pathway. Because deletion of the subunit B was previously associated with PCP defects (Hermle et al. 2010), it is possible that a specific V-ATPase subpool is required in PCP. Further experiments are necessary to test this hypothesis and to examine the exact contribution of the V-ATPase in PCP.

One substantial difference with mutants for PCP core proteins was that lack of (P)RR significantly affected cell viability. It suggested that (P)RR might have additional functions due to its association with the V-ATPase (Hermle et al. 2013). Using elegant experiments based on endocytosis quantification and pH monitoring, they showed that (P)RR regulated acidification of specific apical vesicles but did not interfere with other vesicle populations. Defective apical vesicles led to a mistrafficking of the transmembrane protein E-Cadherin which could not transit through the endolysosomal pathway and undergo lysosomal degradation. Instead, after normal

endocytosis, E-Cadherin was recycling back to the apical membrane. Thus, it appeared that (P)RR had a specific role for recycling apical vesicles in epithelial cells. This role is shared with the V-ATPase as mutants for various subunits of the pump have the same defective apical vesicles. An interesting finding was also that (P)RR was not required for all V-ATPase-mediated proton transport as the acidification of certain compartments was not impaired in (P)RR mutants. In contrast, V-ATPase was required for acidification of all vesicles as mutant flies for Vha6-2 (ATP6V1A) showed impaired endocytosis and subsequent acidification at the apical and basal areas.

Altogether, this study revealed that (P)RR and V-ATPase have overlapping roles in the endolysosomal pathway but seem to exhibit distinct functions in the PCP pathway and for the acidification of certain vesicles.

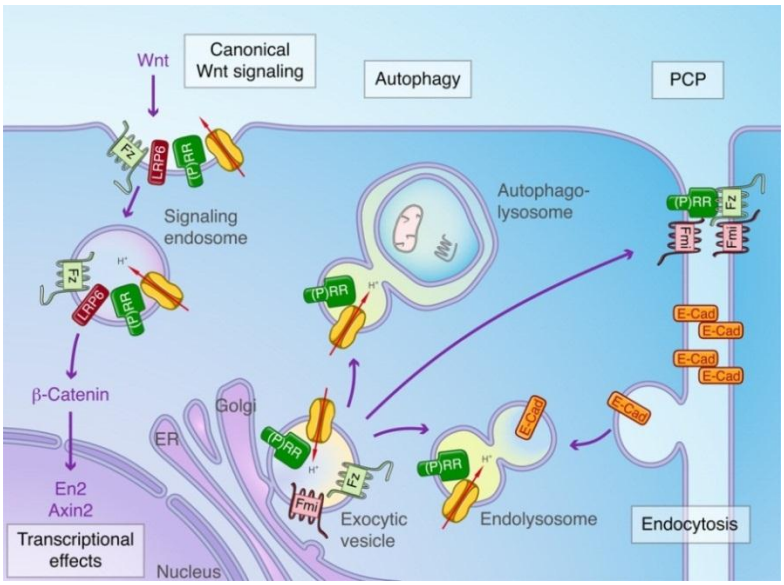

Fig. 5: Functions of (P)RR with the V-ATPase.
In *Xenopus*, (P)RR was shown to be important for canonical Wnt signling. In mice, a role of (P)RR in the regulation of autophagy was described. In *Drosophila*, (P)RR was essential for PCP core proteins trafficking and for endocytosis/recycling of apical proteins. For references see text. (Picture from Rousselle et al. 2014). E-Cad, E-Cadherin; ER, endoplasmic reticulum; Fmi, Flamingo; Fz, Frizzled; LRP6, low-density lipoprotein receptor-related protein 6; PCP, planar cell polarity; (P)RR, (pro)renin receptor; V-ATPase, vacuolar H+ ATPase.

1.2.3.4 Mouse: (P)RR, V-ATPase, autophagy and trafficking

Our early attempts to generate a (P)RR deficient mouse were unsuccessful as no chimera were obtained after re-implantation of blastocysts containing (P)RR deficient embryonic stem cells into foster mothers (Sihn et al. 2010). This suggested that the complete deletion of (P)RR was lethal. Although embryonic lethality could not be ascertained, this was reminiscent of the early death observed in mutant zebrafish. Nevertheless, such early lethality in the mouse would rule out a function of the (P)RR solely as a component of the RAS. Indeed, mice deficient for various RAS components (renin, angiotensinogen…) develop normally (Bader et al. 2001). Thus, it was suggested that this essential role of (P)RR should involve an additional function independently of the RAS.

To circumvent this early death, conditional deletions of (P)RR in mice using the Cre/Lox system were developed. The first tissue-specific deletion of (P)RR in mouse confirmed the potential

influence of (P)RR on V-ATPase function in particular in the process of autophagy. Autophagy is a general term for an essential cellular process allowing the cell to degrade organelles and cytosolic proteins. Autophagy plays important physiological roles for adaptation to starvation, development, elimination of pathogens and cell death. This non-specific process is initiated with the engulfment of a portion of cytoplasm within a specific organelle called autophagosome (Mizushima et al. 2007, Levine et al. 2011). These engulfed components are degraded when this structure further fuses with lysosomes containing pH-dependent hydrolases. The V-ATPase plays a fundamental role in this process by generating the acidic pH necessary for hydrolase activity.

Mice with a specific deletion of (P)RR in cardiomyocytes developed abnormal heart parameters resulting in heart failure and died within 3 weeks after birth (Kinouchi et al. 2010). Histologic observations revealed large fibrotic areas and degenerating cardiomyocytes exhibiting perinuclear accumulation of autophagic vacuoles (Fig. 5). Similar observations were obtained for mice with a conditional deletion of (P)RR in podocytes which developed nephrotic syndrome and fulminant kidney failure leading to death within 2-4 weeks after birth (Oshima et al. 2011, Riediger et al. 2011). Podocyte death was also associated with an accumulation of undigested proteins in autophagic vacuoles and enhanced ER stress. In addition, these cells exhibited features of a more global dysfunction with altered cytoskeleton, loss of differentiation markers and evidence of necrosis. Finally, mice with a specific deletion of (P)RR in vascular smooth muscle cells suffered from collapsed lungs and died within 12-18 weeks after birth (Kurauchi-Mito et al. 2014). Observation of abdominal aortic smooth muscle cells revealed the accumulation of enlarged autophagic vacuoles. These results on autophagy were mimicked *in vitro* in embryonic fibroblasts (Kinouchi et al. 2010), podocytes (Oshima et al. 2011, Riediger et al. 2011) and smooth muscle cells (Kurauchi-Mito et al. 2014) after treatment with Bafilomycin or transfection of Cre adenovirus to delete the floxed *(P)RR/ATP6ap2* allele. In addition, (P)RR ablation in these cells in culture induced a downregulation of several subunits of the V0 sector of the V-ATPase and impaired acidification (Kinouchi et al. 2010, Oshima et al. 2011, Kurauchi-Mito et al. 2014). Such impairment in autophagy is reminiscent of the phenotype observed in yeast lacking a single V0 subunit or proteins involved in the V-ATPase assembly (Hirata et al. 1993, Graham et al. 2000). It is important to note that it can not be excluded that the blockade of autophagy observed *in vivo* might be the long term consequence of other (P)RR-dependent functions. That such defects were observed *in vitro* 24-48h after Bafilomycin treatment but only 6-8 days after Cre transfection (despite fast (P)RR knock down) supports this hypothesis.

A recent study in mice confirmed an important role of (P)RR in cell polarity as it was initially described in *drosophila* but extended this role to the process of retinal lamination during retinal development (Kanda et al. 2013). The mammalian retina is a highly organized laminar tissue serving as an interface between the visual information and its processing and interpretation in the brain (Masland et al. 2001, Swaroop et al. 2010). The partitioning defective 3 homolog (Par3)-Par6-atypical protein kinase C (aPKC) λ complex (also known as Par-aPKC system) is an essential regulator of cell polarity in various cell types (Suzuki et al. 2006). In photoreceptors, this complex interacts with cadherins at adherens junctions to establish and maintain cell shape and tissue integrity. As a consequence, deletion of these various proteins in animals has been

associated with the disruption of the retinal architecture (Horne-Badovinac et al. 2001, Wei et al. 2002, Malicki et al. 2003, Masai et al. 2003, Wei et al. 2004, Koike et al. 2005). Specific deletion of (P)RR in photoreceptors did not affect retinal cell fate determination but led to severe dysfunction of photoreceptors and the loss of proper laminar organization (Kanda et al. 2013). Within cells, (P)RR was described to colocalize and directly interact with Par3 in the ER/Golgi network and to be further targeted to the apical surface through endocytic trafficking. Accordingly, deletion of (P)RR did not alter Par3 protein expression but impaired its apical localization. Co-immunoprecipitation and yeast two-hybrid analysis revealed that the N-terminal domain (with (pro)renin binding properties) was sufficient to bind Par3 but also that the transmembrane domain was required for proper intracellular localization. A role of (P)RR as a receptor for (pro)renin is unlikely to be involved in this mechanism. In addition, the presence of normal retinal lamination in zebrafish mutants for different V-ATPase subunits suggested that the retinal laminated structure was not dependent of a modulation of V-ATPase activity. Thus, like in the *drosophila*, (P)RR appeared to be important for the trafficking of some vesicles without affecting V-ATPase functions.

Altogether, these studies in the mouse have suggested that the lack of (P)RR may impact the V-ATPase assembly, stability or expression, and substantiated a role of (P)RR in trafficking independently of the V-ATPase. However, these exact mechanisms are still unknown and further investigations are necessary.

1.2.3.5 Human: (P)RR, V-ATPase and mental disorders

Various polymorphisms in the (P)RR gene have been associated with increased cardiovascular risks in humans. The description and the relevance of these polymorphisms have been described in a previous section (1.1.5). The first clinical reports suggesting an interaction between (P)RR and V-ATPases has been provided by Ramser et al. in 2005. This study identified a unique exonic splice enhancer mutation (c.321C>T) resulting in the deletion of the exon 4 (Δe4 isoform) and in a 50% reduction in the amount of the functional protein (Ramser et al. 2005). This mutation did not lead to cardiovascular abnormalities but resulted in X-linked mental retardation (XLMR) and epilepsy (Fig. 1). Interestingly, the authors still linked this phenotype to the RAS: indeed, experiments conducted on the lymphocytes of a patient bearing the mutation, showed that the Δe4 isoform was unable to activate ERK1/2 in the presence of renin. This result suggested that the function as a receptor for renin might be involved in neuron physiology (Ramser et al. 2005). At that time, (P)RR was solely described as a receptor for (pro)renin and other potential functions were not expected. With the new functions attributed to (P)RR over the last few years, the scientific community has assumed that a modulation of V-ATPases activity was most likely responsible for the pathology.

A recent study found the same mutation in a patient with another X-linked mental disease (Korvatska et al. 2013). In addition, they described a new mutation c.345C>T associated with X-linked Parkinsonism with spasticity (XPDS). This mutation also resulted in exon 4 skipping and overexpression of the minor splice Δe4 isoform. In human embryonic kidney (HEK293) cells transfected with siRNA, (P)RR ablation impaired autophagy and lysosomal clearance as

observed in XPDS brain sections. Of note, the most drastic effects were found in the striatum, a region involved in Parkinson's disease, and associated with an accumulation of Tau protein (Poorkaj et al. 2010). Interestingly, transfection of the Δe4 isoform into (P)RR-depleted HEK293 cells did not significantly influence the canonical Wnt signaling pathway as assessed by luciferase reporter assay (Korvatska et al. 2013). This study confirmed that (P)RR mutations are associated with various mental diseases but the described mechanism differed from the initial study (Ramser et al. 2005). Even though (pro)renin binding activity of (P)RR was not excluded, the defective autophagy strongly argued for a role of (P)RR as regulator of V-ATPase activity. This conclusion was in line with the work of Contrepas et al. which showed that the truncated (P)RR/ATP6ap2 acted as a dominant negative mutant in transfected neuronal cells by affecting the trafficking of the endogenous receptor (Contrepas et al. 2009). Because only one copy of (P)RR/ATP6ap2 is present per synaptic vesicle (Takamori et al. 2006), it was suggested that intact (P)RR may be important for vesicle trafficking and/or recycling and more globally for neurotransmission. In light of the recent findings, we can assume that this impaired neurotransmission might be a consequence of abnormal cell homeostasis due to impaired autophagy and vesicular acidification.

The association between (P)RR polymorphisms and X-linked intellectual disability has recently been challenged. Indeed, large-scale human exome sequencing from 10,563 X chromosomes has revealed that the mutation (c.321C>T) initially associated with XLMR and later with XPDS is also present in healthy individuals (Piton et al. 2013). This study suggested that one or several other gene(s) were most likely responsible for these pathologies and that the association between (P)RR polymorphisms and these intellectual disabilities needs to be reassessed. The other mutation c.345C>T was not analyzed in this report and therefore no conclusion can be drawn on it.

1.2.4 Conclusion

From its initial description as a receptor for (pro)renin in 2002, the understanding of (P)RR has markedly evolved (Fig. 6). There is now strong evidence from genetic studies that (P)RR is essential for V-ATPase activity and that both proteins are important for canonical Wnt and perhaps PCP signaling, autophagy, endolysosomal sorting and endocytosis/recycling (Fig. 5). The exact mechanism how (P)RR regulates the V-ATPase is still obscure and requires new animal models and experiments. Finally, it is important to note that (P)RR might regulate some vesicle trafficking independently of the V-ATPase. This aspect is also not well understood so far.

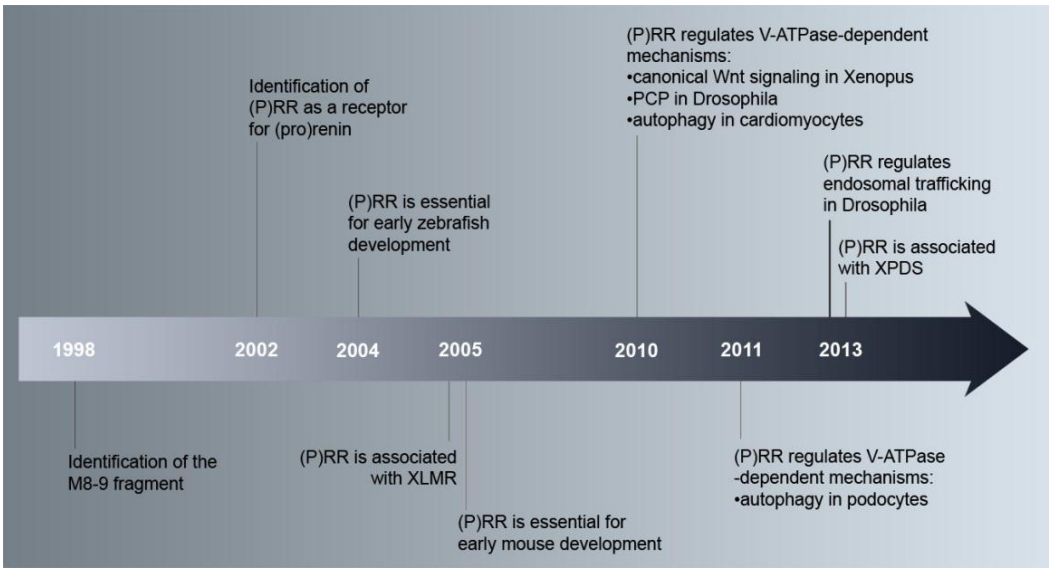

Fig. 6: Timeline of (P)RR characterization. The timeline summarizes the different studies describing an association between (P)RR and V-ATPase (Rousselle et al. 2014). For references see text. PCP, planar cell polarity; (P)RR, (pro)renin receptor; XLMR, X-linked associated mental retardation; XPDS, X-linked Parkinsonism with spasticity.

1.3 Osteoclasts: specialized cells for bone resorption with plasma membrane V-ATPases

The skeleton is a dynamic tissue which undergoes a lifelong remodeling process through the coordinated action of bone-degrading cells (osteoclasts) and bone-forming cells (osteoblasts). Osteoclasts are multinucleated cells resulting of the fusion of several hematopoietic monocytes/macrophage precursors. Their main function is to resorb mineralized bone matrix. It is well established that osteoclasts play essential roles not only in bone homeostasis but also in various skeletal pathologies. For instance, osteoclasts are the primary therapeutic targets to treat osteoporosis (bone loss). A particular feature of mature osteoclasts is the presence of V-ATPases at the plasma membrane facing bone surface. This location allows V-ATPases to pump protons into the extracellular resorptive area, generating an acidic pH crucial for matrix degradation and bone resorption. (P)RR has been described to be upregulated during osteoclast differentiation (Nomiyama et al. 2005), but the exact role of (P)RR in osteoclasts is still unknown. Also, the association between (P)RR and V-ATPases has been mainly described to be important for the acidification of intracellular organelles (Rousselle et al. 2014). Therefore, it is interesting to examine the role of (P)RR in osteoclasts, a cellular model with plasma membrane V-ATPases important to acidify the extracellular environment.

1.3.1 Bone architecture and dynamics

1.3.1.1 Bone structures and functions

Bones are assembled into a highly specialized rigid framework known as the skeleton. It is a dynamic structure characterized by its rigidity and ability to regenerate after a trauma. From an anatomical point of view, two different kinds of bone exist: flat bones such as skull and scapula and long bones such as femur and tibia. According to its shape and location, each bone can fulfill one or several functions including protection of organs, maintenance of mineral homeostasis, support for locomotion and generation of an optimal environment for hematopoietic stem cell niches in the medullary cavity (Taichman et al. 2005). Adult bones contain two types of tissue: cortical bone (compact bone) and trabecular bone (cancellous or spongy bone). Cortical bone is a compact, dense tissue surrounding the marrow compartment and represents 80% of the total bone mass. Trabecular bone is composed of trabecular plates and rods organized in a honeycomb-like structure within the marrow space and represents 20% of the total bone mass (Fig. 7). The bone matrix is constituted by organic structural proteins of which collagen 1 is the main component (90%). Crystalline complexes of calcium carbonate and phosphate (also known as hydroxyapatite crystals) constitute the inorganic components of the matrix and are responsible for the rigidity of the bone.

1.3.1.2 Bone development

Bone formation or ossification is the generation of new bone tissues by osteoblasts and occurs through two distinct modes. Intramembranous ossification takes place in flat bones and involves direct differentiation of mesenchymal cells into osteoblasts. In contrast, endochondral ossification in flat bones is characterized by the replacement of a cartilage template by bone tissue (Mackie et al. 2011). Briefly, chondrocytes from the growth plate undergo a progression in their activity (proliferation, secretion, hypertrophy and apoptosis) leading to the generation of cartilage templates and the invasion of blood vessels (Kronenberg et al. 2003). Mature osteoclasts degrade the cartilage matrix and generate cartilage remnants. Osteoclast activity is also crucial to create cavities important for blood vessels and cell invasion. Defect in osteoclast activity leads to abnormal growth plate size. Through cavities, differentiated osteoblasts migrate and secrete bone matrix around cartilage remnants to give rise to the so-called bone trabeculae (trabecular bone) (Fig. 7). Hydroxyapatite crystals are further incorporated and mineralize the bone tissue. This process is active from fetal development until early adulthood and is responsible of the longitudinal growth of bones.

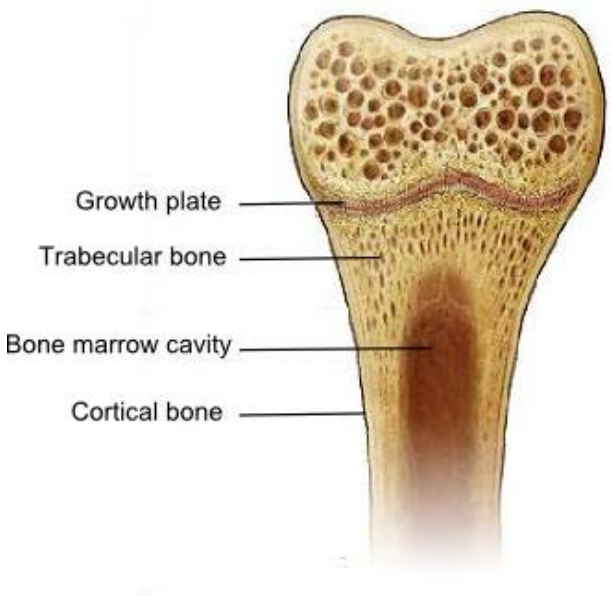

Fig. 7: Schematic view of a long bone.
The scheme represents a longitudinal section of a long bone and highlights in a simplified way the main bone structures.
(Modified from the original picture appearing on www.vanderbilthealth.com website.)

1.3.1.3 Bone remodeling

Although it appears static, the adult skeleton is in a permanent dynamic state. Bone tissues are constantly renewed through a process termed bone remodeling in response to stimuli such as mechanical stress and hormones. This lifelong process is characterized by cycles coupling the destruction of old bone by osteoclasts (resorption) and the generation of new bone by osteoblasts (bone formation). It is estimated that 10 % of our bone tissues are replaced every year through remodeling. Bone remodeling is important to maintain the structural integrity of

bones by replacing old “fatigued” bone and for mineral homeostasis through the release and storage of calcium and phosphates (Heaney et al. 2005).
Bone remodeling is achieved by the concerted action of osteoclasts and osteoblasts and occurs at discrete sites within bones termed Basic Multicellular Units (BMU) (Parfitt 2002). The remodeling process consists of four successive steps: activation, resorption, reversal and formation. Activation corresponds to a modification of the bone surface make it prone to remodeling and the recruitment of monocytes/macrophages from the blood stream. These mononuclear cells further fuse together to form multinucleated osteoclasts. Resorption is performed by fully differentiated osteoclasts which provide an acidic environment essential for pH-dependent enzymes and the subsequent bone dissolution resulting in resorption pits. Following osteoclast apoptosis, the reversal phase is characterized by signals which attract osteoblast precursors (stromal cells) in these cavities. Bone formation is performed by mature osteoblasts which synthetize and secrete an organic matrix (osteoid) and regulate its mineralization. Subsequently, osteoblasts mostly undergo apoptosis but some of them either become bone lining cells or are embedded in osteoid and become osteocytes (Kogianni et al. 2007). Osteocytes are characterized by numerous cellular extensions which create a network within bone tissues and allow them to communicate with each other. They act as strain and stress sensors and regulate bone turnover in response to mechanical stimuli through the secretion of sclerostin (Kogianni et al. 2007, Robling et al. 2008). Therefore, they are essential cells to maintain the bone structure. Recently, osteocytes have also been described to be essential for osteoclasts differentiation (Nakashima et al. 2011, Xiong et al. 2011).
A tight balance between bone resorption and formation is crucial for bone homeostasis and is under the control of a multitude of signal. Dysregulation of this balance due to an abnormal osteoclast activity is associated with several bone pathologies. For instance, increased bone resorption leads to osteoporosis (low bone mass) whereas decreased bone resorption is associated with osteopetrosis (high bone mass). Therefore, osteoclasts are an interesting clinical target to treat these bone diseases.

1.3.2 Osteoclast physiology and importance of plasma membrane V-ATPases

1.3.2.1 Osteoclast progenitors

Pioneer experiments revealed that some blood cells can be recruited in the bone tissue and have the ability to form osteoclasts (Fischman et al. 1962, Jee et al. 1963). Further experiments with osteopetrotic mice confirmed this observation. This high bone mass phenotype could be rescued by transplantation of bone marrow or spleen cells from healthy mice and parabiotic union with normal mice suggesting the presence of osteoclast progenitors in various hematopoietic tissues (Walker et al. 1972, 1973 and 1975). The use of labeled phagocytes provided direct evidence that circulating mononuclear monocytes migrate to the bone and give rise to osteoclasts (Tinkler et al. 1981). Within the bone marrow, hematopoietic stem cells (HSCs) are self-renewing pluripotent progenitors which give rise to all blood cell types including those of the myeloid lineage. The transcription factor PU.1 is essential to direct HSCs to the myeloid lineage. Deletion

of PU.1 in mice not only impaired normal hematopoiesis but also led to severe osteopetrosis due to an absence of osteoclasts (Scott et al. 1994, Tondravi et al. 1997). Therefore, it is now widely accepted that osteoclasts are of hematopoietic origin and derive from myeloid progenitors. It has also been demonstrated *in vitro* that monocytes and macrophages from various tissues can give rise to osteoclasts when cultured in a suitable environment (Bar-Shavit et al. 1983, Udagawa et al. 1990). Thus, researchers have postulated that all cells from the monocyte/macrophage lineage *in vivo* would give rise to osteoclasts in the bone marrow. Several studies have challenged this idea over the last few years and it is now suggested that some subsets of myeloid cells have a better ability to differentiate to osteoclasts (Li et al. 2004, Yao et al. 2006, Jacquin et al. 2006, Muto et al. 2011, Charles et al. 2012, Jacome-Galarza et al. 2013). Despite a better description of osteoclast progenitors, the exact role and involvement of each subset in osteoclastogenesis *in vivo* certainly requires further investigations. However, a common feature of these osteoclast progenitors is that they must reside or migrate into the bone marrow as multinucleated osteoclasts are absent of the blood circulation (Lerner et al. 2000).

1.3.2.2 Osteoclast differentiation: M-CSF and RANKL as stimulators

A major breakthrough in the comprehension of osteoclastogenesis occurred with the development of an *in vitro* system based on co-culture of murine bone marrow or spleen cells and osteoblasts/stromal cells. This system was sufficient to obtain mature osteoclasts suggesting that stromal cells were necessary and sufficient for osteoclastogenesis (Takahashi et al. 1988, Udagawa et al. 1990). Further experiments revealed that osteoblasts/stromal cells produce two essential factors for this process: macrophage colony-stimulating factor (M-CSF) and receptor activator of NF-κB ligand (RANKL) (Arai et al.1999, Suda et al. 1999) (Fig. 8). Both factors initiate a multitude of signaling pathways leading to the regulation of genes important for osteoclast differentiation and function (Boyle et al. 2003, Teitelbaum et al. 2003).

Briefly, M-CSF (also known as colony-stimulating factor 1 or C-SF1) is a homodimeric glycoprotein constitutively expressed *in vivo* by a multitude of cells including osteoblasts and stromal cells. The crucial role of M-CSF in osteoclastogenesis emerged from osteopetrotic (*op/op*) mice which harbor a null mutation in the *M-CSF* gene and hence do not possess functional M-CSF proteins (Wiktor-Jedrzejczak et al. 1990, Yoshida et al. 1990). These animals are characterized by the lack of osteoclasts and the development of severe osteopetrosis which can be rescued by the administration of soluble M-CSF (Kodama et al. 1991, Wiktor-Jedrzejczak et al. 1990). The binding of M-CSF to its receptor c-fms (also termed CSF-1R or M-CSFR) present on osteoclast precursors has several physiological consequences. First, it triggers a regulatory loop which increases c-fms expression. This positive loop involves the transcription factor PU.1 which is essential for the maturation of myeloid cells (Scott et al. 1994, Tondravi et al. 1997). Accordingly, mice deficient in PU.1 or c-fms lack osteoclasts and exhibit severe osteopetrosis similar to *op/op* mice (Tondravi et al. 1997, Dai et al. 2002). Second, M-CSF/c-fms interaction activates downstream pathways important for the proliferation and survival of osteoclast precursors (Ross 2006). Finally, M-CSF induces the expression of receptor activator of NF-κB (RANK) in these maturating precursors, which make them responsive to its ligand RANKL (Arai

et al. 1999). RANKL and RANK belong to the tumor necrosis factor (TNF) and TNF receptor superfamilies respectively (Teitelbaum 2000). RANKL was long thought to be exclusively expressed by osteoblasts. Recent studies have also highlighted that osteocytes are a potential source of RANKL *in vivo* (Nakashima et al. 2011, Xiong et al. 2011). The absence of osteoclastogenesis and the subsequent development of severe osteopetrosis in RANK and RANKL knock-out mice put in light the importance of the RANK/RANKL interaction for this process (Lacey et al. 1998, Yasuda et al. 1998, Li et al. 2000). This interaction is regulated *in vivo* by osteoprotegerin (OPG), a soluble decoy receptor secreted by osteoblasts which competes with RANK for RANKL binding and inhibits osteoclastogenesis (Lacey et al. 1998). Accordingly, OPG-deficient mice have accelerated osteoclastogenesis and develop osteoporosis (Simonet et al. 1997, Bucay et al. 1998). It is now well known that the balance between RANKL and OPG expression directly influences osteoclastogenesis and determines the amount of bone resorbed.
Binding of RANKL to RANK activates numerous intracellular signaling pathways including TNF receptor-associated factor 6 (TRAF6), nuclear factor κB (NF-κB), c-Fos, nuclear factor of activated T-cells cytoplasmic 1 (NFATc1), microphtalmia-associated transcription factor (MITF) and c-src, which are required for the regulation of genes involved in osteoclast differentiation and functions (Teitelbaum 2000, Boyle et al. 2003).

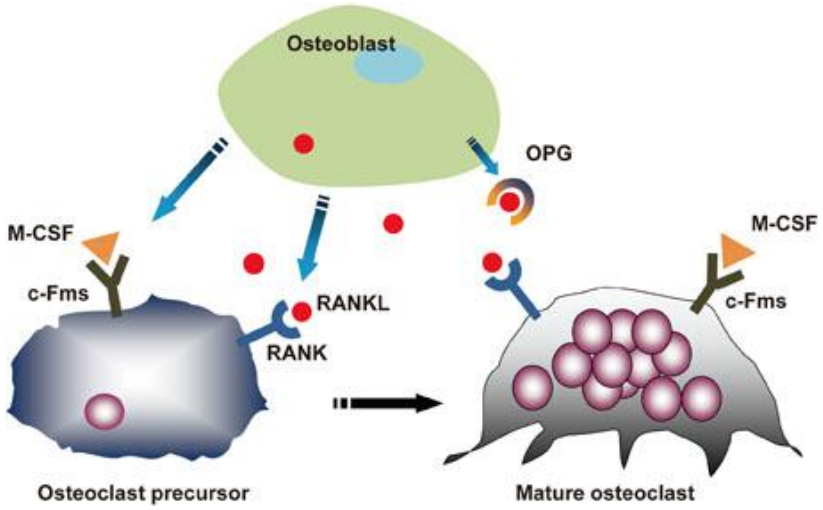

Fig. 8: Molecular control of osteoclast differentiation. Osteoblasts secrete M-CSF and RANKL, two important factors which act on their respective receptors c-fms and RANK present on osteoclast precursors and promote osteoclasts differentiation. Osteoblasts also produce OPG, a soluble decoy receptor which binds RANKL and inhibits osteoclastogenesis (Picture from Lee 2010). For abbreviations, see text.

1.3.2.3 Osteoclast fusion and polarization

Following differentiation, committed pre-osteoclasts then start to fuse to become multinucleated osteoclasts. NFAT1c has been described to upregulate the expression of two key proteins involved in this process: dendritic cell-specific transmembrane protein (DC-STAMP) and subunit

d2 of the V-ATPase V0 domain (ATP6V0d2) (Kim et al. 2008, Feng et al. 2009). Mice lacking either DC-STAMP or ATP6V0d2 do not form multinucleated osteoclasts and develop osteopetrosis (Kukita et al. 2004, Yagi et al. 2005, Lee et al. 2006). In addition, *in vitro* data have suggested that the V-ATPase subunit ATP6V0c and accessory subunit Ac45 (ATP6ap1) might be important for the fusion of pre-osteoclasts (Laitala-Leinonen et al. 1999, Yang et al. 2012). Chemical inhibition of V-ATPases with Bafilomycin also affects the fusion of pre-osteoclasts (Laitala-Leinonen et al. 1999). Therefore, a potential role of membrane V-ATPases in the process of fusion as previously described in neurons (Peri et al. 2008) is also suggested to be involved during osteoclastogenesis. As pre-osteoclasts fuse, sustained RANKL signaling induces the expression of several proteins such as tartrate-resistant acid phosphatase (TRAP), Cathepsin K (CtsK), chloride channel 7 (CLCN7) and osteoclast-specific V-ATPase subunit a3 (also termed ATP6V0a3, ATP6i, OC-116kD or TCIRG1) (Boyle et al. 2003), which will be crucial for bone resorption.

To become fully active, multinucleated osteoclasts undergo a morphological change through cytoskeletal rearrangement and cellular polarization, leading to the formation of a sealing zone. The sealing zone is formed by the intracellular polarization of F-actin fibers to form a cytoskeletal structure named “actin ring” (Vaananen et al. 1995). Malformation of the actin ring structure is associated with impaired resorption. Some studies have reported that V-ATPase subunits such as ATP6V0a3, ATP6V0d2, and ATP6V1C1 are involved in the formation of actin ring (Taranta et al. 2003, Lee et al. 2006, Feng et al. 2009). Because these subunits were described to be specifically associated to V-ATPases targeted to the plasma membrane in osteoclasts, these results suggest that they might have an additional role as a regulator of the actin cytoskeleton. Upon attachment to the bone surface, the sealing zone binds tightly to the matrix and creates a closed environment between the osteoclast and the bone surface called resorption lacunae (Fig. 9). This binding is mediated by $\alpha_v\beta_3$ integrins which are adhesion receptors expressed by osteoclasts during their differentiation. $\alpha_v\beta_3$ integrins are essential for osteoclast function since mice deficient in β_3 subunit develop dysfunctional albeit differentiated osteoclasts and develop osteopetrosis (McHugh et al. 2000).

The final step of maturation is the fusion of V-ATPases-containing lysosomal vesicles with the plasma membrane bound by the sealing zone to create a folded membrane structure termed ruffled membrane (Fig. 9). In addition to the sealing zone and the ruffled border, mature osteoclasts are highly polarized and contain two additional specialized domains with a functional significance yet to be determined: a functional secretory domain and a basolateral domain. The development of these four particular domains results in fully mature osteoclasts able to resorb bone (Fig. 9).

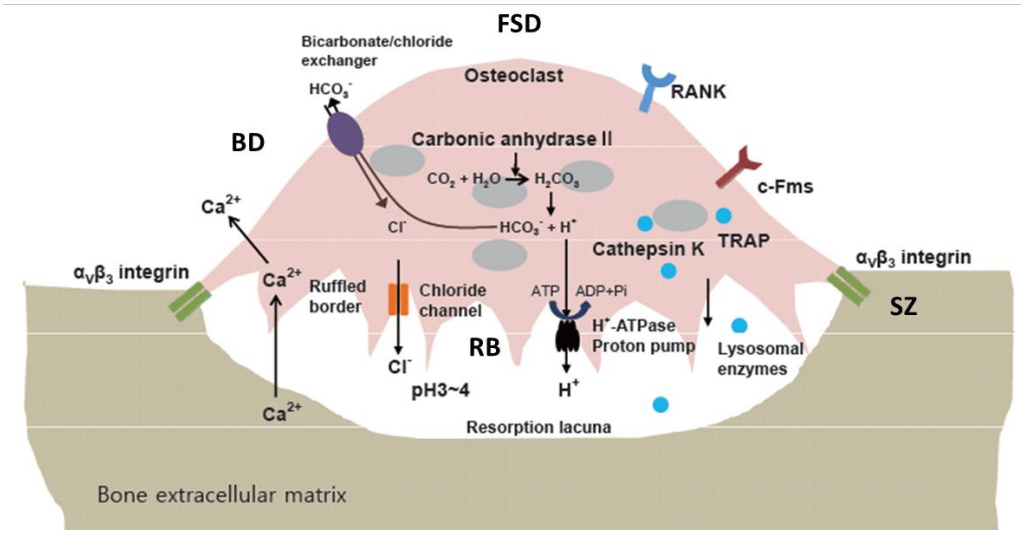

Fig. 9: Osteoclast morphology and bone resorption. Mature osteoclasts are polarized cells with 4 functional domains: a ruffled border (RB), sealing zone (SZ), a basolateral domain (BD) and a functional secretory domain (FSD). Located at the ruffled border, V-ATPases extrude protons into the resorption lacuna and create an acidic environment essential for bone resorption and mediated by enzymes such as Cathepsin K and TRAP. For further details, see text (Picture modified from Lee 2010).

1.3.2.4 Osteoclast and bone resorption

Bone resorption is exclusively taking place in the resorption lacuna and requires the presence of several ions and enzymes secreted by osteoclasts. Dissolution of the bone mineral phase is achieved through acidification of the resorption lacunae (Fig. 9). The generation of a low pH is performed by V-ATPases which are present in great number at the ruffled border and pump protons across the plasma membrane (Teitelbaum 2000). Several studies have demonstrated the importance of V-ATPases for bone resorption. Inhibition of V-ATPase activity with Bafilomycin or antisense RNA abolished *in vitro* bone resorption (Sundquist et al. 1990, Laitala et al. 1994). The ATP6V0a3 (TCIRG1) subunit is primarily expressed in osteoclasts and is important for the trafficking and function of V-ATPases at the ruffled membrane. This essential role is supported by the development of severe osteopetrosis in mice and humans harboring mutations in the *TCIRG* gene (Li et al. 1999, Scimeca et al. 2000, Frattini et al. 2000, Kornak et al. 2000, Susani et al. 2004). In addition to osteopetrosis, the severe phenotype in TCIRG1 knockout mice is characterized by the lack of tooth eruption and the development of splenomegaly (splenic enlargement and hematopoiesis) as a consequence of the bone marrow obliteration by excessive bone tissue (Li et al. 1999). At the cellular level, mutant osteoclasts fully develop and retain an ability to acidify intracellular lysosomes but are unable to secrete protons across the ruffled border and resorb bone (Li et al. 1999).

Protons pumped by V-ATPases are generated by intracellular enzymatic reactions catalyzed by carbonic anhydrase II (CAII) (Gay et al. 1974). The transport of negatively charged chloride ions through CLC-7 chloride channels is important not only to maintain electroneutrality within the cytoplasm but also to generate hydrochloric acid together with positively charged protons (Schlesinger et al. 1997). Within the resorption lacuna, hydrochloric acid creates an acidic environment which can reach pH 4.5. This low pH is important for the dissolution of

hydroxyapatite crystals characterized by the release of calcium ions, phosphate ions and water. Mice and humans lacking CLC-7 and CAII also present osteopetrosis due to abnormal osteoclast activity (Sly et al. 1983, Kornak et al. 2001, Margolis et al. 2008). After bone demineralization, the acidic environment is further essential for the degradation of type I collagen, the main organic component of the bone matrix. Osteoclasts specifically express and secrete key lysosomal pH-dependent proteases such as cathepsin K (CtsK), tartrate resistant alkaline phosphatase (TRAP) and matrix metalloproteinases (MMPs) involved in matrix resorption (Boyle et al. 2003). CtsK and TRAP deficient mice develop osteopetrosis despite normal osteoclast differentiation (Hayman et al. 1996, Saftig et al. 1998, Gowen et al. 1999; Li et al. 2006). Degradation products generated by these enzymes are endocytosed through the ruffled border, transcytosed in vesicles across the cytoplasm and finally secreted into the extracellular space at the basolateral and functional secretory domains (Nesbitt et al. 1997, Mulari et al. 2003). Certain degradation products resulting from the enzymatic cleavage of collagen I fibers such as cross-linked C-telopeptide of type I collagen (CTX-I) can reach the bloodstream and are used as markers of resorption activity (Rosen et al. 2000). The removal of degradation products from the resorption pit allows osteoclasts to degrade bone matrix several days. Once resorption is terminated, osteoclasts detach from bone surface and mainly undergo apoptosis (Teitelbaum 2000).

1.4 Macrophages: specialized cells for phagocytosis

Studies from mice with tissue specific (P)RR deletion using the Cre/Lox system have all observed a blockade in the autophagy pathway characterized by the accumulation of autophagic vacuoles within the cytoplasm due to impaired acidification and leading to cell death. These results have reinforced the concept that (P)RR is important for V-ATPase activity even though the exact mechanism is still unknown. As previously stated, this drastic phenotype might illustrate the long term consequence of (P)RR deletion, masking earlier potential roles of (P)RR. The fact that (P)RR may regulate vesicle trafficking independently of the V-ATPase as described in *Drosophila* supports this hypothesis. Indeed, it is not excluded that the defective autophagy might be the consequence of a disturbed trafficking of vesicles and/or organelles. To test this hypothesis, macrophages represent an interesting cell type as they display an intense intracellular trafficking after the engulfment of foreign bodies into phagosomes. This process known as phagocytosis leads to the destruction of the engulfed material through several maturation stages involving interactions with several organelles and a progressive acidification of the phagosome. The fusion with lysosomes is the endpoint of the process as it is during autophagy. To study a role of (P)RR in phagocytosis, macrophages can easily be studied *in vivo* in the peritoneal cavity and *in vitro* after differentiation of bone marrow cells with M-CSF. However, the deletion of (P)RR in those cells requires the generation of new transgenic animals using a technology not based on the Cre/Lox system.

The development of RNA interference technology has allowed researchers to understand the role of a large number of genes by repressing their expression not only *in vitro* but also *in vivo*. In particular, the use of expression cassette for small hairpin RNA (shRNA) whose expression is triggered by doxycycline has been successfully used to efficiently induce the knockdown of genes of interest in mice and rats. The development of transgenic rats harboring a doxycycline-inducible and reversible shRNA targeting (P)RR is of particular interest and would give the possibility to trigger (P)RR knockdown *in vivo* by treating rats with doxycycline and *in vitro* by culturing primary cell cultures in presence of doxycycline. The role of (P)RR in macrophages can thus be studied as early as the knockdown is effective in those cells.

1.4.1 Macrophages

Macrophages are leukocytes from the myeloid lineage first described by Ilya Metchnikoff in 1882 (Gordon 2008). Macrophages are derived from monocytes which are produced from the bone marrow and released into the bloodstream. Monocytes migrate into organs and under the influence of several factors differentiate into tissue macrophages (Ginhoux et al. 2014). It is also described that some subsets of resident macrophages do not originate from monocytes but are rather maintained through macrophage proliferation (Lavin et al. 2015). Both macrophage branches are highly dependent on M-CSF for their differentiation and proliferation (Davies et al. 2013). Macrophages are found in virtually all tissues in which they regulate several homeostatic functions and as a key component of the innate immune system, they act as local immune sentinels (Epelman et al. 2014, Lavine et al. 2015). Macrophages have the unique capacities to

detect the presence of a pathogen through several receptors. The engulfment and the destruction of the pathogen in a process known as phagocytosis provide a first line of defense to the organism.

1.4.2 Macrophages and phagocytosis

Macrophages are professional phagocytes with the ability to internalize and degrade large particles including microorganisms. The destruction of pathogens is an important event of the innate immune response and promotes antigen presentation to trigger the adaptive response (Mosser et al. 2008). Phagocytosis is initiated by the engulfment of organisms within a structure termed phagosome via several receptors present at the plasma membrane (Flannagan et al. 2009). Once the phagocytic cup is sealed, the phagosome undergoes maturation characterized by successive interactions with different intracellular compartments leading to acquisition of new components and progressive acidification (Fig. 10). After endocytosis, early phagosomes (pH ± 6.2) fuse with early endosomes characterized by markers such as small GTPases Rab5 and early endosome antigen 1 (EEA1) and acquire some properties of early endosomes (Kinchen et al. 2008). For instance, early phagosomes gain the ability to recycle receptors to the plasma membrane via the budding and release of Rab11-positive vesicles known as recycling endosomes (Maxfield et al. 2004). Additional budding events lead to the retrieval of cargo targeted to endosomes and the trans-Golgi network. Intermediate phagosomes represent a maturation step which likely involves interactions with multi-vesicular bodies (MVBs) for protein degradation (Flannagan et al. 2009), though it is not well understood yet.

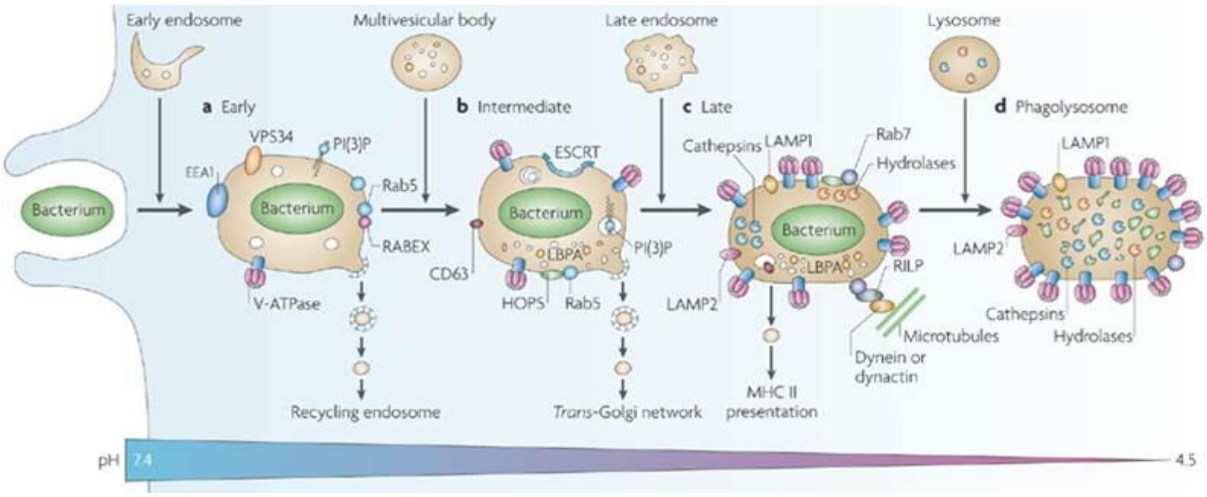

Fig. 10: Successive stages of phagosomal maturation. After pathogen internalization, the phagosome undergoes a maturation process characterized by successive interactions and/or fusions with several intracellular compartments and culminates with the formation of a structure termed phagolysosome. Through these different interactions, the phagosome modifies its composition by acquiring several markers, proteins and enzymes and by progressively decreasing its luminal pH. Phagosomes also release vesicles which are targeted to different organelles. EEA1, early endosome antigen 1; ESCRT, endosomal-sorting complex required for transport; HOPS, homotypic protein sorting; LAMP, lysosomal-associated membrane protein; LBPA, lysobisphosphatidic acid; PI(3)P, phosphatidylinositol-3-phosphate; MHCII, major histocompatibility complex II; RILP, Rab-interacting lysosomal protein; VPS, vacuolar sorting protein. (Picture from Flannagan et al. 2009).

The maturation into late phagosomes occurs with the acquisition of proteases and lysosomal-associated membrane proteins (LAMPs) imported from late endosomes and /or the Golgi apparatus (Flannagan et al. 2009). Late phagosomes also become more acidic (pH ± 5.8) due to an increased presence of V-ATPases. Like late endosomes, the late phagosomes are positive for the small GTPase Rab7 which is an important mediator (among other proteins) of the fusion with lysosomes resulting in the final structure of the phagosomal maturation termed phagolysosome (Bucci et al. 2000). A consequence of this fusion is the presence of a large number of V-ATPases, further decreasing the luminal pH (pH ± 4.5). This low pH is crucial for the activity of hydrolytic enzymes and for reactive oxygen species (ROS) production required to degrade microorganisms (Kinchen et al. 2008, Flannagan et al. 2009). In accordance, inhibition of V-ATPases with Bafilomycin was described to suppress bactericidal activity of alveolar macrophages (Bidani et al. 2000). V-ATPases have also been suggested to be important for the phagosomal maturation itself by regulating vesicle fusion (Peri et al. 2008).
Altogether, phagocytosis is a complex process involving several mechanisms including endocytosis, recycling, fusion and acidification. A role of (P)RR in these different aspects can be studied with the use of latex beads, fluorophore-coupled dead pathogens and macromolecules including dextran and transferrin. To this purpose, we decided to generate a new transgenic model based on the RNA interference technology.

1.4.3 Mechanisms and functions of RNA interference

RNA interference (RNAi) is an evolutionary conserved mechanism of gene silencing which was first suggested occurring in plants (Agrawal et al. 2003). However, the RNAi became popular once it was described in the roundworm *C. elegans* (Fire et al. 1998). This mechanism has since been reported in fungi and almost all eukaryotic organisms including protozoa, flies, rodents and humans (Agrawal et al. 2003). RNAi is a process in which double-stranded RNA (dsRNA) of exogenous or nuclear origin mediates sequence specific degradation of a target messenger RNA (mRNA) and thereby regulates gene expression (Matzke et al. 2001). The RNAi pathway (Fig. 11) begins with the trimming of dsRNA molecules by the endoribonuclease Dicer, resulting in short fragments of 20-25 nucleotides termed short interfering RNA (siRNA) (MacRae et al. 2007). Following processing, siRNAs are incorporated into a multiprotein structure termed RISC (RNA-induced silencing complex)-loading complex composed of Dicer, an Argonaute protein, and a dsRBD (double-stranded RNA-binding domain) protein (Wilson et al. 2013). Within the loading complex, the sense (passenger) strand is cleaved and ejected while the antisense (guide) strand and Argonaute are released and form RISC (Wilson et al. 2013). The guide strand directs RISC to complementary sequences of target mRNA for subsequent cleavage by the endonuclease activity of Argonaute and degradation of the mRNA transcript in a process termed post-transcriptional gene silencing (PTGS). To avoid erroneous gene silencing, efficient and specific PTGS is based on a perfect base pairing between the siRNA guide strand and the target mRNA.
RNAi is a natural function involved in the cellular defense against foreign nucleic acids (virus and transposons) and in the regulation of eukaryotic gene expression during development. In addition to PTGS, siRNAs have been documented to mediate effects in the nucleus on

chromosomal DNA. Several studies showed that siRNAs modulate DNA methylation, heterochromatin formation and DNA elimination (Dernburg et al. 2002, Jenuwein 2002).

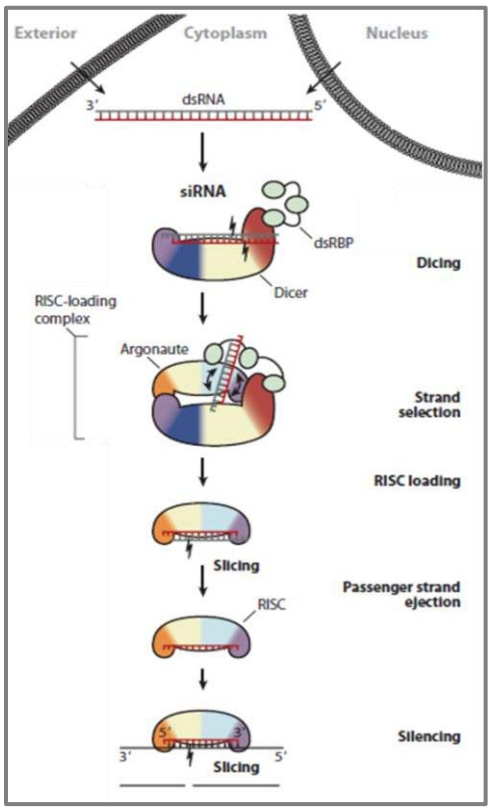

Fig. 11: Mechanism of RNA interference.
Dicer binds to and cleaves dsRNA of endogenous or nuclear origin. The resulting siRNA duplex binds to Argonaute with the help of the RISC-loading complex. After ejection of the passenger strand, the guide strand directs RISC to complementary sequences of target mRNA for subsequent cleavage by the endonuclease activity of Argonaute resulting in gene silencing.
dsRBP, double-stranded RNA-binding domain; dsRNA, double-stranded RNA; RISC, RNA-induced silencing complex; siRNA, short interfering RNA. (Picture modified from Wilson et al. 2013).

1.4.4 Application of RNAi: short hairpin RNA

The development of RNAi has provided a valuable molecular tool to investigate cellular gene functions. Synthetic siRNA duplexes have been extensively used to transfect cells and repress the expression of a gene of interest *in vitro*. Optimization of the design and delivery of siRNA has rendered this method very efficient and RNAi-mediated knockdown has also been performed *in vivo* in adult rodents through several approaches such as hydrodynamic injection, local delivery and intranasal administration (Kumar et al. 2007, Shim et al. 2010). One disadvantage of this method is that siRNA-mediated gene silencing remains a transient event. The advent of short hairpin RNA (shRNA) technology has opened new ways to achieve constitutive and conditional gene knockdown in mammals. ShRNAs are short RNAs containing 19-29 base pairs-complementary sequences separated by a loop of 4-10 nucleotides responsible for the hairpin structure (Kumar et al. 2007). Their expression is achieved with the help of promoters present in vectors which can be easily transfected into cells. Segments encoding shRNA templates are often cloned downstream of RNA polymerase III promoters (U6 or H1) to ensure a strong and permanent expression (Chen et al. 2005). Following cell transfection, vectors reach the nucleus and randomly integrate in the host DNA. Nuclear RNA polymerases III trigger the expression of shRNA transcripts which undergo nuclear export with the karyopherin Exportin 5 (Yi et al.

2003). Once in the cytoplasm, shRNAs are taken in charge by the RNAi machinery as described above (Fig. 11) resulting in gene silencing induced by RISC. Transgenic animals with constitutive shRNA-mediated gene silencing have been generated by pronuclear injection of fertilized eggs or lentiviral infection of embryonic stem cells (Gama Sosa et al. 2010, Podolska et al. 2011).

1.4.5 Transgenic rats with doxycycline-inducible shRNA expression

Under certain circumstances including embryonic lethality, the use of an inducible system may be required. Among several approaches to control the expression of a transgene, a common tool for transgenic animals is the tetracycline (Tet)-mediated system adapted from the Tet resistance operon of Escherichia Coli (Gossen et al. 1992, Stieger et al. 2009, Gama Sosa et al. 2010). In normal conditions, the Tet repressor (TetR) binds to a DNA sequence called Tet operator (TetO) leading to the repression of Tet resistance genes. In the presence of Tet or more often its synthetic analogue Doxycycline (Dox), the binding of TetR to TetO is prevented and the transcription of Tet resistance genes provides a protection to Escherichia Coli strains against Tet antibiotics.

Different Tet-responsive systems have been used *in vivo* in mice and rats. The most widely used strategy is the Tet regulatory system available in two versions differing in the effect of Dox. The Tet regulatory system was developed by fusing the TetR DNA binding domain with the activation domain of the herpes simplex virus VP16 to obtain Tet-controlled transactivators (tTAs) (Gossen et al. 1995). These tTAs activate the transcription of a transgene through TetO sequences cloned upstream of the promoter. Suppression of the transgene expression is achieved by treating transgenic animals with Dox in drinking water and is thus referred to as Tet-Off version (Gama Sosa et al. 2010). In contrast the second version uses reverse Tet-controlled transactivators (rtTAs) which are mutated tTAs and reverse the effect of Dox. The transgene is only expressed in the presence of Dox and is thus termed Tet-On version (Gossen et al. 1995). In this study, we developed an inducible Tet-controlled system based on the original Tet resistance operon mechanism and devoid of any transactivators. Our inducible shRNA vector contains a bimodal expression system (Fig. 12) with a shRNA cassette against (P)RR under the control of the H1 promoter (with TetO sequences) and the TetR cassette followed by a polyadenylation site driven by a CAGGS promoter (Niwa et al. 1991). This technology has been efficient to achieve Dox-inducible and reversible shRNA-mediated gene silencing without any toxicity in mice and rats (Seibler et al. 2007, Kotnik et al. 2009). In this study, a vector containing a shRNA against (P)RR has been developed, linearized and used for pronuclear microinjection to generate transgenic rats.

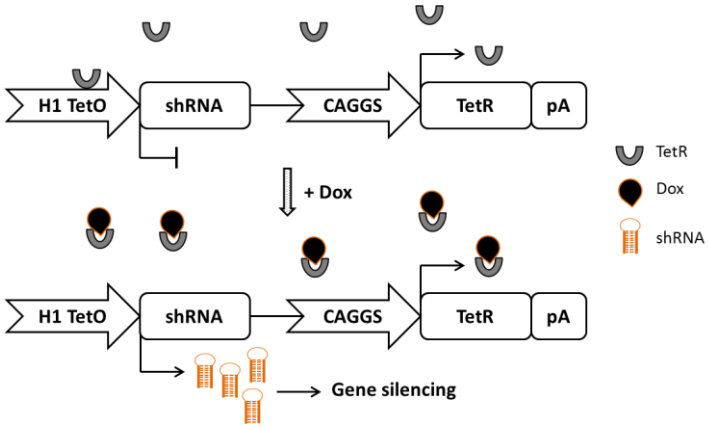

Fig. 12: Transgene construct for doxycycline-inducible shRNA-mediated gene silencing.
Schematic representation of the bimodal expression system used for inducible expression of shRNAs. In the absence of doxycycline (Dox), constitutively transcribed TetR binds to TetO and inhibits the transcription of the shRNA. In the presence of Dox, TetR binds to the antibiotics, loses the ability to bind to TetO and thus allows the expression of the shRNA.
For further information and abbreviations, see text. (Scheme inspired from Kotnik et al. 2009)

1.4.6 Macrophages from transgenic rats as a cellular tool

Tissue resident macrophages, deriving either from circulating monocytes or from local macrophage proliferation, are present in almost all organs in which they have a role in local homeostasis and immunosurveillance (Gordon et al. 2005, Mosser et al. 2008).
Macrophages present in the peritoneal cavity are of particular interest to study a role of (P)RR in these cells *in vivo* as they can be easily collected by peritoneal wash gene after induction of (P)RR knockdown by treating transgenic rats with Dox in drinking water. In addition, gene silencing can also be induced *in vitro* by treating cultured peritoneal macrophages with Dox added in culture medium. Finally, bone marrow cells of these transgenic rats are an additional source of macrophages as they can be differentiated *in vitro* with M-CSF and subsequently treated with Dox. Therefore, transgenic rats with inducible shRNA offer several opportunities to study new roles of (P)RR in macrophages.

AIM OF THE STUDY

CHAPTER 9

The (P)RR was initially described as a member of the Renin Angiotensin System and has since been extensively studied for its potential contribution to hypertension and target-organ damage. However, recent studies have highlighted additional functions of the (P)RR as a potential associated protein of the V-ATPase complex. Such functional association has been described to be important for vesicle acidification and the transduction of intracellular signaling pathways.
Osteoclasts are specialized bone resorbing cells in which V-ATPases are mainly located at the plasma membrane in order to acidify the extracellular environment. Disruption of various V-ATPase subunits in mice led to an osteopetrotic phenotype due to either lacking or dysfunctional osteoclasts.

This work aimed to investigate the role of (P)RR in osteoclast physiology and activity. To this purpose, two mouse models with a specific (P)RR deletion in osteoclasts were generated using the Cre/Lox technology. The growth and the bone density of these animals were evaluated. In addition, differentiation of bone marrow and spleen cells into osteoclasts *in vitro* allowed us to further characterize the role of (P)RR during osteoclast differentiation, maturation and activity.

Another aim of this work was the generation of a novel transgenic animal model to study the role of (P)RR in macrophages. Macrophages are professionalized phagocytes crucial for immune response. As an alternative to the Cre/Lox system, we generated transgenic rats with a conditional depletion of (P)RR with the use of a doxycycline-induced shRNA expression system. These transgenic rats allowed us to deplete (P)RR in macrophages *in vivo* and *in vitro* by treating rats or primary cells cultured from them with doxycycline. Several cellular functions including phagocytosis, endocytosis and receptor recycling were studied in (P)RR-deficient macrophages.

MATERIAL AND METHODS

CHAPTER 3

3.1 Material

3.1.1 Chemicals and reagents

Table 1: Chemicals and reagents.

Chemicals and reagents	Manufacturers (location, country)
2-methoxyethyl-acetate (2-MEA)	Merck (Darmstadt, Germany)
1,4-Dithiothreitol (DTT)	Invitrogen (Darmstadt, Germany)
4',6-Diamidino-2-phenylindole (DAPI)	Sigma-Aldrich (Steinheim, Germany)
ABC Elite reagent	Vector Laboratories (Burlingame, Canada)
Acetic acid (glacial)	Roth (Karlsruhe, Germany)
Acetone	Roth (Karlsruhe, Germany)
Agarose	Lonza (Basel, Switzerland)
Agarose	Biozym (San Diego, USA)
Alcian blue 8GS	Sigma-Aldrich (Steinheim, Germany)
Alizarin red S	Sigma-Aldrich (Steinheim, Germany)
Ammoniumperoxydisulfate	Sigma-Aldrich (Steinheim, Germany)
Ampicillin trihydrate	Serva (Heidelberg, Germany)
Ascorbic acid γ-irradiated	Sigma-Aldrich (Steinheim, Germany)
Bacto Agar	Becton (Heidelberg, Germany)
Bafilomycin A1, *streptomyces griseus*	Merck (Darmstadt, Germany)
β-Glycerophosphate disodium salt pentahydrate	Sigma-Aldrich (Steinheim, Germany)
β-Mercaptoethanol 99%	Sigma-Aldrich (Steinheim, Germany)
Bicinchoninic acid solution	Sigma-Aldrich (Steinheim, Germany)
Bovine Serum Albumin (BSA)	Sigma-Aldrich (Steinheim, Germany)
Bradford Reagent	Sigma-Aldrich (Steinheim, Germany)
Bromophenol blue	Sigma-Aldrich (Steinheim, Germany)
Calcium chloride dihydrate	Sigma-Aldrich (Steinheim, Germany)
Chloroform	Merck (Darmstadt, Germany)
Citric acid	Merck (Darmstadt, Germany)
Complete protease inhibitor cocktail Mini	Roche (Mannheim, Germany)
Complete protease inhibitor cocktail Mini EDTA-free	Roche (Mannheim, Germany)
Copper (II) sulfate solution	Sigma-Aldrich (Steinheim, Germany)
Deoxyribonucleotide (dNTP)	Bioline (Luckenwalde, Germany)
Diethylpyrocarbonate (DEPC)	Sigma-Aldrich (Steinheim, Germany)
Disodium hydrogenophosphate	Sigma-Aldrich (Steinheim, Germany)
E. Coli (K-12 strain) Bioparticles® AF488 conjugate	Invitrogen (Darmstadt, Germany)
Entellan® medium	Merck (Darmstadt, Germany)
Ethanol	Berkel AHK (Berlin, Germany)
Ethidium bromide	Invitrogen (Darmstadt, Germany)
Ethylenglycolmonobutylether	Merck (Darmstadt, Germany)

Ethylene glycol tetraacetic acid (EGTA)	Roth (Karlsruhe, Germany)
Ethylenediaminetetraacetic acid (EDTA)	Serva (Heidelberg, Germany)
Fast red violet LB salt	Sigma-Aldrich (Steinheim, Germany)
First strand buffer	Invitrogen (Darmstadt, Germany)
Fluoromont-G	Southern Biotech (Birmingham, USA)
Fluospheres® carboxylated 2.0µm blue	Invitrogen (Darmstadt, Germany)
Fluospheres® carboxylated 2.0µm yellow/green	Invitrogen (Darmstadt, Germany)
Glucose	Sigma-Aldrich (Steinheim, Germany)
Glycerol	Roth (Karlsruhe, Germany)
Hepes	Sigma-Aldrich (Steinheim, Germany)
Hydrochloric acid	Roth (Karlsruhe, Germany)
Isoflurane	Abott (Wiesbaden, Germany)
Isoprenaline	Sigma-Aldrich (Steinheim, Germany)
Isopropanol	Roth (Karlsruhe, Germany)
Ketavet 100mg/ml	Pfizer (Berlin, Germany)
Kisol-Folie	Kettenbach GmbH (Eschenburg, Germany)
Lysing Buffer Pharm Lyse™	BD (Heidelberg, Germany)
LysoSensor™ Green DND189	Invitrogen (Darmstadt, Germany)
LysoTracker® Red DND99	Invitrogen (Darmstadt, Germany)
Magnesium Chloride	Sigma-Aldrich (Steinheim, Germany)
Methanol	Roth (Karlsruhe, Germany)
Methyl methacrylate	Polyscience (Eppelheim, Germany)
Milk powder	Roth (Karlsruhe, Germany)
Monopotassium phosphate	Sigma-Aldrich (Steinheim, Germany)
Naphtol-AS-Mx-phosphat	Sigma-Aldrich (Steinheim, Germany)
N-N-Dimethylformamid	Sigma-Aldrich (Steinheim, Germany)
Normal donkey serum	Sigma-Aldrich (Steinheim, Germany)
Odyssey® Blocking Buffer	LI-COR Bioscience GmbH (Bad Homburg, Germany)
Paraffin	Roth (Karlsruhe, Germany)
Paraformaldehyde (PFA) 4%	Otto Fischar GmbH & Co. KG (Saarbrücken, Germany)
Phalloidin-Alexa488	Invitrogen (Darmstadt, Germany)
Phenylmethylsulfonylfluorid	Sigma-Aldrich (Steinheim, Germany)
Phosphatase inhibitor cocktail (PhosStop)	Roche (Mannheim, Germany)
Phosphate Buffered Saline (PBS)	Sigma-Aldrich (Steinheim, Germany)
pHrodo™ red *E.Coli* bioparticles®	Invitrogen (Darmstadt, Germany)
Ponceau S solution	Sigma-Aldrich (Steinheim, Germany)
Potassium dihydrogenphosphate	Merck (Darmstadt, Germany)
Potassium hydroxide	Fluka (Steinheim, Germany)
Random Hexamer Primer	Roche (Mannheim, Germany)
Rapamycin	Merck Chemicals GmbH (Schwalbach, Germany)
Restore™ WB stripping buffer	Thermo Fischer Scientific (Rockford, USA)
Rompun 2%	Bayer (Leverkusen, Germany)
Roti®-Load	Roth (Karlsruhe, Germany)
Roti®-Phenol	Roth (Karlsruhe, Germany)
Rotiphorese® Gel 30 (37.5:1)	Roth (Karlsruhe, Germany)
Sirius red F3B (Direct Red 80)	Sigma-Aldrich (Steinheim, Germany)
Saponin	Sigma-Aldrich (Steinheim, Germany)
silver nitrate	Sigma-Aldrich (Steinheim, Germany)
Sodium acetate	Sigma-Aldrich (Steinheim, Germany)
Sodium carbonate	Merck (Darmstadt, Germany)
Sodium chloride	Roth (Karlsruhe, Germany)
Sodium citrate	Merck (Darmstadt, Germany)
Sodium deoxycholate	Merck (Darmstadt, Germany)
Sodium dodecylsulfate (SDS)	Serva (Heidelberg, Germany)
Sodium fluoride	Sigma-Aldrich (Steinheim, Germany)

Sodium hydroxide	Roth (Karlsruhe, Germany)
Sodium pyrosulfate	Sigma-Aldrich (Steinheim, Germany)
Sodium tartrate	Sigma-Aldrich (Steinheim, Germany)
Sucrose	Merck (Darmstadt, Germany)
Tergitol type NP-40	Sigma-Aldrich (Steinheim, Germany)
Tetramethylethylendiamine (TEMED)	Roth (Karlsruhe, Germany)
Tissue-Tek® OCT™ Compound	Sakura (Staufen, Germany)
Toluidine blue O	Sigma-Aldrich (Steinheim, Germany)
Transferrin from human serum, AF647 conjugate	Invitrogen (Darmstadt, Germany)
Tris	Roth (Karlsruhe, Germany)
Tris-HCl	Roth (Karlsruhe, Germany)
Triton X-100	Sigma-Aldrich (Steinheim, Germany)
Trizol®	Invitrogen (Darmstadt, Germany)
Tween-20	Sigma-Aldrich (Steinheim, Germany)
Vectashield® Mounting Medium with DAPI	Vector Laboratories (CA, USA)
Xylene	Roth (Karlsruhe, Germany)

3.1.2 Antibodies

Table 2: Antibodies for Western Blot (WB) and Immunohistochemistry (IHC).

Antibody	Host	Manufacturer (location, country)	Method	Dilution
Primary				
ATP6ap2	rabbit	Sigma-Aldrich (Steinheim, Germany)	WB IHC	1/1000 1/500
beta-actin	rabbit	Cell Signaling (Danvers, USA)	WB	1/1000
GAPDH	rabbit	Cell Signaling (Danvers, USA)	WB	1/1000
GFP/YFP	rabbit	Abcam (Cambridge, UK)	WB IHC	1/1000 1/500
LC3B	rabbit	Cell Signaling (Danvers, USA)	IHC	1/500
LC3B	rabbit	Sigma-Aldrich (Steinheim, Germany)	WB	1/1000
TetR	mouse	MoBiTec GmbH (Göttingen, Germany)	WB	1/2000
Transferrin	rabbit	Dako (Hamburg, Germany)	WB	1/1000
Secondary				
IRDye®-coupled anti-mouse/rabbit	Donkey	LI-COR Bioscience GmbH (Bad Homburg, Germany)	WB	1/5000
Cy3-conjugated anti-rabbit	Donkey	Jackson Immuno (Suffolk, UK)	IHC	1/500

Table 3: Antibodies for Flow Cytometry (FACS).

Antibody	Manufacturer (location, country)	Dilution
B220 PE/Cy7 anti-mouse	Biolegend (San Diego, USA)	1/1000
CD3 APC anti-mouse	Biolegend (San Diego, USA)	1/1000
CD4 PE anti-mouse	Biolegend (San Diego, USA)	1/500
CD8 Alexa Fluor® 700 anti-mouse	Biolegend (San Diego, USA)	1/4000
CD11b APC anti-mouse	Biolegend (San Diego, USA)	1/4000
CD16/32 anti-mouse	Biolegend (San Diego, USA)	1/1000
CD45 PB® anti-mouse	Biolegend (San Diego, USA)	1/1000
Gr1 FITC anti-mouse	Biolegend (San Diego, USA)	1/1000
Ly6C Alexa Fluor® 700 anti-mouse	Biolegend (San Diego, USA)	1/1000
Ly6G PE anti-mouse	Biolegend (San Diego, USA)	1/1000

3.1.3 Oligonucleotides

All oligonucleotides were synthetized by a company located on the campus (BioTeZ Berlin Buch GmbH) and delivered in a lyophilized state. Primers were diluted in sterile water to a concentration of 100 µM and stored at -20°C. For Polymerase Chain Reaction (PCR), primers were diluted with sterile water to a final concentration of 5 µM and stored at 4°C. All oligonucleotides used for genotyping, quantitative real-time PCR and shRNA annealing are listed in the table 4.

Table 4: Primers for PCR and oligonucleotides for shRNA constructs.

Primers	Sequence (5'-3')	Species	Gene and method
Lf2271	AGCACTCTCTTCCAGGTATGTTGTG	mouse	distal LoxP site on *(P)RR/ATP6ap2*
Lr2273	CTGGATCCCGGAGCATGGGTAAAGG		genotyping PCR
Lf2271	AGCACTCTCTTCCAGGTATGTTGTG	mouse	distal LoxP site on *(P)RR/ATP6ap2*
Er2276	GCCCCTCTCTTACAGTTCTATCAGT		genotyping PCR
Cre1 fw	GAACGCACTGATTTCGACCA	mouse	Cre
Cre2 rv	AACCAGCGTTTTCGTTCTGC		genotyping PCR
RosaYFP1	AAAGTCGCTCTGAGTTGTTAT	mouse	R26-YFP transgene
RosaYFP2	GCGAAGAGTTTGTCCTCAACC		genotyping PCR
RosaYFP3	GGAGCGGGAGAAATGGATATG		

TetR fw	CAAGTTGCCAAGGAGGAGAG	rat	Tet Repressor
TetR rv	AACCGGTCTAGAATCGATGG		genotyping PCR
(P)RR1-2 fw	TTCTGGTGGCGGGTGCTTTAGG	mouse	(P)RR/ATP6ap2
(P)RR3 rv	TGGAATAGGTTACCCACGGCAA		qPCR
(P)RR fw	CCACAGGCAGCGTC	rat	(P)RR/ATP6ap2
(P)RR rv	GTCTTGACAGTGTGGCCAATTC		qPCR
Hprt fw	GTAATGATCAGTCAACGGGGGAC	mouse	Hprt - reference gene
Hprt rv	CCAGCAAGCTTGCAACCTTAACCA		qPCR
Hprt fw	CTCATGGACTGATTATGGACAGGAC	rat	Hprt - reference gene
Hprt rv	GCAGGTCAGCAAAGAACTTATAGCC		qPCR
Trap fw	TCCCCTGGTATGTGCTGG	mouse	Trap - osteoclast enzyme
Trap rv	GCATTTTGGGCTGCTGAC		qPCR
Ctsk fw	CAGCAGGATGTGGGTGTTCA	mouse	Cathepsin K - osteoclast enzyme
Ctsk rv	ACACTGGCCCTGGTTCTTGA		qPCR
Gapdh fw	GTCAAGGCCGAGAATGGGAA	mouse	Gapdh - reference gene
Gapdh rv	GCTTCACCACCTTCTTGATG		q-PCR
TBP fw	CGAAGTGCAATGGTCTTTAGGTC	mouse	TBP – reference gene
TBP rv	CCCTATCACTCCTGCCACACC		q-PCR
ATP6V0d2 fw	CATTCCTTGGAGCCCCTGAG	mouse	ATP6V0d2 - V-ATPase subunit
ATP6V0d2 rv	TCTCTGTGAAACGGCCCAGT		q-PCR

Oligos	**Sequence (5'-3')**
rPRRsh1	TCCCGCTTGCTGTGGGCAACCTATTCAAGAGATAGGTTGCCCACAGCAAGCTTTTTTA
rPRRsh2	CGCGTAAAAAAGCTTGCTGTGGGCAACCTATCTCTTGAATAGGTTGCCCACAGCAAGC
rPRRsh3	TCCCCCTACAACCTTGCGTATAATTCAAGAGATTATACGCAAGGTTGTAGGTTTTTTA
rPRRsh4	CGCGTAAAAAACCTACAACCTTGCGTATAATCTCTTGAATTATACGCAAGGTTGTAGG

3.1.4 Kits

Table 5: Kits.

Kits	Manufacturers (location, country)
Amaxa cell line Nucleofactor® kit V	Lonza (Cologne, Germany)
Bicinchoninic Acid (BCA) Protein Assay Kit	Sigma-Aldrich (Steinheim, Germany)
In Situ Cell Death Detection Kit, Fluorescein	Roche (Manheim, Germany)
Mouse CTX-I ELISA kit	USCNK Life Science (Wuhan, China)
QIAquick® Gel extraction kit	Qiagen (Hilden, Germany)
Rneasy ® Mini Kit	Qiagen (Hilden, Germany)
Trap Staining	Sigma-Aldrich (Steinheim, Germany)
Trap Staining	Kamiya Biomedical (Seattle, USA)
Trichrom stain (Masson) Kit	Sigma-Aldrich (Steinheim, Germany)
Wizard ® SV Gel and PCR Clean-Up System	Roche (Manhein, Germany)

3.1.5 Enzymes and markers

Table 6: Enzymes and markers.

Enzymes	Manufacturers (location, country)
Collagenase	Sigma-Aldrich (Steinheim, Germany)
DNase I, recombinant	Roche (Mannheim, Germany)
DNase I, recombinant	Boehringer (Mannheim, Germany)
GoTaq® qPCR Master Mix	Promega (Madison, WI, USA)
Moloney Murine Leukemia Virus Reverse Transcriptase	Invitrogen (Darmstadt, Germany)
Restriction enzymes	NEB (Frankfurt/Main, Germany)
Proteinase K	Invitrogen (Darmstadt, Germany)
RedTaq ® DNA Polymerase	Sigma-Aldrich (Steinheim, Germany)
RNase A	Applichem (Darmstadt, Germany)
RNasin® Ribonuclease Inhibitor	Promega (Madison, WI, USA)
RNase-free DNase set	Qiagen (Hilden, Germany)
SuperScript® RNA Amplification System	Invitrogen (Darmstadt, Germany)
Thermus Aquaticus DNA Polymerase	Invitrogen (Darmstadt, Germany)
Thermus Aquaticus DNA Polymerase	Lab-made

Markers	Manufacturers (location, country)
PCR	
Lambda DNA/EcoRI+HindIII (EH) marker	Fermentas (St. Leon-Rot, Germany)
PhiX174 DNA/BsuRI (Phi) marker	Fermentas (St. Leon-Rot, Germany)
Quick-Load© 100bp DNA ladder	NEB (Frankfurt/Main, Germany)
Quick-Load© 1 kb DNA ladder	NEB (Frankfurt/Main, Germany)

WB	
Odyssey® two-color protein molecular weight marker	Bioscience GmbH (Bad Homburg, Germany)
Precision plus protein™ standards all blue	BioRad Laboratories (München, Germany)
Prestained protein marker, broad range 7-175 kDa	NEB (Frankfurt/Main, Germany)

3.1.6 Recombinant proteins

Table 7: Recombinant proteins.

Recombinant (rec) proteins	Abbreviations	Manufacturers (location, country)
Macrophage colony-stimulating factor (rec, murine)	mM-CSF	PeproTech (Hamburg, Germany)
Macrophage colony-stimulating factor (rec, human)	hM-CSF	R&D Systems (Wiesbaden-Nordenstadt, Germany)
Macrophage colony-stimulating factor (rec, rat)	rM-CSF	PeproTech (Hamburg, Germany)
Receptor activator of nuclear factor κB ligand (rec, rat)	rRANKL	PeproTech (Hamburg, Germany)
Receptor activator of nuclear factor κB ligand (rec, mouse)	mRANKL	R&D Systems (Wiesbaden-Nordenstadt, Germany)

3.1.7 Mouse and rat strains

Mice in which the exon 2 of the *(P)RR/ATP6ap2* gene is flanked with loxP site have been generated in collaboration with the Mouse Clinical Institute based in Illkirch, France. As part of a collaboration, these mice were shipped to our animal house at the Max Delbrück Center (MDC) and were used to generate mice with tissue specific deletions of the (P)RR. Cathepsin K-Cre mice (kind gift from Prof. Dr. Kato, Tokyo, Japan) were used for specific deletion in differentiated osteoclasts. Lysosyme M-Cre mice (kind gift from Dr. Schmidt-Ullrich, Berlin, Germany) were used for deletion in the myeloid lineage. Rosa26-YFP transgenic mice (kind gift from Prof. Dr. C. Birchmeier, Berlin, Germany) were used to control the specificity of the Cre expression. Transgenic rats expressing an inducible shRNA against (P)RR after doxycycline treatment were generated in the lab of Prof. Dr. Michael Bader using the Sprague Dawley® (SD) rat strain. All transgenic animal models used in this study are listed in the table 8.

Table 8: Transgenic animals.

Mice	Rats
(P)RR/ATP6ap2 flox	sh(P)RR
Cathepsin K-Cre	
Lysozyme M-Cre	
Rosa26-YFP	

3.1.8 Cell culture materials

Table 9: Cells, cell lines and material used for cell culture.

Cells and Cell lines	Origins
Cos-7	fibroblast-like cell line
RAW264.7	monocytes/macrophages cell line
Macrophages	Primary culture from bone marrow/peritoneal cavity
Macrophage-derived osteoclasts	Primary culture from bone marrow/spleen

Materials	Abbreviations	Manufacturers (location, country)
Media		
Dulbecco's Phosphate Buffered Saline	PBS	Gibco (Darmstadt, Germany)
Dulbecco's Modified Eagle Medium (+ glutamine)	DMEM	Gibco (Darmstadt, Germany)
Dulbecco's Modified Eagle Medium Glutamax	DMEM HG	Gibco (Darmstadt, Germany)
Hank´s balanced salt solution	HBSS	Sigma-Aldrich (Steinheim, Germany)
α-Minimum Essential Medium (+ Glutamine)	α-MEM	PAA (Cölbe, Germany)
α-Minimum Essential Medium (+ Glutamine)	α-MEM	Gibco (Darmstadt, Germany)
α-Minimum Essential Medium (- Glutamine)	α-MEM	Lonza (Cologne, Germany)
Supplements		
Dimethylsulfoxide	DMSO	Sigma-Aldrich (Steinheim, Germany)
Doxycyclin	Dox	Sigma-Aldrich (Steinheim, Germany)
Fetal Bovine serum	FBS	Sigma-Aldrich (Steinheim, Germany)
L-Glutamine	Glu	Gibco (Darmstadt, Germany)
2-Mercaptoethanol 99%	β-mercapto	Sigma-Aldrich (Steinheim, Germany)
Penicillin-streptomycin (100x)	P/S	Gibco (Darmstadt, Germany)
Penicillin-streptomycin (100x)	P/S	Biochem (Berlin, Germany)
Transfection reagents		
Lipofectamine LTX		Invitrogen (Darmstadt, Germany)
Opti-MEM®I		Gibco (Darmstadt, Germany)
Enzymes		
TripLE™ Express		Gibco (Darmstadt, Germany)
Trypsin		Gibco (Darmstadt, Germany)
Equipments and expandable materials		
Cell culture dishes and plates Cellstar®		Greiner bio-one (Frickenhausen, Germany)
Cell culture incubator		Heracell GFL (Burgwedel, Germany)
Cell strainer (100, 70, 50 µm)		BD Falcons (Heidelberg, Germany)
Cryovial		Simport (Beloeil, Canada)
KOVA Glasstic® Slide 10 with grids		Hycor Biomedical (Garden Groove, USA)
Nalgene Mr. Frosty containers		Thermo Scientific (Rockford, USA)
Nunc and Nalgene® cryogenic storage tubes		Thermo Scientific (Rockford, USA)
Sterile filter (0.2 and 0.45µm)		Sartorius (Goettingen, Germany)
Syringe (1 ml)		Braun (Melsungen, Germany)
Water bath		GFL (Burgwedel, Germany)

3.1.9 Lab equipment and expendable materials

Table 10: Lab equipment and expendable materials.

Instruments and materials	Manufacturers (location, country)
384-well optical plate MicroAmp®	Applied Biosystems (Darmstadt, Germany)
8 - channel - pipette M300	Biohit (Rosbach v.d Höhe, Germany)
96-well clear microplates	R&D Systems (Wiesbaden-Nordenstadt, Germany)
Agarose gel electrophoresis chamber	Biometra (Göttingen, Germany)
Automatic Pipette Witoped XP	Witeg Labortechnik GmbH (Wertheim, Germany)
Bacteria shaker Certomat®H	Braun (Melsungen, Germany)
BD™ LSR II	BD (Heidelberg, Germany)
BD™ LSRFortessa cell	BD (Heidelberg, Germany)
Binocular MZFLIII	Leica (Wetzlar, Germany)
Cell scraper	TPP (Trasadingen, Switzerland)
Cell scraper	Greiner bio-one (Frickenhausen, Germany)
Centrifuge 5415C	Eppendorf (Hamburg, Germany)
Centrifuge G5-6R	Beckman Coulter (Krefeld, Germany)
Centrifuge Sorvall RC 5C	Heraeus Instuments GmbH (Hanau, Germany)
Cooling centrifuge Megafuge 1.0R	Heraeus Instuments GmbH (Hanau, Germany)
Cooling centrifuge Sigma 3K12	Sigma-Aldrich (Steinheim, Germany)
Cooling centrifuge Sorvall®PC5C Plus	Kendro (Langensebald, Germany)
Costar stripette (2, 5, 10, 25 m)	Corning (NY, USA)
Cryostat CM3050 S	Leica (Wetzlar, Germany)
Disposable pipettes Cellstar®	Greiner bio-one (Frickenhausen, Germany)
EDTA tubes MiniCollect®	Greiner bio-one (Frickenhausen, Germany)
Electronic pipette Xplorer©	Eppendorf (Hamburg, Germany)
Electroporator 2510	Eppendorf (Hamburg, Germany)
Falcon tubes (15 and 50 ml)	Greiner bio-one (Frickenhausen, Germany)
FastPrep™ lysing matrix tubes	MP Biomedicals (Illkirch, France)
FastPrep™-24 instrument	MP Biomedicals (Illkirch, France)
Filter tips (10, 20, 200 and 1000 ml)	Biozym (San Diego, USA)
Fine balance	Kern&Sohn GmbH (Balingen, Germany)
Fluorescence microscope BZ-9000	Keyence (Neu-Isenburg, Germany)
GenePulse® electroporationcuvettes	BioRad Laboratories (München, Germany)
Hematocytometer Scil Vet abc	Scil GmbH (Viernheim, Germany)
Hybond™ XL nylon membrane	Amersham Biosciences (Little Chalfon, UK)
Inverted microscope DMI6000B	Leica (Wetzlar, Germany)
Latex gloves	Sänger (Schrozberg, Germany)
Membrane filter	Millipore (Morlsheim, Germany)
Microbalance	Sartorius (Göttingen, Germany)
Microplate Reader Infinite® M200	Tecan (Crailsheim, Germany)
Micro-slide 8 well ibi-treat	Ibidi (München, Germany)

Microwave 8020	Privileg (Fürth, Germany)
Multipette® plus	Eppendorf (Hamburg, Germany)
NanoDrop™ 1000 spectrophotometer	Peqlab (Erlangen, Germany)
Normal chow (0.25%sodium)	Ssniff (Soest, Germany)
Nitrile gloves	Cardinal Health (The Hague, The Netherlands)
Nucleofactor® 2b device	Lonza (Cologne, Germany)
Odyssey®infrared imaging system	LI-COR Bioscience GmbH (Bad Homburg, Germany)
Pasteur pipettes	Roth (Karlsruhe, Germany)
PCR tubes	Biozym Scientific GmbH (Oldendorf, Germany)
pH Meter pH Level 1	WTW (Weilheim, Germany)
Pipetboy acu	Integra Biosciences (Zizers, Switzerland)
Pipettes Gilson Disposable CellstarR	Gilson (Middleton, WI, USA)
Power supply PowerPac™ HC	BioRad Laboratories (München, Germany)
Precision balance 440-43N	Kern & Sohn GmbH (Balingen, Germany)
PVDF membranes	Amersham Biosciences (Little Chalfon, UK)
Real time PCR system 7900HT AbiPrism	Applied Biosystems (Darmstadt, Germany)
Roller mixer SRT1	Snijders (Tilburg, Netherlands)
Rotable platform Polymax 1040	Heidolph Instruments (Schwabach, Germany)
Rotary microtome HM 355 S	Microm (Walldorf, Germany)
Save-Lock Tubes	Eppendorf (Hamburg, Germany)
SDS-PAGE gel electrophoresis chamber	BioRad Laboratories (München, Germany)
Serological pipettes	Sarstedt (Nümbrecht, Germany)
Single pipettes	Discovery Abimed (Langenfeld, Germany)
Skyscan micro-CT 1172	Skyscan (Kontich, Belgium)
Special accuracy weighing machine	Sartorius (Göttingen, Germany)
SpeedVac SVC100	Savant Instruments (NY, USA)
Sterile laminar flow work Laminair®HB2448	Heraeus Instuments GmbH (Hanau, Germany)
Sterile laminar flow work bench safe 2020	Thermo-Scientific (Rockford, USA)
SuperFrost® Plus slides	Menzel Gläser (Braunschweig, Germany)
Syringe filter	Sartorius (Göttingen, Germany)
Tank blotter	BioRad Laboratories (München, Germany)
Thermocycler PTC-200	BioRad Laboratories (München, Germany)
Thermometer	Thermo Fischer Scientific (Rockford, USA)
Thermomixer 5437	Eppendorf (Hamburg, Germany)
Ultrasound Sonoplus	Bandelin electronic (Berlin, Germany)
UV Stratalinker 1800	Stratagene (La Jolla, USA)
UV transilluminator MultiImage®	Alpha Innotech (CA, USA)
Vacuum pump Vacusafe comfort	Integra Biosciences (Zizers, Switzerland)
Vortex Genie 2	Bender & Hobein AG (Zürich, Switzerland)
Water bath	GFL (Burgwedel, Germany)
Whatman paper (3 mm)	Whatman (Madison, USA)

3.2 Methods

3.2.1 DNA analysis

3.2.1.1 DNA isolation for animal genotyping

At the time of weaning (separation from the parents), mice and rats were given an identification number characterized by a combination of small holes on ears. The resulting pieces of ear or tail biopsies were used for the isolation of genomic DNA by incubating them with 100 µl Ear buffer containing 1 g/l proteinase K and shacking overnight at 55°C.

Ear buffer (pH 7)	
NaCl	200 mM
Tris-HCl	100 mM
EDTA	0.1 mM
SDS	1%

TE buffer	
Tris-HCl	10 mM
EDTA	1 mM

Enzyme activity was inactivated by incubation at 95°C for 10 min. Degradation of RNA was performed by adding 750 µl tris-EDTA (TE) buffer containing 20 µg/ml RNase A. Samples were mixed vigorously with a vortex and stored at 4°C until Polymerase Chain Reaction (PCR).

3.2.1.2 Genotyping PCR

DNA amplification by genotyping PCR was performed to distinguish wild type from transgenic animals. The amplification of the gene of interest was achieved with the use of Taq DNA polymerase (Invitrogen) in a reaction mixture described in the table 11. PCR efficiency was optimized by adjusting the amount of some of these components such as primers, dNTPs or enzyme.

Table 11: PCR reaction mix.

Components	Volume (µl)
10X PCR buffer	3
dNTP mixture (5mM)	2
$MgCl_2$ (50 mM)	1.5
Primer Forward (5 µM)	1
Primer Reverse (5 µM)	1
DNA sample	2
Taq polymerase (5U/µl)	0.3
Sterile water	19.2

The mix was pipetted and kept on ice before being transferred into a pre-heated thermocycler (BioRad Laboratories) and the reaction was achieved with the basic program illustrated in the table.12. As explained above, optimal reaction conditions can be variable and need to be optimized. For this purpose, duration and temperature for annealing and elongation steps were adjusted for each reaction. At the end of the PCR, samples were immediately analyzed or stored at -20°C until further analysis.

Table 12: Basic PCR program

PCR steps	Time	Temperature	Cycles
Initial denaturation	3 min	94°C	x1
Denaturation	30 sec	94°C	x35-40
Annealing	30 sec	55-65°C	
Elongation	30-60 sec	72°C	
Final elongation	10 min	72°C	x1

3.2.1.3 Analysis of PCR products by agarose gel electrophoresis

According to the desired resolution and the size of PCR products, an optimum agarose concentration (1-3%) was chosen. Agarose was dissolved in tris-acetate-EDTA (TAE) buffer and ethidium bromide was added (5 µl/50 ml). PCR reactions were mixed with DNA loading buffer at a ratio 4:1 and half of the total volume was loaded into the gel slots. PCR products were then electrophoretically separated at constant voltage (100-120 V) for 20-40 min. Gels were then placed under a UV light using a Transilluminator MultiImage™Light Cabinet (Alpha Innotech Corpororation, USA) and observed via the AlphaView software. The size of the different PCR fragments was estimated by comparison with adequate molecular weight markers (Table 6).

DNA loading buffer	
Sucrose	4 g
Bromophenol blue	2.5 mg
TE buffer	10 ml

TAE buffer	
Tris-HCl	242 g
EDTA	18.5 g
Sodium acetate	68 g
H_2O	1 l

3.2.2 RNA analysis

3.2.2.1 RNA extraction from cells

RNA from cultured cells was extracted and purified using the RNeasy® Mini Kit (Qiagen) according to the manufacturer's instructions. In detail, cell lines or primary cells grown in a

monolayer (< 5 x 10^6 cells) were washed with cold PBS and lysed by addition of 350 µl buffer RLT containing 1% β-mercaptoethanol. Cells were scraped into the buffer and 350 µl of 75% ethanol were further added. Lysates were homogenized by passing them 3 times through a 21-gauge needle and transferred immediately into QIAshredder spin columns placed in 2 ml collection tubes. After centrifugation for 30 s at 10,000 rpm, columns were then transferred into new 2 ml collection tubes and washed with 500 µl buffer RW1. After centrifugation for 30 s at 10,000 rpm, flow-through was discarded and DNase treatment was performed directly in columns using the DNase kit (Qiagen). Briefly, after resuspension of the lyophilized DNase with 550 µl RNase-free water (kit), 80 µl of a solution containing 10 µl DNase and 70 µl RDD buffer (kit) were added to each column and incubated 15 min at room temperature. After an additional wash with 500 µl RW1 buffer, columns were further washed two times with 500 µl RPE buffer (containing ethanol). Columns were then transferred to new collection tubes and dried by centrifugation at 13,000 rpm for 1 min before being placed into new 1.5 ml collection eppendorf tubes. For RNA elution, 20-50 µl RNase-free water were added to the column membrane and RNA eluates were recovered by centrifuging 30-45 s at 10,000 rpm. RNA concentration was measured using the NanoDrop™ spectrophotometer (Peqlab) and stored at -80°C until use.

3.2.2.2 RNA extraction from tissues (organs)

From dissected organs, small tissue samples were collected in FastPrep™ lysing matrix tubes containing 3-5 matrix beads (MP Biomedical), immediately frozen in liquid nitrogen and stored at -80°C until use. For RNA extraction, 1 ml Trizol® reagent per 100 mg of tissue and samples were homogenized one or two times for 40 s at speed level 4 using the FastPrep™-24 instrument (MP Biomedical). The amount of beads and rounds of homogenization were optimized according to the specific organ. After 10 min incubation at room temperature to ensure a complete dissociation of the nucleoprotein complex, 200 µl of chloroform per 1 ml Trizol® reagent were added and samples were shaken for 15 s. After 3 min incubation at room temperature, samples were centrifuged at 12,000 g for 15 min at 4°C and the upper phase was transferred into 1.5 ml eppendorf tubes. After addition of 500 µl isopropanol, samples were incubated at room temperature for 10 min and further centrifuged at 10,000 g for 15 min at 4°C. Pellets containing RNA were washed with 1 ml 70% ethanol (per 1 ml Trizol® reagent) and centrifuged at 7,500 g for 10 min at 4°C. Ethanol was then discarded with a pipette and pellets were air-dried at room temperature for 15-30 min. Finally, RNA pellets were resuspended in DEPC-treated water, vortexed and incubated 15 min at 55-60°C. RNA concentration was measured using the NanoDrop™ spectrophotometer (Peqlab) and stored at -80°C until use.

3.2.2.3 Measurements of RNA concentration and purity

After extraction from cells or tissues, RNA concentration was measured with the NanoDrop™ spectrophotometer (Peqlab) using 1.5 µl sample. In addition, purity of nucleic acid samples was

also assessed via the ratio of sample absorbances at 260 and 280 nm. RNA is generally considered as "pure" (absence of salt and proteins) when the 260/280 ratio is around 2.0.

3.2.2.4 Reverse transcription (complementary DNA synthesis)

Before reverse transcription (RT), DNase treatment was performed to avoid any amplification of potential genomic DNA. For RNA extracted from cells, this step was performed directly in columns as described above. For RNA extracted from tissues, 1-2 µg total RNA were incubated with 1 µl DNase I (Roche), 1 µl 10X PCR buffer and an adequate volume of DEPC-treated water to reach 9 µl for 30 min at 37 °C. Enzyme activity was then inactivated by incubation at 75°C for 10 min. After this step, these samples were used as templates to synthetize complementary DNA (cDNA) by RT.
The volume containing the desired amount of RNA was adjusted to 9µl with DEPC-treated water. Then, 1 µl of random hexamer primers (RH) and 2 µl of deoxynucleotidephosphates (dNTPs) were added and the mixture was incubated at 65°C for 5 min and directly chilled on ice to avoid formation of RNA secondary structures. The RT was performed by adding 8µl of a master mix and following a program as described in Table 13. Until use, cDNAs were stored at -20°C.

Table 13: Reverse transcription master mix and reaction

Components	Volume (µl)
5X First-strand buffer	4
DTT (0.1 M)	2
RNase inhibitor	1
M-MLV	1

RT steps	Time	Temperature
Priming	10 min	25°C
Transcription	50 min	37°C
Enzyme inactivation	15 min	70°C
Conservation	for ever	4°C

3.2.2.5 Polymerase Chain Reaction and analysis

Procedures to perform PCR and analyze PCR products on agarose gels were performed as described in the section 3.2.1 DNA analysis.

3.2.2.6 Quantitative Real Time PCR (qRT-PCR)

Quantitative Real Time PCR (qRT-PCR) was used to amplify and quantify cDNA as a reflection of mRNA levels (gene expression) in cells or tissues. Reaction was performed using the qRT-PCR system 7900HT (Applied Biosystems) with the SYBR© green protocol in 384-well plate. For each experiment, samples were diluted (2-20 ng/µl), primers concentrations optimized and an adequate housekeeping gene selected. For the reaction, 9 µl of each cDNA template was mixed

with primers specific for a selected gene, the GoTaq® qPCR master mix and the CXR reference dye. The precise mixture and the typical thermal profile are depicted in Table 14. A melting curve analysis was carried out at the end of the PCR program. Expression of the gene of interest was normalized to the housekeeping gene expression. The method of Livak and Schmittgen (Livak et al. 2001) was applied to compare gene expression levels between groups, using the equation $2^{-\Delta\Delta CT}$.

Table 14: qRT-PCR components and program

Components	Volume (µl)
cDNA	9
GoTaq® master mix (2X)	10
Primer Forward (5 µM)	0.4
Primer Reverse (5 µM)	0.4
CXR reference dye (100X)	0.2

qRT-PCR steps	Time	Temperature	Cycles
Initial denaturation	10 min	95°C	x1
Denaturation	15 sec	95°C	x40
Annealing and elongation	60 sec	60°C	

3.2.3 Protein analysis

3.2.3.1 Protein isolation

To extract proteins from cells, culture plates were placed on ice and washed one time with cold PBS. Cells were harvested in an adequate volume of RIPA buffer or protein lysis buffer containing protease and phosphatase inhibitors. Cell homogenates were sonicated 30 s and mixed gently 30 min at 4°C. Nuclei and undissolved debris were removed by centrifugation at 10,000 x g for 10 min at 4°C. Finally, protein-containing supernatants were transferred into new Eppendorf tubes and stored at -20°C until usage.

RIPA buffer (pH 7)	
NaCl	150 mM
Tris (pH 8.0)	50 mM
Tergitol-NP40	1%
Sodium deoxycholat	0.5%
SDS	0.1%

Cell lysis buffer	
NaCl	150 mM
Tris (pH 7.5)	25 mM
NaF	10 mM
EDTA	0.5 mM
Triton	1%

To isolate proteins from organs, 100 to 200 mg of tissue were homogenized with beads in an adequate volume of RIPA buffer containing protease and phosphatase inhibitors using the FastPrep™-24 instrument. Cell homogenates were sonicated, centrifuged and stored as described above.

3.2.3.2 Determination of protein concentration

The amount of proteins was measured using the bicinchoninic acid protein assay (BCA) either from a commercial kit (Sigma) or an internal protocol. In principle, the assay (similar to Lowry and Bradford assays) is based on a colorimetric biochemical reaction between bicinchoninic acid and copper sulfate. Briefly, peptide bonds reduce Cu^{2+} ions from copper sulfate into Cu^{+} ions at 37°C. The amount of copper reduced is proportional to the amount of protein present in the solution. Molecules of bicinchoninic acid chelate each Cu^{+} ion forming a purple-colored complex which is measurable by absorption spectrophotometry. Solutions containing known concentration of bovine serum albumin (BSA) were used as standards (0.078 – 5 µg BSA/µl) to calculate the amount of proteins.

Samples were diluted if necessary and 5 µl of each sample or standard were mixed with 200 µl of bicinchoninic acid solution (containing 2% copper sulfate) in 96-well plate. After 30-40 min incubation at 37°C, absorbance was measured at 562 nm using a microplate reader (Tecan). Protein concentrations were graphically determined using the standard curve based on BSA standards.

3.2.3.3 SDS-Polyacrylamide gel electrophoresis (SDS-PAGE)

Protein samples (10-50 ug) were denaturated with an appropriate volume of 4X Roti®-load SDS loading buffer (at a ratio 3:1) 10 min at 95°C and cooled on ice. Resolving gel containing 8-15% acrylamide and stacking gels containing 5% acrylamide were casted using Bio-Rad electrophoretic cells. After polymerization, gels were immersed in electrophoresis buffer and combs removed. The protein samples and a prestained marker were loaded onto the stacking gel and migration was performed at 80V. Once the migration line reached the resolving gel, the voltage was fixed at 100-120V until the end. Afterwards, gels were subjected to western blotting.

Electrophoresis buffer	
Glycine	196 mM
Tris-HCl (pH8.4)	20 mM
SDS	0.1%

3.2.3.4 Western blots (WB)

Proteins were transferred onto pre-activated (with methanol) PVDF membranes using a tank-blotter filled with transfer buffer. The blotting was performed at constant intensity (0.25 mA) during 2 hours in a cold environment.

Membranes were then incubated with an adequate blocking buffer (2.5% milk powder, 5% BSA or Odyssey® blocking buffer) for 1 hour at room temperature, followed by the application of primary antibody either in Tris-buffered saline (TBS) containing 0.1% tween (TBS-T) or in blocking buffer at a dilution of 1:500-1:1000. Incubation was performed overnight at 4°C under

constant rolling. To remove unspecifically bound antibodies, membranes were washed 3 times for 10 min each with TBS-T. Membranes were then probed with Odyssey® IRDye secondary antibodies (diluted 1:10000 in TBS-T) for 1 hour at room temperature. After washing 3 times for 10 min each with TBS-T, signals were detected using the Odyssey® infrared imaging system.

Transfer buffer	
Glycine	200 mM
Tris	20 mM
Methanol	20%

TBS-T buffer	
NaCl	150 mM
Tris	50 mM
Tween 20	0.5%

3.2.3.5 Enzyme-linked immunosorbent assay (ELISA)

A commercially available ELISA kit (USCN Life Science Inc.) was used to measure serum mouse Cross Linked C-Telopeptide of Type I Collagen (CTX-I) which is a metabolite of bone resorption. The kit is a sandwich enzyme immunoassay for the *in vitro* quantitative measurement of mouse CTX-I in serum, plasma and other biological fluids. Analysis was performed according to the manufacturer's protocol.

3.2.4 Isolation, culture and treatments of mouse and rat macrophages

Mice and rats were sacrificed by cervical dislocation and several organs were used as a source of progenitor or differentiated resident macrophages.

3.2.4.1 Isolation and differentiation of progenitors from bone marrow

After a dorsal incision, the skin was peeled from both hindlimbs and long bones were collected (tibias and femurs). Bones were then aseptically cleaned off muscles with gaze and quickly washed with 70% ethanol. After epiphyses were cut out, diaphyses were flushed with sterile cold PBS using a 1ml-syringe and 25-G needle until bone cavity appeared empty (transparent). Cells were centrifuged 5 min at 1000 rpm, resuspended in complete DMEM medium (DMEM containing 1g/l glucose, glutamine, pyruvate, 100 U/ml penicillin/streptomycin and 10% FBS) and seeded in 2 culture dishes (150 mm diameter). After overnight incubation, nonadherent cells were collected, centrifuged 5 min at 1000 rpm and resuspended in complete DMEM medium. After counting, $8x10^5$ cells were seeded per well (for a 6 well-plate format) with 2 ml complete DMEM medium containing 25 ng/ml recombinant macrophage colony stimulating factor (M-CSF). After 3 days, 2 ml of complete medium containing 25 ng/ml M-CSF were added. On day 6, culture supernatants were removed and adherent differentiated macrophages were incubated in fresh complete medium containing 10 ng/ml M-CSF and used for further analysis.

3.2.4.2 Isolation of resident macrophages from peritoneal cavity

Upon sacrifice, the abdominal skin was carefully removed and 10 ml cold PBS (1% FBS) was injected with a syringe into the peritoneal cavity. After shaking the abdomen, an incision was performed to collect resident macrophages in suspension. The peritoneal wash was then centrifuged 5 min at 1000 rpm and the cell pellet was resuspended in complete DMEM medium. The cell suspension was seeded for 2 hours, nonadherent cells were removed and adherent macrophage cells were used for further experiments.

3.2.4.3 Doxycycline treatment *in vitro*

Macrophages differentiated and isolated from shRNA transgenic rats were treated 2-6 days with 1 µg/ml doxycycline in complete DMEM medium (with 10 ng/ml rat M-CSF) to induce the expression of the shRNA against (P)RR/ATP6ap2 and the subsequent reduction of (P)RR/ATP6ap2 protein levels.

3.2.4.4 Starvation-induced autophagy

To induce autophagy, differentiated macrophages were washed 2-3 times with PBS and incubated 2-6 hours with Hanks balanced salt solution (HBSS), a medium without amino acids and serum. Alternatively, autophagy was induced chemically using complete medium containing 1 µM Rapamycin, an mTOR inhibitor. To block the fusion of lysosomes with phagosomes and the resolution of autophagy, 1µM of Bafilomycin, a specific inhibitor of V-ATPases, was used in some conditions. After treatments, cells were washed 2-3 times with PBS and used for live staining, fixed for immunostaining or frozen for proteins and RNA extraction.

3.2.4.5 Analysis of intracellular pH

To have an indication of the pH in intracellular compartments, several pH sensitive dyes were used. After appropriate treatment, macrophages were incubated with 1 µM LysoSensor™ Green DND189 or 50-75 nM LysoTracker® Red DND99 for 15-45 min. After addition of DAPI (to stain nuclei) 10 min before the end of the experiment, cells were washed with PBS and live imaging was immediately performed using confocal microscopy.
Macrophages were also incubated with 100-200 ng/ml pHrodo™ red *E.Coli* bioparticles® for 30-60 min, washed with PBS and intracellular labeling was analyzed by FACS or confocal microscopy.
Some experiments were conducted in the presence of Rapamycin (1 µM) to block endocytosis or Bafilomycin (1µM) to inhibit V-ATPases with both treatments starting 30 min before incubation with the dyes.

3.2.4.6 Analysis of phagocytosis

After differentiation, macrophages were incubated with Fluospheres® carboxylate-modified microspheres, 2 µm, blue or yellow/green fluorescent beads (2.5 x 10^6 beads/ml) for 30-60 min. After several washes with PBS, cells were analyzed by FACS or incubated with DAPI and fixed with PFA for confocal microscopy observation.

3.2.4.7 Analysis of membrane receptor recycling

Macrophages were washed 2 times with PBS, serum starved for 30-60 min and pulsed with medium (complete DMEM medium without FBS) containing 25 µg/ml transferrin-Alexa Fluor 647 conjugate for 15-25 min. Cells were washed 3 times with PBS to withdraw the excess of transferrin, and chase was performed in complete DMEM medium without FBS for 15-45 min. Cells were then washed 2 times with PBS, fixed with 4% PFA for 15 min and finally conserved in PBS. Macrophages were immediately observed under confocal microscopy or further immunostaining were performed.

3.2.4.8 Immunohistochemistry

After fixation with 4% PFA, macrophages were washed with PBS and permeabilized 30 min with PBS-Tr (1X PBS, 0.1% triton). To block unspecific binding of the antibodies, macrophages were incubated with PBS-Tr containing 3% normal donkey serum for 30 min. Macrophages were washed 3 times with PBS and incubated with first antibody in TBS-Tr overnight at 4°C. Cells were washed 3 times (5 min) with PBS and incubated 1 hour with the adequate fluorochrome-conjugated secondary antibody in PBS-Tr at room temperature in dark. DAPI (1/2000) was added for 15 min and macrophages were washed 3 times with PBS (5-10 min). Cells were immediately observed under a confocal microscope or conserved in PBS at 4°C in the dark.

3.2.5 Isolation and differentiation of mouse osteoclasts

3.2.5.1 Primary cells and osteoclastogenesis

Bone marrow cells were isolated from long bones in α-MEM medium as previously described. Primary splenic cells were isolated as follow: spleens were aseptically removed, minced in pieces in α-MEM medium (α-MEM medium, 10% FBS, 100U/ml P/S, 1% glutamine) and passed through 70µm sieves.

Cell suspensions were centrifuged 5 min at 1,000 rpm. Cell pellets were resuspended in α-MEM medium and cells were seeded in 6-well plates overnight. After 18-24 h incubation, non-adherent cells were harvested counted and the desired amount of cells was resuspended in α-

MEM medium (2.10^6 cells/ml) containing 15 ng/ml recombinant human M-CSF (hM-CSF). Cells were seeded either on plastic or sterile glass surface at a density of 650,000 cells/cm^2 for splenic macrophages and 500,000 cells/ cm^2 for BMMs. After 2 days, medium was changed for α-MEM medium containing 15 ng/ml hM-CSF and 50 ng/ml recombinant mouse RANKL (mRANKL). Medium was changed every 3 days until multinucleated osteoclasts were observed.

3.2.5.2 Bone-resorbing activity

After overnight incubation, non-adherent cells were harvested and seeded on Biocoat™ Osteologic™ Discs (BD Biosciences) or ivory slices (gift from Prof. Uwe Kornak). Cells were differentiated as described above for 6-9 days. For the discs, resorption was assessed immediately by microscopy. For the ivory slices, osteoclasts were removed by sonication and black ink was added on slices. After 1 min incubation, the excessive ink was removed carefully with a wet tissue and resorption pits were observed by microscopy

3.2.5.3 Trap and phalloidin staining

Fully differentiated osteoclasts grown on glass cover slips were fixed with 4% PFA for 15 min at 4°C, washed 3 times with PBS and then incubated with trap staining solution for 15 min at 37°C. Osteoclasts were washed 3 times with PBS and permeabilized with 0.1% Saponin/3% BSA in PBS for 10 min at room temperature. After 3 additional PBS washes, cells were incubated with Phalloidin Alexa Fluor 488 conjugate (1:400 dilution) and DAPI (1:1000 dilution) in PBS for 1 hour in dark at room temperature. Cover slips were washed 3 times with PBS and mounted on slides with Fluoromont-G water-soluble compound for microscopy.

Trap staining solution	
Trap buffer	5 ml
Fast Red Violet LB	3 mg
Naphtol solution	50 µl

Trap buffer	
Sodium acetate	40 mM
Sodium tartrate	10 mM

Naphtol solution	
Naphtol-phosphate	10 mg
N-N-dimethylformamide	1 ml

3.2.6 Flow cytometry

3.2.6.1 Collection of cells from different organs

Peripheral blood was collected into EDTA-coated tubes, inverted and kept on ice. Suspensions of bone marrow cells were obtained by flushing femurs with FACS buffer (cold PBS containing 2% FBS) using a 1ml syringe and a 23G needle. Spleens were collected and cells were dissociated through 70 and 40 µm meshes with FACS buffer to obtain single splenic cell suspension. Peritoneal cells were collected form peritoneal wash.

All cell suspensions were transferred into 15 ml falcons and incubated 2 min with 1 ml of 1X BD™ Pharm Lyse™ in order to lyse red blood cells. The reaction was stopped by addition of 5 ml of FACS buffer and centrifuged for 5 min at 1000 rpm. The supernatant was discarded and cells were resuspended in 1 ml FACS buffer and kept on ice.

3.2.6.2 Preparation, blocking and staining of cells for flow cytometry

To analyze myeloid and lymphoid subsets, cells were resuspended in FACS buffer, distributed in 96-well plate and centrifuged 5 min at 4°C and 1000 rpm. Supernatants were removed and cells resuspended in blocking buffer (FACS buffer for rat cells and FACS buffer containing anti-mouse CD16/32 Ab (1:1000) and kept 20 min at 4°C. After centrifugation 5min at 4°C and 1000rpm, cells were resuspended in FACS buffer containing a panel of fluorescent dye-labeled antibodies (Table 3) and incubated at 4°C in the dark for 30 min. Samples were centrifuged 5min at 1000 rpm, then washed one time with FACS buffer and fixed with 2% PFA (in FACS buffer) 10 min in the dark at room temperature. After a last centrifugation, cells were finally resuspended in FACS buffer and stored in the dark at 4°C until use.
To study mouse stem cells markers, cells were processed as described for myeloid and lymphoid cells without blocking the cells with anti-mouse CD16/32 Ab since it is described as a marker of myeloid progenitors.

3.2.6.3 Flow cytometry

Dilution and efficiency of all antibodies have been previously optimized. Single staining of bone marrow or splenic cells was used for compensation to avoid spectra overlap.
For flow cytometry, cells were transferred into FACS tubes together with approximately 0.5 ml of PBS and analyzed using the BD™ LSRFortessa™ or LSR II FACS analyzers and BD FACSDiva software. Data were subsequently treated with the FlowJo software.

3.2.7 Cloning

3.2.7.1 Vectors

Table 15: Vectors

Inserts	Vectors	Company (location)
rat (P)RR	pGEM-T	Promega (Madison, WI, USA)
rat (P)RR	pcDNA3.1 (+/-)	Invitrogen (Darmstadt, Germany)
sh(P)RR	pINV7	Taconic (Cologne, Germany)

3.2.7.2 Restrictive digestion of DNA

Digestions of double-stranded DNA molecules were performed with appropriate restriction enzymes in their respective buffers as recommended by the manufacturer. Digestion with 2 enzymes was carried out with adequate commercial buffer either in one step or in sequential steps. The reaction mixture (Table 16) was incubated 1 hour at 37°C. Digestions were performed to linearize vectors, to control a construct or to validate the correct ligation of an insert into a vector.

Table 16: Reactive components for restrictive digestion.

Components	Quantity
Each enzyme	5 µl
Each buffer	10 µl
Plasmid DNA	10 µg
H2O	x µl
Total volume	100 µl

3.2.7.3 Gel purification

Products from digestions were loaded into agarose gels with an adequate ladder to assess their molecular weights. After migration at constant voltage (100 V), gels were observed under a UV lamp and fragments of interest were excised with a scalpel. These fragments were purified using the Wizard® SV Gel and PCR Clean-up System (Promega) following the manufacturer's instructions.

3.2.7.4 Ligation of linear fragments

Highly efficient ligation of linear DNA fragments into an appropriate vector was performed using the T4 DNA ligase enzyme (Promega). The ligation reaction (Table 17) was incubated 1 hour at room temperature and then maintained at 4°C until being electroporated into *Escherichia Coli* (*E. coli*) bacteria.

Table 17: Reactive components for ligation.

Components	**Quantity**
Vector DNA	50 ng
Insert DNA	100-300 ng
T4 DNA ligase (5 U/µl)	1 µl
Ligation buffer 10X	1 µl
H2O	x µl
Total volume	10 µl

3.2.7.5 Preparation of electrocompetent *E. coli*

For initial bacterial growth, 100 ml of lysogeny broth (LB) medium were inoculated with a single colony of *E. coli* (DH5α strain) and shaken overnight at 37˚C. For the second growth, 1 ml of overnight culture was transferred into 250 ml of LB medium and bacteria were allowed to growth at 37˚C until an optical density of 0.6. The bacterial culture was then placed on ice for 15 min and centrifuged at 2600 g for 15 min at 2˚C. *E. coli* were washed two times with 250 ml and 10 ml of 10% glycerol (in water), centrifuged again and finally resuspended in 2 ml of 10% glycerol. Bacteria were split into 30 µl aliquots and stored at -80˚C until use.

3.2.7.6 Transformation of electrocompetent *E. coli*

One aliquot of competent cells was gently thawed on ice for 5 min and mixed with 1-5 µl of the ligation reaction. The mixture was transferred to a prechilled cuvette on ice and electroporation was performed at 1350 V for 5 ms (Electroporator 2510). Immediately, 1 ml of LB medium was added and transformed cells were transferred to a sterile Eppendorf tube. After shaking 30-60 min at 37˚C, 2 µl were mixed with 50 µl LB medium and disposed on ampicillin-agar plate.

LB medium	
Yeast extract	5 g
Bactotrypton	10 g
NaCl	10 g
Ampicillin	100 µg/ml
H2O	1 l

LB plates	
Agar	15 g
LB medium	1l

Sterile beads were added and shaking allowed a proper dispersion of the cells over the agar. After carefully removing beads, the plate was incubated overnight at 37˚C to allow bacterial growth.

3.2.7.7 Plasmid extraction and purification

After overnight growth and ampicillin selection, the LB plate contains many bacterial colonies. Most of them are formed by transformed *E. coli* (containing the plasmid). A sterile tip was used to pick a single colony and transferred immediately into a falcon tube containing 5 ml LB medium. This was performed for several colonies to increase the chance of collecting one with bacteria containing the correct construct. Falcons were shaken (180 rpm) overnight at 37˚C. Two milliliters of culture were transferred to an Eppendorf tube and centrifuged 5 min at 8000 rpm. The pellet was resuspended in 250 µl of Solution A (table 18) by vortexing. Cells were lysed by adding 250 µl of Solution B (Table 18) and mixed gently by inversion. The lysate was incubated 5 min at room temperature. For neutralization, 250 µl of Solution C (Table 18) were

added before mixing again by inverting to obtain a white clot made of DNA/proteins/SDS. Afterwards, the homogenate was incubated on ice for 15-30 min. Cell debris and chromatins were pelleted by centrifugation at 13,000 g for 10 min. The supernatant was transferred to a new tube and 500 µl of isopropanol were added to precipitate the DNA (plasmid). After a further centrifugation, the pellet was washed with 500µl of 70% ethanol and centrifuged again 15 min at 13,000 g. The pellet was then dried under a hood to allow the total evaporation of ethanol and finally dissolved in 20-50 µl DNase-free water or TE buffer.

Table 18: Solutions for extraction and purification of plasmids.

Solution A		Solution B		Solution C	
Glucose	50 mM	NaOH	100 mM	Potassium acetate	3.1 M
EDTA pH 8.0	10 mM	SDS	0.5%		
Tris HCl pH 8.0	25 mM				
RNaseA	0.4 mg/ml				

3.2.7.8 Quality control of plasmids

Plasmid concentration was measured using a Nanodrop2000 (Thermo Scientific).
Control of the construct was performed by restrictive digestion as described above. In addition, samples were sent to the Invitek Company (Berlin Buch) for sequencing.

3.2.8 Cell culture

3.2.8.1 Cell lines

Cos7 is a fibroblast-like cell line derived from the kidney of an African green monkey and immortalized with SV40 virus. These cells were used for transfection of plasmids.
RAW264.7 is a mouse leukemic monocyte/macrophage cell line derived from tumors induced in male BALB/C mice by the Abelson murine leukemia virus. These cells were used as osteoclast precursors.

Table 19: Cell lines and respective culture media

Cell lines	Medium
Cos7 (fibroblast-like cells)	DMEM high glucose 10% FBS - 100 U/ml P/S - 1% β-mercaptoethanol
RAW264.7 (monocytes/macrophages)	DMEM high glucose 10% FBS - 100 U/ml P/S 1%

Both cell lines originated from stocks of the ATCC Global BioRessource Center (USA) and were cultured in the appropriate medium (table 19) under Mycoplasma-free conditions in Heracell incubators (Heraeus Instruments GmbH) at 37°C and 5 % CO2 under water-saturated atmosphere.

3.2.8.2 Preparation and maintenance of cell lines

Cells were obtained and maintained frozen in vials at -190°C. Cells were thawed quickly in warm water (37°C) and immediately resuspended in their respective pre-warmed medium (Table 19). Cells were centrifuged 5 min at 1000 rpm to eliminate DMSO present in freezing medium (see below), resuspended in warm culture medium and transferred to a culture dish. Media were changed every 2-3 days until cells reached 80 % confluence. To split the cells (passage), they were washed with warm PBS and trypsinized with trypsin (Gibco) or Triple™ Express (Gibco) for 5 min at 37°C. Cells in suspension were collected with fresh medium and seeded into new dishes at the desired dilution. To freeze the cells, they were trypsinized, centrifuged 5 min at 1000 rpm and resuspended in freezing medium (FBS containing 10% DMSO). Cells were transferred to a Cryovial (Simport) and placed in frost container (Nalgen) containing isopropanol overnight at -80°C to ensure a homogeneous cooling. Frozen vials were finally stored either in a normal box at -80°C or in liquid nitrogen.

3.2.8.3 Differentiation of RAW264.7 cells into osteoclasts

RAW264.7 cells were trypsinized and 5.10^5 cells were suspended in differentiation medium (α-MEM medium, 5 % FBS, P/S) containing 50 ng/ml RANKL (Peprotech) in 6 well-plate. The medium was changed every 2 days until osteoclasts were formed (6-8 days). Cells were collected at different time points for protein and RNA extraction.

3.2.8.4 Transfection of Cos7 cells and efficiency of the shRNA construct

Cos7 cells were trypsinized, counted and seeded at a density of 8.10^5 cells/well in 12 well-plates. After overnight culture, cells were incubated with 800 µl medium in absence of antibiotics (P/S) for 4-6 hours. Cos7 cells were then co-transfected by addition of 200 µl of Opti-MEM (4% lipofectamine) containing plasmids coding for rat (P)RR/ATP6ap2 and ptetO-sh(P)RR/ATP6ap2-tetR or shegfp. Doxycycline (Dox) was added in some wells to the final concentration of 1µg/ml. Media (+/- Dox) were refreshed everyday. After 72 hours, cells were washed with PBS, scrapped in RIPA buffer and protein extracted as previously described. Efficiency of the shRNA construct was assessed controlling (P)RR/ATP6ap2 protein level by western blot as previously described.

3.2.9 Animal work

3.2.9.1 Animal husbandry

All animals were kept in pathogen-free conditions at the Max Delbrück Center animal facility according to the German Animal Protection Law. Mice and rats were housed in individually ventilated cages at a constant temperature of 21±2˚C, with a 12h light/12h dark cycle and a free access to standard chow (0.25% sodium, SSNIF) and drinking water *ad libitum*.
Breedings were performed by crossing 2 females and 1 male in a single cage and pups were weaned and genotyped (tail cut) 21 days postpartum. A maximum of 6 animals of the same sex were further maintained per cage.
All animal procedures were in accordance with the guidelines provided by the Landesamt für Gesundheit und Soziales (LAGeSo).

3.2.9.2 Generation of shRNA transgenic rats

Transgenic rats were generated in the group of Prof. Michael Bader at the MDC, according to established methods with the help of Dr. Elena Popova (Popova et al. 2004, Kotnik et al. 2009). Briefly, complementary sense and antisense oligos (shRNA) specifically targeting a sequence in the exon 9 of the rat (P)RR/ATP6ap2 mRNA were designed and ordered (BioTeZ Berlin Buch-GmbH). Both oligonucleotides were annealed and cloned into the bimodal pINV7 vector (Taconic) and tested *in vitro*. To generate transgenic rats, a 4 kb DNA fragment containing ptetO-sh(P)RR/ATP6ap2-tetR was cut out with *PacI* and *KpnI* restriction enzymes. The fragment was purified from an agarose gel using a QIAquick Gel Extraction Kit following manufacturer's instruction, dissolved at 3 ng/µl with microinjection buffer (8 mM Tris-HCl, pH 7.4 and 0.15 mM EDTA) and microinjected into fertilized oocytes of SD rats. Eggs were maintained in culture for 2 hours and subsequently transferred into pseudo-pregnant SD foster mothers. The transgenic rat line was named sh3/4 rats. Integration of the transgene was detected by transgene specific PCR on genomic DNA isolated from tail biopsies with the primers TetRfor: 5′-CAA GTT GCC AAG GAG GAG AG -3′ and TetRrev: 5′-AAC CGG TCT AGA ATC GAT GG -3′.

3.2.9.3 Doxycyclin treatment *in vivo*

To induce expression of shRNA against (P)RR/ATP6ap2, animals were treated with doxycycline (Dox; Sigma) in the drinking solution. The Dox solution was freshly prepared each day and kept dark due to the light sensitivity of Dox. To check the functionality of the system, animals were treated with 0.5 g/l Dox in the drinking water for 8 days and (P)RR/ATP6ap2 protein and RNA levels were analyzed in organs by western blot and real time PCR, respectively.

3.2.9.4 Blood composition

Blood was taken either from the tail of conscious animals (2 drops) or from cardiac puncture of deeply anesthetized animals (100 mg/kg ketamine hydrochloride (Ketavet) and 10 mg/kg xylazine (Rompun)). Blood was homogenized in EDTA tubes (Greiner bio-one) and cell composition was analyzed using a Scil Vet abc hematocytometer (Scil).

3.2.10 Skeleton and bone analysis

3.2.10.1 Skeleton preparation for bone and cartilage staining

After sacrifice, skin and organs were removed and animals were fixed in 95% ethanol for five days, changing ethanol every day. Skeletons were then immersed in staining solution containing alcian blue and alizarin red (Table 20) for 3 days in darkness. Samples were rehydrated with 70%, 40% and 15% ethanol, each dilution for one hour. After 2 hours in water, tissues were cleared with 1% KOH for 3 days, changing solution every day. Finally, samples were cleared through 20%, 50% and 80% glycerol in 1% KOH for 1-3 days each. Skeletons were then stored in 100% glycerol.

Table 20: Composition of the alcian blue/alizarin red staining solution

Components	Volume (ml)
0.3% alcian blue 8GS in 70% ethanol	10
0.2% alizarin red S in 95% ethanol	10
glacial acetic acid	10
70% ethanol	170

3.2.10.2 Micro-computed tomography

Tibias and spines were collected after mice were sacrificed by cervical dislocation. Bone were cleaned carefully and stored in 4% PFA. Bones were analyzed by micro-computed tomography (µCT) using the Skyscan 1172 system (Skyscan). For bone density, samples were measured with a multi-sample holder at a 9 µm pixel size, 180° rotation, rotation angle 0.5°, filter AI 0.5 mm, random movement 2, voltage 80 kV and current 124 µA. Raw data reconstruction was performed with NRecon software. Quantitative analysis occurred with CTan software after definition of regions of interest (ROIs). In tibias, trabecular and cortical parameters were assessed through ROIs comprising 50 consecutive scan slices as described in Fig 13. In lumbar vertebrae, the entire trabecular bone was analyzed.

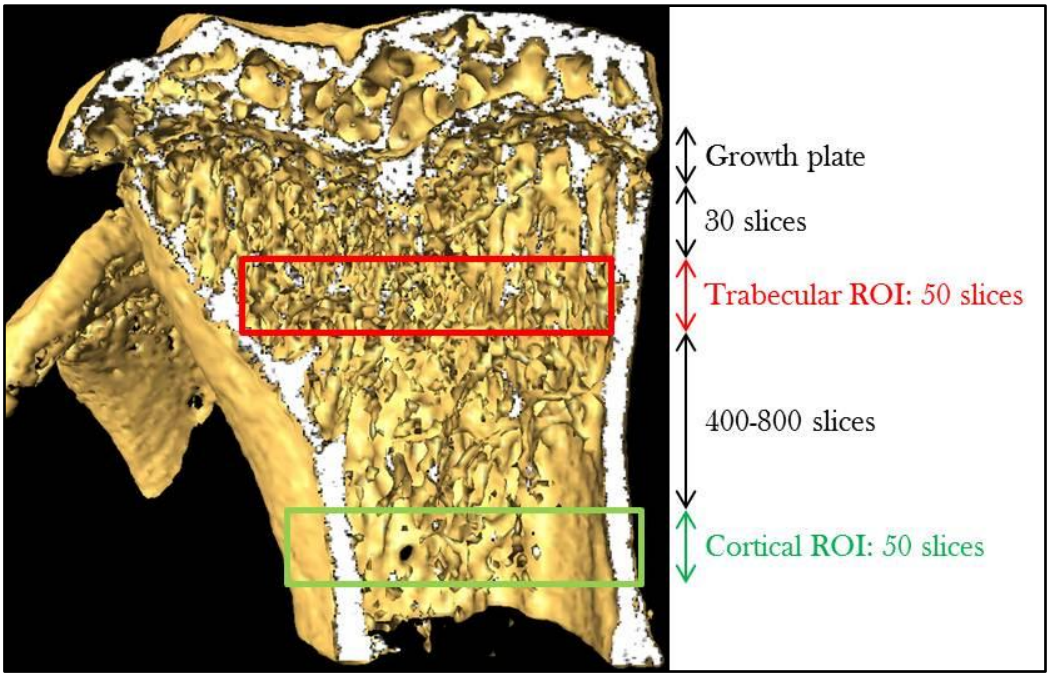

Fig. 13: Areas for trabecular and cortical bone measurements.

3.2.11 Histology

3.2.11.1 Preparation of paraffin sections

For paraffin sections, tissue samples were fixed 48 hours in 4% PFA at 4˚C. Incubation in 0.5 M EDTA (pH 7.4) was additionally performed for bones in order to decalcify them and obtain a soft tissue easier to cut. After fixation, samples were washed twice with PBS and dehydrated through a serie of ethanol solutions (50%, 70%, 80%, 96% and 100%) for 1 hour each step. Complete dehydration was achieve by successive incubation in methanol and toluene for 1 hour each step. For paraffin embedding, samples were pre-infiltrated with paraffin for 2 hours at 67˚C and finally embedded in fresh paraffin at 67˚C. Tissue sections (4-6 µm) were produced with a rotary microtome, placed on glass slides, air-dried overnight and stored at room temperature. For further staining, sections were deparaffinized by successive incubations: 3 times xylol for 5 min, 3 times 100% ethanol for 5 min, 1 time in 90%, 80%, 70% and 50% ethanol for 5 min each, washed in distilled water for 5 min and finally incubated in TBS.

3.2.11.2 Hematoxylin and Eosin staining (HE)

The hematoxylin and eosin staining was based on the recommendations of the manufacturer's instructions. Briefly, deparaffinized and rehydrated sections were stained with hematoxylin solution for 3 min, rinsed with running tap water for 10-20 min, dipped in acid ethanol 10 times and rinsed again in deionized water for 2 min. Sections were then stained with eosin solution for 30 s, rinsed in deionized water and dehydrated through a serie of ethanol solutions (50, 70, 80,

96 and 100%) for 5 min each step. Samples were cleared 3 times in xylene for 5 min, coverslipped in mounting medium and stored at 4˚C in the dark until observation.

3.2.11.3 Picrosirius (Sirius) red staining

Deparaffinized and rehydrated sections were stained with picrosirius red solution (0.1% Sirius red F3B in saturated aqueous solution of picric acid) for one hour at room temperature. Sections were then rinsed 2 times with acidified water (0.5% glacial acetic acid) and dehydrated 3 times in 100% ethanol for 5 min. Sections were cleared 5 min in xylene, mounted, coverslipped and stored at 4˚C in dark until observation.

3.2.11.4 Toluidine blue staining

Deparaffinized and rehydrated sections were stained with toluidine blue working solution (Table 21) for 2-3 min, rinsed 3 times with distilled water, quickly dehydrated 2 times in 100% ethanol and cleared in xylene for 3 min. Sections were mounted, coverslipped and stored at 4˚C until observation.

Table 21: Composition of the toluidine blue working solution.

Components	Volume (ml)
1% Toluidine blue O in 70% ethanol	10
1% Sodium chloride in water (pH 2.3)	10

3.2.11.5 Trap staining

Deparaffinized and rehydrated sections were stained either with the “acid phosphatase, leukocyte (TRAP) kit” (Sigma) following the manufacturer’s instructions or with the Trap staining solution used for osteoclasts in culture and described in part 3.2.5.3.

3.2.11.6 Terminal deoxynucleotidyl transferase dUTP nick end labeling

Deparaffinized and rehydrated sections were stained for DNA fragments (as a result of apoptosis) using the “In situ cell death detection kit, Fluorescein” (Roche). A positive control was generated by incubation of a section with DNase-I for 10 min at 25˚C. Sections were permeabilized with permeabilization solution (PBS, 0.1% triton, 0.1% sodium citrate) for 2 min, washed with PBS and stained following the manufacturer’s instructions. Sections were mounted

with Vectashield-DAPI mounting medium, coverslipped and stored at 4˚C in the dark until observation with fluorescence microscope.

3.2.11.7 Immunohistochemistry

Deparaffinized and rehydrated sections were incubated 20 min in Tris-EDTA buffer pH 9.0 at 95˚C for antigen retrieval. After washing 2 times in PBS at room temperature for 15 min, sections were blocked 30 min in blocking solution (10% normal donkey serum in PBS) at room temperature to prevent unspecific antibody binding. Sections were then incubated with primary antibody diluted in blocking solution overnight at 4˚C in wet chamber. After washing 3 times 10 min with PBS, sections were incubated with appropriate secondary antibody conjugated to a fluorophore diluted in PBS for 2 hours at room temperature in wet chamber. Sections were washed 3 times 3 min with PBS, mounted with Vectashield-DAPI medium, coverslipped and stored at 4˚C in the dark until observation with fluorescence microscope.

3.2.11.8 Preparation of plastic sections

For plastic sections, bones were fixed 48h in 4% PFA at 4˚C and stored in 70% ethanol at 4˚C. Bones were dehydrated in subsequent ethanol steps (70, 80, 90, 100%) of 24h each, incubated in 50% ethanol in acetone for 12h, washed in 100% ethanol for 12h, cleared in xylene 2 times for 2h and embedded in methyl methacrylate (MMA) according to standard laboratory procedures. Tissue sections (5 µm) were generated using a rotary microtome and collected in 0.5% Triton in water. Sections were incubated 5-10 min in 70% ethanol/ethylene glycol monobutyl ether (3:2 v/v), compressed between Kisol-Folie and dried 24h at 58˚C. For deplastification, sections were incubated 3 times in 2-methoxyethyl-acetate for 10 min and 2 times in xylene for 3 min. For rehydration, sections were incubated in subsequent ethanol steps (100, 90, 70 and 50%) for 1 min each and washed 5 min in distilled water. Sections were kept dry until further staining.

3.2.11.9 Von Kossa/Toluidine blue staining

Deplasticized sections were rehydrated 5 min in distilled water, incubated 2 min in 1% nitrate silver solution, washed 3 times with distilled water for 1-2 min, incubated 2min in 5% sodium carbonate/10% formaldehyde and washed 10 min under running water. Sections were then incubated 5 min in 5% sodium pyrosulfate, washed 10 min under running water, rinsed in distilled water, counterstained 1-5 min in 0.025% toluidine blue solution and quickly rinsed again in distilled water. Color contrast was obtained by incubation in subsequent ethanol steps (70, 90 and 100 %) for 2 min each, cleared 2 min in xylene, mounted with Entellan® medium, coverslipped and stored at room temperature in dark until observation.

3.2.12 Statistics

All data were subjected to statistical analysis using the GraphPad Prism 6 software (San Diego, CA, USA). Results in this study are presented as mean ± SEM (standard error of mean). The Student's t-test was applied for comparisons between independent pairs of means. Three or more groups were analyzed using one-way ANOVA with Bonferroni post-test. Differences with a P-value (Pv) of $Pv<0.05$ were considered to be statistically significant.

RESULTS

CHAPTER 4

4.1 Osteoclast-specific deletion of (P)RR leads to growth retardation and bone loss in mice

4.1.1 RANKL induces (P)RR expression *in vitro* and *in vivo*

(P)RR expression level was examined in RAW264.7 cells (monocytes/macrophages) treated with RANKL. At the protein level, little (P)RR expression could be detected in RAW264.7 cells at baseline. RANKL induced an increase of (P)RR protein level already detected after 1 day and further significantly increased after 4 and 5 days of treatment (Fig. 14A). Quantitative RT-PCR revealed that (P)RR mRNA level was significantly induced after RANKL treatment already at day 1 and reached a maximum at day 2 which was concordant with protein level. This upregulation occurred at different amplitudes when using either β-actin (Fig. 14B) or Hprt (Fig. 14C) as reference genes.

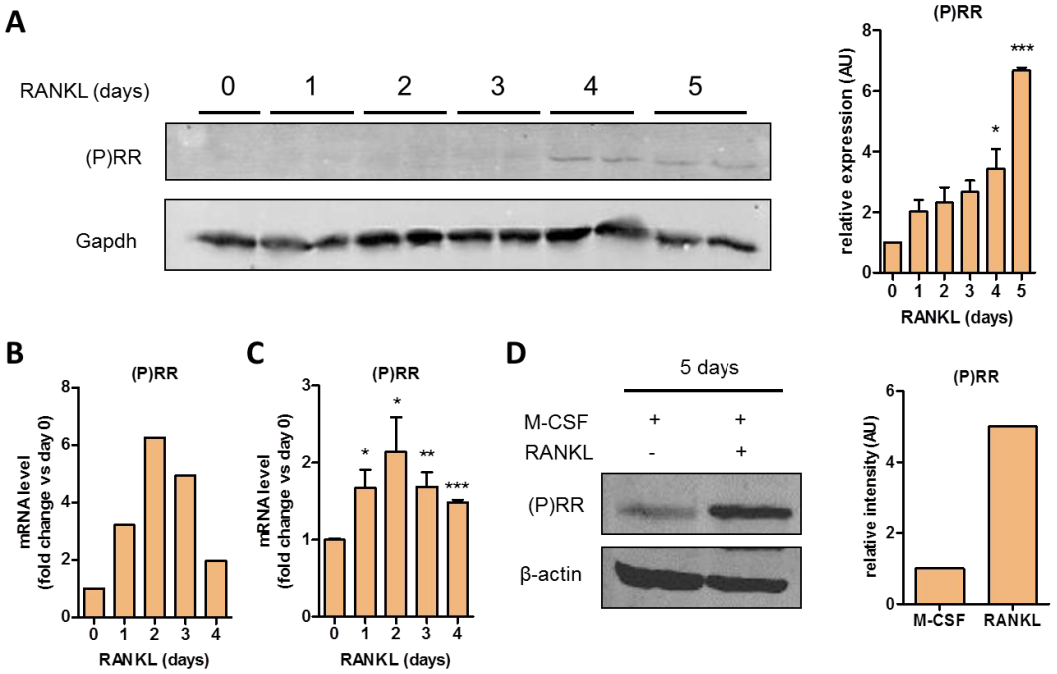

Fig. 14: (P)RR expression is upregulated during RANKL-mediated osteoclast differentiation. (A) (P)RR protein level was detected by western blot in RAW264.7 cells treated with RANKL (50 ng/ml) and normalized to Gapdh. Untreated RAW264.7 cells (day 0) were used as reference (n=2). **(B)** (P)RR mRNA levels were measured by quantitative RT-PCR in RAW264.7 cells treated with RANKL (50 ng/ml) using β-actin (n=1) or **(C)** Hprt (n=5) as reference genes. **(D)** (P)RR protein level was detected by western blot in BMMs treated with M-CSF (10 ng/ml) and RANKL (50 ng/ml) and normalized to β-actin. BMMs treated with M-CSF (10 ng/ml) served as reference. AU, arbitrary unit. **P<0.05; **P<0.01, ***P<0.001 vs. reference.*

In addition, we also found that (P)RR protein level was increased in bone marrow-derived macrophages (BMMs) treated 5 days with RANKL and M-CSF in comparison to control BMMs treated with M-CSF alone (Fig. 14D).

In order to analyze (P)RR expression in osteoclasts *in vivo*, (P)RR immunofluorescence staining was performed on tibia sections. Fluorescence analysis revealed that cells with the strongest signals are most likely osteoclasts as they appeared multinucleated and at the surface of trabecular bone (Fig. 15A and 15B). Other cell types including chondrocytes, osteoblasts and osteocytes displayed a weak (P)RR immunostaining. Altogether, these results suggested that (P)RR might be important during osteoclast differentiation and/or function.

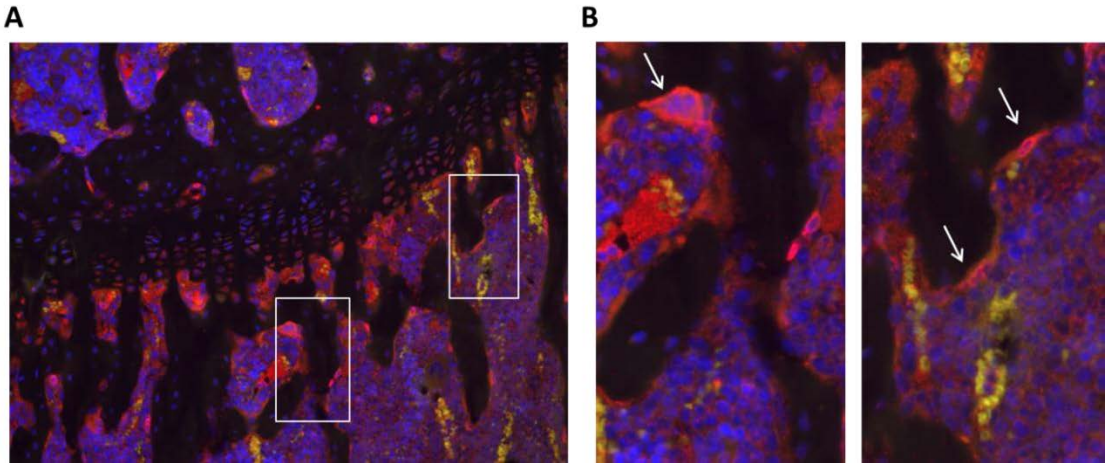

Fig. 15: (P)RR is strongly expressed *in vivo* by osteoclasts. (A) Representative picture of (P)RR immunostaining on tibia section. Strong fluorescence signals characterized multinucleated osteoclasts present on the surface of bone trabeculae. Image is magnified X20 **(B)** Increased size of the two white rectangular inserts. Arrows identified multinuclear osteoclasts. Nuclei were stained with DAPI (blue).

4.1.2 Generation of mice with a specific (P)RR deletion in osteoclasts

Our early attempts to generate mice with a global (P)RR deletion were unsuccessful as it likely resulted in early embryonic lethality (Sihn et al. 2010). To circumvent this early death, conditional deletions of (P)RR in mice using the Cre/Lox system were developed. Mice in which the exon 2 of the *(P)RR* gene is flanked with LoxP site have been generated (Riediger et al. 2011). To assess the role of (P)RR in osteoclasts, we crossed *(P)RR*$^{flox/wt}$ heterozygous females to transgenic mice expressing the Cre recombinase under the control of the endogenous Cathepsin K (CtsK) promoter (Fig. 16A). Mice with a homozygous deletion of the *CtsK* gene develop osteopetrosis whereas heterozygous mice have normal bone architecture (Li et al. 1996). To avoid homozygousity of the knockin allele, *(P)RR*$^{wt/y}$ males with one copy of the Cre (*Cre*$^{+/0}$) were used for breedings (Fig. 16A). The resulting *(P)RR*$^{flox/y}$, *Cre*$^{+/0}$ males were osteoclast-specific conditional knockout (cKO) animals (Fig. 16A and 16B). We used *(P)RR*$^{wt/y}$, *Cre*$^{+/0}$ and *(P)RR*$^{flox/y}$, *Cre*$^{0/0}$ male littermates as controls (Ctrl) to exclude any Cre- and flox-mediated toxicity (Fig. 16B). Unless otherwise specified, females were not studied. While the CtsK promoter has been documented to drive Cre expression only in mature osteoclasts (Nakamura et al. 2007), we

sought to confirm the specificity in our model. To this purpose, genomic excision of the exon 2 was assessed via the amplification of a 326 bp PCR product specific to the null allele and reflecting the Cre activity. The excision product was detected in the cKO bone as expected and remained absent in other organs from cKO animals and in bone from Ctrl animal (Fig. 16C).

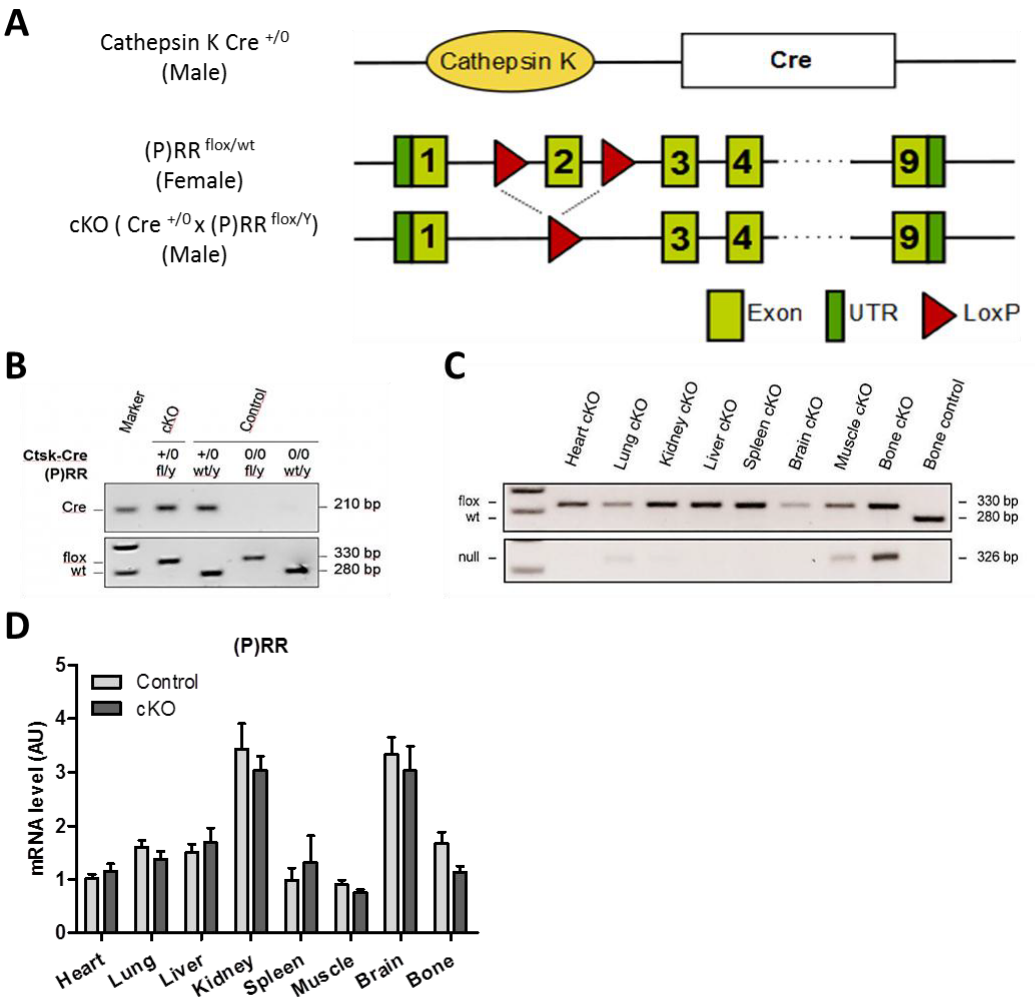

Fig. 16: Conditional inactivation of the *(P)RR* gene using the CtsK-Cre. (A) Floxed (P)RR mice were generated by homologous recombination with a construct in which exon 2 was flanked by loxP sites. Osteoclast-specific excision was performed using transgenic mice expressing the Cre recombinase under the control of the Cathepsin K (CtsK) promoter (adapted from Riediger et al. 2011). **(B)** PCR genotyping depicting the different genotypes: wt (P)RR allele (280bp), floxed (P)RR allele (330bp) and Cre (210bp). **(C)** A 326bp PCR product specific for *(P)RR* excision was only detected in cKO bone. **(D)** Quantitative RT-PCR analysis in various organs did not show any significant difference in (P)RR expression level between cKO and Ctrl animals. TBP was used as reference gene (n=5-8). AU, arbitrary unit.

In addition, (P)RR expression level was assessed in several organs by quantitative RT-PCR and no significant difference between cKO and Ctrl animals was observed although a slight decrease of (P)RR expression in cKO bone was found (Fig. 16D). To explain this weak effect in bone, we have to remember that the deletion of (P)RR occurred only in osteoclasts and not in other cell types of the bone tissue. Therefore, the detection of a drastic difference in bone (P)RR expression is not expected. Altogether, these results validated the efficiency and the specificity of the Cre recombinase in our model.

4.1.3 (P)RR cKO mice have a normal early development

Knowing that newborn mice with a deletion of ATP6V0a3 (Li et al. 1999) and ATP6V0d2 (Lee et al. 2006) V-ATPase subunits are normal, we also monitored the early development of (P)RR cKO mice to rule out any embryonic abnormalities. The cKO mice were born with the expected mendelian frequency without any gross morphological abnormality (data not shown). The body weight of animals at different ages during embryonic development (E16.5 and E17.5) and after birth (1 day and 1 week) was measured and no difference was found in cKO mice compared to Ctrl mice (Fig. 17A and 17B).

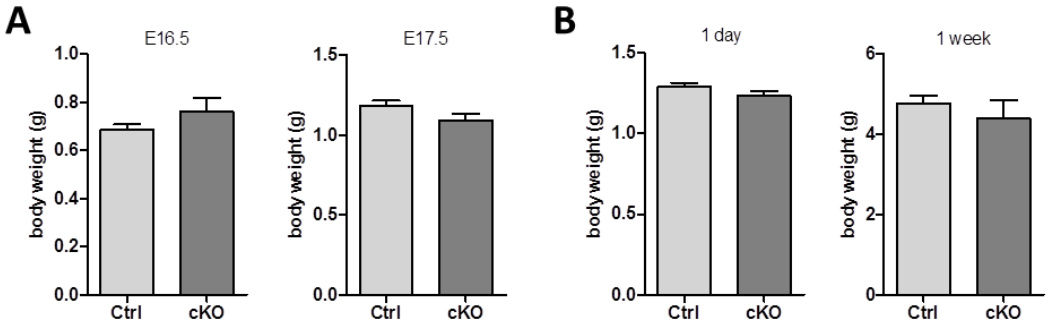

Fig. 17: Body weight of embryos and young mice. (A) Body weight of cKO and Ctrl embryos was measured at the age of 16.5 (E16.5) and 17.5 days (E17.5) *in utero* (n=2-6). **(B)** Body weight of cKO and Ctrl young mice was measured at birth (1 day) and 1 week after birth (n=4-12).

During embryonic development, the liver is the major hematopoietic site before the bone marrow takes over after birth (Godin et al. 2002). As osteoclasts arise from monocytes, we quantified the percentage of CD11b+ Gr1- monocytes by flow cytometry in the liver at 16.5 days of embryonic development (E16.5) and at birth (D1) (Fig. 18A). We also control CD11b+ Gr1+ Ly6G+ neutrophils and CD3- B220+ B lymphoid cells to exclude any abnormalities in the differentiation of myeloid and lymphoid cells (Fig. 18A and 18B). For these three cell types, no difference was observed between cKO mice and Ctrl mice. These different results confirm that (P)RR cKO mice have a normal embryonic and early development.

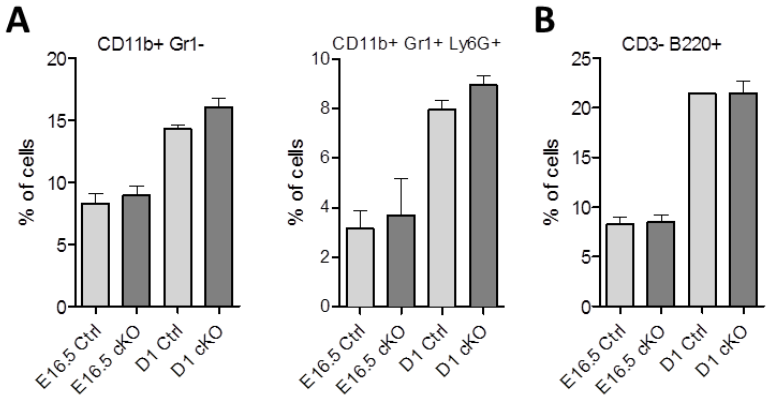

Fig. 18: Hepatic hematopoiesis in embryos and at birth. Flow cytometry was performed on liver from cKO and Ctrl mice at the embryonic stage 16.5 (E16.5) and at birth (D1). **(A)** Percentage of myeloid cells including CD11b+ Gr1- monocytes and CD11b+ Gr1+ Ly6G+ neutrophils. **(B)** Percentage of CD3- B220+ B lymphoid cells. Males and females were pooled (n=2-4).

4.1.4 (P)RR cKO mice exhibit growth retardation

After birth, cKO mice developed progressively a growth retardation which becomes visible after 4 weeks. We monitored the body weight of cKO mice at different ages and indeed detected a significant difference compared to Ctrl mice at 4 weeks of age. The growth retardation aggravated up to 24 weeks of age and was further maintained during the lifetime (Fig. 19A). As cKO mice also appeared shorter, we measured the body length of some animals at 4 and 12 weeks of age. In addition to the decreased body weight (Fig. 19B), these mice were significantly shorter compared to Ctrl mice at both ages (Fig. 19C). This phenotype is illustrated by the picture of 12 week-old cKO and Ctrl mice (Fig. 19D).

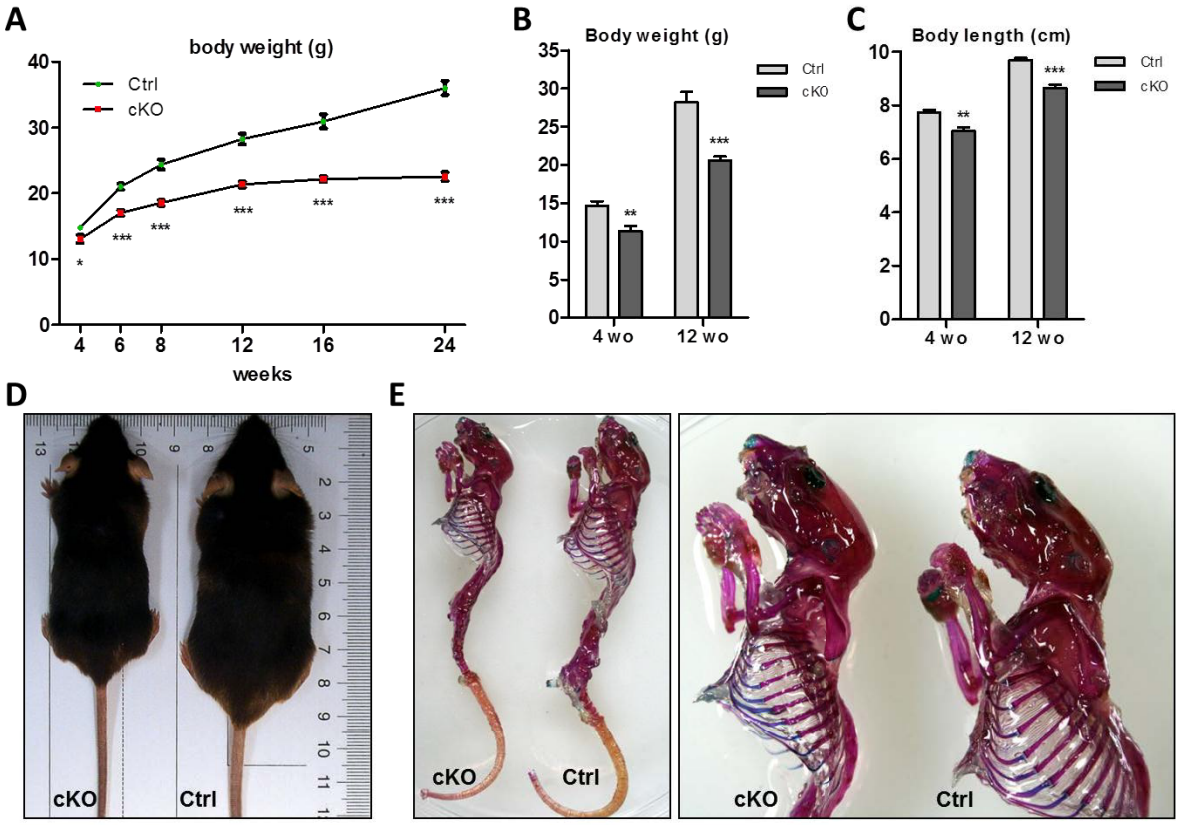

Fig. 19: Growth retardation in young and adult cKO males. (A) Body weight (g) of Ctrl and cKO mice at the age between 4 and 24 weeks (n=11). **(B)** Body weight (g) and **(C)** body length (cm) of Ctrl and cKO mice at the age of 4 and 12 weeks (n=5). **(D)** Picture of Ctrl and cKO at the age of 12 weeks. **(E)** Skeleton morphology of 12 week-old Ctrl and cKO mice revealed by alizarin red (bone) and alcian blue (cartilage) staining. **P<0.05; **P<0.01, ***P<0.001 vs. Control.*

Despite the growth retardation, the skeletal architecture of cKO mice was not perturbed. Skeleton staining with alizarin red/alcian blue solution revealed that bone (red) and cartilage (blue) tissues were similar in appearance and proportions (Fig. 19E) in cKO and Ctrl mice. Absence of teeth eruption has previously been observed in mice with severe osteopetrosis. However, all mice in this study had normal teeth eruption (Fig. 19E and data not shown). To confirm that this phenotype was not transient but maintained throughout life, some animals were observed at one year of age. Pictures of such mice illustrated that the growth retardation in

cKO was maintained during lifetime (Fig. 20A). In accordance, all the parameters measured including body weight, body length, femur and tibia lengths were significantly decreased in cKO mice compared to Ctrl mice (Fig. 20B). Some morphological abnormalities of the face (skin of the nose, semi-closed eyes, orientation of the ears) already observed at adult stage appeared more obvious in old cKO mice (Fig. 20A). More generally, old cKO mice exhibited a deteriorated health status characterized by a sick appearance and a decreased activity (data not shown).

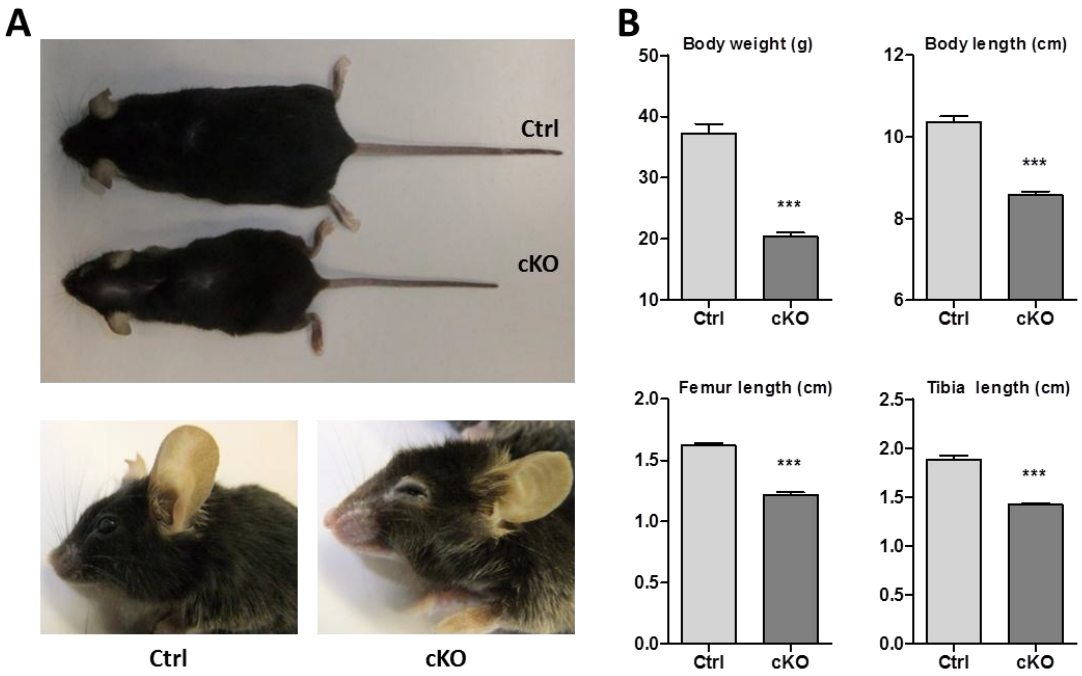

Fig. 20: Growth retardation is maintained in old cKO males. (A) Appearance of Ctrl and cKO mice at the age of 1 year. **(B)** Body weight (g), body length (cm) (n=9-11), femur and tibia length (cm) (n=5) of Ctrl and cKO mice at the age of 1 year. ****P<0.001 vs. Control.*

We also monitored female cKO mice to exclude a sex specific phenotype and to study heterozygous animals. Indeed, only females can be heterozygous for the floxed allele due the gene location on the X chromosome. It was therefore interesting to observe the consequence of (P)RR heterozygous deletion. From our breedings, the *(P)RR*$^{flox/flox}$, *Cre*$^{+/0}$ genotype corresponds to osteoclast-specific conditional knockout (cKO) females and the *(P)RR*$^{flox/wt}$, *Cre*$^{+/0}$ genotype corresponds to heterozygous (Het) females (Fig. 21A). We used *(P)RR*$^{flox/wt}$, *Cre*$^{0/0}$ and *(P)RR*$^{flox/flox}$, *Cre*$^{0/0}$ female littermates as controls (Ctrl) (Fig. 21A). As observed for males, the body weight of cKO females was significantly decreased at 4 weeks of age compared to Ctrl mice (Fig. 21B). The growth retardation of cKO mice aggravated up to 16 weeks of age and was further maintained during lifetime whereas the body weight of Het mice was identical to Ctrl mice at each age (Fig. 21B). A decreased body length was also observed in 12 week-old cKO mice compared to Ctrl mice (Fig. 21C and 21D). In contrast, Het mice were indistinguishable from Ctrl mice. Finally, skeleton staining of cKO females confirmed the normal appearance and proportions of bone and cartilage observed in cKO males in comparison to Ctrl animals (Fig. 21D

and 21E). These results demonstrate that the growth retardation is also present in cKO females but absent in Het female mice and therefore suggest that only homozygous deletion of (P)RR in osteoclasts has deleterious consequences.

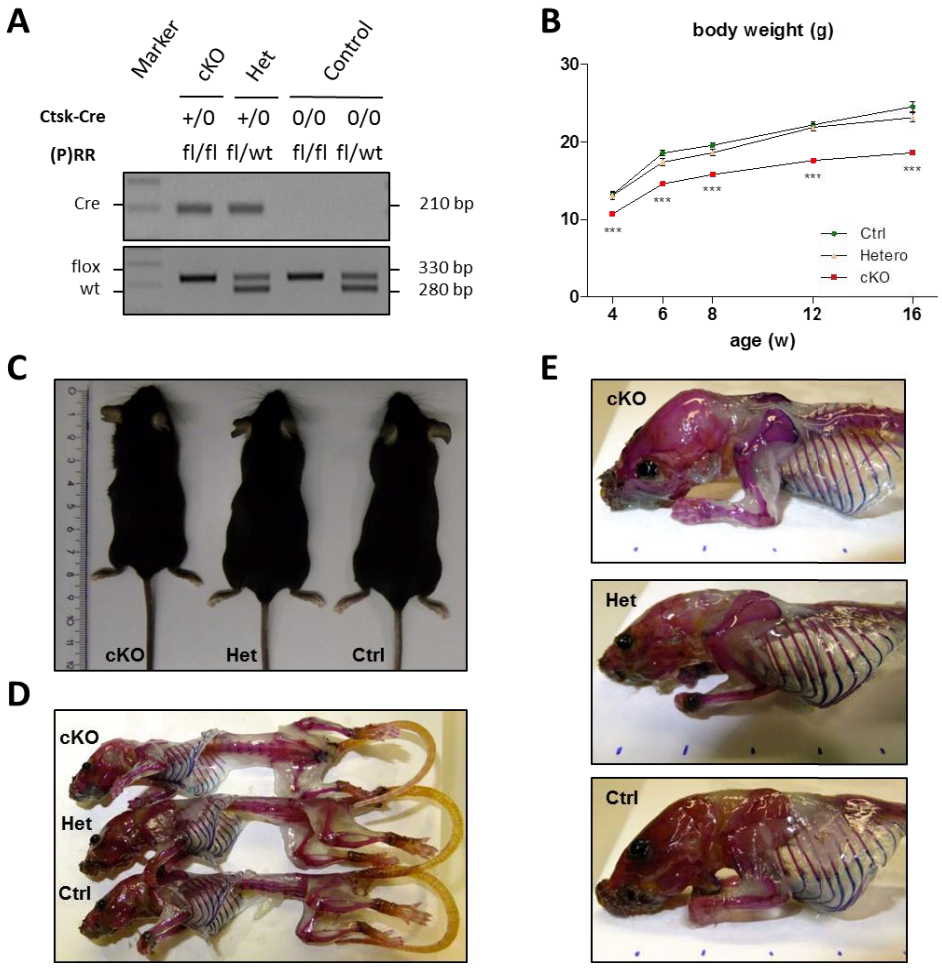

Fig. 21: Growth retardation in cKO female mice. (A) PCR genotyping depicting the different genotypes: wt (P)RR allele (280bp), floxed (P)RR allele (330bp) and Cre (210bp). **(B)** Body weight (g) of Ctrl, Het (heterozygous) and cKO mice at the age between 4 and 16 weeks (n=11). **(C)** Picture of 12 week-old cKO, Het and Ctrl mice. **(D)** and **(E)** Skeleton morphology of 12 week-old cKO, Het and Ctrl mice revealed by alizarin red (bone) and alcian blue (cartilage) staining. ****P<0.001 vs. Control.*

4.1.5 (P)RR cKO mice do not develop osteopetrosis but rather exhibit a decreased bone density

Mice with a deletion of ATP6V0a3 (Li et al. 1999) and ATP6V0d2 (Lee et al. 2006) are characterized by an increased bone density (osteopetrosis). To detect such a skeletal disorder in (P)RR cKO mice, bones were studied in more details. General observation of femurs (Fig. 22A) and tibias (Fig. 22B) of 12 week-old animals confirmed the growth retardation as the length of these bones were significantly decreased in cKO mice compared to Ctrl mice. Nevertheless, the structure and the shape of these bones appeared normal in cKO mice and we also observed red bone marrow denoting the presence of a bone marrow cavity (Fig. 22A and 22B).

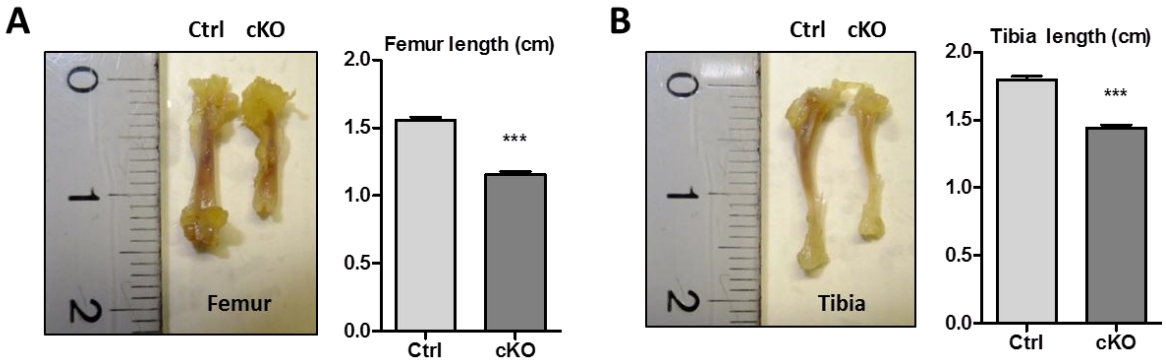

Fig. 22: Femur and tibia lengths. (A) Femur length (cm) and **(B)** tibia length (cm) of 12 week-old cKO and Ctrl mice (n=7). ****P<0.001 vs. Control.*

In order to examine the bone mineral density, we performed radiographic (X-ray) examination of several bones. This technique is commonly used in clinics to detect several bone abnormalities. A radiographic examination highlights the minerals present in bone tissue and thus reflects its density. Spine (Fig. 23A), femur and tibia (Fig. 23B) were exposed to X-rays and no differences in bone mineral density were observed on radiographs between cKO and Ctrl mice at 12 weeks of age. This result contrasts with the increased mineralization and bone density depicted in most of osteopetrotic mice including those with an impaired V-ATPase (Li et al. 1999; Lee et al. 2006) and therefore suggest that (P)RR cKO mice do not develop such a high bone mass phenotype.

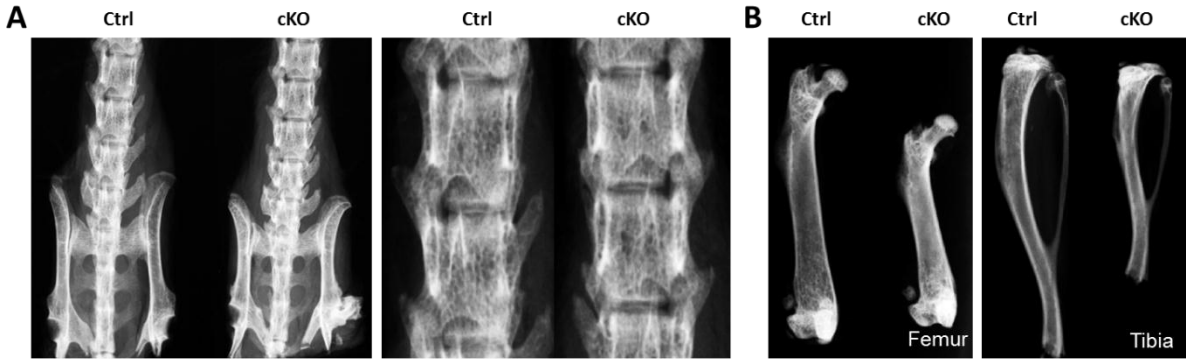

Fig. 23: Radiographic examination of cKO mice. Euthanized 12 week-old Ctrl and cKO mice were exposed to radiographic (X ray) analysis. The white intensity on radiograms reflects the bone density. No difference was observed between Ctrl and cKO bone density. **(A)** Radiograms of spines. **(B)** Radiograms of femurs and tibias.

To further detail the bone phenotype, micro-computed tomography (µCT) was performed following the parameters described in the material and methods section (part 3.2.10.2) and 3D reconstruction was performed using the NRecon software. Tibias from 12 week-old mice were analyzed. A posterior view of the proximal tibia did not reveal any abnormalities in the general shape of the bone in cKO mice (Fig. 24A). In contrast, an anterior view revealed an abnormal shape of the epiphysis and the upper metaphysis of cKO mice compared to Ctrl mice (Fig. 24B).

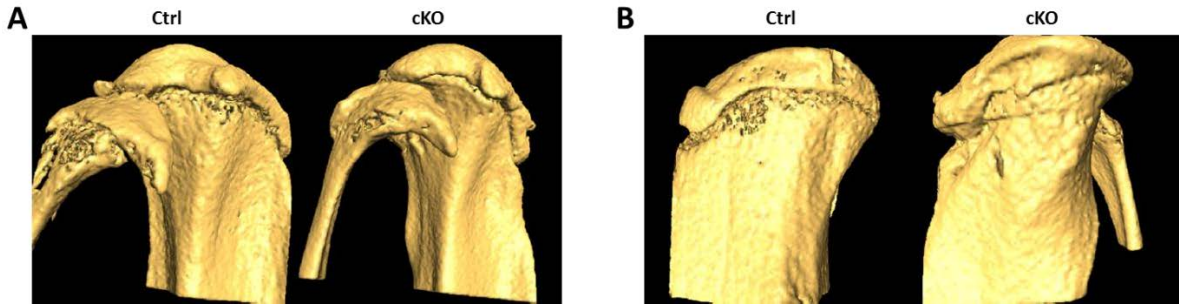

Fig. 24: µCT examination and external tibia shape. Tibias from euthanized 12 week-old Ctrl and cKO mice were fixed in 4% PFA, stored in 70% ethanol and exposed to micro-computed tomography (µCT) analysis. **(A)** Posterior and **(B)** anterior view of reconstructed tibias using the NRecon software.

To better characterize the bone phenotype, regions of interest (ROIs) were delimited to examine the trabecular and cortical bones in the upper tibia and the vertebra as described in the material and methods section (part 3.2.10.2). Animals were observed at different age to detect any evolution and variation of the bone phenotype.

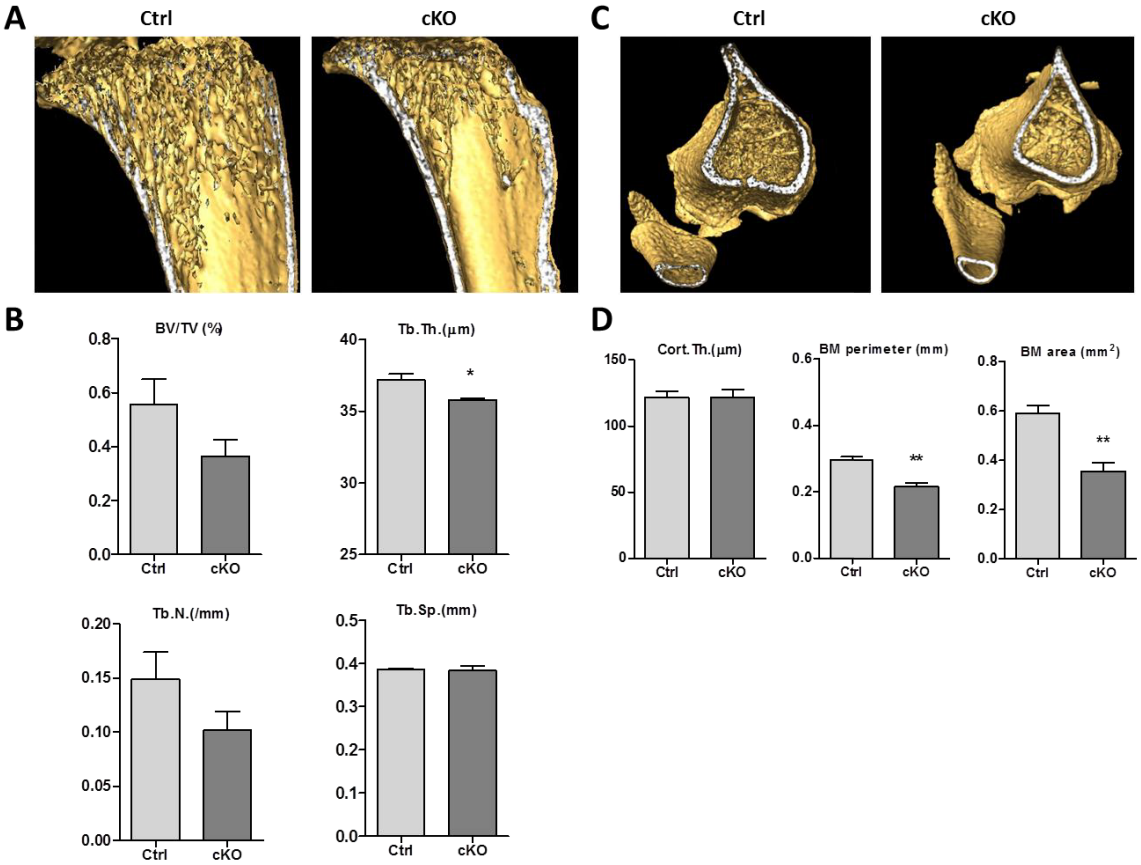

Fig. 25: µCT examination of 4 week-old mice did not reveal any osteopetrosis. Tibias from 4 week-old Ctrl and cKO mice were examined by micro-computed tomography (µCT) analysis and 3D reconstructed. **(A)** Representative image (3D) of trabecular bone. **(B)** Three-dimensional trabecular structural parameters in the secondary spongiosa of the proximal tibia: bone volume per tissue volume (BV/TV, %), trabecular thickness (Tb.Th., µm), trabecular number (Tb.N., /mm) and trabecular spacing (Tb.Sp., mm). **(C)** Representative image of cortical bone. **(D)** Cortical thickness (Cort.Th., µm), bone marrow perimeter (BM perimeter, mm), bone marrow area (BM area, mm^2). (n=4). **P<0.05, **P<0.01 vs. Control*

At 4 weeks of age, the upper tibia did not reveal any increase in bone density. Instead, the bone density seemed to be slightly decreased in cKO mice compared to Ctrl mice (Fig. 25A). This observation was confirmed by several parameters measuring the density of the trabecular bone mass. Bone volume/tissue volume (BV/TV, %) was decreased, albeit not significantly, in cKO compared to Ctrl mice (Fig. 25B). This tendency was also observed for the trabecular number (Tb.N., /mm) which reflects the number of trabeculae (Fig. 25B). However, the trabecular thickness (Tb.Th., µm) which measures the thickness of the trabeculae was significantly decreased in cKO mice (Fig. 25B). In contrast, the trabecular separation (Tb.Sp., mm), which reflects the distance between the trabeculae, was unchanged (Fig. 25B).
This decrease in bone density was specific to the trabecular bone and was not observed in the cortical bone. Indeed, measurement of the cortical thickness (Cort.Th., µm) revealed no difference between cKO and Ctrl mice (Fig. 25C and 25D). A significant decreased of the BM perimeter (BM perimeter, mm) and area (BM area, mm^2) as a consequence of the growth retardation was observed (Fig. 25C and D).
These results highlight the fact that young cKO mice do not exhibit a high bone mass phenotype but rather tend to have a decreased bone density. These results contrast with our hypothesis and with animals deficient for ATP6V0a3 (Li et al. 1999) and ATP6V0d2 (Lee et al. 2006) V-ATPase subunits.

The bone density parameters were also assessed in adult mice at the age of 12 weeks. At this age, representative image of the upper tibia did not reveal any increase in bone density but rather showed a slight decrease of the bone density in cKO mice compared to Ctrl mice as it was described for young animals (Fig. 26A). Concordantly, parameters such as bone volume/tissue volume (BV/TV, %), trabecular number (Tb.N., /mm) and trabecular thickness (Tb.Th., µm) were still lower in cKO whereas the trabecular separation (Tb.Sp., mm) was still unchanged between cKO and Ctrl mice (Fig. 26B). The only difference was the absence of a significant difference for the trabecular thickness in 12 week-old cKO mice compared to Ctrl mice (Fig. 26B). Analysis of the cortical bone confirmed the previous observation made in young animals. Indeed, the cortical thickness (Cort.Th., µm) was identical in both groups whereas the BM perimeter (BM perimeter, mm) and area (BM area, mm^2) were still significantly decreased in cKO mice compared to Ctrl mice (Fig. 26C and 26D).

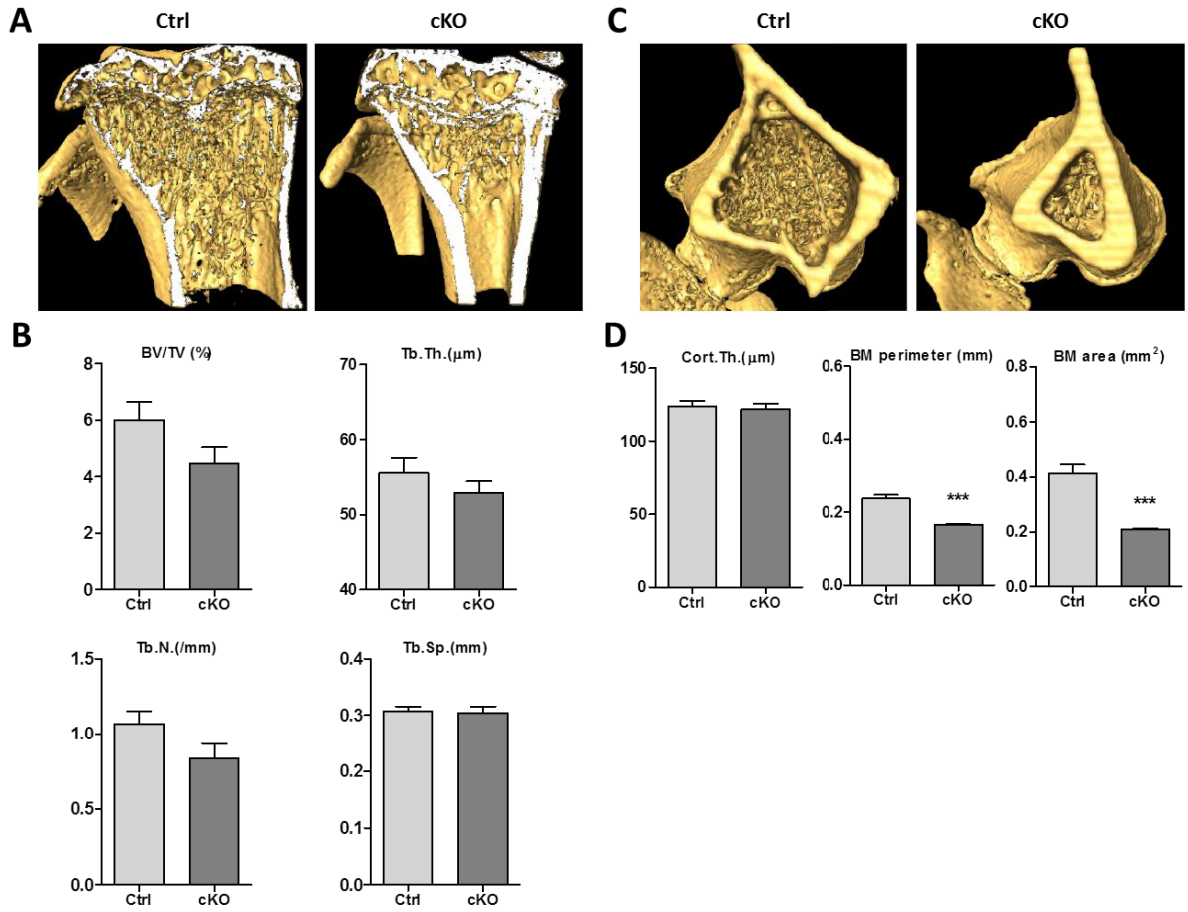

Fig. 26: µCT examination of 12 week-old mice confirmed the absence of osteopetrosis. Tibias from 12 week-old Ctrl and cKO mice were examined by micro-computed tomography (µCT) analysis and 3D reconstructed. **(A)** Representative image (3D) of trabecular bone. **(B)** Three-dimensional trabecular structural parameters in the secondary spongiosa of the proximal tibia: bone volume fraction (BV/TV, %), trabecular thickness (Tb.Th., µm), trabecular number (Tb.N., /mm) and trabecular spacing (Tb.Sp., mm). (n=7-8) **(C)** Representative image of cortical bone. **(D)** Cortical thickness (Cort.Th., µm), bone marrow perimeter (BM perimeter, mm), bone marrow area (BM area, mm^2). (n=4). ****P<0.001 vs. Control*.

In addition to tibias, the bone density of the fifth lumbar vertebrae from 12 week-old mice was also analyzed. Picture of trabecular bone within the lower part of the vertebra did not reveal any osteopetrosis in cKO mice (Fig. 27A) but rather a slightly decreased bone density in cKO mice as described in tibias. The bone volume fraction (BV/TV, %) was decreased, albeit not significantly, in cKO mice (Fig. 27B). The trabecular thickness (Tb.Th., µm) was significantly lower in cKO whereas the trabecular number (Tb.N., /mm) and the trabecular separation (Tb.Sp., mm) remained constant between cKO and Ctrl mice (Fig. 27B). These various parameters were very similar to those observed in tibias and therefore suggest that the decreased bone density was present not only in long bones but also in short bones (vertebra) of the axial skeleton.

In summary, these results show that adult cKO mice have a decreased bone density and do not develop osteopetrosis as it was already observed in young animals.

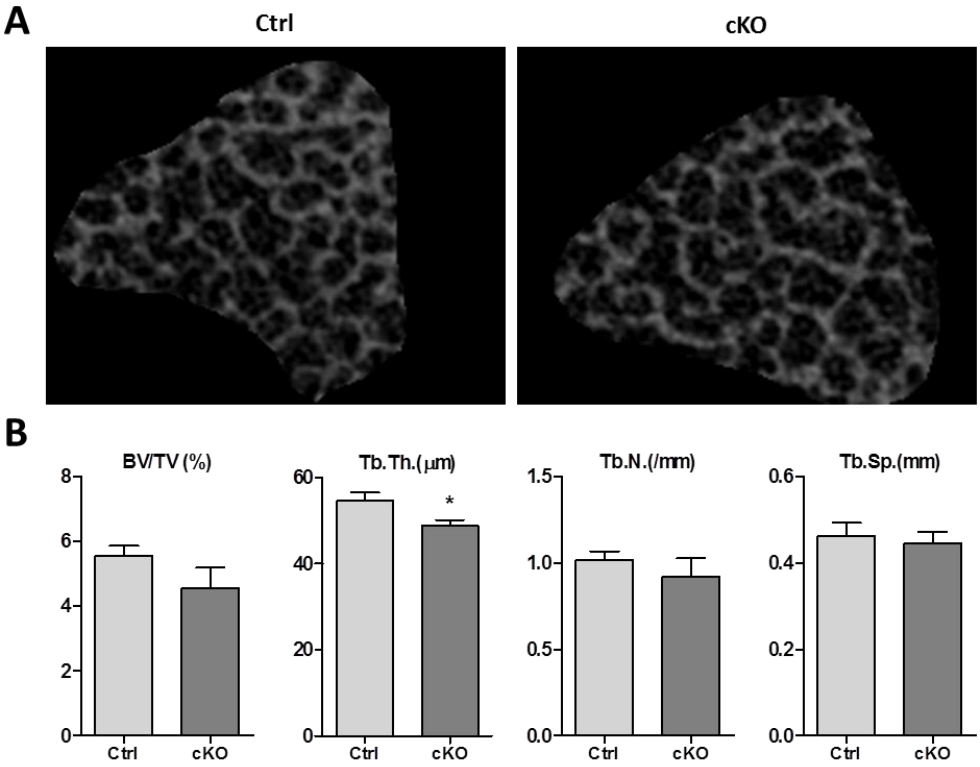

Fig. 27: Absence of osteopetrosis in vertebrae of 12 week-old cKO mice. Spines from 12 week-old Ctrl and cKO mice were examined by micro-computed tomography (µCT) analysis and fifth lumbar vertebrae were 3D reconstructed. **(A)** Representative image (2D) of trabecular bone in the lower part of vertebrae. **(B)** Three-dimensional trabecular structural parameters from the entire vertebra: bone volume fraction (BV/TV, %), trabecular thickness (Tb.Th., µm), trabecular number (Tb.N., /mm) and trabecular spacing (Tb.Sp., mm). (n=5). **P<0.05 vs. Control*

Finally, we also assessed the bone density parameters in tibias of old mice (1 year old) to exclude a potential late development of osteopetrosis. The bone volume fraction (BV/TV, %), the trabecular number (Tb.N., /mm) and the trabecular separation (Tb.Sp., mm) were similar in cKO and Ctrl mice (Fig. 28). In contrast, the trabecular thickness (Tb.Th., µm) was significantly lower in cKO mice (Fig. 28).

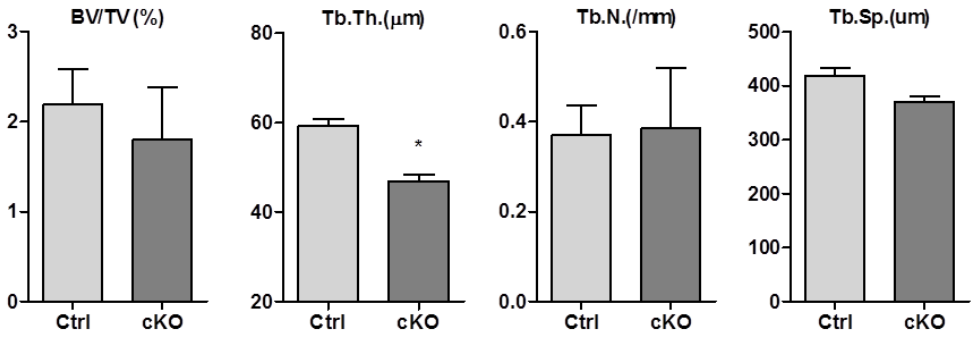

Fig. 28: Absence of osteopetrosis in 1 year-old cKO mice. Tibias from 1 year-old Ctrl and cKO mice were examined by µCT analysis and 3D reconstructed. Three-dimensional trabecular structural parameters from the upper tibia: bone volume fraction (BV/TV, %), trabecular thickness (Tb.Th., µm), trabecular number (Tb.N., /mm) and trabecular spacing (Tb.Sp., µm). (n=2-3). **P<0.05 vs. Control*

These observations show the absence of osteopetrosis in old cKO mice compared to Ctrl mice. Also, the decreased bone density described in young and adult mice remains present in 1 year-old cKO mice.

Contrary to our initial hypothesis, all these µCT data at different ages confirmed that mice with a specific deletion of (P)RR in osteoclasts do not develop osteopetrosis but rather exhibit a growth retardation associated with a decreased bone density in tibias and vertebrae.

4.1.6 (P)RR cKO mice have a normal spleen

Spleen enlargement or splenomegaly has been described in mice with osteopetrosis. This pathological adaptation is a consequence of the increased bone density which leads to an impaired hematopoiesis in long bones. To provide an adequate amount of blood cells to the body, the spleen becomes the prominent hematopoietic organ (extramedullary hematopoiesis) characterized by the presence of a large amount of stem cells which further differentiate in various proportions into all types of circulating cells. As a result of this increased cellularity, the spleen undergoes an increase in size and weight.

Despite the absence of osteopetrosis in our model, we wanted to check whether the complex bone phenotype of the (P)RR cKO mice had an impact on the spleen morphology and function.

To this purpose, spleens from 12 week-old mice were used to conduct visual analysis and flow cytometry. Representative picture of spleens did not reveal any morphological differences between Ctrl and cKO mice (Fig 29A).

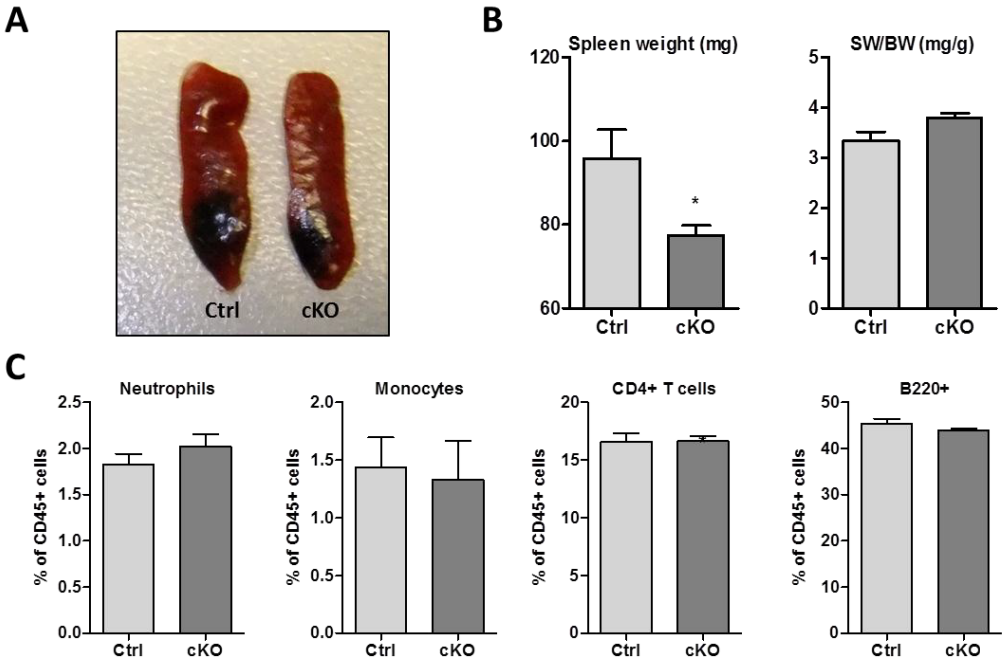

Fig. 29: Absence of splenomegaly in 12 week-old cKO mice. (A) Representative picture of spleens. **(B)** Spleen weight (mg) and spleen weight (mg)/body weight (g) (SW/BW) ratio. (n=6-7). **(C)** Flow cytometry was performed on spleen homogenates. Neutrophils (CD45+ CD11B+ Ly6G+), monocytes (CD45+ CD11B+ Ly6G-), CD4+ T cells (CD45+ CD3+ B220- CD4+) and B cells (CD45+ CD3- B220+) were quantified and expressed as percentage of CD45+ cells. (n=4). **P<0.05 vs. Control*

The spleen weight was significantly decreased in cKO mice compared to Ctrl mice (Fig. 29B). However, due to the growth retardation and the lower body weight of cKO mice, we calculated the spleen weight/body weight (SW/BW) ratio and found no difference between Ctrl and cKO mice (Fig. 29B). These results showed that (P)RR cKO mice have a normal spleen morphology. We further analyzed the proportion of some myeloid and lymphoid cells by flow cytometry. Neutrophils (CD45+ CD11B+ Ly6G+), monocytes (CD45+ CD11B+ Ly6G-), CD4+ T cells (CD45+ CD3+ B220- CD4+) and B cells (CD45+ CD3- B220+) in spleens were found in the same proportions in Ctrl and cKO mice (Fig. 29C). Although we did not directly quantify the amount of stem cells, these results and the absence of splenomegaly strongly suggest that spleens of 12 week-old cKO mice have a normal function and that extramedullary hematopoiesis does not occur. These findings concord with the absence of osteopetrosis and suggest that hematopoiesis in bone is normal in cKO mice.

4.1.7 (P)RR cKO mice have a normal blood composition

To confirm a normal hematopoiesis in (P)RR cKO mice, blood samples from 16 week-old mice were collected and automated blood composition analysis was carried out using a hematocytometer (Scil GmbH). All parameters measured such as levels of white and red blood cells, platelets, hemoglobin and hematocrit as well as percentage of lymphocytes, granulocytes and monocytes were identical in Ctrl and cKO mice (Fig. 30).

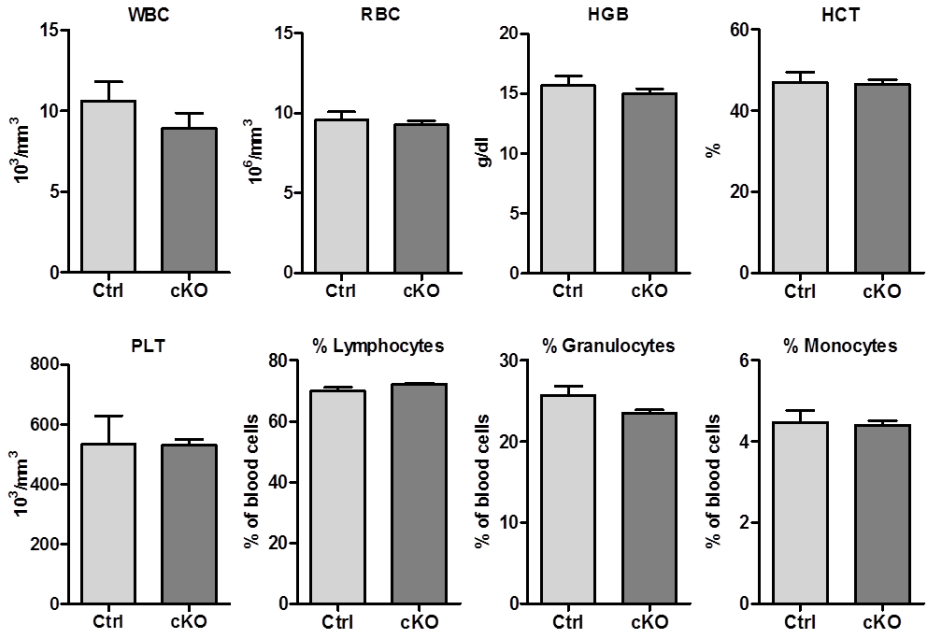

Fig. 30: Blood composition of 16 week-old mice. Blood from 16 week-old mice was taken and subjected to automated blood composition using a hematocytometer (Scil GmbH): number of white blood cells (WBC), red blood cells (RBC) and platelets (PLT); level of hemoglobin (HGB) and hematocrit (HCT); percentage of lymphocytes, granulocytes and monocytes. (n=4)

These results show a normal blood composition and confirm that in the absence of any spleen abnormalities, cKO mice have a normal bone hematopoiesis. Also, it suggests that the decreased bone density observed in these animals alters neither the hematopoietic environment nor stem cell differentiation as all blood cell lineages are present in normal proportions.

4.1.8 Bone histology confirms a decreased bone density in (P)RR cKO mice

After µCT examination, tibias and vertebrae from Ctrl and cKO mice were plastic embedded, sectioned and subjected to Von Kossa staining which stains calcified bone tissue in black. Von Kossa staining on tibia sections from 4 and 12 week-old animals revealed a decreased density of trabecular bone in cKO mice (Fig. 31A) much more pronounced in comparison to the µCT analysis which showed only a slightly decreased bone density (Fig. 26A and B).

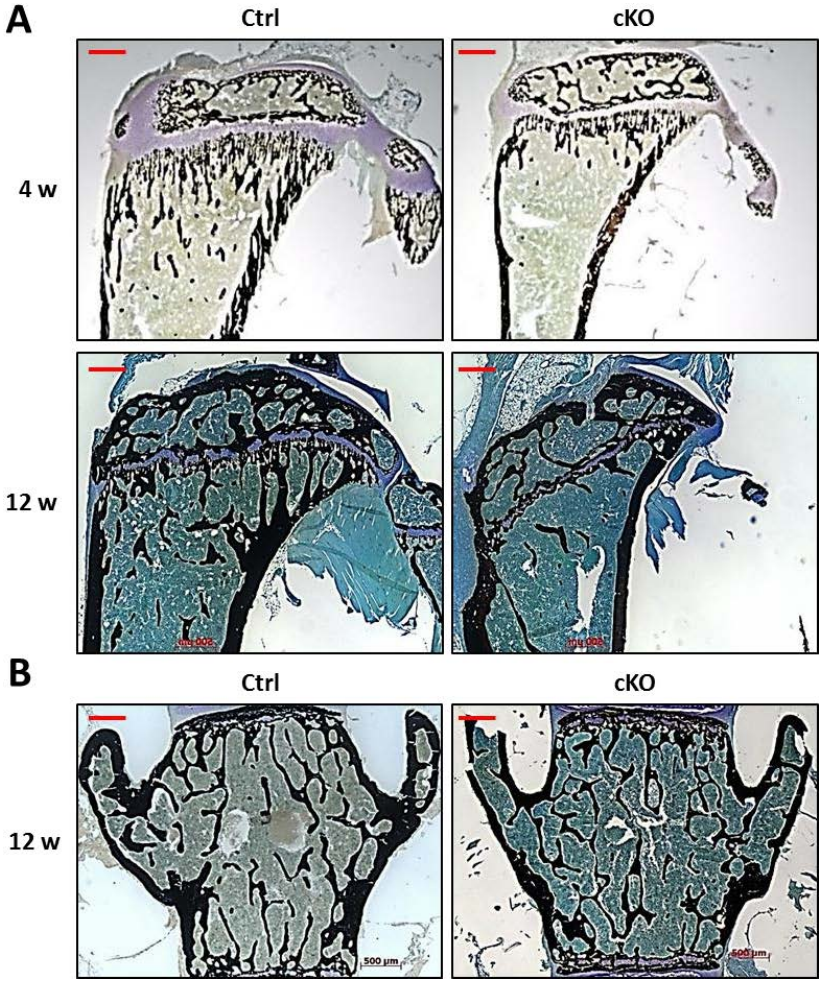

Fig. 31: Von Kossa staining in tibias and vertebrae of 4 and 12 week-old mice. Von Kossa staining (black) on plastic sections of tibias and vertebrae from 4 and 12 week-old mice (A) Representative image of Von Kossa staining on tibias from 4 and 12 week old Ctrl and cKO mice. (B). Representative image of Von Kossa staining on vertebrae from 12 week-old Ctrl and cKO mice. Sections were counterstained in 0.025% toluidine blue solution. Scale bar=500 µm.

As previously observed (Fig. 24B and 25A), cortical bone staining showed that epiphysis and upper metaphysis of cKO mice have an abnormal shape compared to Ctrl mice (Fig. 31A). Additional observation of cortical bone did not reveal any further defects between Ctrl and cKO mice. Von Kossa staining on vertebrae sections from 12 week-old mice confirmed the µCT results with a slight decrease of bone density in cKO compaired to Ctrl mice (Fig. 31B). No defects were observed in the cortical bone.
In summary, µCT analysis and Von Kossa staining show that (P)RR cKO mice have a decreased bone density. These results suggest that (P)RR-deficient osteoclasts have an increased differentiation and/or activity.

4.1.9 (P)RR-deficient osteoclasts have a normal differentiation but an increased resorptive activity *in vitro*

To determine the consequence of (P)RR deletion in osteoclasts, we first assessed whether the (P)RR knockdown was efficient and effective *in vivo*. To this purpose, we performed (P)RR immunostaining on tibia sections from 12 week-old Ctrl and cKO mice. Osteoclasts were identified as multinucleated cells on bone surface (Fig. 32 white arrows). Intensity of (P)RR immunostaining appeared to be decreased in cKO osteoclasts compared to Ctrl osteoclast (Fig. 32). These results confirm that (P)RR deletion in osteoclasts is effective *in vivo*.

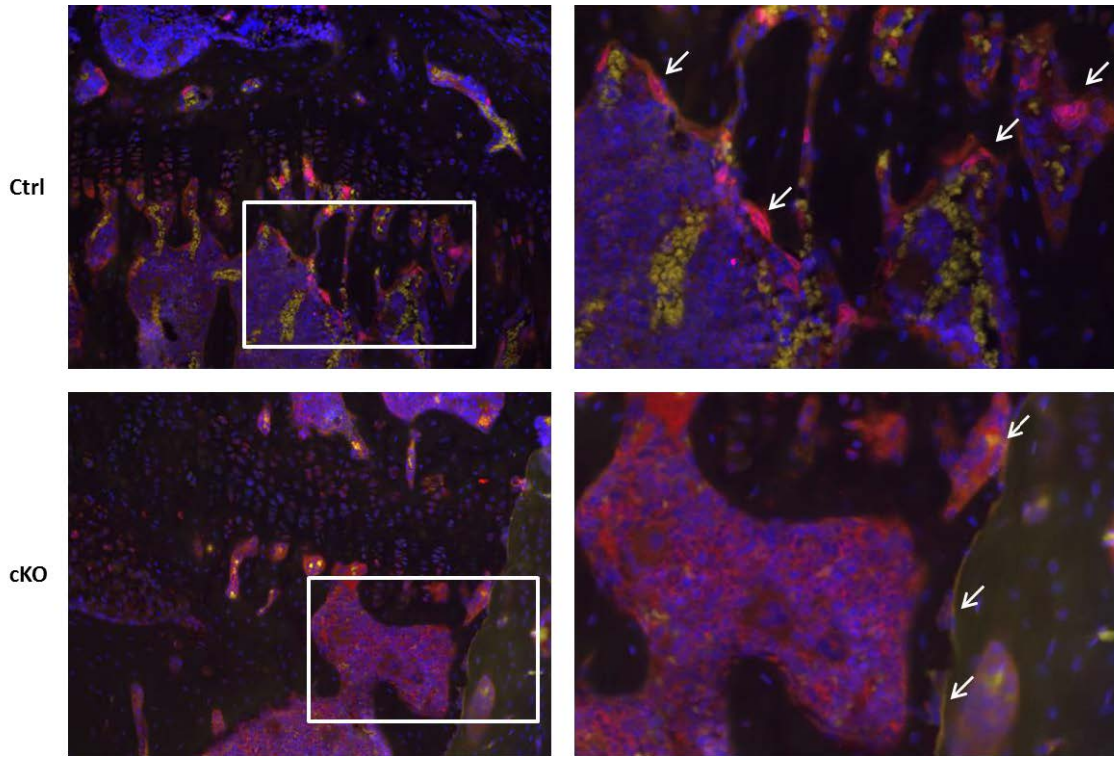

Fig. 32: (P)RR immunostaining in tibia sections of 12 week-old mice. Immunofluorescence staining of (P)RR (red) in paraffin sections of tibias from 12 week-old Ctrl and cKO mice. Representative pictures of trabecular bone within the primary spongiosa (left panel). Images are magnified X20. White boxed areas were enlarged (right panel). White arrows show mature osteoclasts (multinucleated cells). Nuclei were stained with DAPI (blue).

We next aimed to analyze the consequence of (P)RR deficiency on osteoclast differentiation and apoptosis. (P)RR immunostaining provided a first hint that mature osteoclasts were present in cKO mice. To gain further quantitative information, we performed Trap staining on tibia sections from 4 and 12 week-old mice. Trap staining is a common procedure which stains osteoclasts in purple/red. In 4 week-old mice, Trap staining showed numerous osteoclasts on trabeculae with no differences between Ctrl and cKO (Fig. 33A). This result suggested that (P)RR deletion did not interfere with osteoclasts differentiation and did not lead to premature apoptosis. In 12 week-old animals, the number of Trap positive cells (osteoclasts) was decreased in cKO compared to Ctrl mice and suggested that less mature osteoclasts were present in cKO mice (Fig. 33B). However, this effect can be explained by the decreased bone density of cKO mice which was previously characterized by µCT analysis and histology and is also apparent on the bone section subjected to Trap staining (Fig. 33B). Indeed, on the few trabeculae present on cKO tibia sections, Trap positive cells were present in the same proportion as on trabeculae of Ctrl tibia sections. Although not precisely measured, the ratio osteoclast number/bone surface did not seem to be impaired in cKO tibias. Altogether, these data suggest that deletion of (P)RR in osteoclasts do not affect their differentiation *in vivo*. This result was expected since the CtsK-cre is expressed when the differentiation process is already engaged. In addition, these data exclude any premature cell death which has often been described in other cell types after deletion of (P)RR using the cre/Lox technology (Kinouchi et al. 2010, Oshima et al. 2011, Riediger et al. 2011).

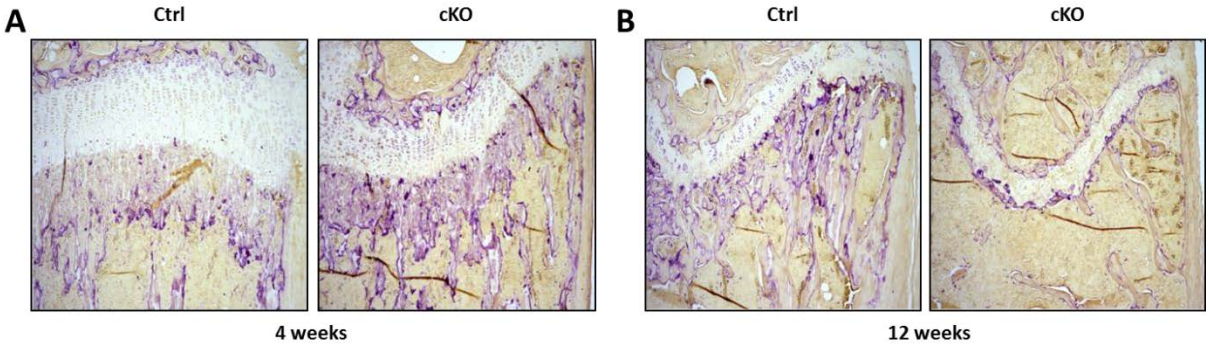

Fig. 33: Trap staining on tibia sections from 4 and 12 week-old mice. Trap staining was performed on paraffin sections using a commercial kit (Sigma). **(A)** Representative Trap staining observed in tibias from 4 and **(B)** 12 week-old Ctrl and cKO mice. Images are magnified X10.

The decreased bone density in cKO mice pointed to a potentially increased activity of (P)RR-deficient osteoclasts. In young animals, osteoclasts are important to invade and resorb the mineralized cartilage matrix during long bone development. Briefly, hypertrophic chondrocytes from the growth plate provide a cartilaginous matrix which is further mineralized (calcified). Invading osteoclasts are important to partially resorb this calcified matrix and create cartilage remnants which serve as template for further bone formation.

To characterize a defect in cartilage resorption, decalcified tibias were embedded in paraffin, sectioned and toluidine blue staining was performed. This histological method stains cartilage

tissue in blue. The amount of cartilage remnants appeared similar in tibia sections from 4 week-old Ctrl and cKO animals (Fig. 34A). In contrast, in tibia sections from 12 week-old mice, persistant cartilage remnants could be observed in Ctrl mice but were totally absent in cKO (Fig. 34B). These results suggest that increased osteoclasts activity in cKO mice have led to an increased cartilage resorption and might explain the decreased in trabecular bone.

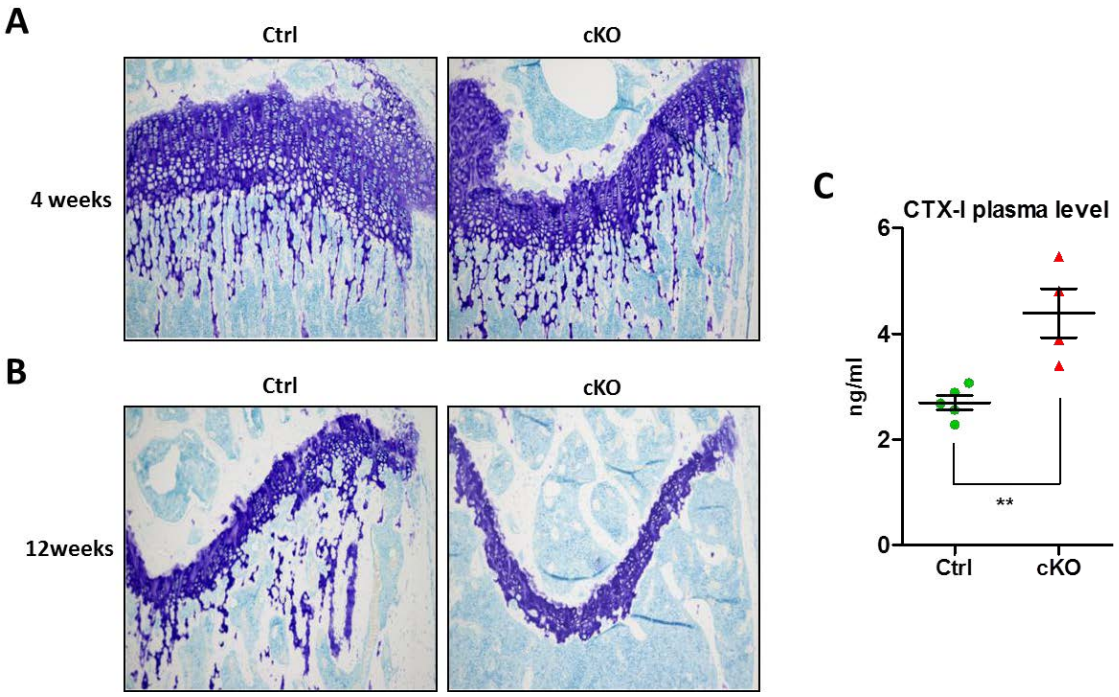

Fig. 34: Increased osteoclast activity *in vivo*. (A) Toluidine blue staining on tibia sections from 4 and **(B)** 12 week-old Ctrl and cKO mice. Images are magnified X10 **(C)** CTX-I plasma level (ng/ml) was measured by ELISA in 12 week-old animals (n=4). ***P<0.01 vs. Control*

In adult animals, bone remodeling is important to maintain bone integrity and renewal. Increased osteoclast activity during this process is associated with bone loss. To determine the activity of (P)RR-deficient osteoclasts, we assessed the plasma level of a marker for bone resorption (C-telopeptide of type I collagen, CTX-I) by ELISA in 12 week-old mice. This degradation product of type I collagen is released during bone resorption. We found a significant increase of CTX-I plasma levels in cKO mice suggesting that (P)RR-deficient osteoclasts have an increased activity during bone remodeling (Fig. 34C).

In summary, these data show that efficient (P)RR deletion in osteoclasts does not impair neither their differentiation nor their apoptosis but rather increases their resorptive activity. (P)RR-deficient osteoclasts seem to have an increased ability to degrade cartilage matrix during bone growth and bone matrix during bone remodeling.

4.1.10 (P)RR-deficient osteoclasts have an increased differentiation *in vitro*

To better understand the consequence of (P)RR deletion on osteoclast physiology, we examined *in vitro* osteoclast differentiation, maturation and activity using bone marrow and spleen cells stimulated with M-CSF and RANKL. We first assessed the efficiency of the CtsK-Cre to delete (P)RR during osteoclast differentiation in culture. To this purpose, genomic excision of the exon 2 was analyzed by PCR and characterized by a 326 bp PCR product. Neither adherent cells (fibroblasts and macrophages) nor bone marrow cells treated 48h with M-CSF (macrophages) were positive for this PCR product (Fig. 35A). In contrast, deletion of the exon 2 was present in macrophages treated with RANKL at each time point from day 1 until day 7. Although these results suggest that the CtsK-Cre was induced by RANKL treatment as early as after 24h, it did not allow any quantification in terms of global gene deletion.

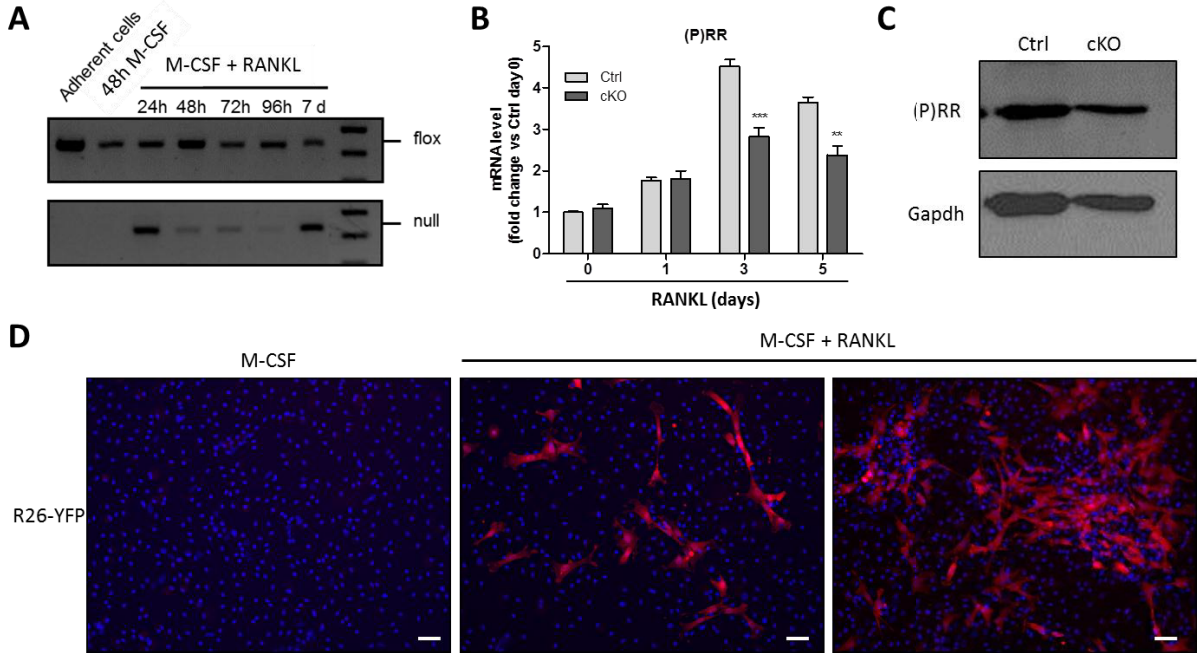

Fig. 35: CtsK-Cre-mediated (P)RR knockdown during *in vitro* osteoclastogenesis. (A) PCR for the floxed (330 bp) and null (326 bp) (P)RR allele. Adherent cells (fibroblasts and macrophages), macrophages treated 48h with M-CSF (20 ng/ml) and macrophages treated with M-CSF (10 ng/ml) and RANKL (50 ng/ml) were analyzed. **(B)** (P)RR mRNA levels were measured by quantitative RT-PCR in BM-derived macrophages treated with M-CSF (10 ng/ml) and RANKL (50 ng/ml) for 0, 1, 3 and 5 days. Hprt was used as reference gene. (n=4). **(C)** (P)RR protein level was detected by western blot in BMMs treated with M-CSF (10 ng/ml) and RANKL (50 ng/ml). Gapdh was used as loading control. **(D)** BM-derived macrophages from (P)RR$^{wt/y}$, Cre$^{+/0}$, YFP$^{+/-}$ were stimulated 5 days with M-CSF (10 ng/ml) and RANKL (50 ng/ml) and immunohistochemistry using anti-GFP antibody was performed. Unstimulated macrophages (day 0) were used as control. Scale bar =50 µm. ***P<0.01, ***P<0.001 vs. Ctrl.*

We examined (P)RR mRNA levels at different stages of differentiation. As previously described, (P)RR expression in Ctrl cells was increased after RANKL treatment with a peak at 3 days of stimulation (Fig. 35B). In cKO cells, we found (P)RR expression level to be significantly decreased after 3 and 5 days of RANKL treatment (Fig. 35B). However, this decrease was not total and matched approximately 40% of Ctrl level. In accordance, (P)RR protein level was

unchanged after 3 days of RANKL treatment (data not shown) and decreased by 50% after 5 days (Fig. 35C). One explanation for this incomplete *in vitro* knockdown was the late induction of the CtsK-Cre during osteoclastogenesis as previously described (Nakamura et al. 2007).

To monitor the induction of the CtsK-Cre at the cellular level, we bred CtsK-Cre positive mice with ROSA26-YFP reporter mice. In this murine model, Cre-positive cells are characterized by the expression of the fluorescent YFP protein present within the R26 locus. Bone marrow cells from *CtsK-Cre$^{+/0}$, YFP$^{+/-}$* were treated with M-CSF and RANKL to induce osteoclastogenesis and YFP expression was assessed by immunohistochemistry using an anti-GFP antibody. After 5 days of treatment, most of the osteoclasts and osteoclast progenitors were positive for the YFP staining (Fig. 35D). In contrast, all mononuclear cells remained negative for the YFP staining. Therefore, the late induction of the Cre (2-3 days) and the presence of these mononuclear cells with no Cre activity during in vitro osteoclastogenesis likely explained results on (P)RR mRNA and protein levels. To determine the impact of (P)RR deletion on osteoclast differentiation, we cultured bone marrow cells with M-CSF and RANKL for 5 days and subsequently observed the formation of Trap-positive multinucleated cells.

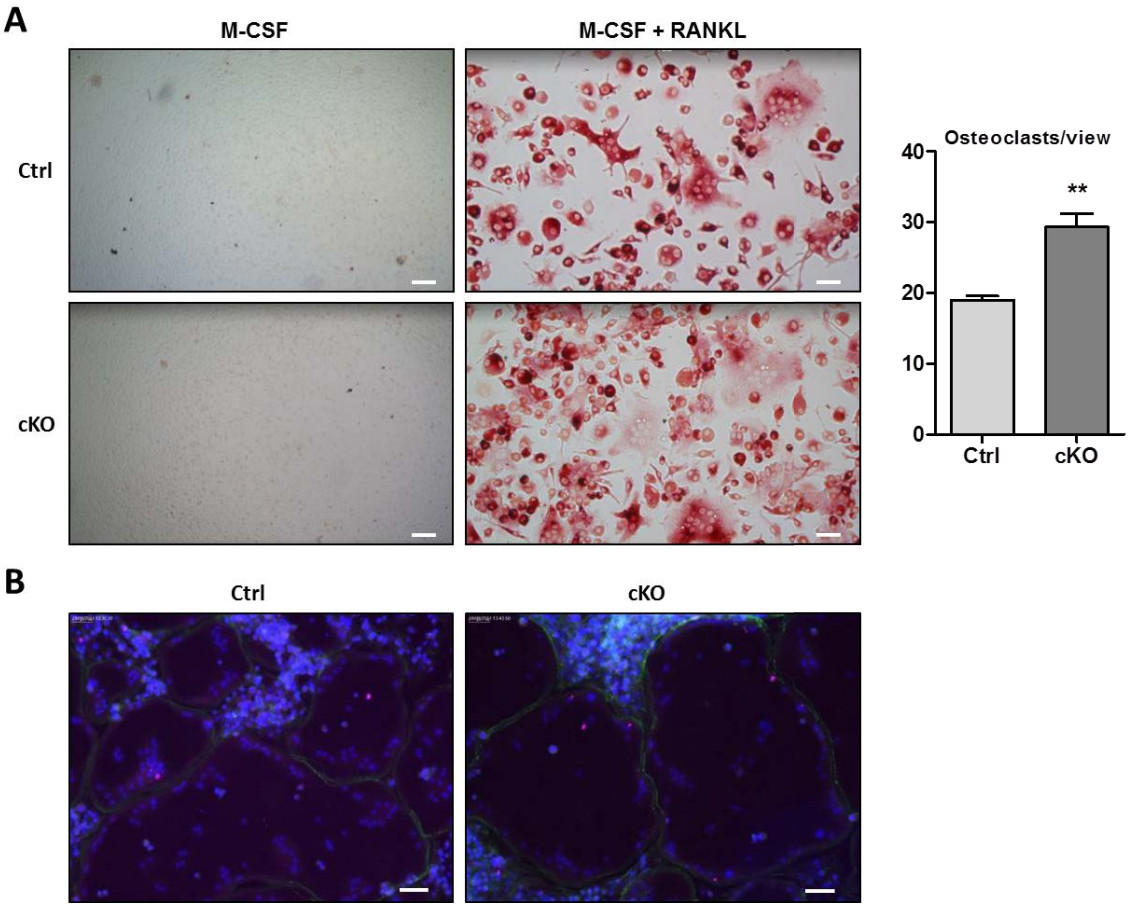

Fig. 36: BM-derived osteoclasts lacking (P)RR have an increased *in vitro* differentiation. (A) BM-derived macrophages were stimulated 5 days with M-CSF (10 ng/ml) alone or in combination with RANKL (50 ng/ml). Trap staining was further performed using a commercial kit (Sigma) and cells with at least 2 nuclei were counted. (n=3) **(B)** Actin ring formation was also observed in differentiated osteoclasts using Alexa-Fluor-488-phalloidin staining (green). Nuclei were stained with DAPI (blue). Scale bar=50 µm.

Treatment with M-CSF alone did not induce osteoclast formation whereas combination of M-CSF and RANKL led to the formation of multinucleated Trap-positive osteoclasts (Fig. 36A). By counting, we found that cKO cells formed more Trap-positive cells with at least two nuclei in comparison to Ctrl cells (Fig. 36A). We further stained the actin cytoskeleton with Alexa-Fluor-488-phalloidin and observed normal actin rings in both Ctrl and cKO osteoclasts (Fig. 36B). These findings suggest that the development to fully differentiated osteoclasts (Trap-positive and actin ring) containing multiple nuclei is increased *in vitro* in cKO mice.

To confirm these results, we also treated spleen cells with M-CSF and RANKL for 5 days and observed osteoclast differentiation. In this experiment, we performed Trap and actin staining simultaneously and cells were ranked in 3 categories according to the amount of nuclei. The number of cells with 1 or 2 nuclei was not different in Ctrl and cKO cultures. Although the amount of large osteoclasts (more than 5 nuclei) remained also unchanged, we found a significantly increased number of cells with 3, 4 or 5 nuclei in cKO cultures compared to Ctrl. Actin rings were present in all multinucleated cells from both groups.

Altogether, these in vitro analyses show that osteoclasts lacking (P)RR have an increased differentiation with all the features characterizing functional osteoclasts.

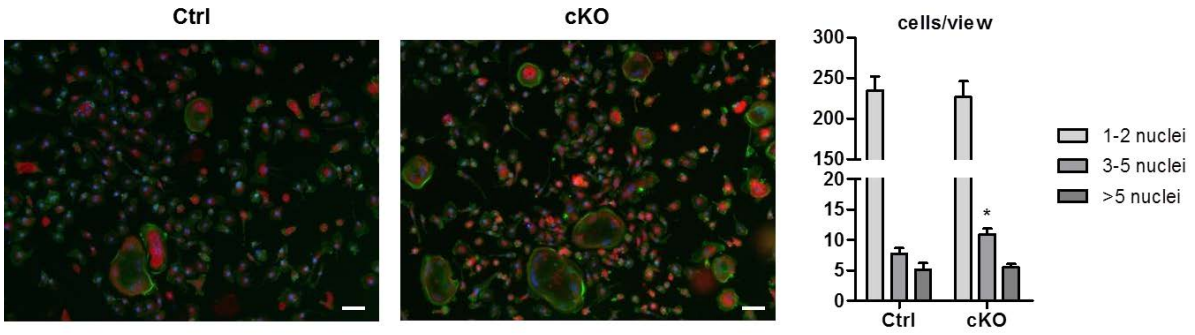

Fig. 37: Spleen-derived osteoclasts lacking (P)RR have an increased *in vitro* differentiation. Spleen-derived macrophages were stimulated 5 days with M-CSF (10 ng/ml) and RANKL (50 ng/ml). Trap staining (red) was further performed using a commercial kit (Sigma). Actin ring was simultaneously observed using Alexa-Fluor-488-phalloidin staining (green). Nuclei were stained with DAPI (blue). Cells were counted according to the number of nuclei. Representative pictures from a total of 10 for each group. **P<0.05 vs. Ctrl.*

4.1.11 Increased expression of osteoclast markers in (P)RR-deficient osteoclasts

We next monitored the expression of markers generally associated with mature osteoclasts using bone marrow cells treated with M-CSF and RANKL. Trap, CtsK and ATP6V0d2 expressions were assessed at different time points by quantitative RT-PCR. All 3 genes were markedly increased following RANKL stimulation in Ctrl and cKO cells. Trap expression was higher, albeit not significantly, in cKO cells after 3 and 5 days of treatment compared to Ctrl. On the other hand, CtsK and ATP6V0d2 levels were significantly increased in cKO cells after 5 days of treatment compared to Ctrl cells.

These results show that the increased differentiation of cKO osteoclasts is associated with an increased expression of genes important for cell fusion and/or proton extrusion (ATP6V0d2) and for bone resorption (Trap and CtsK).

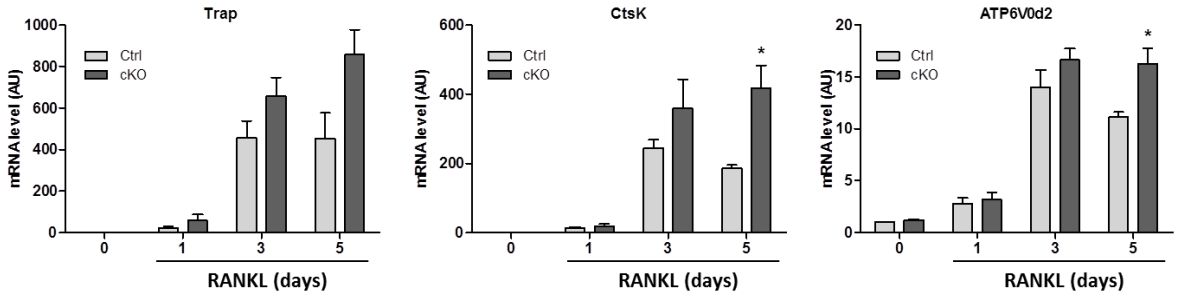

Fig. 38: Regulation of osteoclast functional markers during *in vitro* differentiation. BM-derived macrophages were stimulated with M-CSF (10 ng/ml) and RANKL (50 ng/ml). Trap, CtsK and ATP6V0d2 gene expressions were assessed after 0, 1, 3 and 5 days of stimulation. Hprt was used as reference gene. (n=4). **P<0.05 vs. Ctrl.*

4.1.12 (P)RR-deficient osteoclasts have a slightly increased bone resorption activity

We next evaluated the bone-resorbing activity of fully differentiated osteoclasts by pit formation assay. To this purpose, bone marrow and spleen cells were cultured 5 days with M-CSF and RANKL on artificial bone matrix and ivory slices, respectively. At the end of the treatment, cells were washed away and pit formation observed on both supports.

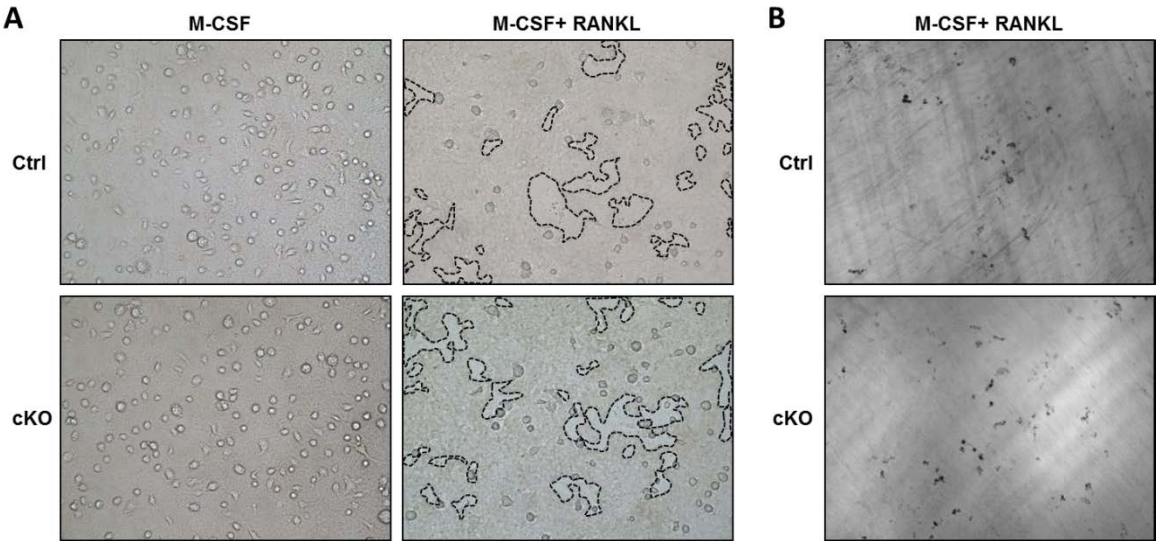

Fig. 39: BM- and spleen-derived osteoclasts lacking (P)RR tend to have an increased resorbing activity *in vitro*. (A) BM-derived macrophages were stimulated 5 days with M-CSF (10 ng/ml) alone or in combination with RANKL (50 ng/ml) on OsteologicTM discs (BD Biosciences) and resorption was observed and outlined. **(B)** Spleen-derived macrophages were stimulated 5 days with M-CSF (10 ng/ml) and RANKL (50 ng/ml) on ivory slices. Osteoclasts were washed out and ivory slices were stained with black ink. After washing, resorption pits appeared black.

Osteoclasts differentiated from BM and spleen cells of cKO mice exhibited a slightly increased bone-resorbing activity compared with osteoclasts from Ctrl mice. Although it coincided with the *in vivo* data, we have to mention that this difference in term of resorbing-activity was not quantified and therefore not subjected to statistical analysis. In conclusion, the increased mRNA expression of osteoclast markers in cKO cells is therefore associated with a slight increase of bone-resorbing activity *in vitro* and might explain the decreased bone density observed in cKO mice.

4.1.13 CtsK-Cre is expressed by a new cell population in bone

During staining of bone sections from 4 week-old cKO mice, we also observed a striking reduction of the growth plate thickness compared to age-matched Ctrl mice (Fig. 40). Because the growth plate is responsible of the longitudinal bone growth, this observation raised concerns about the specificity of the CtsK-Cre and therefore prompted us to further analyze its expression pattern by using R26-YFP reporter mice.

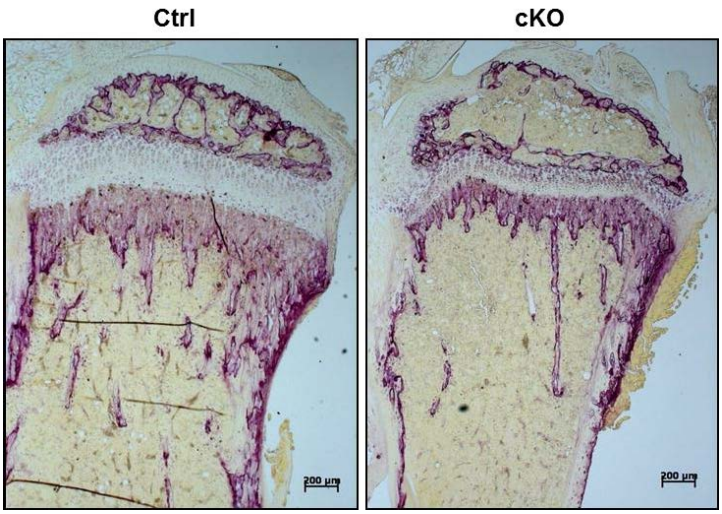

Fig. 40: (P)RR-deficient mice have a decreased growth plate size. Representative image of femur sections from 4 week-old mice subjected to Trap staining. The thickness of the growth plate appeared strongly reduced in cKO compared to Ctrl mice. Scale bar=200 µm.

YFP staining using an anti-GFP antibody was performed to detect CtsK-Cre expression and activity in R26-YFP mice. YFP expression was confirmed in osteoclasts from Cre-positive mice (*Cre*$^{+/0}$ *YFP*$^{+/-}$) and was absent in Cre-negative mice (*Cre*$^{0/0}$ *YFP*$^{+/-}$) confirming the specificity of the antibody (Fig. 41A). With the exception of few YFP-positive cells within the growth plate, chondrocytes did not exhibit any CtsK-Cre activity (Fig. 41A). Thus, the reduction of the growth plate thickness did not appear to be a consequence of an unspecific (P)RR deletion in chondrocytes. In addition, cortical bone was also negative for YFP staining suggesting that bone-embedded cells also termed osteocytes did not express the CtsK-Cre (Fig. 41B). Because osteocytes are derived from osteoblasts, it also implied that osteoblasts did not express the CtsK-Cre.

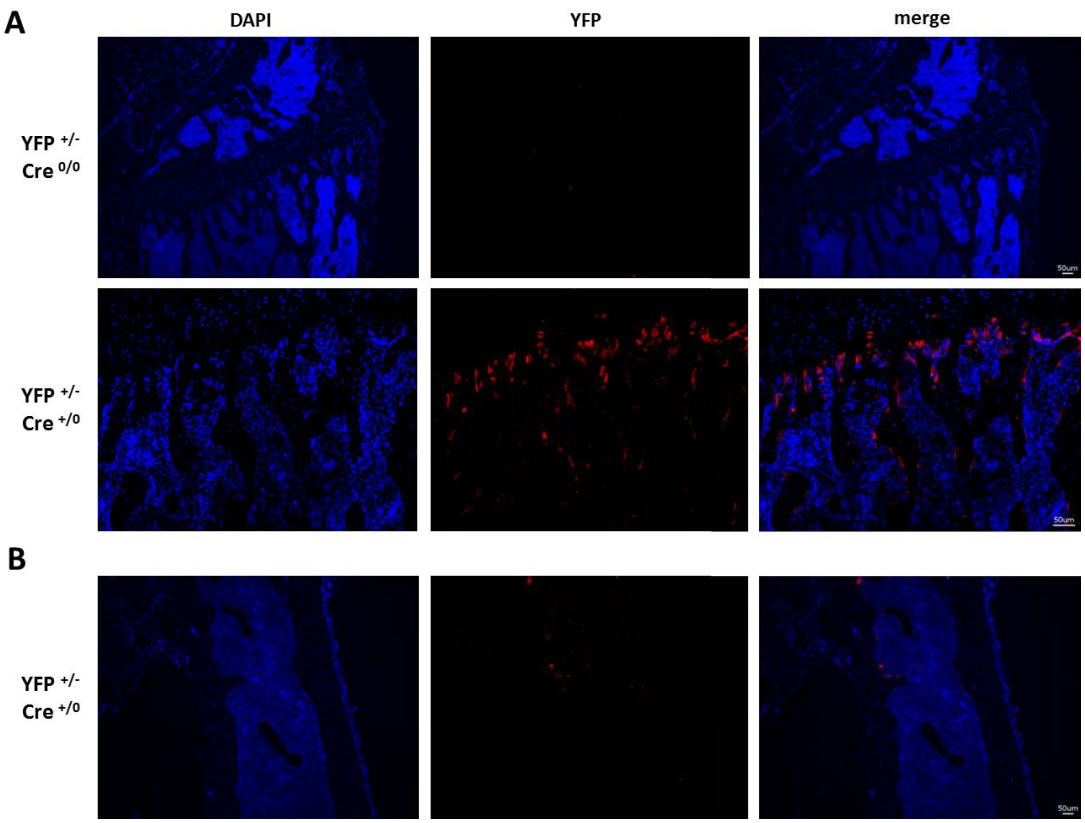

Fig. 41: CtsK-Cre expression pattern using R26-YFP reporter mice. CtsK-Cre expression was assessed in tibias from 4 week-old reporter mice using an anti-GFP antibody (red). **(A)** Cre expression in osteoclasts from Cre-positive mice (*YFP$^{+/-}$ Cre$^{+/0}$*). Animals with no Cre expression (*YFP$^{+/-}$ Cre$^{0/0}$*) were used as negative control. **(B)** Cre expression in cortical bone from Cre-positive mice (*YFP$^{+/-}$ Cre$^{+/0}$*). Nuclei were stained with DAPI (blue). Scale bar=50 µm.

In contrast, we identified a subset a cells with YFP signal in the periphery of the growth plate. The characterization and the role of these cells were not assessed in this work and require further investigations.

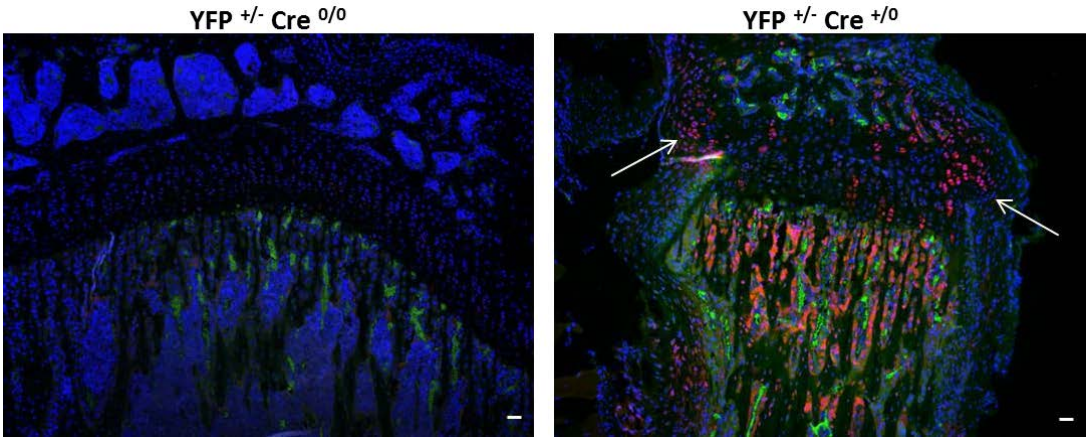

Fig. 42: CtsK-cre expression in a new cell population using R26-YFP reporter mice. CtsK-cre expression was assessed in tibias from 8 week-old reporter mice using an anti-YFP antibody (red). Mice with no Cre expression (*YFP$^{+/-}$ Cre$^{0/0}$*) were used as negative control for the staining (left). In Cre-positive mice (*YFP$^{+/-}$ Cre$^{+/0}$*), Cre expression was identified in a new cell population (white arrows) located in the periphery of the growth plate. Nuclei were stained with DAPI (blue). Scale bar=50 µm.

4.1.14 Additional phenotype of cKO mice: increased penis size

In addition to the growth retardation and the craniofacial abnormalities, external observation of cKO mice also revealed an additional intriguing feature. Indeed, cKO mice were characterized by a penis size which appeared increased compared to Ctrl mice (Fig. 43A). Although the general penis morphology of cKO mice appeared normal, its length was significantly increased compared to Ctrl penis (Fig. 43B and 43C). Due to the growth retardation, the difference between Ctrl and cKO mice was further increased when the penis length (cm)/body length (cm) ratio was calculated (Fig. 43C). We also found that the penis weight of cKO mice was increased, albeit not significantly, compared to Ctrl mice (Fig. 43D). However, due to the growth retardation of cKO mice the penis weight (mg)/body weight (g) ratio was significantly increased compared to Ctrl mice (Fig. 43D).

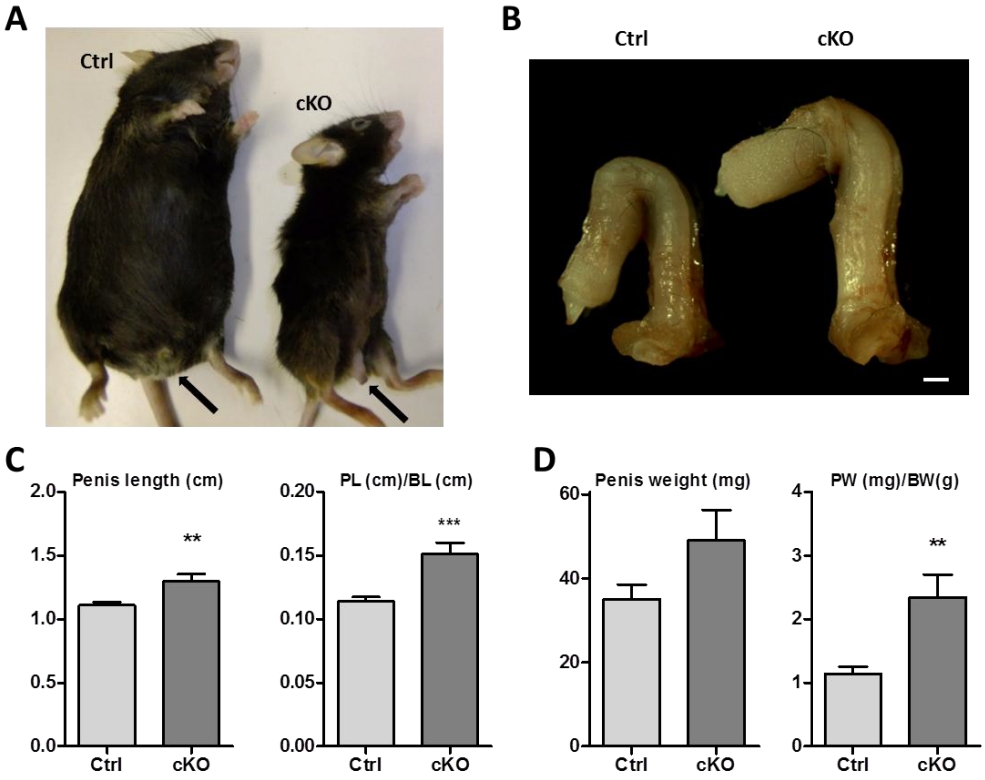

Fig. 43: cKO mice have an increased penis size. (A) Picture of 16 week-old mice showing the increased penis size of cKO compared to Ctrl. **(B)** Representative picture of penis from 16 week-old Ctrl and cKO mice. **(C)** Penis length (cm) and ratio penis length (PL, cm)/body length (BL, cm) from 16 week-old Ctrl and cKO mice. **(D)** Penis weight (mg) and ratio penis weight (PW, mg)/body weight (BW, g) from 16 week-old Ctrl and cKO mice. Scale bar=1 mm. (n=5-10). ***P<0.01, ***P<0.001 vs. Control.*

In summary, we observed that cKO mice have a penis which is significantly increased in size compared to Ctrl mice. Erectile function is the consequence of local vasodilation and increased blood volume within the penis. Priapism is an erectile dysfunction characterized by a permanent erection. It is however unlikely that (P)RR cKO mice have a permanent erection since their penis remained unchanged after sacrifice and the stop of blood supply. It is also interesting to note

that the penis enlargement of cKO males did not impair their ability to copulate and obtain offsprings when bred with female mice (data not shown).
We performed histologic analysis on penis sections to look for any tissue abnormalities which might explain the increased size of the penis. HE staining did not reveal any structural defects in cKO penis compared to Ctrl (Fig. 44). Bone and cartilage tissues which are present in mouse penis appeared normal in cKO mice. In addition, collagen staining (Sirius red staining) did not reveal any fibrosis in cKO penis compared to Ctrl (Fig. 44).
These results show that neither structural defects nor fibrosis can explain the increased penis size of cKO mice.

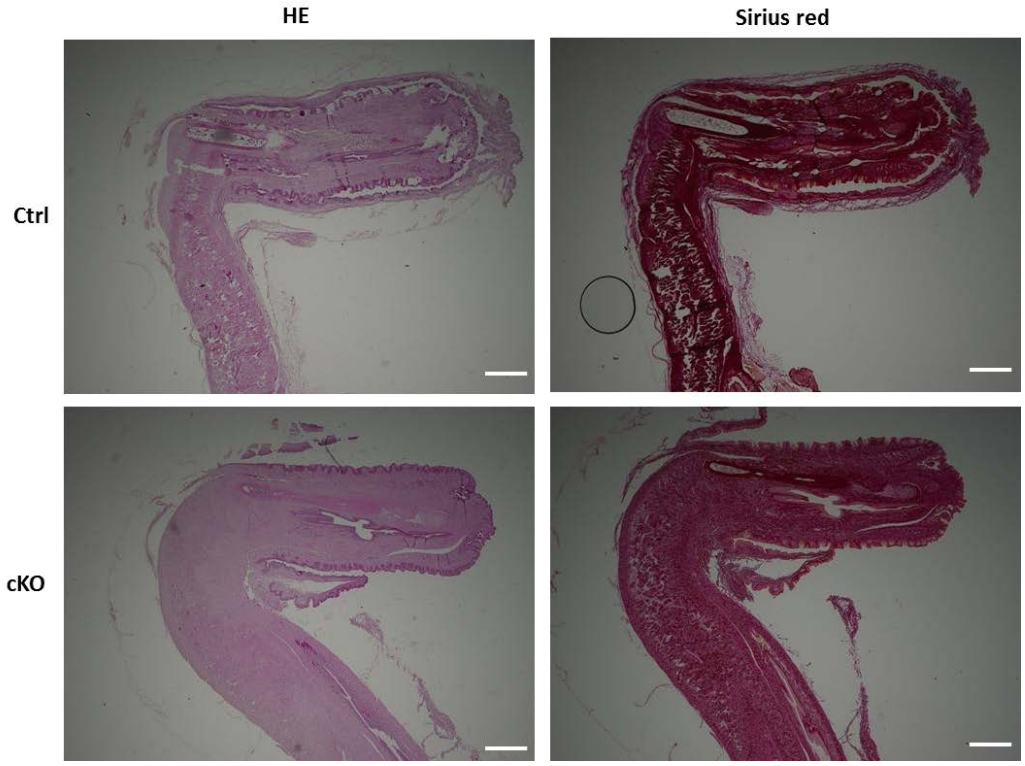

Fig. 44: Histological analysis of penis from 12 week-old mice. Hematoxylin and eosin (HE) and Sirius red staining were performed on penis sections from 12 week-old Ctrl and cKO mice. Scale bar=1 mm.

In addition, immunostaining to observe autophagy and apoptosis were conducted on penis sections. Autophagy was analyzed by staining with anti-LC3 antibody whereas apoptosis was measured by TUNEL assay. We first focused our attention on the bone area of the penis which might contain cellular defects due to the presence of (P)RR-deficient osteoclasts (Fig 45A). LC3 staining within this area did not reveal any significant difference between cKO and Ctrl mice (Fig. 45B). Also, the number of apoptotic cells put in evidence by TUNEL assay was not modified between Ctrl and cKO mice (Fig. 45B).
These data suggest that the penis phenotype of cKO mice is not a consequence of increased autophagy and/or apoptosis within the bone tissue.

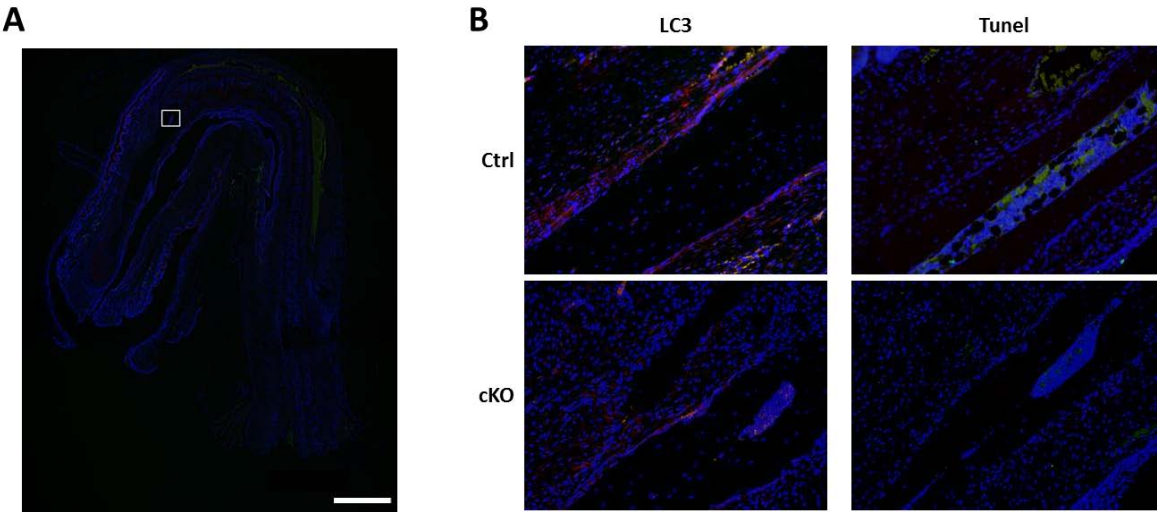

Fig. 45: Autophagy and apoptosis staining in penis bone area from 12 week-old mice. (A) White box depicts bone area in which pictures were taken. **(B)** LC3 (autophagy, red) and Tunel (apoptosis, green) staining on bone area from 12 week-old Ctrl and cKO mice. Nuclei were stained with DAPI (blue). Scale bar=1 mm.

The corpus cavernosum was also subjected to the autophagy and apoptosis staining (Fig. 46A). As described for the bone area, autophagy (LC3 staining) and apoptosis (TUNEL assay) were not impaired in cKO compared to Ctrl mice (Fig. 46B). Therefore, increased autophagy and/or apoptosis are absent within the corpus cavernosum and are not the cause of the increased penis size of cKO mice.

Altogether, the histologic analysis did not reveal any gross abnormalities in the penis from cKO and therefore, further experiments are required to find the relation between osteoclasts activity and size of the penis.

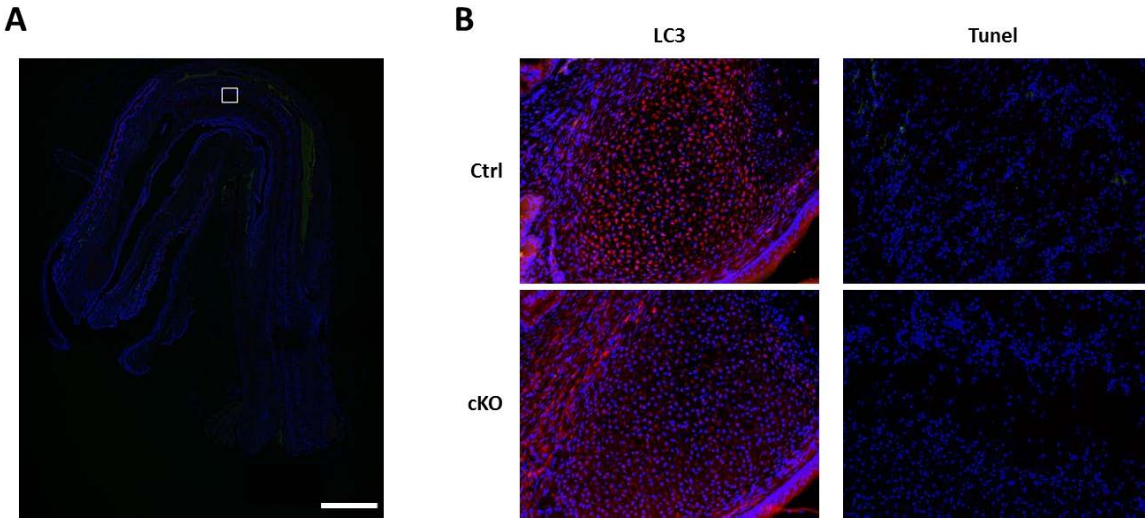

Fig. 46: Autophagy and apoptosis staining in corpus cavernosum area from 12 week-old mice. (A) White box depicts corpus cavernosum area in which pictures were taken. **(B)** LC3 (autophagy, red) and Tunel (apoptosis, green) staining on corpus cavernosum area from 12 week-old Ctrl and cKO mice. Nuclei were stained with DAPI (blue). Scale bar=1 mm.

4.1.15 Conclusion

Mice with a (P)RR specific deletion in osteoclasts exhibit bone loss (and no osteopetrosis) and growth retardation. (P)RR-deficient osteoclasts develop normally *in vitro* and *in vivo* but seem to mature faster and to express more osteoclast markers *in vitro* compared to Ctrl cells. In addition, the bone resorption activity of cKO osteoclasts appears to be increased *in vivo* and to a lesser extent *in vitro*. We also revealed that the CtsK-Cre is express by a new cell population which was not further characterized in this work. Finally, through an unknown mechanism, cKO mice have a penis which is enlarged compared to Ctrl mice.

4.2 (P)RR deletion in myeloid cells and osteoclast sleads to bone loss in mice

Contrary to our hypothesis, (P)RR deletion in osteoclasts did not lead to osteopetrosis but rather to bone loss and growth retardation. Using the CtsK-Cre, we deleted (P)RR in committed osteoclasts and therefore a role of (P)RR during the early differentiation phase could not be excluded. In addition to osteoclasts, the new cell population described to express Cre in the CtsK-Cre mice may also contribute to the development of the bone phenotype in cKO mice. To circumvent these issues, we decided to develop a second mouse model with a conditional deletion of *(P)RR* in osteoclasts using a different Cre recombinase-expressing transgenic mouse.

4.2.1 Generation of mice with a deletion of (P)RR in myeloid cells and osteoclasts

For our second mouse model, we crossed *(P)RR*$^{flox/wt}$ heterozygous females to transgenic mice expressing the Cre recombinase under the control of the endogenous Lysozyme M (LysM) promoter (Fig. 47A).

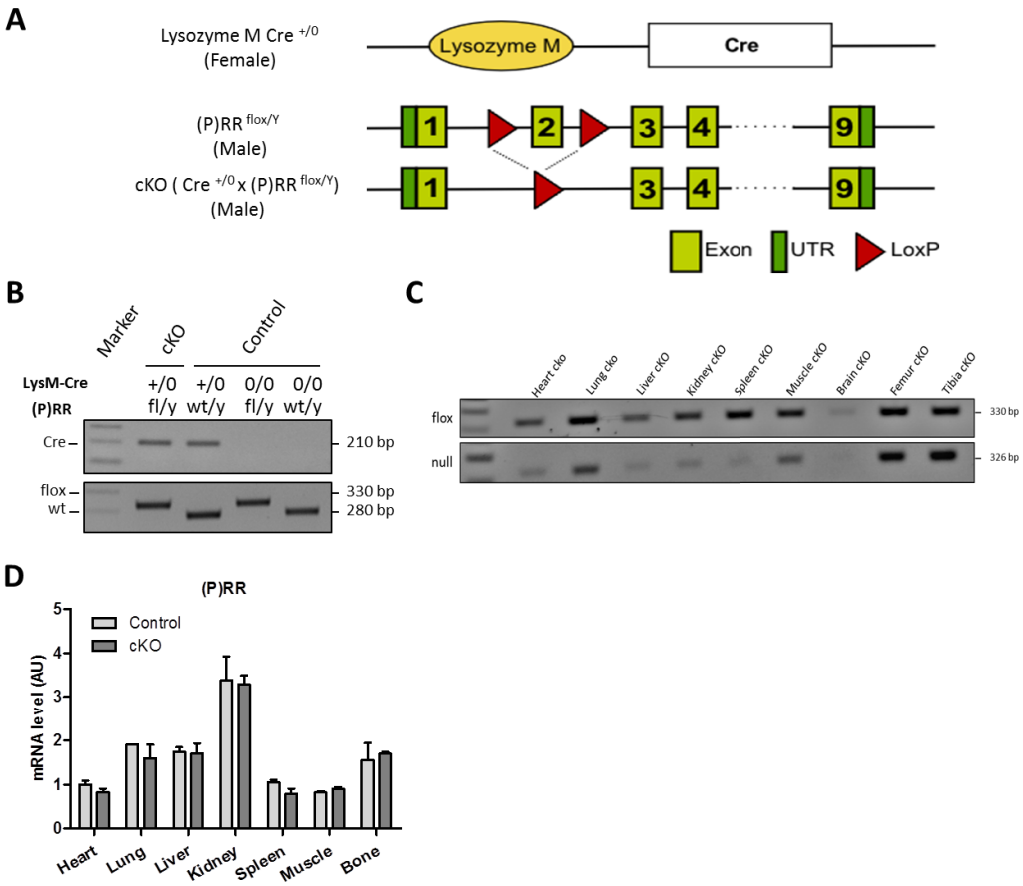

Fig. 47: Conditional inactivation of the *(P)RR* gene using the LysM-Cre mice. (A) Floxed (P)RR mice were generated by homologous recombination with a construct in which exon 2 was flanked by loxP sites. Deletion of (P)RR in osteoclasts was performed using transgenic mice expressing the Cre recombinase under the control of the Lysozyme M (LysM) promoter (adapted from Riediger et al. 2011). **(B)** PCR genotyping depicting the different genotypes: wt (P)RR allele (280bp), floxed (P)RR allele (330bp) and Cre (210bp). **(C)** A 326bp PCR product specific for *(P)RR* excision was detected in bone and other organs from cKO mice. **(D)** Quantitative RT-PCR analysis in various organs did not show any significant difference in (P)RR expression level between cKO and Ctrl animals. TBP was used as reference gene (n=2).

The lysM-Cre targets all myeloid cells including monocytes and macrophages which give rise to osteoclasts. *(P)RR$^{wt/y}$* males with one copy of the Cre (Cre$^{+/0}$) males were used for breedings (Fig. 47A). The resulting *(P)RR$^{flox/y}$, Cre$^{+/0}$* genotype corresponds to conditional knockout (cKO) males with (P)RR-deficient osteoclasts (Fig. 47A and 47B). We used *(P)RR$^{wt/y}$, Cre$^{+/0}$* and *(P)RR$^{flox/y}$, Cre$^{0/0}$* male littermates as controls (Ctrl) to exclude any Cre- and flox-mediated toxicity (Fig. 47B). Only males were studied in this work.

To test the LysM-Cre expression pattern, genomic excision of exon 2 was assessed via the amplification of a 326 bp PCR product specific to the null allele. The excision product was strongly detected in the cKO bone as expected and to a lesser extends in all other organs due to the presence of circulating and/or resident myeloid cells (Fig. 47C). In addition, (P)RR expression level was assessed in several organs by quantitative RT-PCR and no significant difference between cKO and Ctrl animals was observed (Fig. 47D). Although (P)RR deletion occurred in myeloid cells and osteoclasts, other cell populations still expressed (P)RR and therefore a difference of (P)RR mRNA level in the whole bone was not expected.

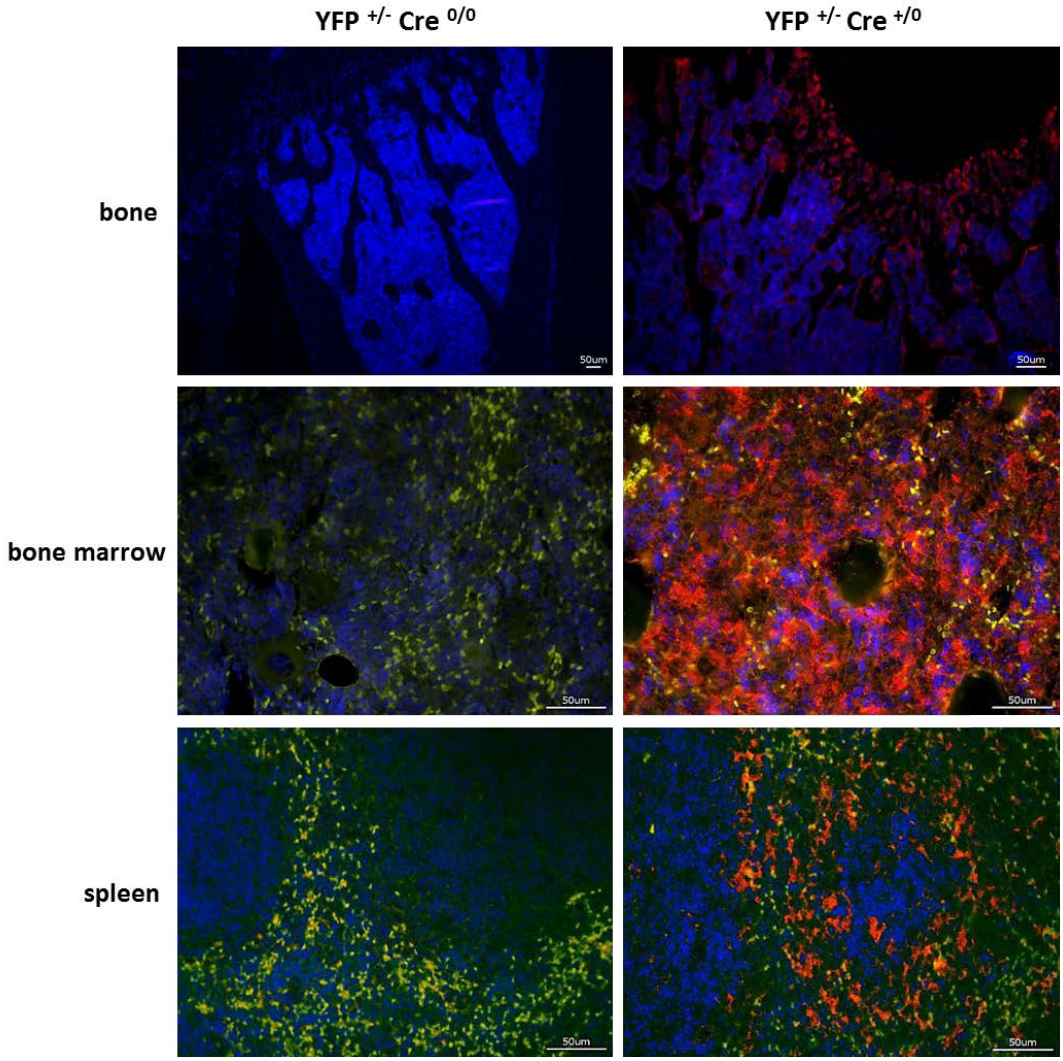

Fig. 48: LysM-Cre expression pattern using R26-YFP reporter mice. LysM-Cre expression was assessed in bone, bone marrow and spleen from 12 week-old *YFP$^{+/-}$ Cre$^{+/0}$* mice using an anti-GFP antibody (red). Animals with no Cre expression (*YFP$^{+/-}$ Cre$^{0/0}$*) were used as negative control. Nuclei were stained with DAPI (blue). Scale bar=50 µm.

As we did for the CtsK-Cre, we bred LysM-Cre positive mice with R26-YFP reporter mice. LysM-Cre expression and activity was detected by immunohistochemistry using an anti-GFP antibody in different organs from Cre-positive mice (*Cre$^{+/0}$ YFP$^{+/-}$*). Cre-negative mice (*Cre$^{0/0}$ YFP$^{+/-}$*) were used as negative control for the staining (Fig. 48). In bone sections, we confirmed LysM-Cre expression in cells which resemble osteoclasts lying on trabecular bone (Fig. 48). We also detected YFP staining in cells from the bone marrow and spleen which can be explained by the presence of myeloid and macrophage cells within these organs.
In summary, these results show that the LysM-Cre is expressed and active in myeloid cells, macrophages and osteoclasts in our model.

4.2.2 cKO mice with LysM-Cre-mediated (P)RR deletion have a normal growth and development

The cKO mice were born with the expected mendelian frequency without any gross morphological abnormalities (data not shown). After birth, cKO mice had a normal development and growth. We monitored the body weight of cKO mice at different ages and did not detect any difference between Ctrl and cKO mice (Fig. 49A).

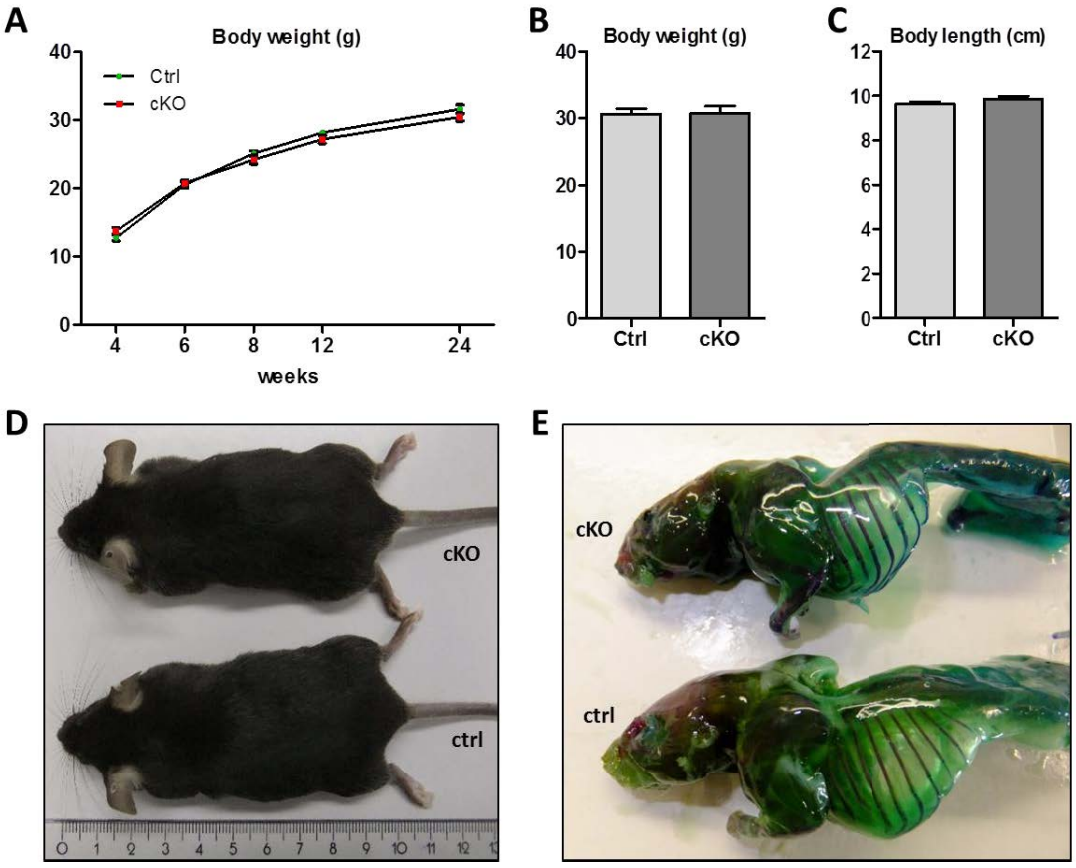

Fig. 49: cKO mice with LysM-Cre-mediated (P)RR deletion have a normal growth. (A) Body weight (g) of Ctrl and cKO mice between 4 and 24 weeks of age. (n between 9 and 16) **(B)** Body weight (g) and **(C)** Body length (cm) of Ctrl (n=5) and cKO mice (n=3) at the age of 12 weeks. **(D)** Picture of Ctrl and cKO at the age of 12 weeks. **(E)** Skeleton morphology of 12 week-old Ctrl and cKO mice revealed by alizarin red (bone) and alcian blue (cartilage) staining.

We also measured the body length of some animals at 12 weeks of age. In addition to the normal body weight at this age, cKO mice had a normal body length and were indistinguishable from Ctrl mice (Fig. 49B and C). This phenotype was further illustrated by the picture of 12 week-old cKO and Ctrl mice (Fig. 49D). Also, skeleton staining with alizarin red/alcian blue solution did not reveal any skeletal abnormalities in cKO mice (Fig. 49E). All mice in this study had normal teeth eruption (data not shown). These data show that cKO mice have a normal development and growth.

General observation of femurs and tibias of 12 week-old animals showed that the bone of cKO mice had a normal structure and shape (Fig. 50A) We also observed red bone marrow denoting the presence of a bone marrow cavity. Femur and tibia lengths from cKO mice were similar to Ctrl mice (Fig. 50B). These data confirm that cKO mice have a normal growth and bone architecture.

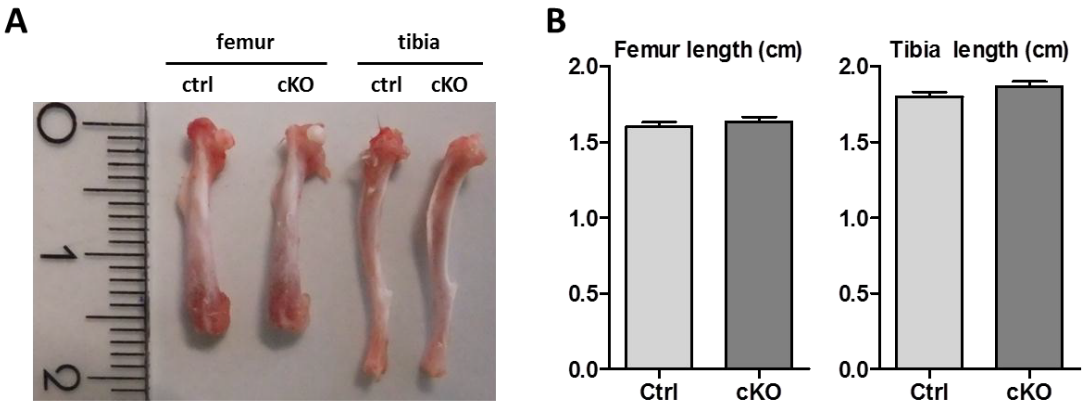

Fig. 50: Femur and tibia lengths of 12week-old mice. (A) Picture of femurs and tibias from 12 week-old Ctrl and cKO mice. **(B)** Femur and tibia lengths (cm) of 12 week-old Ctrl (n=5) and cKO (n=3) mice.

To confirm that the normal aspect of cKO mice was not transient but maintained throughout life, some animals were observed at one year of age. At this age, the body weight and body length of cKO mice remained similar to Ctrl mice (Fig. 51A).

Some morphological abnormalities of the face (skin of the nose, closed eyes, orientation of the ears) were observed in cKO mice with CtsK-Cre-mediated (P)RR deletion (Fig. 20A). In contrast, cKO mice with LysM-Cre-mediated (P)RR deletion did not develop such craniofacial defects compared to Ctrl mice as illustrated by picture of the heads (Fig. 51B). We also observed spleen morphology in this second cKO mice model. Consistent with the observation in CtsK mice, spleens from LysM mice did not present any morphological differences compared to Ctrl mice (Fig 51C) and the spleen weight and the spleen weight/body weight (SW/BW) ratio of cKO mice were also not different compared to Ctrl mice (Fig. 51C).

Altogether, these results show that cKO mice with LysM-Cre-mediated (P)RR deletion have a normal global development which is maintained through life. In addition, the normal spleen size of cKO mice already suggests that the presence of osteopetrosis in these animals is unlikely.

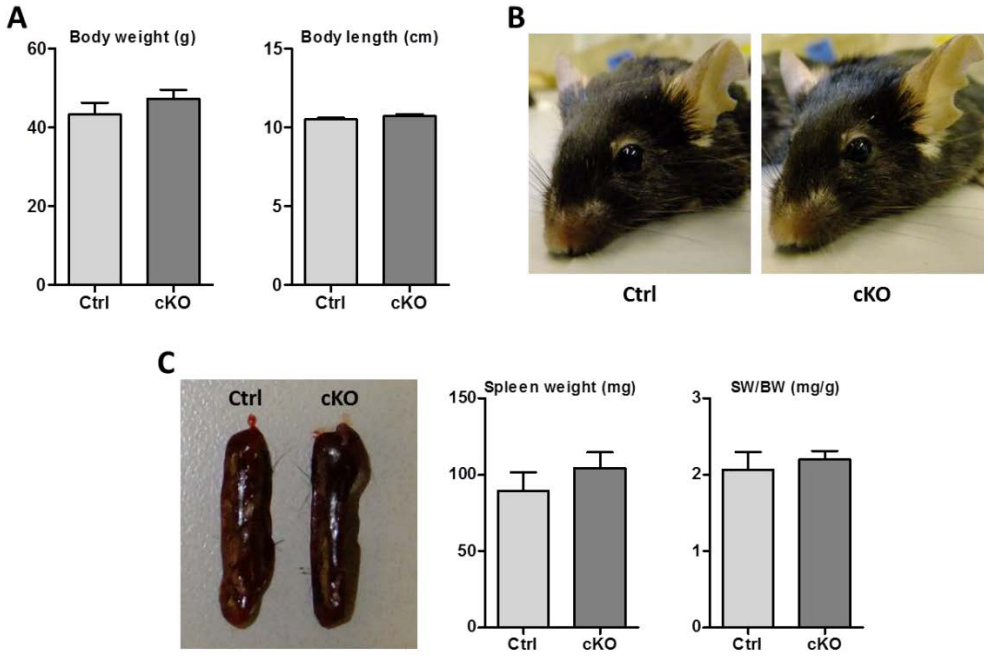

Fig. 51: General aspect of 1 year-old cKO mice. Body and spleen dimensions were analyzed in 1 year-old Ctrl and cKO mice **(A)** Body weight (g) and body length (cm). **(B)** Representative picture of the head. **(C)** Representative picture of spleens, spleen weight (mg) and spleen weight (mg)/body weight (g) (SW/BW) ratio. (n=3).

4.2.3 cKO mice with LysM-Cre-mediated (P)RR deletion have a decreased bone density

To analyze the bone density, micro-computed tomography (µCT) was performed following the parameters described in the material and methods section (part 3.2.10.2) and 3D reconstruction was performed using the NRecon software. Proximal tibias from 12 week-old mice were scanned and bone density parameters were assessed.

At this age, 3D reconstructions of proximal tibia did not show any increase in bone density but rather put in evidence a decreased bone density in cKO mice compared to Ctrl mice (Fig. 52A). In accordance, the bone volume/tissue volume (BV/TV, %) ratio was significantly decreased in cKO compared to Ctrl mice (Fig. 52B). Parameters such as trabecular number (Tb.N., /mm) and trabecular thickness (Tb.Th., µm) were lower in cKO but not significantly different compared to Ctrl mice. The trabecular separation (Tb.Sp., mm) remained unchanged between cKO and Ctrl mice (Fig. 52B). Observation of the cortical bone showed no difference in terms of cortical bone thickness between both groups (Fig. 52C). The diameter of the bone marrow cavity was also unchanged.

In summary, these results highlight a decreased bone density in cKO mice with LysM-Cre-mediated (P)RR deletion and confirm the bone phenotype previously observed in cKO mice with CtsK-Cre-mediated (P)RR deletion.

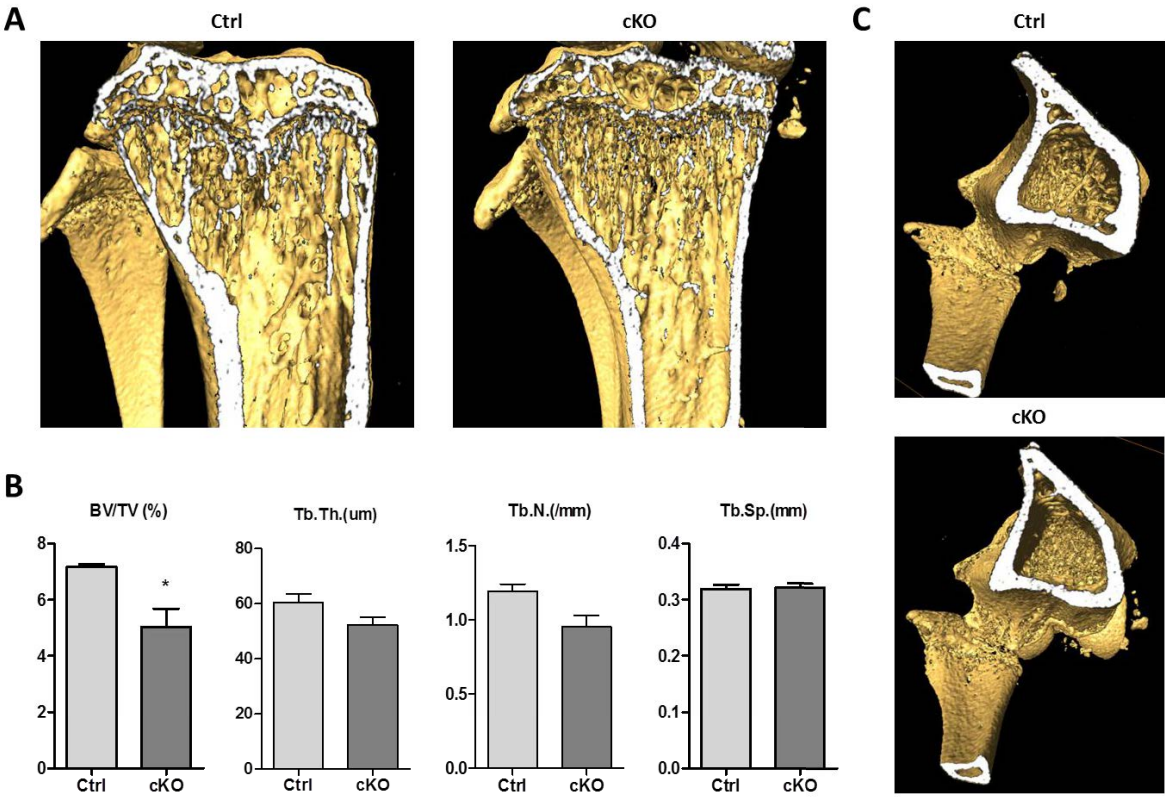

Fig. 52: µCT examination of 12 week-old mice. Tibias from 12 week-old Ctrl and cKO mice were examined by micro-computed tomography (µCT) analysis and 3D reconstructed. **(A)** Representative image (3D) of trabecular bone. **(B)** Three-dimensional trabecular structural: bone volume per tissue volume (BV/TV, %), trabecular thickness (Tb.Th., µm), trabecular number (Tb.N., /mm) and trabecular spacing (Tb.Sp., mm). (n=3-4)**. (C)** Representative image of cortical bone. **P<0.05 vs. Control*

4.2.4 Osteoclasts lacking (P)RR have a normal differentiation *in vitro*

The consequence of LysM-Cre-mediated (P)RR deletion on osteoclast differentiation was further investigated *in vitro* using cell culture. First, we treated BM cells with M-CSF (20 ng/ml) for 5 days to generate macrophages and (P)RR protein level was analyzed by western blot. (P)RR protein level was strongly reduced in cKO macrophages compared to Ctrl macrophages (Fig. 53A). To generate osteoclasts, we used spleen-derived macrophages treated with M-CSF (10 ng/ml) and RANKL (50 ng/ml). With the LysM-Cre being already expressed at the macrophage stage, (P)RR protein level was drastically reduced after 3 and 5 days of osteoclast differentiation (Fig. 53B). Effective (P)RR deletion did not impair osteoclast differentiation and maturation as they become multinucleated and rearranged their actin skeleton (Fig. 53C). Cells were counted and ranked according to their number of nuclei. The number of cells with 1-2, 3-5 and more than 5 nuclei was similar in cKO and Ctrl cell cultures (Fig. 53C) suggesting that the differentiation occurred normally in cKO cells.

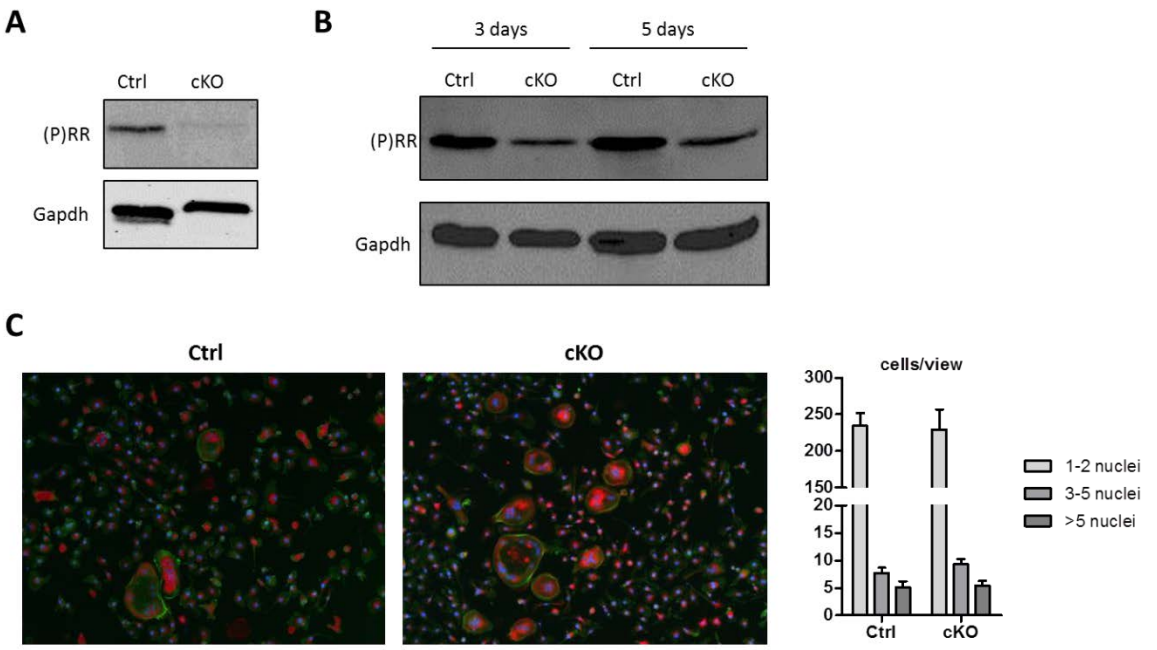

Fig. 53: Spleen-derived osteoclasts lacking (P)RR have a normal *in vitro* differentiation. (A) (P)RR protein level was detected by western blot in BMMs treated with M-CSF (10 ng/ml) for 5 days and **(B)** in spleen-derived osteoclasts treated 3 and 5 days with M-CSF (10 ng/ml) and RANKL (50 ng/ml). Gapdh was used as loading control. **(C)** Spleen-derived macrophages were stimulated 5 days with M-CSF (10 ng/ml) and RANKL (50 ng/ml). Trap staining (red) was further performed using a commercial kit (Sigma). Actin ring was simultaneously observed using Alexa-Fluor-488-phalloidin staining (green). Nuclei were stained with DAPI (blue). Cells were counted according to the number of nuclei. Representative pictures from a total of 10 for each group.

These results show that the LysM-Cre strongly decreases (P)RR protein expression in differentiated osteoclast and in osteoclast progenitors (macrophages). Efficient (P)RR deletion in these cells do not impair their differentiation and maturation.

4.2.5 Osteoclasts lacking (P)RR have an increased resorption acitivity *in vitro*

To assay bone resorption activity, spleen-derived macrophages were cultured on ivory slices and treated 5 days with M-CSF (10 ng/ml) and RANKL (50 ng/ml). Osteoclasts were washed away and resorption pits were stained with black ink, washed and finally subjected to microscopy. An increased number of resorption pits was observed in cKO compared to Ctrl cells suggesting that the resorption activity of cKO osteoclasts was increased compared to Ctrl osteoclasts (Fig. 54).

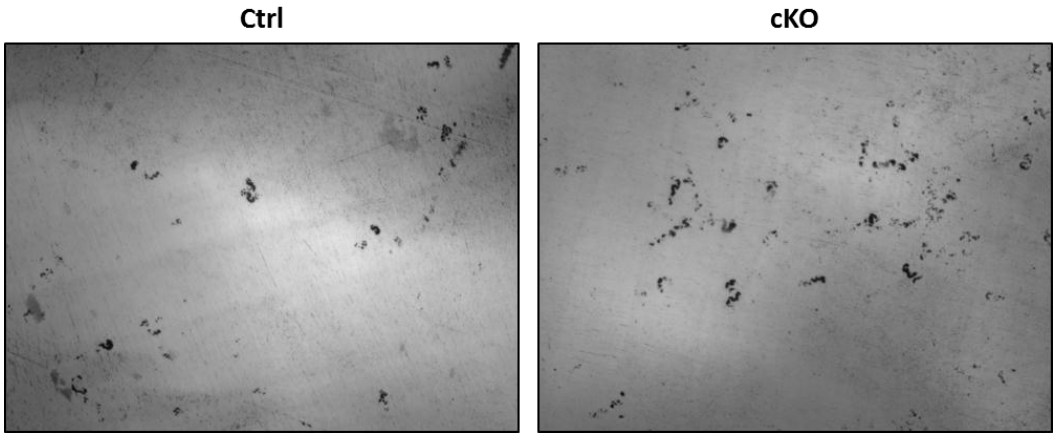

Fig. 54: Spleen-derived osteoclasts lacking (P)RR have an increased *in vitro* resorbing activity. Spleen-derived macrophages were stimulated 5 days with M-CSF (10 ng/ml) and RANKL (50 ng/ml) on ivory slices. Osteoclasts were washed out and ivory slices were stained with black ink. After washing, resorption pits appeared black.

4.2.6 cKO mice with LysM-Cre-mediated (P)RR deletion have a normal penis size

The presence of an intriguing penis phenotype in cKO mice with CtsK-Cre-mediated (P)RR deletion prompted us to look for such a phenotype in our LysM-Cre model. We observed penises from 12 week-old animals and did not find any difference between cKO and Ctrl mice (Fig. 55).

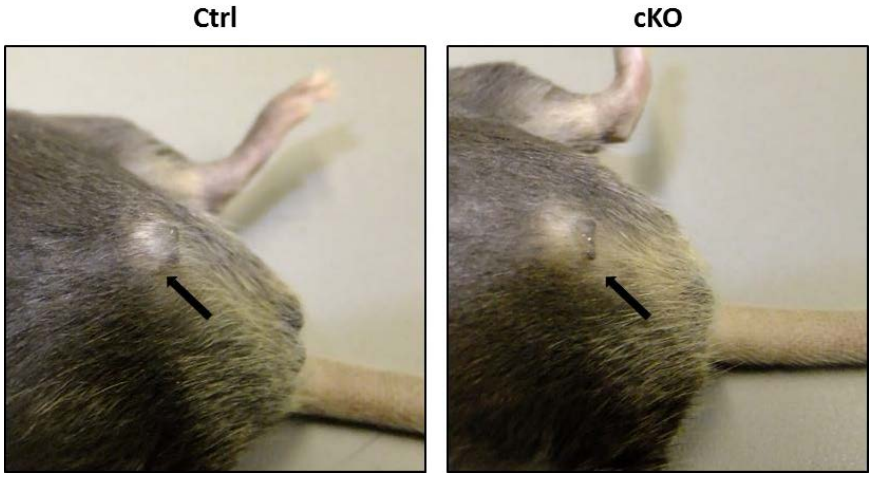

Fig. 55: cKO mice have a normal penis size. Picture of 12 week-old mice showing a normal penis size in Ctrl and cKO mice.

4.2.7 Conclusion

Mice with a (P)RR deletion in myeloid cells and macrophages (LysM-Cre) do not develop osteopetrosis but rather exhibit the same decreased bone density as mice with a (P)RR deletion in differentiated osteoclasts (CtsK-Cre). This phenotype appears to be the consequence of an increased osteoclast activity in both models. There are however some phenotypic differences between the two mouse models. Indeed, in contrast to our CtsK-Cre model, mice with a (P)RR deletion in myeloid cells and macrophages have a normal growth development, cranio-facial features and penis size.

4.3 Generation of *sh(P)RR* transgenic rats and role of (P)RR in macrophages

Studies from mice with tissue specific (P)RR deletion using the Cre/Lox system have all observed an accumulation of autophagic vacuoles within the cytoplasm due to impaired acidification and leading to cell death. As previously stated, this drastic phenotype might illustrate the long term consequence of (P)RR deletion masking earlier potential roles of (P)RR.
Macrophages represent an interesting cell type as they display an intense intracellular trafficking after the engulfment of foreign bodies into phagosomes. This process known as phagocytosis leads to the destruction of the engulfed material through several maturation stages involving interactions with several organelles and a progressive acidification of the phagosome. To assess a role of (P)RR in phagocytosis and trafficking, macrophages can easily be studied *in vivo* in the peritoneal cavity and *in vitro* after differentiation of bone marrow cells with M-CSF. In this regard, the development of a transgenic rat harboring a doxycycline-inducible shRNA targeting (P)RR was of particular interest as it would give the possibility to trigger (P)RR knockdown in macrophages *in vivo* by giving doxycycline (Dox) in drinking water and *in vitro* by treating primary cell cultures.

4.3.1 Efficiency of (P)RR *shRNA in vitro*

Two different *sh(P)RR* oligos were designed targeting exon 3 (*sh1/2*) and exon 9 (*sh3/4*) of the rat *(P)RR* gene. To test their efficiency in vitro, COS7 cells were co-transfected with plasmids coding for rat *(P)RR* fused with a YFP tag (pUb-YFPr(P)RR) and *sh(P)RR* (pTetO-sh(P)RR-TetR) or *shegfp* (pUb-shegfp) (Fig. 56A). The use of YFP-tagged r(P)RR was dictated by the difficulty to obtain a detectable and specific signal for (P)RR protein in western blot with the use of commercial antibodies available at that time. Also, there was a risk to detect the endogenous (P)RR proteins expressed in COS7 cells and not targeted by our rat-specific shRNA oligos.

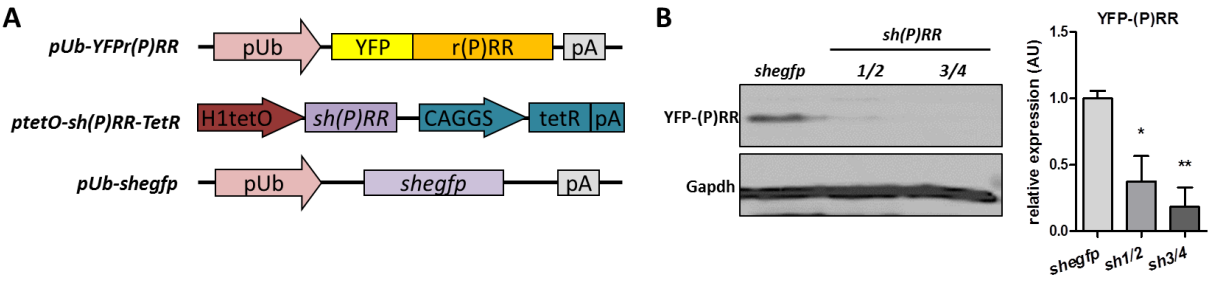

Fig. 56: Validation of *r(P)RR* shRNAs efficiency *in vitro*. (A) Plasmids used for transfection of COS7 cells. **(B)** Western blot analysis of YFP-tagged (P)RR protein expression level using an anti-YFP antibody. COS7 cells were co-transfected with YFPr(P)RR and *shegfp* or *sh(P)RR* and further treated 48h with doxycyclin (1µg/ml) to trigger shRNA expression. Two different shRNA oligos targeting *r(P)RR* (named *1/2* and *3/4*) were tested. Gapdh was used as internal control**.** *Shegfp*-transfected cells were used as reference for the quantification (n=3)**.** For further information about *sh(P)RR* plasmid, see fig. 11 in Introduction. egfp, enhanced green fluorescent protein; pA, polyadenylation site; pUB, ubiquitin C promoter; YFP, yellow fluorescent protein. **P<0.05; **P<0.01 vs. reference.*

The constitutive expression of YFPr(P)RR and *shegfp* was mediated by the ubiquitin promoter whereas *sh(P)RR* expression was triggered by adding Dox (1 µg/ml) in the culture medium. Following 48h Dox treatment, western blot analysis using anti-YFP antibody showed a significant reduction of YFPr(P)RR protein level for both *sh(P)RR* plasmids compared to *shegfp* plasmid (Fig. 56B).
These experiments showed that both *sh(P)RR* oligos target efficiently r(P)RR mRNA and result in the drastic reduction of r(P)RR protein level. The construct containing the *sh3/4* oligos was selected and used to generate transgenic rats.

4.3.2 Generation of sh3/4 transgenic rats

A linear plasmid fragment containing the bimodal expression cassette with *sh(P)RR* and TetR (Fig. 11) was generated with restriction enzymes and used to produce transgenic rats by pronuclear microinjection into fertilized oocytes of Sprague Dawley (SD) rats (see material and methods 3.2.9.2). Positive founders were further used for the breeding and establishment of the transgenic rat line termed sh3/4. Transgenic rats were characterized using a genotyping PCR protocol generating a 195-bp product (Fig. 57A). SD rats with no transgene integration were used as control during experiments.

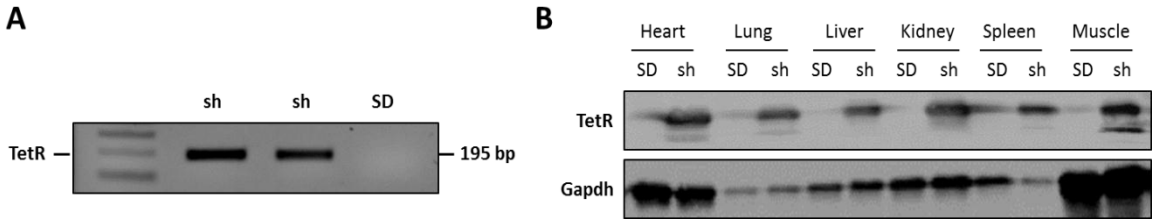

Fig. 57: Genotyping PCR and TetR protein expression. (A) Genotyping PCR was performed on tails from newborn rats and a 195-bp PCR product characteristic of transgenic animal (sh). **(B)** Western blot analysis of tetracycline repressor (TetR) expression in various tissues isolated from Sprague-Dawley (SD) and transgenic (sh) rats. Gapdh was used as loading control.

While absent in SD control rats, TetR protein expression was confirmed by Western blot in several tissues isolated from transgenic rats (Fig. 57B) suggesting that the construct was transcriptionally active.
Altogether, these observations demonstrate the efficient generation of *sh(P)RR* transgenic rats.

4.3.3 Doxycyclin treatment efficiently decreases (P)RR expression *in vivo*

To trigger *sh(P)RR* expression, transgenic and control rats were treated with Dox (100 mg/kg) present in drinking water. After 8 days of treatment, (P)RR protein level was assessed by Western blot in tail biopsies. In Dox-treated transgenic rats, we observed that (P)RR protein

level was decreased by 90% when compared to untreated transgenic rats (Fig. 58A). In contrast, Dox treatment in control SD rats did not alter (P)RR expression excluding a off-target effect of the Dox (Fig. 58A). To validate the efficiency of the Dox treatment, we also analyzed (P)RR mRNA levels in several organs by quantitative RT-PCR. We found that these levels were strongly decreased in spleen (by 100%), lung (by ~80%), kidney (by ~70%) and to a lesser extend in liver (by ~30%) in Dox-treated transgenic rats compared to Dox-treated SD rats (Fig. 58B).
These results showed that Dox treatment in drinking water efficiently triggers *sh(P)RR* expression *in vivo* in transgenic rats, leading to a strong downregulation of (P)RR expression in several tissues.

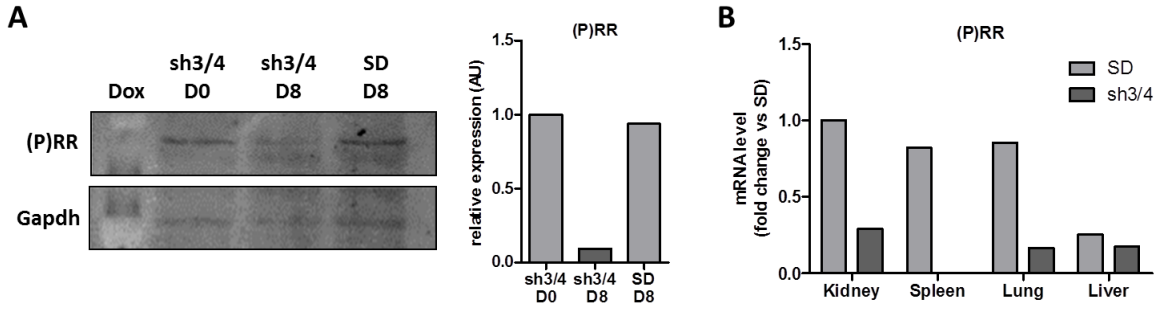

Fig. 58: *In vivo* doxycyclin (Dox) treatment decreases (P)RR expression in tissues. Doxycyclin (100 mg/kg/day) in drinking water was administred to rats for 8 days. **(A)** (P)RR protein level in tails isolated from Sprague-Dawley (SD) and transgenic (sh3/4) rats before (D0) and after 8 days (D8) of Dox treatment. (P)RR expression was quantified using Gapdh as loading control. **(B) (**P)RR mRNA levels in various organs of SD and sh3/4 rats after 8 days of Dox treatment determined by quantitative RT-PCR using Hprt as a reference gene. AU, arbitrary unit.

4.3.4 Doxycyclin treatment treatment *in vivo* leads to premature death

Although (P)RR expression was strongly reduced in organs from transgenic rats after 8 days of Dox treatment, animals did not exhibit any particular physiological defects. Animal reaction and mobility were also normal. Therefore, we extended the Dox treatment and observed the physiological consequences of long term (P)RR knockdown.
The body weight and the water intake were monitored every day during the Dox treatment as parameters of general homeostasis. For both parameters, we did not observe any difference between Dox-treated SD and Dox-treated transgenic rats during the first ten days of the treatment (Fig. 59A and B). However, after 11 days of Dox treatment, both parameters started to decline strongly and constantly in transgenic rats until reaching a critical point after 15 days of treatment. During these 4 days, while both parameters remained normal in SD rats, the body weight of transgenic rats decreased by approximately 17%, and water intake was reduced to almost zero (Fig. 59A and B). An absence of movement also characterized these animals (data not shown). At this point, the health of transgenic rats was so compromised that Dox treatment was interrupted and animals were sacrificed. These observations show that long term (P)RR deletion impairs general homeostasis and leads to premature death, which is in line with the

observations made in mice with tissue-specific (P)RR deletion (Kinouchi et al. 2010, Oshima et al. 2011, Riediger et al. 2011).

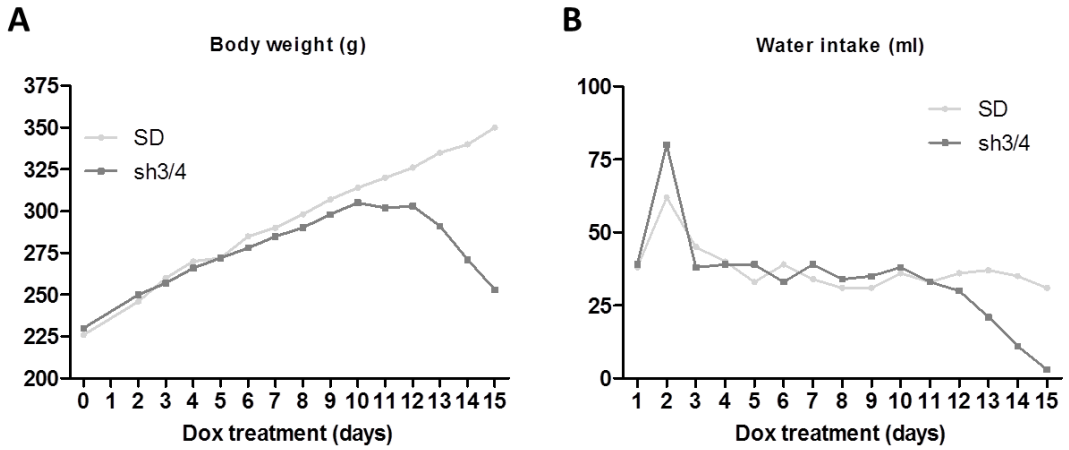

Fig. 59: *In vivo* doxycyclin (Dox) treatment impairs general homeostasis and leads to premature death. Sprague-Dawley (SD) and sh3/4 rats were treated with Dox (100 mg/kg) in drinking water. **(A)** Body weight and **(B)** water intake (ml) were monitored for 15 days, after which Dox treatment was suppressed due to a strong deterioration of the sh3/4 rats.

To better understand and characterize the health decline of transgenic rats treated with Dox, we observed the consequences of (P)RR depletion on blood homeostasis. Blood composition was analyzed in SD and transgenic rats before and after 15 days of Dox treatment. All parameters measured such as white and red blood cells, hemoglobin and hematocrit stayed constant in both animals before and after Dox treatment (Fig. 60A). We also measured blood glucose level (glycemia, mg/dl) in SD and transgenic rats before and after 9 and 13 days of Dox treatment. Blood glucose level was not different in both animals before and after 9 days of Dox treatment Fig. 60B). In contrast, after 13 days of Dox treatment, glycemia from transgenic rat was severely increased by a factor 2 compared to SD animal (Fig. 60B) suggesting that glucose homeostasis was impaired following (P)RR depletion.

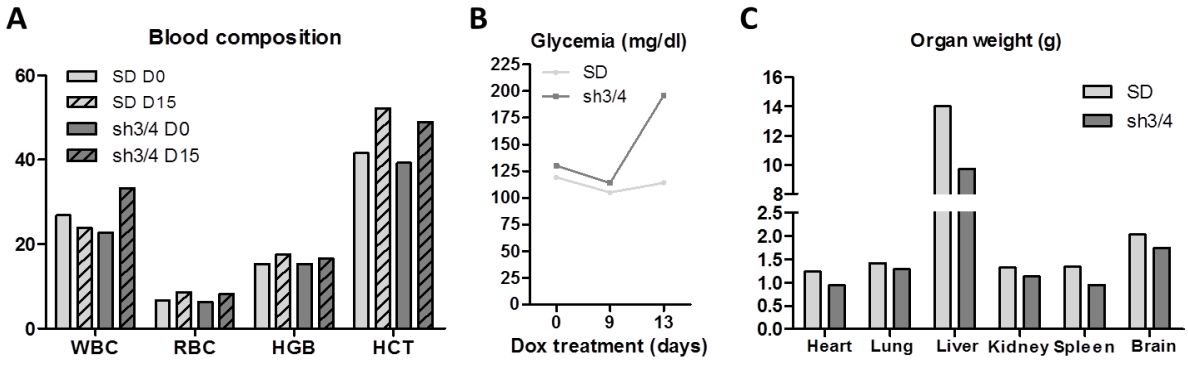

Fig. 60: *In vivo* doxycyclin (Dox) treatment impairs glycemia and organ physiology. Sprague-Dawley (SD) and sh3/4 rats were treated 15 days with Dox (100 mg/kg). **(A)** Blood composition of SD and sh3/4 rats at the beginning (D0) and the end (D15) of Dox treatment: white blood cells (WBC, 10^3/mm^3), red blood cells (RBC, 10^6/mm^3), hemoglobin levels (HGB, g/dl) and hematocrit (HCT, %). **(B)** Blood was collected before (day 0) and after 9 and 13 days of Dox treatment and glycemia (mg/dl) was measured. **(C)** Weight (g) of several organs from SD and sh3/4 rats after 15 days of Dox treatment.

After 15 days of Dox treatment, animals were sacrificed and organs were observed to detect any abnormality. The weight of all organs from Dox-treated transgenic rat was decreased compared to organs from Dox-treated SD rat with the strongest effect occurring in the liver (-30%) (Fig. 60B).
Altogether, these results showed that the degraded health status observed in transgenic rats treated 2 weeks with Dox (stop drinking, immobility and high blood glucose) is likely the consequence of multiple organ failure as a result of efficient (P)RR deletion.

4.3.5 Phagocytosis in (P)RR-deficient peritoneal macrophages *in vivo*

Macrophages are professional phagocyte cells, in which no role for (P)RR has been described yet. We used our sh3/4 rats to study the effects of (P)RR knockdown in macrophage phagocytosis *in vivo*. After induction of (P)RR knockdown for 8 days with Dox (100mg/kg) in drinking water, fluorescent latex beads were injected into the peritoneal cavity of anesthetized animals. After 30 min incubation, rats were sacrificed and primary peritoneal macrophages were collected by peritoneal lavage. After centrifugation and resuspension, macrophages were gated and phagocytosis was assessed by flow cytometry. In all experiments, macrophages from SD rats exhibited normal phagocytosis. In contrast, macrophages from transgenic rats gave conflicting data. Indeed, despite identical Dox treatment for all experiments, we observed that transgenic macrophages exhibited either a normal phagocytosis or an absence of phagocytosis (data not shown). Therefore, we were not able to confirm a role of (P)RR in macrophage phagocytosis *in vivo*. The reason for these discrepancies is not clear but several hypotheses can be emitted. First and most likely, the efficiency of Dox treatment to deplete (P)RR in peritoneal macrophages might differ from one rat to another. Variations in parameters such as the age, body weight or drinking volume might modify the efficiency of the Dox treatment. Also, for ethical reasons, we could not treat rats with Dox more than 8 days. Other explanations involve technical problems occurring during genotyping or beads injection.
Altogether, a role of (P)RR in macrophage phagocytosis could not be confirmed *in vivo* by treating transgenic rats with Dox during 8 days. To study such a role of (P)RR and to have a better monitoring of the Dox treatment, we decided to perform experiments on macrophages differentiated *in vitro*.

4.3.6 Characterization of (P)RR-deficient macrophages *in vitro*

To study the role of (P)RR in macrophages *in vitro*, we established a well-described cell culture system based on bone marrow (BM) cells. BM cells from SD and sh3/4 rats were collected and cultured 6 days with M-CSF (30 ng/ml) to obtain pure macrophage populations. To validate our model, macrophages were further treated with Dox (1 µg/ml) and (P)RR expression was assessed at different time of treatment. (P)RR mRNA levels in transgenic macrophages was significantly decreased (more than 90%) after 48h of Dox treatment compared to Dox-treated

Ctrl macrophages (Fig. 61A). Accordingly, western blot analysis revealed that (P)RR protein levels in transgenic macrophages was also strongly reduced after 48h of Dox treatment (Fig. 61B).

In addition, we tested the reversibility of our system. To this purpose, transgenic macrophages were treated for 3 consecutive days with Dox (1 µg/ml) and further maintained 4 days in Dox-depleted medium. (P)RR protein level was assessed by western blot. As described above, (P)RR protein level was efficiently reduced by Dox after 1 day of treatment and no longer detected after 2 and 3 days of treatment (Fig. 61C). Interestingly, (P)RR proteins were not detected for several days after Dox depletion suggesting that (P)RR knockdown persisted in these cells despite the absence of Dox in the medium (Fig. 61C). This suggested that intracellular Dox remained present and active after Dox depletion in culture medium.

These results showed that Dox in culture medium induces *sh(P)RR* expression and efficiently decreased (P)RR mRNA and protein levels *in vitro*. Therefore, this model represents a good alternative to the peritoneal macrophages isolated from Dox-treated rats.

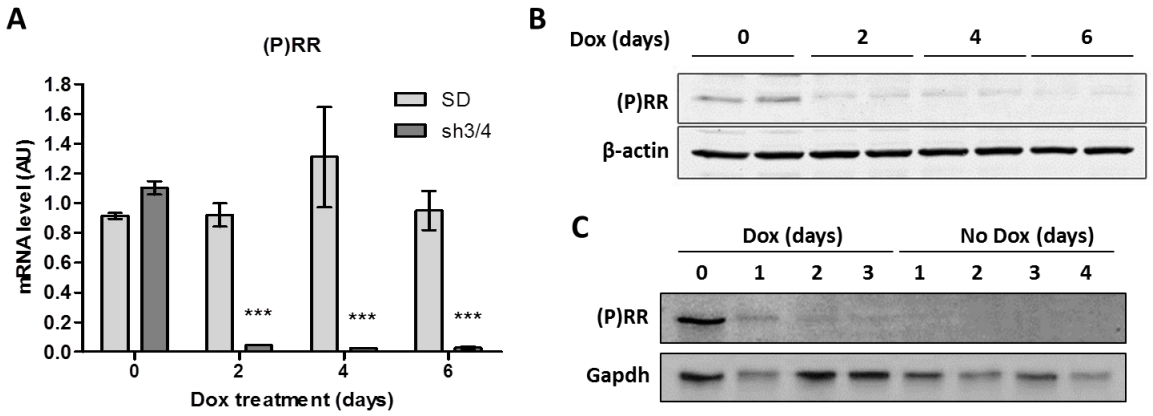

Fig. 61: Doxycycline (Dox) treatment decreases (P)RR expression in macrophages *in vitro*. BM-derived macrophages were treated with doxycycline (1 µg/ml) in medium for several days. **(A)** (P)RR mRNA levels in Dox-treated macrophages were measured by qPCR using Hprt as a reference gene (n=2). **(B)** (P)RR protein levels in Dox-treated macrophages was detected by western blot using β-actin as a loading control (n=2). **(C)** (P)RR protein level in macrophages during and after Dox treatment was detected by western blot using Gapdh as a loading control. ****P<0.001 vs. SD rat*

A defective autophagy characterized by the accumulation of autophagolysosomes (LC3bII positive compartments) within cells has been described in most (P)RR-deficient tissues (Kinouchi et al. 2010, Oshima et al. 2011, Riediger et al. 2011). Therefore we aimed to observe whether such phenotype was present in our (P)RR-deficient macrophages. To this purpose, we first studied LC3bI conversion into LC3bII by western blot in macrophages cultured under several conditions (Fig. 62A). Control and transgenic macrophages were first cultured 4 days in Dox-containing medium. At basal level, we did not observe any difference in LC3bII/LC3bI ratio between both groups. After Dox treatment, some cells were further cultured in starvation medium for 4 hours or in presence of Rapamycin for 2 hours in order to induce autophagy. In both conditions, we detected a similar increase of the LC3bII/LC3bI isoform in (P)RR-deficient

and control macrophages. Finally, the presence of Bafilomycin (V-ATPase inhibitor) in starvation medium further increased the LC3bII/LC3bI ratio in both groups compared to starvation alone. This last result suggested that (P)RR-deficient macrophages retained the ability to correctly process and degrade the LC3bII isoform in autophagolysosomes under starvation conditions as the accumulation of LC3bII isoform occurred after V-ATPase inhibition (Bafilomycin-dependent).

Immunostaining using an antibody targeting both LC3b isoforms confirmed the results obtained by western blots. LC3bI/II immunofluorescence was identical in Control and (P)RR-deficient macrophages at basal level or after incubation with Rapamycin (Fig. 62B) confirming a normal autophagy in those cells.

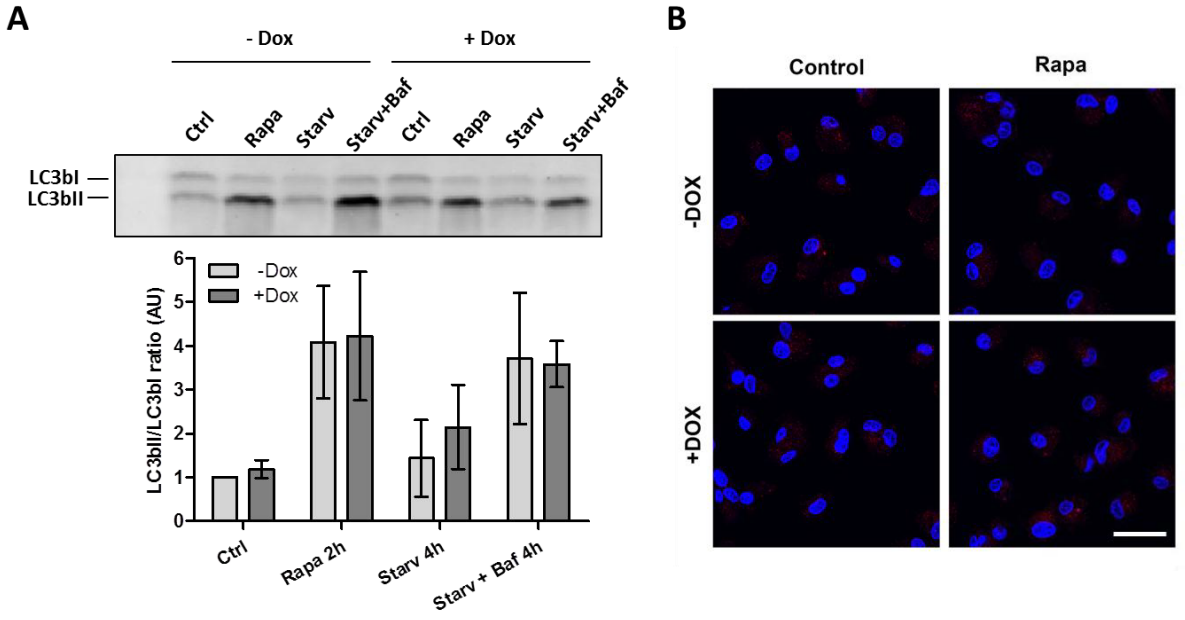

Fig. 62: (P)RR-deficient macrophages have a normal autophagy *in vitro*. BM-derived macrophages from sh3/4 rats were kept in culture 4 days with or without Dox (1 µg/ml) in culture medium and used in experimental setups. To induce autophagy, macrophages were either treated 2 hours with Rapamycin (1 µM) or incubated 4 hours in starvation medium (Hank's balanced salt solution). Bafilomycin (Baf, 1 µM) was used to inhibit V-ATPases. **(A)** The conversion of LC3bI into LC3bII is a hallmark of autophagy and was assessed by western blot using an LC3 antibody targeting both isoforms. Induction of autophagy was assessed by LC3bII/LC3bI ratio using macrophages in normal conditions (Ctrl, -Dox) as reference (n=2). **(B)** LC3bI/II immunofluorescence staining (red) in Control and Dox-treated macrophages either in normal medium or treated 2 hours with Rapamycin (1µM) to induce autophagy. Nuclei were stained with DAPI (blue). Confocal imaging using 63X objective. Scale bar=25 µm. AU, arbitrary unit.

In conclusion, these results show that 1-2 days of Dox treatment induces *sh(P)RR* expression and efficiently decreases (P)RR expression in macrophages *in vitro*. In addition, the normal autophagy observed in (P)RR-deficient macrophages after 4 days of Dox treatment suggests that the defective autophagy (associated with apoptosis/necrosis) observed in (P)RR-deficient tissues (Kinouchi et al. 2010, Oshima et al. 2011, Riediger et al. 2011) is a long term consequence of (P)RR deletion. Altogether, our (P)RR-deficient macrophages cultured *in vitro* are an adequate

tool to study a role of (P)RR in these cells before the defective autophagy can interfere with cellular mechanisms.

4.3.7 (P)RR-deficient macrophages have a normal phagocytosis of beads *in vitro*

To study phagocytosis *in vitro*, we first used fluorescent beads. Macrophages from transgenic rats were treated with Dox (1 µg/ml) for several days and fluorescent latex beads were added into the medium (5.10^6 beads/well). After 30 min of incubation, cells were washed, collected and fluorescence was assessed by flow cytometry. Untreated macrophages from SD or transgenic rats, and Dox-treated macrophages from SD rats were used as control. After 2 and 4 days of Dox treatment, we observed a similar fluorescence profile with FACS, indicative of similar uptake capacities in (P)RR-deficient macrophages and the different control macrophages (data not shown). We extended the Dox treatment up to 6 days but macrophages from all groups showed again an identical uptake of fluorescent beads (Fig. 63).
These results suggest that short and long term (P)RR deletion in macrophages do not impair the bead engulfment *in vitro*.

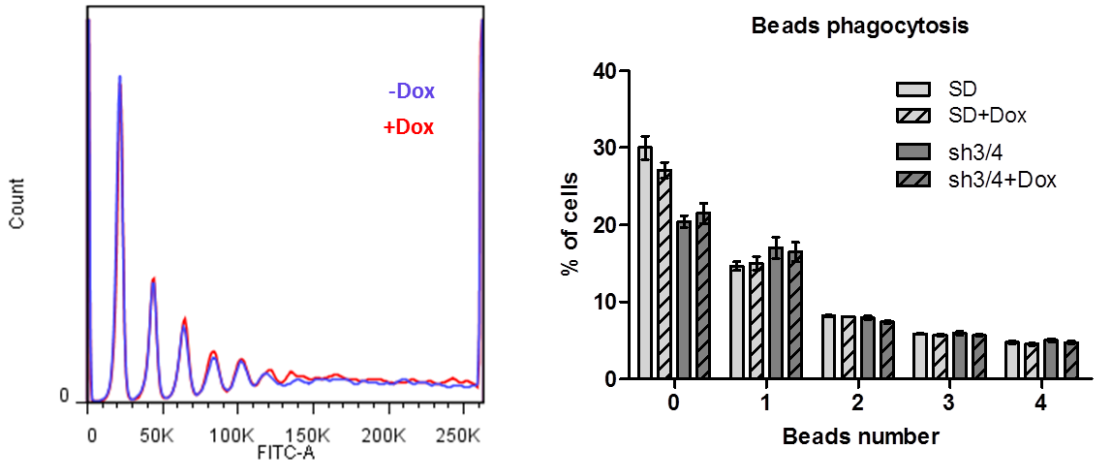

Fig. 63: (P)RR-deficient macrophages have a normal phagocytosis of beads *in vitro*. BM-derived macrophages from SD and sh3/4 rats were treated with or without doxycycline (Dox, 1 µg/ml) in medium for 6 days. To assess phagocytosis, yellow-green fluorescent latex beads were added to the culture medium (5.10^6 beads/well). After 30 min incubation, macrophages were scrapped, collected and subjected to FACS analysis. After exclusion of doublet cells, the fluorescence of phagocytosed beads was observed (FITC laser) in macrophages (n=2).

4.3.8 (P)RR-deficient macrophages have a delayed acidification and/or vesicle trafficking after phagocytosis of *E. coli* bioparticles *in vitro*

Phagocytosis is a complex mechanism involving several cellular functions. After engulfment, foreign bodies are trafficked in maturating vesicles through the cytoplasm and are targeted to the highly acidic lysosomal compartment. Experiments with beads *in vitro* revealed that the

capacity of (P)RR-deficient macrophages to engulf particles was not impaired but did not provide additional hints about vesicle trafficking and acidification. To gather information about pH, we used different methods. We performed our initial experiments using pH-dependent fluorescent dyes such as LysoTracker Red which stains highly acidic lysosomes, and LysoSensor Green which reacts more widely and stains mildly and highly acidic compartments. We applied these dyes to transgenic macrophage cultures treated with or without Dox during 4 days. In some conditions, macrophages were starved (no serum and no amino acids) before the addition of the dyes in order to induce autophagy and the generation of acidic autophagolysosomes. For all conditions, we observed the fluorescence by confocal microscopy. We did not observe any difference for LysoTracker Red fluorescence between control and Dox-treated macrophages either in normal or starvation conditions (Fig. 64A). In contrast, 1 hour pretreatment with Bafilomycin to inhibit V-ATPases totally abolished LysoTracker Red signal (Fig. 64B). Finally, LysoSensor Green signal in control and Dox-treated macrophages was identical and did not reveal any differences in terms of overall pH (Fig. 64C).

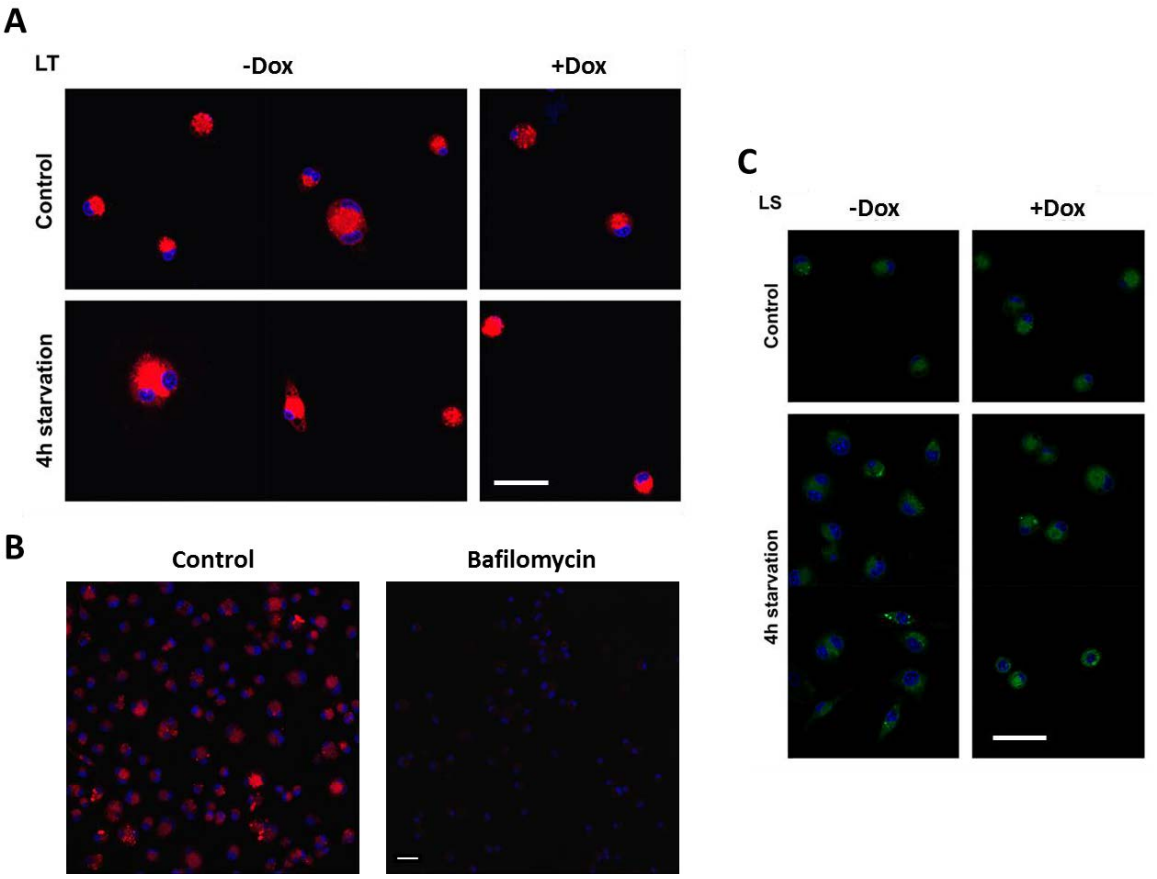

Fig. 64: (P)RR-deficient macrophages have acidic cytoplasmic organelles. BM-derived macrophages from sh3/4 rats were kept in culture for 4 days with or without Dox in culture medium. pH-dependent fluorescence was assessed in normal medium (Control) or after 4h starvation medium. **(A)** LysoTracker Red (LT) fluorescence in macrophages. Cells were incubated with LysoTracker Red (50 nM) and observed using confocal microscopy. **(B)** Effect of Bafilomycin on LysoTracker Red signal. Macrophages were treated with Bafilomycin (1 µM) for 30 min before LysoTracker Red staining. **(C)** LysoSensor Green (LS) fluorescence in macrophages. Cells were incubated with LysoSensor Green (1 µM) and observed using confocal microscopy. DAPI (blue) stained nuclei. Scale bars= 25 µm.

All these results suggested that 48-72 hours after (P)RR depletion, the pH is not impaired in intracellular compartments. It also suggested that the total absence of acidification observed in (P)RR-depleted cells using the Cre/Lox system might be a late consequence of (P)RR deletion.
However, these pH-dependent dyes give only a rough idea of the pH at a certain point and do not reflect the dynamic of pH variations. Therefore, we decided to use fragments of dead bacteria coupled with a low pH-sensitive fluorochrome (pHrodo™ Red *E. coli* BioParticles) to follow the trafficking and acidification of vesicles after internalization.
Control and Dox-treated macrophages were incubated with pHrodo™ Red *E. coli* BioParticles during 1 hour and phagocytosis was analyzed by confocal microscopy. Multiple acidic vesicles characterized by a very strong fluorescence were observed in macrophages from both groups without any differences (Fig. 65). Inhibition of phagocytic engulfment with Rapamycin strongly reduced the fluorescence emission.
These results confirmed that the uptake of bacteria fragments is not impaired in (P)RR-deficient macrophages. Microscopy also revealed that vesicles with acid pH are present in those cells. However, the fluorescence observed by confocal microscopy is not adapted for precise and fine pH quantification. Therefore, we performed additional analysis using flow cytometry to detect more accurately the fluorescence emitted by the bioparticles.

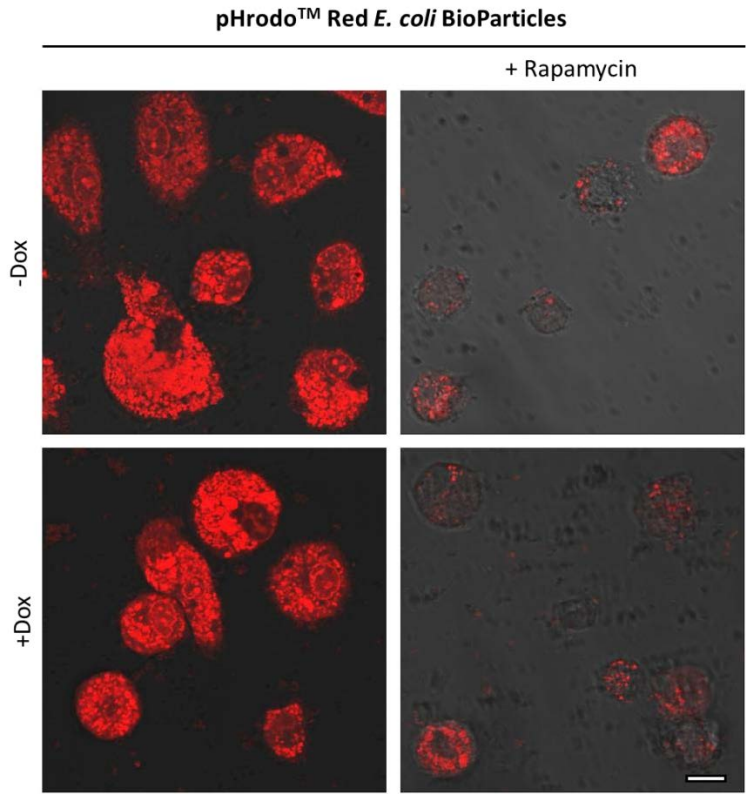

Fig. 65: Dead bacteria are targeted to acidic compartments in (P)RR-deficient macrophages. BM-derived macrophages from sh3/4 rats were kept in culture 4 days with or without Dox (1 µg/ml) in culture medium. pHrodo™ Red *E. coli* BioParticles (sensitive to low pH) were added to the medium (100 µg/ml). Rapamycin (1 µM) was added to block phagocytosis. After 1h incubation, macrophages were washed, fixed and mounted. Endocytosis and pH were assessed by confocal microscopy. Scale bar=10 µm.

Control and Dox-treated macrophages were incubated with pHrodo™ Red *E. coli* BioParticles during 1 hour and pH-dependent fluorescence was analyzed by flow cytometry. For both tested concentrations (200 and 40 µg/ml), we observed in control macrophages (-Dox) a single fluorescence peak (intensity 10^4) characterizing a low pH in bacteria-containing vesicles (Fig.

66). In contrast, in Dox-treated macrophages (+Dox), we also observed an additional peak partially shifted to the left (denoted by an arrow in both panels of Fig. 66) suggesting that some (P)RR-deficient cells have a higher pH in bacteria-containing vesicles.

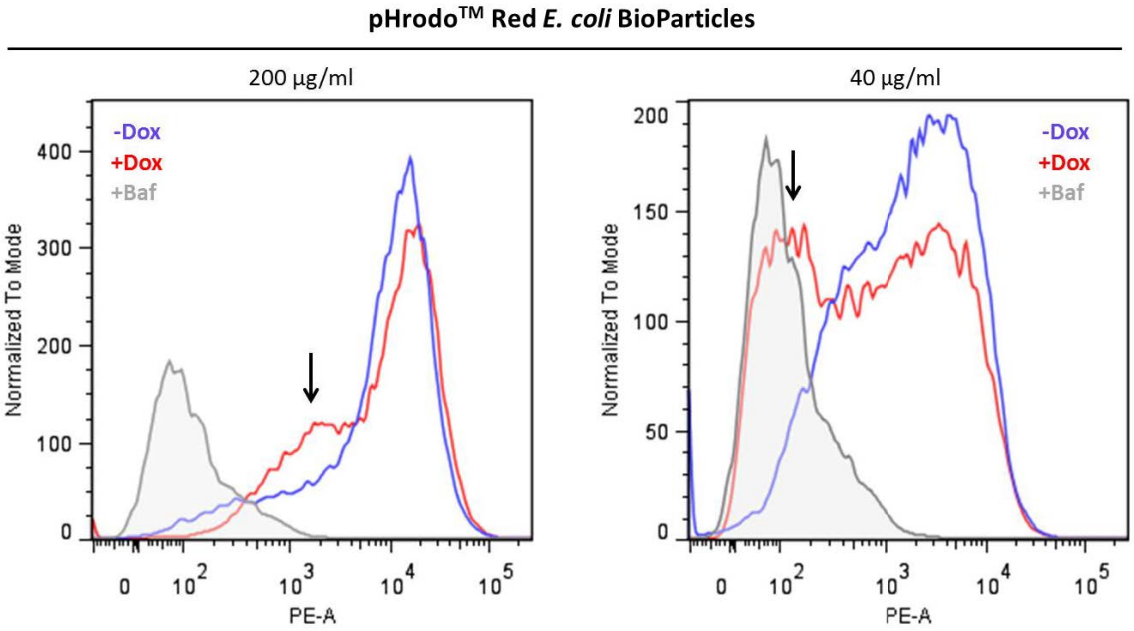

Fig. 66: Acidification of bacteria-containing vesicles is reduced in (P)RR-deficient macrophages. BM-derived macrophages from sh3/4 rats were kept in culture 4 days with or without Dox (1 µg/ml) in culture medium. pHrodo™ Red *E. coli* BioParticles (sensitive to low pH) were added to the medium and two concentrations were tested (200 and 40 µg/ml). Bafilomycin (Baf, 1µM) was also added in some conditions to inhibit intracellular acidification. After 1h incubation, macrophages were washed and the fluorescence was detected by flow cytometry. A shift in fluorescence (arrows) towards higher pH could be observed in Dox-treated macrophages.

Inhibition of V-ATPase with Bafilomycin (Baf) totally blocked acidification as no fluorescence peak was observed.

These data suggested that acidification takes place but is somehow impaired in (P)RR-deficient macrophages. To further characterize this effect, we performed flow cytometry at different time after bacteria uptake. To this purpose, control and Dox-treated macrophages were incubated with pHrodo™ Red *E. coli* BioParticles during 30, 60 and 90 min and fluorescence was further assessed by flow cytometry. After 30 min of incubation, there was no significant difference in the early acidification between Dox-treated and control macrophages (Fig. 67). In contrast, after 1 hour incubation, a lower pH was observed in controls compared to Dox-treated macrophages (Fig. 67). This effect is likely a consequence of a decreased acidification of bacteria-containing vesicles as the uptake was not impaired in (P)RR-deficient macrophages. Finally, after 90 min of incubation, a high intensity fluorescence peak characteristic of a low pH was identified in both groups. It suggested that (P)RR-deficient macrophages have the ability to generate a low pH in phagolysosomes although the process is delayed (Fig. 67). It is important to note that the acidification of bacteria-containing vesicles in (P)RR-deficient macrophages was back to normal after 90 min in this experiment but was sometimes already observed after 45 or 60 min in other

experiments. Despite these experimental variations, these results confirmed that (P)RR-deficient macrophages target bacteria to acidic compartments but the maturation process requires more time compared to control macrophages.

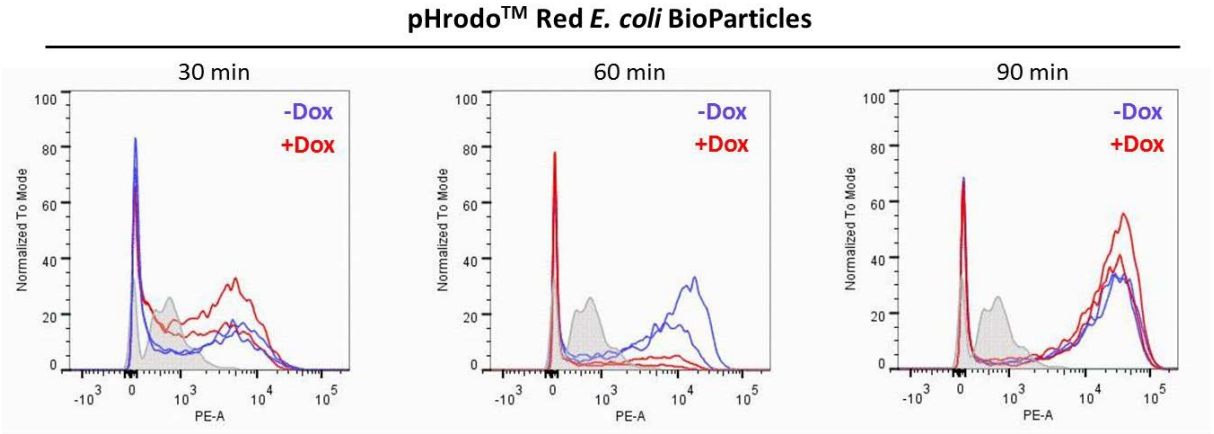

Fig. 67: Acidification of bioparticles-containing vesicles is delayed in (P)RR-deficient macrophages. BM-derived macrophages from sh3/4 rats were kept in culture 4 days with or without Dox (1 µg/ml) in culture medium. pHrodo™ Red *E. coli* BioParticles (sensitive to low pH) were added to the medium (40 µg/ml). After 30, 60 and 90 min incubation, macrophages were washed and the fluorescence was detected by flow cytometry. Shaded curves represent background fluorescence of pHrodo *E. coli* incubated in medium alone.

4.3.9 (P)RR-deficient macrophages have a normal endocytosis but an impaired receptor recycling

In parallel to the phagocytosis process, we also aimed to study a potential role of (P)RR in the process of endocytosis and receptor recycling. After endocytosis of a receptor/ligand complex by clathrin-coated pits, both partners dissociate within acidic endosomes and most ligands are further targeted to lysosomes for degradation whereas receptors returned back to the plasma membrane through several pathways involving different organelles. In contrast, transferrin and its receptor are not dissociated in acidic endosomes but are rather recycled together to the plasma membrane. This association is actually a tripartite collaboration as the transferrin is bound to two irons (Fe^{3+}) and is therefore an important regulator of cellular iron uptake. After endocytosis, the acidic pH (~6.0) in early (sorting) endosomes (Rab5 positive) leads to the dissociation of the iron and iron-free transferrin remains bound to its receptor. The bipartite complex is recycled to the plasma membrane within recycling endosomes (Rab11 positive) and the extracellular neutral pH leads to the dissociation of the transferrin from its receptor (Maxfield et al. 2004). One particular advantage of transferrin over other ligands (albumin for instance) is the possibility to study both endocytosis and recycling processes. We decided to study the endocytosis and recycling of the transferrin/transferrin receptor complex in our (P)RR-deficient macrophages.

We first aimed to observe the kinetics of transferrin uptake and release in macrophage. To this purpose, macrophages were allowed to internalize human transferrin for 10 min followed by 0, 15 and 45 min chase. Intracellular transferrin was detected by western blot using an anti-transferrin antibody and quantified using Gapdh as loading control. Immediately after the 10 min pulse (0 min chase), a large amount of intracellular transferrin was detected in macrophages suggesting an efficient uptake. We observed that intracellular transferrin level was increased by approximately 50% in (P)RR-deficient macrophages (Dox-treated) compared to control macrophages (Fig. 68A). After 15 min of chase, intracellular transferrin was strongly reduced in control macrophages suggesting an efficient recycling process (Fig. 68A). Although this reduction was also observed in (P)RR-deficient macrophages, the amount of intracellular transferrin was 3 times higher in those cells. After 45 min chase, almost all transferrin was recycled in control macrophages whereas (P)RR-deficient cells still had a double amount of intracellular transferrin in comparison (Fig. 68A).

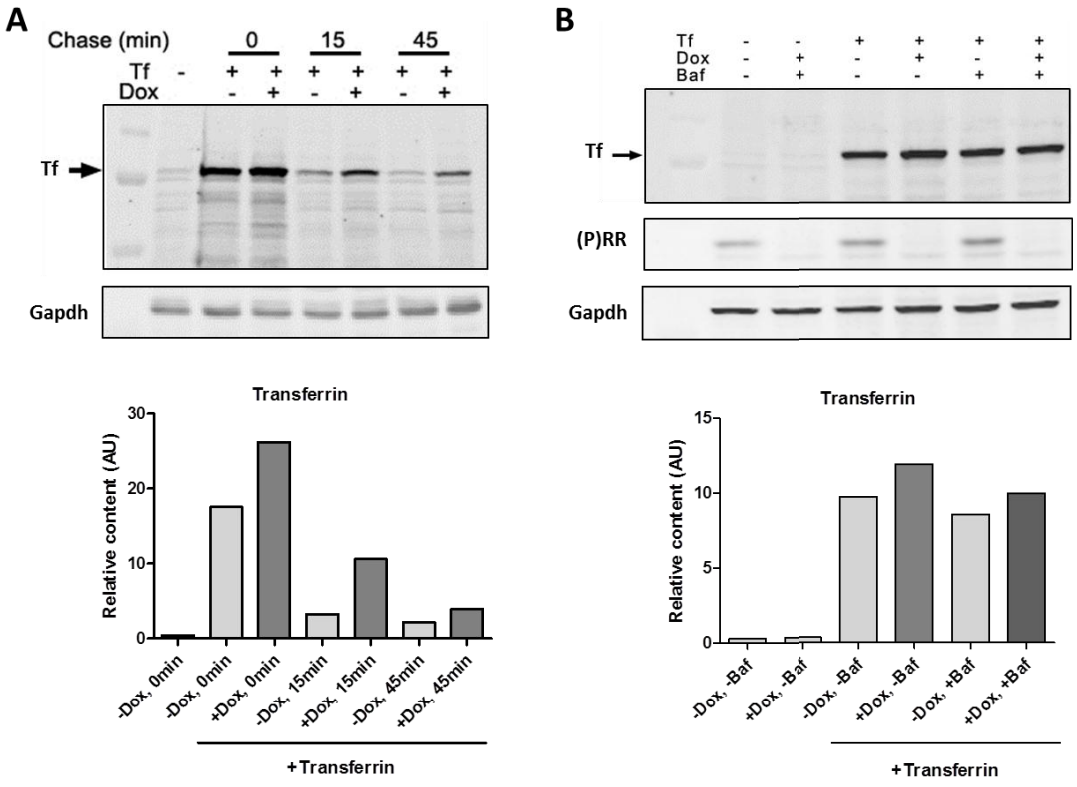

Fig. 68: (P)RR-deficient macrophages have an impaired transferrin receptor recycling. BM-derived macrophages from sh3/4 rats were kept in culture 4 days with or without Dox (1 µg/ml) in culture medium and used in experimental setups. **(A)** Intracellular transferrin is increased in (P)RR-deficient macrophages (Dox-treated). Macrophages were pulsed with human transferrin (1.5 µg/ml) for 10 min and transferrin internalization was monitored after 0, 15 and 45 min chase periods by western blot using an anti-transferrin (Tf) antibody. Signals were quantified using Gapdh as loading control. **(B)** Transferrin recycling is impaired in (P)RR-deficient macrophages. Macrophages were treated with Bafilomycin (Baf, 1 µM) for 30 min to block receptor recycling and further pulsed with human transferrin (1.5 µg/ml) for 5 min. Cells were washed and cytoplasmic transferrin was assessed by western blot using an anti-transferrin (Tf) antibody. Signals were quantified using Gapdh as loading control. (P)RR deletion was confirmed in Dox-treated macrophages using an anti-(P)RR antibody. AU, arbitrary unit.

These results showed that (P)RR-deficient macrophages have more intracellular transferrin after a 10 min pulse and this effect was maintained after 15 and 45 min of chase. Either a defective recycling or increased endocytosis were the most likely reasons to explain this effect. Indeed, after endocytosis, 95% of the transferrin molecules are recycled from sorting endosomes to the plasma membrane with a $t_{1/2}$ of 2 min (Maxfield et al. 2004). An impairment of this recycling dynamics taking already place during the 10 min pulse may explain the effects observed in (P)RR-deficient macrophages. Although the uptake of particles during phagocytosis was normal in (P)RR-deficient macrophages, an increase of transferrin endocytosis during the 10 min pulse can not be excluded in our experiment.

To test whether endocytosis was involved, macrophages were treated with Bafilomycin for 30 min to block recycling processes (no vesicle acidification) and further incubated with human transferrin during a short pulse of 5 min without any chase. Quantification of intracellular transferrin at the end of the pulse was assessed by western blot. Blockade of recycling with Bafilomycin almost totally abolished the difference in the amount of intracellular transferrin observed by western blot between Dox-treated and control macrophages (Fig. 68B). (P)RR deletion was also assessed and confirmed in Dox-treated macrophages by western blot (Fig. 68B). These results suggest that (P)RR-deficient macrophages have a normal transferrin endocytosis. The increased intracellular transferrin observed in these cells is most likely the consequences of an impaired recycling of the transferrin/transferrin receptor complex.

We then performed histochemistry to further characterize the intracellular location of the transferrin in (P)RR-deficient macrophages. To this purpose, we first incubated macrophages with fluorescent human transferrin (transferrin-AF647) for 10 min and observed by confocal imaging the intracellular transferrin after 15 and 45 min of chase. At both times we observed more fluorescent transferrin in Dox-treated macrophages compared to control (Fig. 69).

Interestingly, strongest fluorescence appeared to be located at the cell periphery suggesting that transferrin molecules were likely located in vesicles such as sorting, early and/or recycling endosomes (Fig. 69). These results validate our previous data from western blot and confirm that transferrin recycling is impaired in (P)RR-deficient macrophages. In those cells, the transferrin appeared mainly at the cell periphery but the exact subcellular localization requires further experiments, including the tracking of transferrin through the different vesicles involved in the recycling process using double immunohistological labeling.

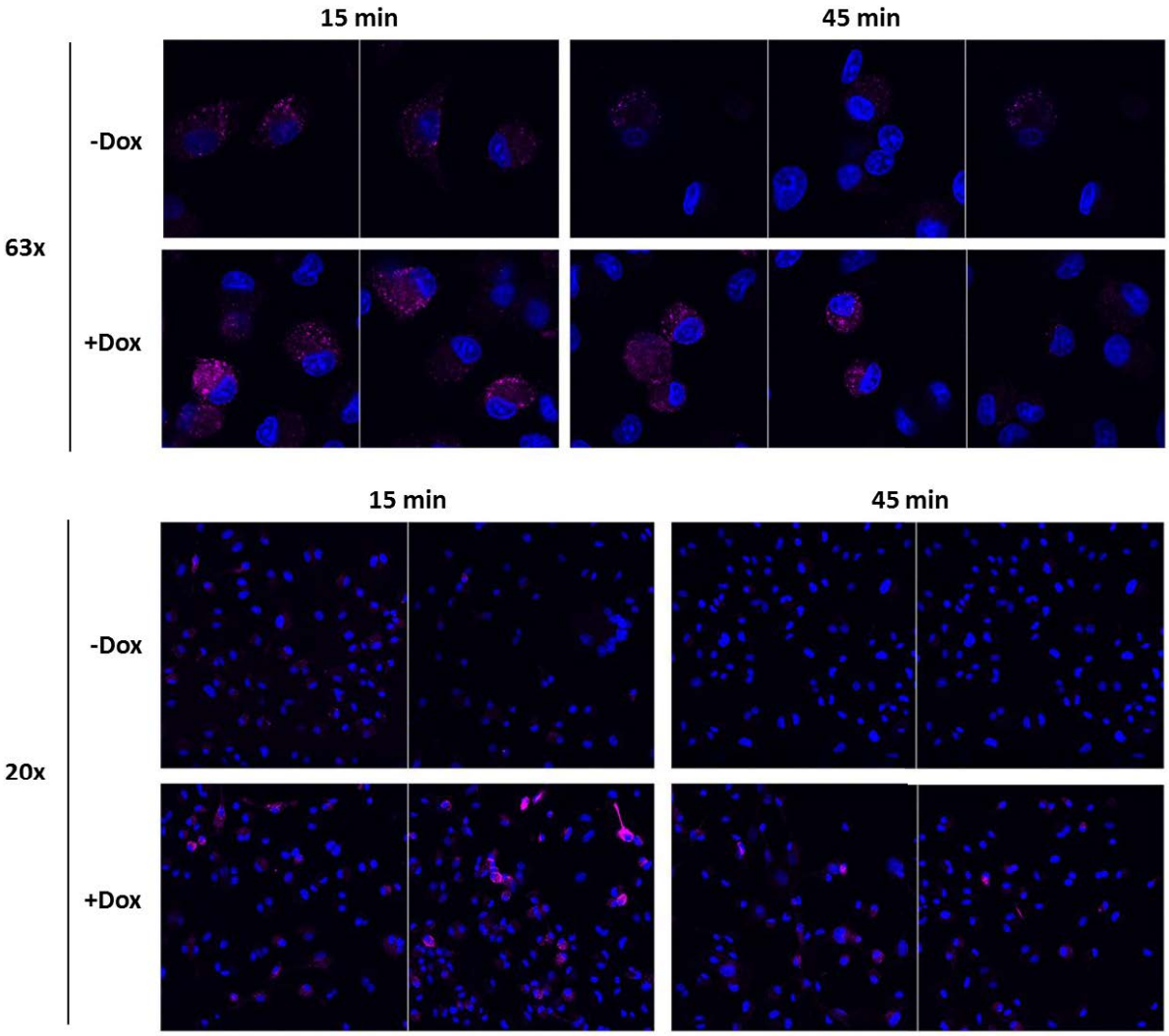

Fig. 69: Intracellular transferrin accumulates in (P)RR-deficient macrophages. BM-derived macrophages from sh3/4 rats were kept in culture 4 days with or without Dox (1 µg/ml) in culture medium and used in experimental setups. Macrophages were pulsed with human transferrin-AF647 (25 µg/ml) for 15 min and transferrin internalization was monitored after 15 and 45 min chase periods by confocal imaging using 63x (upper panel) and 20x (lower panel) objectives. Nuclei were stained with DAPI (blue).

4.3.10 Conclusion

We successfully generated transgenic rats with a conditional depletion of (P)RR based on Doxycycline-induced shRNA expression system. Efficient (P)RR depletion *in vivo* was accomplished by treating rats with Doxycycline in drinking water and led to premature death after two weeks of treatment. To study a role of (P)RR in macrophages, we were able to generate (P)RR-deficient macrophages *in vitro* by adding Doxycyclin in the culture medium. (P)RR deletion in mouse tissues has been associated with cell death due to an alkalization of intracellular vesicles and subsequent accumulation of autophagic vacuoles. In (P)RR-deficient macrophages, we found that the impairment of vesicular pH is not an early event but rather a late consequence after (P)RR deletion. Finally, we found that (P)RR depletion in macrophages

did not impair neither phagocytosis nor endocytosis but rather perturbed the recycling of the transferrin receptor to the plasma membrane. This effect occurred quickly after (P)RR depletion and was not associated with a defective pH. In conclusion, our findings suggest that (P)RR might be important for cellular processes other than vesicle acidification. However, further experiments are required to understand by which mechanisms it occurs.

5 CHAPTER DISCUSSION

The role of the (Pro)renin receptor in osteoclasts and macrophages was in the focus of the present study.

The (pro)renin receptor [(P)RR/ATP6ap2] is a 37-kDa single transmembrane protein discovered a decade ago and depicted as a new member of the tissue renin-angiotensin system (Nguyen et al. 2002). It binds renin and prorenin, leading to increased catalytic activity of these molecules and subsequent local AngII generation. In addition, both ligands can activate pro-fibrotic signaling pathways via the (P)RR, in an AngII-independent manner (Nguyen et al. 2002). For this reason, the role of the (P)RR in cardiovascular diseases and diabetes has been particularly studied in the last decade. However, the discovery of embryonic lethality after (P)RR gene deletion in zebrafish (Amsterdam et al. 2004, Nuckels et al. 2009, http://zfin.org) and mouse (Sihn et al. 2010) paved the way for additional roles of (P)RR in cell homeostasis. Indeed, a 8.9 kDa segment of the (P)RR has been shown to associate with the vacuolar H^+-ATPase (V-ATPase), hence its other name ATP6ap2 (V-ATPase associated protein 2) (Ludwig et al. 1998).

V-ATPases are multiprotein complexes composed of a peripheral V1 domain (eight subunits) responsible for ATP hydrolysis, a membrane –embedded V0 domain (six subunits) responsible for proton translocation and two accessory subunits (Forgac et al. 2007). V-ATPases regulate the pH of various intracellular compartments and are therefore essential for numerous cellular processes including membrane trafficking, molecule transport, receptor recycling and protein degradation. Developmental studies in *Xenopus* and *Drosophila* have revealed a functional association between (P)RR and V-ATPases to promote the canonical and non-canonical Wnt signaling pathways (Cruciat et al. 2010, Buechling et al. 2010, Hermle et al. 2010), whereas studies with tissue-specific gene deletion have pointed out a role in autophagy (Kinouchi et al. 2010, Oshima et al. 2011, Riediger et al. 2011). The defective acidification of a particular intracellular compartment including endosomes and lysosomes was the common observation in these studies.

Mainly intracellular in almost all cells, V-ATPases can be located at the plasma membrane in some specialized cell types including osteoclasts in order to acidify the extracellular environment (Forgac et al. 2007). Mice deficient for some V-ATPase subunits develop osteopetrosis as a consequence of abnormal osteoclast activity (Li et al. 1999, Lee et al. 2006). A role of (P)RR in the regulation of membrane V-ATPases and in osteoclasts in general remained unknown. Therefore, two genetic mouse models with (P)RR deletion in osteoclasts and *in vitro* experiments were used to investigate the role of (P)RR in these cells.

Macrophages are immune cells specialized in the engulfment and degradation of pathogens in a process known as phagocytosis (Stuart et al. 2005). In addition, an intense trafficking of endosomes including recycling endosomes occurs in these cells and is crucial for a normal immune response (Steinman et al. 1983, Flannagan et al. 2009). Phagocytosis and endosome trafficking are highly dependent on V-ATPase activity (Flannagan et al. 2009). A role of (P)RR in macrophage functions was not described. Therefore, transgenic rats with inducible (P)RR deletion were generated and *in vitro* experiments with transgenic macrophages were performed to analyse the role of (P)RR in macrophage functions.

5.1 Role of (P)RR in osteoclast physiology

Osteoclasts are highly specialized cells with the unique ability to resorb bone tissue. They play a fundamental role not only in bone homeostasis but also in several skeletal pathologies. Osteoclasts are multinucleated cells resulting from the fusion of myeloid cells (macrophages/monocytes) directed by specific extracellular cues including M-CSF and RANKL. During their maturation, osteoclasts rearrange their actin cytoskeleton, become polarized and develop a ruffled membrane. Upon attachment to the bone surface, a sealed zone also known as resorption lacunae is created between the osteoclast ruffled membrane and the bone surface. Acidification of the resorption lacunae is ensured by V-ATPases present at high density at the ruffled membrane and is responsible for the dissolution of bone minerals and degradation of bone matrix. To become such specialized cells, differentiating osteoclasts execute a particular genetic program and regulate many genes. Though a prior study described an upregulation of (P)RR mRNA levels during osteoclast differentiation *in vitro* (Nomiyama et al. 2005), little is know about the role of (P)RR in osteoclast functions.

In this study, we confirmed that (P)RR expression is indeed upregulated during *in vitro* differentiation of mouse progenitors (RAW264.7 and bone marrow cells) in presence of M-CSF and RANKL. In addition, immunostaining on bone sections showed that osteoclasts *in vivo* also have a strong (P)RR expression when compared with other bone cells including chondrocytes and osteoblasts. These results suggested a potential role of (P)RR in osteoclast functions.

To assess a functional role of (P)RR in osteoclasts, we bred (P)RR flox mice with two different Cre-expressing mouse models. To disrupt specifically (P)RR in mature osteoclasts, we used mice in which the Cre was knocked into the endogenous *CtsK* (*Cathepsin K*) locus. This model was recently generated and was described to be specifically confined to differentiated osteoclasts (Nakamura et al. 2007). Efficency of the CtsK-Cre was further validated in several studies (Ito et al. 2010, Myauchi et al. 2010, Tsuji-Takichi et al. 2012). To delete (P)RR in osteoclast progenitors (monocytes/macrophages), we additionaly crossed (P)RR flox mice with mice in which the Cre was knocked into the *LysM* (*Lysozyme M*) locus (Clausen et al. 1999). This model has been extensively used to study functional relevance of genes in myeloid cells including granulocytes, monocytes, macrophages and in osteoclast progenitors (Hume et al. 2011). Efficient gene deletion in osteoclasts was previously published by different groups (Kenner et al. 2004, Kim et al. 2006, Lamothe et al. 2013, Qi et al. 2014) while others have pointed out an inefficient

recombination (Aliprantis et al. 2008, Croke et al. 2011). For a better comprehension and comparison of our genetic models, the denomination CtsKcKO and LysMcKO will be hereafter used to refer to the Cre used to delete (P)RR. Both CtsKcKO and LysMcKO mice were born with the expected mendelian frequency without any gross morphological abnormalities. For both models, we confirmed the Cre expression pattern by PCR. The CtsK-Cre was found to be restricted to bones while the LysM-Cre was found in almost all organs tested as a consequence of the presence of myeloid cells (circulating and/or resident) in those tissues.

Impaired V-ATPase activity in osteoclasts has been associated with severe osteopetrosis (high bone density) in mice and humans (Li et al. 1999, Scimeca et al. 2000, Frattini et al. 2000, Kornak et al. 2000, Lee et al. 2006). In case (P)RR is important for membrane V-ATPase activity in osteoclasts, we hypothetized that CtsKcKO and LysMcKO mice would develop such a bone phenotype. In contrast, micro-computed tomography revealed a decreased bone density in tibias from CtsKcKO and LysMcKO mice compared to control mice. These results showed that (P)RR is not important for the trafficking and activity of membrane V-ATPases in osteoclasts as the bone phenotype is the result of an active and efficient bone resorption. Histological examination (TRAP staining) showed that (P)RR-deficient osteoclasts are fully mature in CtsKcKO mice. Several lines of evidence suggested an increased activity of these cells *in vivo*. Histological analysis showed an absence of cartilage core in trabeculae of 12 week-old CtsKcKO mice indicating such an increased resorption activity. In addition, increased plasma levels of CTX-I (a marker of bone resorption) were also observed in CtsKcKO mice.

To determine the impact of (P)RR deletion on osteoclast number and activity, we generated osteoclasts *in vitro* using bone marrow and spleen cells stimulated with M-CSF and RANKL for 5-6 days. Deletion of (P)RR in differentiated osteoclast was assessed by western blot to confirm the efficiency of the different Cre. In CtsKcKO cells, (P)RR protein levels were found to be decreased by only 50% after 5 days of RANKL treatment. The late expression of the CtsK-Cre and the presence of mononuclear cells with no Cre activity, both discovered using a reporter gene (R26-YFP), likely explained the incomplete (P)RR deletion. Whether these non-committed osteoclast precursors (no Ctsk-Cre expression) could fuse with committed cells (with CtsK-Cre) is still a matter of debate (Croke et al. 2011). In LysMcKO cells, (P)RR protein levels were found reduced by 70-80% after 3 and 5 days of RANKL stimulation reflecting an early and efficient expression of the LysM-Cre. Although there has been concerns about the efficiency of the LysM-Cre, we achieved such a reduction in (P)RR protein levels by using mice with only one copy of the LysM-Cre.

Both CtsKcKO and LysMcKO osteoclasts were efficiently generated *in vitro*. These cells displayed all the characteristics of fully mature osteoclast: multinucleated, TRAP-positive and a normal cytoskeletal organization characterized by the presence of an actin ring. These results confirm that (P)RR deletion does not impair the fusion and the maturation of osteoclasts. However, we found a somehow impaired rate of differentiation and/or resorption activity in both models.

Indeed, we observed that CtsKcKO osteoclasts displayed an increased differentiation and resorption activity. These effects were accompanied by an increased expression of osteoclast markers such as Trap, CtsK and ATP6V0d2. These genes are regulated by the RANKL signaling

pathway through the activation of transcription factors such as NFATc1 and MITF (Teitelbaum 2000). In LysMcKO osteoclasts, we detected only a slight increase of the resorption activity despite a normal osteoclast differentiation. Our present experiments using two genetic models demonstrate that reduced (P)RR expression in mature osteoclasts and osteoclast progenitors leads to enhanced osteoclast differentiation and/or activity. Our results further show that (P)RR does not regulate the localization and the activity of membrane V-ATPase in osteoclasts but rather modulates the RANKL signaling pathway. The mechanism by which (P)RR might regulate the RANKL signaling remains unknown. Also, whether the abnormal RANKL signaling is the only consequence of (P)RR deletion in osteoclasts remains to be proven and certainly requires additional experiments. It is indeed possible that (P)RR regulates other signaling pathway and physiological functions in osteoclasts as (P)RR has been described to be important for Wnt signalings (Cruciat et al. 2010, Buechling et al. 2010, Hermle et al. 2010 and 2013), autophagy (Kinouchi et al. 2010, Oshima et al. 2011, Riediger et al. 2011, Kurauchi-Mito et al. 2014) and the endolysosomal pathway (Hermle et al. 2013) in different animal models.

Wnt proteins belong to the family of secreted glycoprotein and signal through two signaling pathways: the canonical Wnt (β-catenin-dependent) pathway and the noncanonical pathway. Genetic studies have initially described that activation of the canonical Wnt pathway promotes osteoblast differentiation and activity, while indirectly inhibiting osteoclastogenesis through the secretion of OPG protein (Glass et al. 2005 and 2006). Following these works, the canonical Wnt pathway has largely been studied in osteoblasts and Wnt pathways in general were thought to play no direct role in osteoclasts. However, a series of recent studies have challenged this dogma. Elegant work from Wei et al. revealed a complex, stage-dependent role of β-catenin in osteoclast precursors and in differentiating osteoclasts (Wei et al. 2011). Importantly, they described that β-catenin inhibition in committed osteoclasts stimulates their differentiation. Accordingly, the Wnt3a ligand was shown to activate the canonical Wnt pathway in osteoclasts and further repress osteoclastogenesis in an osteoblast-independent manner (Albers et al. 2013). In general, the canonical Wnt pathway has been described to decrease osteoclast differentiation. In contrast, activation of the noncanonical pathway has consequences on osteoclastogenesis which are ligand-dependent. For instance, Wnt5a ligand has been shown to enhance osteoclastogenesis (Maeda et al. 2012) whereas Wnt4 and Wnt16 ligands repress osteoclastogenesis (Yu et al. 2014, Moverare-Skrtic et al. 2014). From our work, a role of (P)RR in these various Wnt signaling in osteoclasts can not be excluded and requires additional experiments.

Autophagy is a process by which proteins are engulfed into a structure called autophagosome and delivered to lysosomes (autophagolysosome) for degradation (Levine et al. 2011). (P)RR has been described to be required for a normal autophagy in several murine cell types (Kinouchi et al. 2010, Oshima et al. 2011, Riediger et al. 2011, Kurauchi-Mito et al. 2014). The exact role of autophagy in osteoclasts remains largely unknown. A link between autophagy genes and osteoporosis has been suggested in human genome-wide data (Pan et al. 2010, Zhang et al. 2010). Proteins essential for autophagy including Atg5, Atg7 and LC3 were further shown to be

important for the secretory function of osteoclasts and bone resorption *in vitro* and *in vivo*. Osteoclasts deficient for these various autophagy genes were characterized by an impaired autophagy and a decreased resorption activity (DeSelm et al. 2011). In contrast, we found that (P)RR-deficient osteoclasts have an increased activity *in vitro* and *in vivo*. Although we have not studied autophagy in detail, it is therefore unlikely that the lack of (P)RR impairs autophagy in osteoclasts.

Osteoclasts are polarized cells with the sealing zone (integrins-dependent) separating the basal compartment (ruffled border) from the apical area where RANK receptors are located. Although the signaling and functions of RANK/RANKL in osteoclast have been extensively studied, the desensitization and trafficking of RANK receptor remains largely unknown. The involvement of clathrin-dependent endocytosis has been suggested (Narducci et al. 2010). Recently, the retromer complex has been shown to regulate RANK trafficking after endocytosis (Xia et al. 2013). The retromer complex is an element of the endosomal protein sorting machinery and is responsible of the retrieval and trafficking of transmembrane proteins from endosomes to the Golgi apparatus (Seaman 2012). Genetic deletion of Vps35 (Vacuolar protein sorting-associated protein 35), a component of the retromer complex, resulted in osteoporosis in mice as a consequence of a sustained RANK signaling (Xia et al. 2013). In Vps35-depleted cells, RANK was not trafficked to the Golgi but remained in early and late endosomes and at the cell periphery leading to sustained RANKL signaling. In epithelial (polarized) cells of flies, (P)RR has been shown to be important for the endolysosomal degradation of apical vesicles (Hermle et al. 2013). This study revealed that (P)RR is dispensable for the endocytosis of the transmembrane E-Cadherin but is instead required for its targeting to lysosomal degradation. In absence of (P)RR, E-Cadherins were accumulating at the cell surface and in early and recycling endosomes.

A role of (P)RR as a regulator of protein sorting and trafficking might therefore be involved in the modulation of RANKL signaling in osteoclasts. Using fluorophore-coupled antibody, we have tried to localize RANK in (P)RR-deficient osteoclasts without any success until now. This hypothesis thus remains to be verified.

Bone remodeling is a tightly regulated balance (or coupling) between bone formation and bone resorption. Osteoblasts are bone-forming cells derived from bone marrow mesenchymal cells. Osteoblast differentiation and maturation (osteogenesis) are regulated by a multitude of signals including hormones, cytokines, mechanical stress and aging (Chau et al. 2009). In addition to synthetize and mineralize bone, mature osteoblasts directly regulate osteoclast differentiation through the secretion of RANKL and OPG (Boyce etal. 2007). In contrast, osteoclasts were long thought to be bone-resorbing cells with no abilities to regulate osteogenesis in return. However, several studies have recently challenged this dogma. First, it was described that osteoclasts were indirectly regulating osteogenesis via factors such as TGF-β (transforming growth factor-β) and IGF-1 (insulin-like growth factor type 1) released from the bone matrix during resorption (Tang et al. 2009, Xian et al. 2012). Finally, S1P (sphingosine-1 phosphate) and CTHRC1 (collagen triple helix repeat containing 1) were identified as two factors released by resorbing osteoclasts and directly promoting osteogenesis and bone formation (Lotinun et al. 2013, Takeshita et al. 2013).

In this work, we discovered that (P)RR deletion in osteoclasts led to a decrease in bone density in mice. We linked this phenotype to an increased activity of (P)RR-deficient osteoclasts *in vivo* and *in vitro*. Whether (P)RR deletion could impair the secretion of osteogenic factors and further have an impact on bone formation is still unknown. If it is the case, a decreased number of osteoblasts in bone should be observed. Our attempts to stain and count osteoblast on bone sections have until now remained inconclusive. Such histomorphometric information is of high importance to validate or exclude a role of (P)RR in the osteogenic activity of osteoclasts.

(P)RR has been widely described to act as a receptor for (pro)renin (RAS-dependent) and as a regulator of V-ATPase activity (RAS-independent) in various signaling and homeostatic functions (Rousselle et al. 2014). It has also emerged that (P)RR might regulate the PCP signaling in *drosophila* independently of these two roles (Hermle et al. 2010). It is tempting to speculate about the underlying function(s) by which (P)RR deletion interferes with osteoclast physiology.
All components of the RAS have been identified in bone (Tamargo et al. 2015). AngI and AngII have been described as potent stimulators of bone resorption in osteoclast and osteoblast co-cultures (Hatton et al. 1997). This effect actually occurred through a direct action on osteoblasts and on RANKL secretion as AngII had no effect on osteoclast differentiation and activity when osteoclasts were cultured alone and generated by exogenous RANKL treatment (Hatton et al. 1997). The direct action of AngII on osteoblasts was confirmed *in vivo* as it led to osteoporosis in mice (Shimizu et al. 2008). Although (P)RR might act as a receptor for (pro)renin at the osteoclast membrane and generate local AngII, this function likely plays no important role in osteoclast physiology and does not account for the hyperactive osteoclasts described in our study. From the bone phenotype observed in our two mouse models, it is clear that (P)RR does not regulate the location and the activity of membrane V-ATPases in osteoclasts. However, it is still possible that (P)RR modulates the V-ATPase activity in intracellular compartments with consequences on signaling pathways and homeostatic functions described above (Wnt, autophagy, vesicle trafficking) and leading to the potentiation of the RANKL signaling in (P)RR-deficient osteoclasts. Studies in macrophages from our lab and from the group of Prof. Saftig have brough substantial information regarding the role of (P)RR in those cells and potentially in osteoclasts by extension. Our data on (P)RR-deficient macrophages come from our transgenic rats whith an inducible shRNA (Dox treatment) which will be discussed more in detail in the following part of the discussion. Aiming to clarify the importance of the V-ATPase during membrane fusion events, Kissing et al. generated (P)RR-deficient macrophages crossing (P)RR flox mice with LysM-cre animals (Kissing et al. 2015). Previous works in mice have shown that deletion of (P)RR resulted in a reduced protein level of several Vo subunits (Kinouchi et al. 2010, Oshima et al. 2011). Based on these data, they reasoned that (P)RR-deficient macrophages would be an interesting cellular model with V-ATPase deficiency. The disappearence of Vo subunits was indeed confirmed by western blot following efficient (P)RR deletion by the LysM-cre. Interestingly, acidification of intracellular compartments including endosomes and lysosomes was found normal in (P)RR-deficient macrophages which is in accordance with our own results. In addition, they demonstrated that functional V-ATPases are not required for proper fusion events between phagosomes and lysosomes. In contrast, they observed that these

fusion event were even enhanced in (P)RR-deficient macrophages. In our work, we observed that bacteria are indeed targeted to lysosomes for degradation in (P)RR-depleted macrophages, indirectly confirming that fusion beween phagosomes and lysosomes is normal in these cells. Altogether, these data show that macrophages lacking (P)RR have a normal lysosomal acidification and fusion events involving lysosomes are enhanced. Whether such characteristics would be maintained in osteoclasts is unknown but one might hypothetize so. Osteoclasts resulting from the fusion of these cells would likely have an increased fusion of acidic lysosomes with the ruffled membrane resulting in an increased amount of protons released into the extracellular space. Such explanation would be in perfect accordance with the increased activity of (P)RR-deficient osteoclasts revealed in our work. It is also conceivable that this cellular phenotype would thus not be the consequence of an abnormal intracellular acidification with an impact on other cellular functions. These hypotheses are very tempting but remain to be proven in osteoclasts.

Finally, our work reveals that expression of the *Cathepsin K* gene in bone is not restricted to osteoclasts, but also occurs in a new cell population which remains to be fully characterized. Aiming to delete (P)RR in osteoclasts, we crossed (P)RR-floxed mice with transgenic mice in which the Cre recombinase was knocked into the endogenous *CtsK* locus and whose expression was driven by the endogenous *CtsK* promoter (Nakamura et al. 2007). Only cKO mice with one copy of the CtsK-Cre were generated as heterozygous mutant mice of *CtsK* have a normal bone phenotype (Saftig et al. 1998, Gowen et al. 1999). CtsK are lysosomal cysteine proteases predominantly expressed in osteoclasts. They are essential for bone resorption and are therefore becoming a therapeutic target to treat osteoporosis (Costa et al. 2011). CtsK expression has been reported in other cell types but such descriptions have been often associated to a particular pathology including arthritis, atherosclerosis and cancer (Novinec et al. 2013). In bone, osteocytes have been described to express CtsK in the very particular context of lactating females (Qing et al. 2012). Nakamura et al. generated the CtsK-Cre mouse model and performed several experiments to confirm that the CtsK-Cre was exclusively expressed in differentiating osteoclast *in vivo* and *in vitro* (Nakamura et al. 2007). Importantly, CtsK-Cre expression was absent in other bone cells including osteoblasts and osteocytes. In our model, we confirmed that the CtsK-Cre expression was restricted to the bone tissue and had no effect on (P)RR expression in all the organs we tested. Of note, we found a very low expression in skeletal muscle as previously described (Rantakokko et al. 1996) but (P)RR expression was not affected. Whether this weak expression reflects the activity of the CtsK-Cre in a particular cell type present in skeletal muscles or is a technical artifact remains enigmatic. Based on these results and on the description from Nakamura et al. (Nakamura et al. 2007), we assumed that the CtsK-Cre would be specific enough to study a role of (P)RR in osteoclasts. CtsKcKO mice were born at the expected mendelian ratios and appeared normal for the first 2-3 weeks. Subsequently, CtsKcKO mice developed growth retardation which was maintained the whole life. This phenotype did not alarm us at the time as growth retardation has been previously described in some forms of osteopetrosis in mice and humans (Sobacchi et al. 2013). Several intriguing aspects emerged while we were further characterizing these mice. Notably, CtsKcKO mice did

not develop osteopetrosis but rather tended to have a decreased bone volume. Also, histological examination of bones from 4 week-old CtsKcKO mice revealead a striking reduction of the growth plate thickness by approximately 50% compared to control age-matched control littermates. Such observation was consistent with the growth retardation further developed by these mice but could hardly be explained with the increased activity of (P)RR-deficient osteoclasts. CtsKcKO mice were also characterized by a global sick appearance and a decreased activity. In addition, CtsKcKO mice exhibited some morphological abnormalities mainly concentrated on the head: the shape of the face and the nose were altered, the ears were misoriented and the eyes were semi-closed with deteriorated eyelids. Finally, CtsKcKO mice were curiously characterized to have a penis whose size was significantly increased compared to control mice. Altogether, these observations raised serious concerns about the specificity of the CtsK-Cre and prompted us to develop two additional animal models. We first aimed to confirm the phenotype of the CtsKcKO mice in a second mouse model with a conditional deletion of (P)RR in osteoclasts. To this purpose, we used LysM-Cre-expressing transgenic mice and generated LysMcKO mice. These animals were born at mendelian ratios without any malformation. We found a decreased bone density in tibias from LysMcKO mice and an increased resorptive activity of LysMcKO osteoclasts generated *in vitro*. These results are consistent with the observations made in CtsKcKO mice and therefore confirm that the decreased bone density in both models is indeed the consequence of a specific deletion of (P)RR in osteoclasts. In contrast, all other morphological (size, head and penis) and physiological (aspect and activity) abnormalities described above in CtsKcKO mice were absent in LysMcKO mice suggesting that these aspects are not the consequence of (P)RR deletion in osteoclasts but rather involved a distinct, unknown cell population likely targeted only by the CtsK-Cre. To better characterize the expression of the CtsK-Cre in bone, we used R26-YFP reporter mice. On bone sections, we confirmed a strong expression of the CtsK-Cre in osteoclasts. With the exception of very few CtsK-Cre-positive chondrocytes, we did not detect any expression of the CtsK-Cre in the growth plate. However, we observed an expression of the CtsK-Cre in a subset of cells present in the perichondrium, a connective tissue surrounding the cartilage of developing bone also known as the Groove of Ranvier. The perichondral groove of Ranvier remains a poorly-described structure and is believed to contain multipotent cartilage progenitors (chondroprogenitors) (Langenskiöld 1998). Evidence suggests that these cells are important for cartilage growth and homeostasis (Rodríguez et al. 1985, Karlsson et al. 2009). While trying to characterize these new CtsK-expressing cells in our lab, an elegant study published in the journal *Nature* revealed the exact nature of these cells (Yang et al. 2013). This work aimed to better characterize the role of the the tyrosine phosphatase SHP2 (encoded by *Ptpn11*) in metachondromatosis, a particular form of cartilage tumour syndrome in human associated to *Ptpn11* mutations and characterized by hyperproliferating chondrocytes (Bowen et al. 2011). As Yang et al. hypothetized that osteoclasts might be involved in the development of the syndrome, they used CtsK-Cre mice to delete SHP2 specifically in osteoclasts and obtained SHP2 CtsKcKO mice with a dramatic skeletal phenotype and characteristic features of human metachondromatosis. In contrast, when LysM-Cre mice were used, the resulting SHP2 cKO mice did not develop such phenotype suggesting that the abnormal skeleton and the

metachondromatosis observed in SHP2 CtsKcKO mice were not related to impaired osteoclast activity. Using R26-YFP reporter mice, they showed that the CtsK-Cre was expressed by perichondrial cells in the Groove of Ranvier. Using FACS analysis, they purified and further characterized these CtsK-positive cells *in vitro* as potential mesenchymal stem cells which are precursors that can differentiate into osteoblasts, adipocytes and chondrocytes. In absence of SHP2, these cells differentiate into chondrocytes, proliferate and form cartilaginous protrusions (exostoses). These new CtsK-positive progenitor cells are therefore important for normal cartilage growth. Deletion of (P)RR in those cells most likely alters their functions and might explain the morphological abnormalities exhibited by our CtsKcKO mice as they can be related to abnormal cartilaginous homeostasis. The growth retardation can be linked to a defective cartilage growth in long bones. The nose and the ears are cartilaginous tissues. Also, in mice, the penis contains bone and cartilage tissues. These new CtsK-positive progenitors have been described to proliferate in metachondromatosis syndrome (Yang et al. 2013) but the exact mechanism by which these cells regulate cartilage tissues in our CtsKcKO mice remains to be determined. These results also suggest that one should be careful using the CtsK-Cre mice to study the role of a gene in osteoclasts as these new progenitors are also targeted. In conclusion, we showed that (P)RR-deficient osteoclasts are responsible for the decreased bone density in CtsKcKO and LysMcKO whereas a new CtsK-expressing progenitor cell within the Groove of Ranvier is involved in the morphological abnormalities exhibited by CtsKcKO mice.

In conclusion, our work showed that (P)RR is not important for the trafficking and activity of membrane V-ATPases in osteoclasts as (P)RR-deficient osteoclasts were characterized by an increased resorptive activity leading to a reduction of the bone density in two mice models with a conditional deletion of (P)RR in osteoclasts using LysM- and CtsK-Cre. (P)RR seems to be important for the RANK/RANKL pathway in osteoclasts by a mechanism which remains to be described. In addition, we and others (Yang et al. 2013) revealed that the expression of Cathepsin K, previously thought to be restricted to osteoclasts, is also occuring in some cells in the Groove of Ranvier. These Ctsk-expressing progenitor cells better characterized by Yang et al. are important for cartilage growth and homeostasis (Yang et al. 2013) and are thus likely implicated in the morphological abnormalities (growth retardation, face, penis) observed in our CtsKcKO mice. The role of (P)RR in these cells and the exact functions and properties of these cells remain to be investigated.

5.2 Role of (P)RR in macrophage physiology

An RNAi approach was chosen to create a new transgenic animal model to study the role of (P)RR in macrophages, resulting in the successful generation of an inducible *sh(P)RR* transgenic rat line.

The generation of mice with constitutive deletion of (P)RR was unsuccessful in mice, likely resulting in embryonic lethality (Sihn et al. 2010). Conditional deletion of (P)RR in cardiomyocytes, podocytes and smooth muscle cells have been achieved in mice using the

Cre/Lox system (Kinouchi et al. 2010, Oshima et al. 2011, Riediger et al. 2011, Kurauchi-Mito et al. 2014). These differerent mice also died within 2-3 weeks after birth following heart, kidney and lung failure, respectively. (P)RR-deficient cells were all characterized by an accumulation of cytoplasmic autophagic vacuoles containing partially digested cellular components as the consequence of impaired acidification. These cellular observations were always associated with cellular degeneration and death. This drastic phenotype might illustrate the long term consequence of (P)RR deletion masking earlier potential roles of (P)RR. We hypothetized that the deletion of (P)RR in macrophages using the Cre/Lox system would result in such cellular defects and would not allow us to study the role of (P)RR in macrophage functions. For this reason, we decided to develop a new animal model with an inducible (P)RR deletion not based on the Cre/Lox system. We fixed our choice on the development of transgenic rats harboring a doxycycline-inducible shRNA targeting (P)RR. Rats are of particular interest as they are more similar to human physiology and recapitulate many aspects of human diseases (Twigger 2004). The advent of short hairpin RNA (shRNA) technology, based on RNA interference, has opened new ways to achieve constitutive and conditional gene knockdown in mammals. Their expression is achieved with the help of promoters present in vectors which randomly integrate in the host DNA after cell transfection. Once the promoter is activated, shRNAs are expressed, translocated into the cytoplasm, processed by the RNAi machinery and finally bind the target mRNA for subsequent degradation (Fig. 11). Transgenic animals including rats with constitutive shRNA-mediated gene silencing have been successfully generated (Gama Sosa et al. 2010, Podolska et al. 2011). For the inducible expression of shRNA against (P)RR, we used a Tet-inducible system based on the original Tet operon mechanism: expression of the transgene (shRNA) is achieved in presence of doxycycline while remaining silent in absence of antibiotics. The construct used in this work is based on a bimodal system previously developed in our lab and used to generate transgenic rats with inducible shRNA-mediated knockdown (Kotnik et al. 2009).

We designed two different sh(P)RR oligos targeting either exon (*sh1/2*) or exon 9 (*sh3/4*) of the rat (P)RR gene. Both oligos were expressed following doxycycline treatment and strongly reduced (P)RR protein level by approximately 60% for *sh1/2* and 80% for *sh3/4*. The vector containing *sh3/4* was chosen for pronuclear injection and transgenic rats were successfully generated. Transgenic rats were born at Mendelian frequency without any morphological abnormalities. The presence of TetR protein in several organs of transgenic animals confirmed that the construct was transcriptionally active. To induce *sh(P)RR* expression, we treated these rats with doxycycline (100mg/kg) in drinking water. After 8 days of treatment, (P)RR expression was found to be decreased in various organs including kidney, spleen and lung confirming an efficient expression of the *sh3/4* although having no consequences on the phenotype and behavior of the rats. We pursued Dox treatment for an additional week and observed a progressive degradation of several physiological parameters: a decreased body weight, a reduced water intake and an increased glycemia. After 15 days of Dox treatment, these different parameters were so drastically impaired that transgenic rats, appearing sick and staying static, had to be sacrificed. With longer Dox treatment, it is likely that these rats would have simply died one or two days later. These results are in line with the lethality observed at embryonic

stage after total (P)RR deletion (Sihn et al. 2010) and at 2-3 weeks of age in mice with a tissue-specific (P)RR deletion (Kinouchi et al. 2010, Oshima et al. 2011, Riediger et al. 2011, Kurauchi-Mito et al. 2014). We first aimed to use this model to study the role of (P)RR in macrophages *in vivo*. Importantly, we wanted to perform such investigations in Dox-treated transgenic rats in which efficient (P)RR knockdown is achieved but not associated with a deteriorated health status. For these reasons, we decided to treat these animals 8 days with Dox and performed phagocytosis assay by injecting fluorescent latex beads into the peritoneal cavity. Peritoneal macrophages were collected and intracellular fluorescence was assessed by flow cytometry. Unfortunately, the phagocytic activity of peritoneal macrophages from Dox-treated transgenic rats was highly fluctuating (data not shown) and despite several assays, we could not conclude on a role of (P)RR in phagocytosis *in vivo*. The exact reason of this variability remains unclear although several hypotheses have been emitted: variability of the Dox treatment to silence (P)RR in peritoneal macrophages, variations in biological parameters (age, body weight, water intake), technical problem during genotyping or injection of the beads into the gut. To have a better monitoring on the Dox treatment, we decided to perform experiments on bone marrow-derived macrophages *in vitro*. Mature macrophages were treated with Dox in culture medium for several days to induce (P)RR knockdown. Already after two days of Dox treatment we showed an almost complete reduction (more than 90%) of (P)RR mRNA and proteins levels. This effect was still observed after four and six days of Dox treatment. These results show that shRNA expression is induced in presence of Dox and efficiently reduce (P)RR expression. (P)RR-depleted cells were previously characterized by an accumulation of LC3bII-positive autophagic vacuoles in the cytoplasm and by a defective acidification (using LysoTracker fluorescence) of intracellular organelles (Kinouchi et al. 2010, Oshima et al. 2011, Riediger et al. 2011, Kurauchi-Mito et al. 2014). These two parameters were succinctly analyzed in (P)RR-depleted macrophages after 4 days of Dox treatment. Autophagy induction is characterized by the conversion of LC3bI isoform into LC3bII isoform. Western blot and immunofluorescence for LC3bI/II revealed that autophagy, either in normal or starvation medium, is not impaired in (P)RR-depleted macrophages compared to control macrophages. Also, (P)RR-deficient macrophages were responsive to Bafilomycin suggesting that the V-ATPases activity was not impaired in those cells. In accordance, labeling acidic compartments in (P)RR-depleted macrophages with LysoTracker and LysoSensor fluorescent dyes, we observed a normal intracellular acidification comparable to control macrophages. Altogether, these results show that (P)RR knockdown after 4 days of Dox treatment does not impair the process of autophagy and the acidification of intracellular compartments revealing that V-ATPase activity is not impaired in those cells. The absence of such cellular dysfunctions (autophagy, pH) in this cellular model also suggests that observations made in (P)RR-deficient cells (using the Cre/Lox technology) were likely the long-term consequences of (P)RR deletion. It is also possible that macrophages are cells less sensitive to (P)RR deletion. (P)RR-depleted macrophages after 4 days of Dox treatment thus represent a very interesting model to investigate new roles of (P)RR as those cells still have normal cellular functions.

Phagocytosis of non-opsonized fluorescent latex beads (already used for *in vivo* experiments) has been described to be mediated by scavenger receptors which recognize and engulf a wide

variety of substances and waste material from the body (Palecanda et al. 2001). We used flow cytometry to analyse intracellular fluorescence and found that (P)RR-depleted macrophages have a normal uptake of latex beads. However, such phagocytosis assays with beads do not give further information relative to the trafficking and the lysosomal degradation of these particles. To better monitor these aspects, we used *E. coli* bioparticles coupled to a pH-sensitive fluorochrome. The fluorescence of these bioparticles dramatically increases as pH decreases in intracellular vesicles. Gram-negative bacteria such as *E. coli* can be engulfed by scavenger receptors and by Toll-like receptors (Underhill et al. 2012). After incubation with *E. coli* bioparticles, intracellular fluorescence in macrophages was analyzed using confocal microscopy and flow cytometry. These different experiments revealed that the uptake of *E. coli* bioparticles is not impaired in (P)RR-depleted macrophages. In addition, we showed that *E. coli* bioparticles-containing phagosomes undergo a normal acidification and are delivered to lysosomes for degradation in these cells. Despite these effects, it seems that the maturation of phagosomes takes longer in (P)RR-depleted macrophages compared to control cells. The exact mechanism by which (P)RR might influence the maturation of phagosomes remains unclear. (P)RR might be important for the direct acidification of phagosomes through the regulation of V-ATPases. In mice, (P)RR deletion result in a striking reduction of several V0 subunits protein levels raising the concept that (P)RR is important for V-ATPase assembly and/or stability (Kinouchi et al. 2010, Oshima et al. 2011, Kurauchi-Mito et al. 2014). The lack of a specific antibody against V0 subunits of the rat V-ATPase did not allow us to confirm these data in our rat macrophages. We can only hypothesize that in (P)RR-depleted macrophages, either the V-ATPase V0 subunits are normally expressed or they are indeed downregulated but the remaining pool of functional V-ATPases efficiently acidifies intracellular vesicles. During the various maturation stages, phagosomes interact with multiple intracellular compartments including endosomes (early, recycling and late endosomes), multivesicular bodies and Golgi apparatus before fusing with lysosomes. A role of (P)RR in one or more of these different interactions is also possible. (P)RR has been described to regulate the trafficking of particular apical vesicles in epithelial cells (Hermle et al. 2013) but (P)RR might be important for the trafficking of additional vesicles in macrophages.

The work from Kissing et al. in murine macrophages confirmed our results and revealed additional information about the role of (P)RR in these cells (Kissing et al. 2014). As previously described in the discussion on osteoclasts (paragraph 5.1), Kissing et al. bred (P)RR floxed mice with LysM-Cre and Mx1-Cre mice to delete (P)RR in macrophages and further used these cells as a cellular model for V-ATPase loss of function. The LysM-Cre is constitutively expressed in myeloid cells including macrophages. In contrast, Mx1cKO mice were treated 1 week with polyinosinic-polycytidylic acid to induce Mx1-Cre expression in interferon α-responsive cells including peritoneal macrophages and bone marrow progenitors. In both models, (P)RR-deficient macrophages were characterized by a significantly decreased concentration of several V0 subunits confirming previous data (Kinouchi et al. 2010, Oshima et al. 2011, Kurauchi-Mito et al. 2014). In contrast to these studies, deletion of (P)RR in macrophages was not associated with defective acidification. The lysosomal pH in LysMcKO macrophages was not affected whereas in Mx1cKO macrophages it was slightly less acidic compared to control macrophages. These cells

remained sensitive to Bafilomycin indicating that functional V-ATPases remain present and are sufficient to acidify lysosomes in both models. In accordance, they also showed that pH-dependent lysosomal hydrolases such as β-hexosaminidases, cathepsins D and L had a normal enzymatic activity in (P)RR-deficient macrophages. These results confirmed our own data and show that (P)RR-deficient macrophages retain the ability to acidify intracellular compartments including lysosomes. Interestingly, the work from Kissing et al. is the first to describe a normal acidification, and indirectly a normal autophagy, in (P)RR-deficient cells obtained with the Cre/Lox system. Kissing et al. further showed that efficient phagocytosis was present in (P)RR-deficient macrophages (Kissing et al. 2014). Indeed, beads and non-pathogenic Gram-negative *E. coli* and Gram-positive *L. innocua* were engulfed and delivered to lysosomes. Surprisingly, (P)RR-deficient macrophages degraded both bacteria more efficiently than control macrophages suggesting that the absence of (P)RR and most of V-ATPases did not alter their bactericidal functions. In contrast to previous studies (Bidani et al. 1995, Frankenberg et al. 2008), alkalinization of lysosome pH by treatment with Bafilomycin did not impair the bactericidal activity of macrophages (Kissing et al. 2014). Finally, the exact mechanism by which (P)RR interferes with the protein level of V0 subunits remains an important question to be solved. Kinouchi et al. have suggested that (P)RR is important for V-ATPase assembly in the endoplasmic reticulum (Kinouchi et al. 2010). Kissing et al. showed that while V0 proteins were almost absent in (P)RR-deficient macrophages, the mRNA expression of the same V0 subunits remained unchanged suggesting that (P)RR might be important in the regulation of posttranscriptional events.

In addition to the phagocytosis, we also aimed to study a potential role of (P)RR in the process of endocytosis and receptor recycling in macrophages. After endocytosis of a receptor/ligand complex, acidification of the endosomes allow the dissociation of both partners. Most ligands are further targeted to lysosomes for degradation whereas receptors transit back to the plasma membrane in particular vesicles. In contrast, transferrin and its receptor remain bound in acidic endosomes and are rather recycled together to the plasma membrane. This association is actually a tripartite collaboration as the transferrin is bound to two irons (Fe^{3+}). After endocytosis, the weak acidification (pH~6.0) in early endosomes (Rab5 positive) leads to the dissociation of the iron from the transferrin/transferrin receptor complex and iron-free transferrin remains bound to its receptor. This complex is further recycled to the plasma membrane within recycling endosomes (Rab11 positive). In contact with the extracellular neutral pH, the transferrin is released from its receptor (Maxfield et al. 2004). One particular advantage of transferrin over other ligands is the possibility to follow transferrin trafficking to gather information on its endocytosis and on the transferrin receptor recycling in the same time. To this purpose, we used transferrin and performed pulse-chase experiments in macrophages. In such experiments, the transferrin is endocytosed by macrophages during a short incubation (pulse) and accumulates in intracellular vesicles. At the end of the pulse, macrophages are incubated in chase medium (no transferrin). During the chase, the intracellular transferrin is recycled back to the membrane and is released into the medium. The intracellular transferrin can be quantified by western blot after the pulse and at different time of chase. In control

macrophages, we found a normal recycling as intracellular transferrin was strongly decreased after 15 and 45 min of chase. In contrast, we observed an accumulation of transferrin in intracellular vesicles of (P)RR-deficient macrophages at both time points during the chase compared to control macrophages. We showed that these effects were not the consequence of abnormal transferrin endocytosis in (P)RR-depleted macrophages but rather the result of a perturbed recycling of the transferrin/transferrin receptor complex in these cells. The recycling of the transferrin actually occurred in (P)RR-deficient macrophages but seemed to be delayed.
To characterize the localization of the transferrin, we performed the same experiment using fluorescent transferrin. We confirmed our previous data and showed that fluorescent transferrin indeed accumulate in (P)RR-depleted cells. Interestingly, the strongest fluorescent signals were found in vesicles located at the cell periphery. These vesicles might be sorting, early and /or recycling endosomes as the transferrin and its receptor traffic through these compartments to be recycled. Additional experiments are required to identify and characterized these vesicles.
The exact mechanism by which (P)RR regulates transferrin recycling remains also unclear. It is possible that (P)RR is important for the acidification of these particular vesicles. We showed that phagosome acidification is slightly delayed in (P)RR-deficient macrophages. Also, (P)RR has already been shown to regulate the acidification and the trafficking of specific apical vesicles in polarized cells (Hermle et al. 2013). Whether (P)RR deletion has the same consequences on the acidification of vesicles involved in transferrin recycling is unknown but it might explain why the recycling of the transferrin is perturbed. Because (P)RR is not important for the acidification of all intracellular vesicles (Hermle et al. 2013, Kanda et al. 2013), it remains possible that (P)RR regulates receptor recycling independently of its role as a regulator of V-ATPase activity.

In conclusion, this work resulted in the generation of a new transgenic rat model with a conditional deletion of (P)RR using a doxycycline-inducible shRNA expression system. We showed that Dox treatment *in vivo* efficiently decreased (P)RR in several organs and led to premature death after two weeks of treatment. Our work focused on macrophages but this model gives the opportunity to study (P)RR in a variety of cell types. Deletion of (P)RR in macrophages was efficiently achieved in vitro. (P)RR-deficient macrophages were characterized by a normal acidification (possibly slightly delayed) and normal autophagy. We further demonstrated that (P)RR is not required during the phagocytosis of beads/bioparticles and endocytosis of transferrin but is rather important for the recycling of transferrin receptors.

6 CHAPTER BIBLIOGRAPHY

Abrami, L., Lindsay, M., Parton, R.G., Leppla, S.H., and van der Goot, F.G. (2004). Membrane insertion of anthrax protective antigen and cytoplasmic delivery of lethal factor occur at different stages of the endocytic pathway. J Cell Biol *166*, 645-651.

Adams, D.S., Robinson, K.R., Fukumoto, T., Yuan, S., Albertson, R.C., Yelick, P., Kuo, L., McSweeney, M., and Levin, M. (2006). Early, H+-V-ATPase-dependent proton flux is necessary for consistent left-right patterning of non-mammalian vertebrates. Development *133*, 1657-1671.

Advani, A., Kelly, D.J., Cox, A.J., White, K.E., Advani, S.L., Thai, K., Connelly, K.A., Yuen, D., Trogadis, J., Herzenberg, A.M., *et al.* (2009). The (Pro)renin receptor: site-specific and functional linkage to the vacuolar H+-ATPase in the kidney. Hypertension *54*, 261-269.

Agrawal, N., Dasaradhi, P.V., Mohmmed, A., Malhotra, P., Bhatnagar, R.K., and Mukherjee, S.K. (2003). RNA interference: biology, mechanism, and applications. Microbiol Mol Biol Rev *67*, 657-685.

Albers, J., Keller, J., Baranowsky, A., Beil, F.T., Catala-Lehnen, P., Schulze, J., Amling, M., and Schinke, T. (2013). Canonical Wnt signaling inhibits osteoclastogenesis independent of osteoprotegerin. J Cell Biol 200, 537-549.

Alcazar, O., Cousins, S.W., Striker, G.E., and Marin-Castano, M.E. (2009). (Pro)renin receptor is expressed in human retinal pigment epithelium and participates in extracellular matrix remodeling. Exp Eye Res *89*, 638-647.

Aliprantis, A.O., Ueki, Y., Sulyanto, R., Park, A., Sigrist, K.S., Sharma, S.M., Ostrowski, M.C., Olsen, B.R., and Glimcher, L.H. (2008). NFATc1 in mice represses osteoprotegerin during osteoclastogenesis and dissociates systemic osteopenia from inflammation in cherubism. J Clin Invest 118, 3775-3789.

Allan, A.K., Du, J., Davies, S.A., and Dow, J.A. (2005). Genome-wide survey of V-ATPase genes in Drosophila reveals a conserved renal phenotype for lethal alleles. Physiol Genomics *22*, 128-138.

Amsterdam, A., Nissen, R.M., Sun, Z., Swindell, E.C., Farrington, S., and Hopkins, N. (2004). Identification of 315 genes essential for early zebrafish development. Proc Natl Acad Sci U S A *101*, 12792-12797.

Arai, F., Miyamoto, T., Ohneda, O., Inada, T., Sudo, T., Brasel, K., Miyata, T., Anderson, D.M., and Suda, T. (1999). Commitment and differentiation of osteoclast precursor cells by the sequential expression of c-Fms and receptor activator of nuclear factor kappaB (RANK) receptors. J Exp Med *190*, 1741-1754.

Bader, M., and Ganten, D. (2000). Regulation of renin: new evidence from cultured cells and genetically modified mice. J Mol Med (Berl) *78*, 130-139.

Bader, M., Peters, J., Baltatu, O., Muller, D.N., Luft, F.C., and Ganten, D. (2001). Tissue renin-angiotensin systems: new insights from experimental animal models in hypertension research. J Mol Med (Berl) *79*, 76-102.

Bader, M. (2010). Tissue renin-angiotensin-aldosterone systems: Targets for pharmacological therapy. Annu Rev Pharmacol Toxicol *50*, 439-465.

Bar-Peled, L., and Sabatini, D.M. (2014). Regulation of mTORC1 by amino acids. Trends Cell Biol *24*, 400-406.

Bar-Shavit, Z., Teitelbaum, S.L., Reitsma, P., Hall, A., Pegg, L.E., Trial, J., and Kahn, A.J. (1983). Induction of monocytic differentiation and bone resorption by 1,25-dihydroxyvitamin D3. Proc Natl Acad Sci U S A *80*, 5907-5911.

Bartscherer, K., Pelte, N., Ingelfinger, D., and Boutros, M. (2006). Secretion of Wnt ligands requires Evi, a conserved transmembrane protein. Cell *125*, 523-533.

Batenburg, W.W., Krop, M., Garrelds, I.M., de Vries, R., de Bruin, R.J., Burckle, C.A., Muller, D.N., Bader, M., Nguyen, G., and Danser, A.H. (2007). Prorenin is the endogenous agonist of the (pro)renin receptor. Binding kinetics of renin and prorenin in rat vascular smooth muscle cells overexpressing the human (pro)renin receptor. J Hypertens *25*, 2441-2453.

Beyenbach, K.W., and Wieczorek, H. (2006). The V-type H+ ATPase: molecular structure and function, physiological roles and regulation. J Exp Biol *209*, 577-589.

Bidani, A., and Heming, T.A. (1995). Effects of bafilomycin A1 on functional capabilities of LPS-activated alveolar macrophages. J Leukoc Biol 57, 275-281.

Bidani, A., Reisner, B.S., Haque, A.K., Wen, J., Helmer, R.E., Tuazon, D.M., and Heming, T.A. (2000). Bactericidal activity of alveolar macrophages is suppressed by V-ATPase inhibition. Lung 178, 91-104.

Bilic, J., Huang, Y.L., Davidson, G., Zimmermann, T., Cruciat, C.M., Bienz, M., and Niehrs, C. (2007). Wnt induces LRP6 signalosomes and promotes dishevelled-dependent LRP6 phosphorylation. Science *316*, 1619-1622.

Blitzer, J.T., and Nusse, R. (2006). A critical role for endocytosis in Wnt signaling. BMC Cell Biol *7*, 28.

Bonifacino, J.S., and Traub, L.M. (2003). Signals for sorting of transmembrane proteins to endosomes and lysosomes. Annu Rev Biochem *72*, 395-447.

Boyce, B.F., and Xing, L. (2007). The RANKL/RANK/OPG pathway. Curr Osteoporos Rep *5*, 98-104.

Boyle, W.J., Simonet, W.S., and Lacey, D.L. (2003). Osteoclast differentiation and activation. Nature *423*, 337-342.

Brisseau, G.F., Grinstein, S., Hackam, D.J., Nordstrom, T., Manolson, M.F., Khine, A.A., and Rotstein, O.D. (1996). Interleukin-1 increases vacuolar-type H+-ATPase activity in murine peritoneal macrophages. J Biol Chem *271*, 2005-2011.

Brown, D., and Breton, S. (2000). H(+)V-ATPase-dependent luminal acidification in the kidney collecting duct and the epididymis/vas deferens: vesicle recycling and transcytotic pathways. J Exp Biol *203*, 137-145.

Brugts, J.J., Isaacs, A., de Maat, M.P., Boersma, E., van Duijn, C.M., Akkerhuis, K.M., Uitterlinden, A.G., Witteman, J.C., Cambien, F., Ceconi, C.*, et al.* (2011). A pharmacogenetic analysis of determinants of hypertension and blood pressure response to angiotensin-converting enzyme inhibitor therapy in patients with vascular disease and healthy individuals. J Hypertens *29*, 509-519.

Bucay, N., Sarosi, I., Dunstan, C.R., Morony, S., Tarpley, J., Capparelli, C., Scully, S., Tan, H.L., Xu, W., Lacey, D.L.*, et al.* (1998). osteoprotegerin-deficient mice develop early onset osteoporosis and arterial calcification. Genes Dev *12*, 1260-1268.

Bucci, C., Thomsen, P., Nicoziani, P., McCarthy, J., and van Deurs, B. (2000). Rab7: a key to lysosome biogenesis. Mol Biol Cell *11*, 467-480.

Buechling, T., Bartscherer, K., Ohkawara, B., Chaudhary, V., Spirohn, K., Niehrs, C., and Boutros, M. (2010). Wnt/Frizzled signaling requires dPRR, the Drosophila homolog of the prorenin receptor. Curr Biol *20*, 1263-1268.

Burckle, C.A., Jan Danser, A.H., Muller, D.N., Garrelds, I.M., Gasc, J.M., Popova, E., Plehm, R., Peters, J., Bader, M., and Nguyen, G. (2006a). Elevated blood pressure and heart rate in human renin receptor transgenic rats. Hypertension *47*, 552-556.

Burckle, C., and Bader, M. (2006b). Prorenin and its ancient receptor. Hypertension *48*, 549-551.

Campbell, D.J., Karam, H., Menard, J., Bruneval, P., and Mullins, J.J. (2009). Prorenin contributes to angiotensin peptide formation in transgenic rats with rat prorenin expression targeted to the liver. Hypertension *54*, 1248-1253.

Carnell, M., Zech, T., Calaminus, S.D., Ura, S., Hagedorn, M., Johnston, S.A., May, R.C., Soldati, T., Machesky, L.M., and Insall, R.H. (2011). Actin polymerization driven by WASH causes V-ATPase retrieval and vesicle neutralization before exocytosis. J Cell Biol *193*, 831-839.

Charles, J.F., Hsu, L.Y., Niemi, E.C., Weiss, A., Aliprantis, A.O., and Nakamura, M.C. (2012). Inflammatory arthritis increases mouse osteoclast precursors with myeloid suppressor function. J Clin Invest *122*, 4592-4605.

Chau, J.F., Leong, W.F., and Li, B. (2009). Signaling pathways governing osteoblast proliferation, differentiation and function. Histol Histopathol 24, 1593-1606.

Chen, M., Du, Q., Zhang, H.Y., Wahlestedt, C., and Liang, Z. (2005). Vector-based siRNA delivery strategies for high-throughput screening of novel target genes. J RNAi Gene Silencing *1*, 5-11.

Clausen, B.E., Burkhardt, C., Reith, W., Renkawitz, R., and Forster, I. (1999). Conditional gene targeting in macrophages and granulocytes using LysMcre mice. Transgenic Res 8, 265-277.

Clavreul, N., Sansilvestri-Morel, P., Magard, D., Verbeuren, T.J., and Rupin, A. (2011). (Pro)renin promotes fibrosis gene expression in HEK cells through a Nox4-dependent mechanism. Am J Physiol Renal Physiol *300*, F1310-1318.

Clevers, H., and Nusse, R. (2012). Wnt/beta-catenin signaling and disease. Cell *149*, 1192-1205.

Connelly, K.A., Advani, A., Kim, S., Advani, S.L., Zhang, M., White, K.E., Kim, Y.M., Parker, C., Thai, K., Krum, H.*, et al.* (2011). The cardiac (pro)renin receptor is primarily expressed in myocyte transverse tubules and is increased in experimental diabetic cardiomyopathy. J Hypertens *29*, 1175-1184.

Contrepas, A., Walker, J., Koulakoff, A., Franek, K.J., Qadri, F., Giaume, C., Corvol, P., Schwartz, C.E., and Nguyen, G. (2009). A role of the (pro)renin receptor in neuronal cell differentiation. Am J Physiol Regul Integr Comp Physiol *297*, R250-257.

Costa, A.G., Cusano, N.E., Silva, B.C., Cremers, S., and Bilezikian, J.P. (2011). Cathepsin K: its skeletal actions and role as a therapeutic target in osteoporosis. Nat Rev Rheumatol 7, 447-456.

Cousin, C., Bracquart, D., Contrepas, A., Corvol, P., Muller, L., and Nguyen, G. (2009). Soluble form of the (pro)renin receptor generated by intracellular cleavage by furin is secreted in plasma. Hypertension *53*, 1077-1082.

Croke, M., Ross, F.P., Korhonen, M., Williams, D.A., Zou, W., and Teitelbaum, S.L. (2011). Rac deletion in osteoclasts causes severe osteopetrosis. J Cell Sci 124, 3811-3821.

Cruciat, C.M., Ohkawara, B., Acebron, S.P., Karaulanov, E., Reinhard, C., Ingelfinger, D., Boutros, M., and Niehrs, C. (2010). Requirement of prorenin receptor and vacuolar H+-ATPase-mediated acidification for Wnt signaling. Science *327*, 459-463.

Dai, X.M., Ryan, G.R., Hapel, A.J., Dominguez, M.G., Russell, R.G., Kapp, S., Sylvestre, V., and Stanley, E.R. (2002). Targeted disruption of the mouse colony-stimulating factor 1 receptor gene results in osteopetrosis, mononuclear phagocyte deficiency, increased primitive progenitor cell frequencies, and reproductive defects. Blood *99*, 111-120.

Danser, A.H., Derkx, F.H., Schalekamp, M.A., Hense, H.W., Riegger, G.A., and Schunkert, H. (1998). Determinants of interindividual variation of renin and prorenin concentrations: evidence for a sexual dimorphism of (pro)renin levels in humans. J Hypertens *16*, 853-862.

Danser, A.H., and Deinum, J. (2005). Renin, prorenin and the putative (pro)renin receptor. Hypertension *46*, 1069-1076.

Davis-Kaplan, S.R., Compton, M.A., Flannery, A.R., Ward, D.M., Kaplan, J., Stevens, T.H., and Graham, L.A. (2006). PKR1 encodes an assembly factor for the yeast V-type ATPase. J Biol Chem *281*, 32025-32035.

Deinum, J., Ronn, B., Mathiesen, E., Derkx, F.H., Hop, W.C., and Schalekamp, M.A. (1999). Increase in serum prorenin precedes onset of microalbuminuria in patients with insulin-dependent diabetes mellitus. Diabetologia *42*, 1006-1010.

Derkx, F.H., Deinum, J., Lipovski, M., Verhaar, M., Fischli, W., and Schalekamp, M.A. (1992). Nonproteolytic "activation" of prorenin by active site-directed renin inhibitors as demonstrated by renin-specific monoclonal antibody. J Biol Chem *267*, 22837-22842.

Dernburg, A.F., and Karpen, G.H. (2002). A chromosome RNAissance. Cell *111*, 159-162.

DeSelm, C.J., Miller, B.C., Zou, W., Beatty, W.L., van Meel, E., Takahata, Y., Klumperman, J., Tooze, S.A., Teitelbaum, S.L., and Virgin, H.W. (2011). Autophagy proteins regulate the secretory component of osteoclastic bone resorption. Dev Cell 21, 966-974.

EauClaire, S.F., Cui, S., Ma, L., Matous, J., Marlow, F.L., Gupta, T., Burgess, H.A., Abrams, E.W., Kapp, L.D., Granato, M.*, et al.* (2012). Mutations in vacuolar H+ -ATPase subunits lead to biliary developmental defects in zebrafish. Dev Biol *365*, 434-444.

Feldt, S., Batenburg, W.W., Mazak, I., Maschke, U., Wellner, M., Kvakan, H., Dechend, R., Fiebeler, A., Burckle, C., Contrepas, A.*, et al.* (2008a). Prorenin and renin-induced extracellular signal-regulated kinase 1/2 activation in monocytes is not blocked by aliskiren or the handle-region peptide. Hypertension *51*, 682-688.

Feldt, S., Maschke, U., Dechend, R., Luft, F.C., and Muller, D.N. (2008b). The putative (pro)renin receptor blocker HRP fails to prevent (pro)renin signaling. J Am Soc Nephrol *19*, 743-748.

Feng, H., Cheng, T., Steer, J.H., Joyce, D.A., Pavlos, N.J., Leong, C., Kular, J., Liu, J., Feng, X., Zheng, M.H.*, et al.* (2009). Myocyte enhancer factor 2 and microphthalmia-associated transcription factor cooperate with NFATc1 to transactivate the V-ATPase d2 promoter during RANKL-induced osteoclastogenesis. J Biol Chem *284*, 14667-14676.

Feng, S., Deng, L., Chen, W., Shao, J., Xu, G., and Li, Y.P. (2009). Atp6v1c1 is an essential component of the osteoclast proton pump and in F-actin ring formation in osteoclasts. Biochem J *417*, 195-203.

Fethiere, J., Venzke, D., Madden, D.R., and Bottcher, B. (2005). Peripheral stator of the yeast V-ATPase: stoichiometry and specificity of interaction between the EG complex and subunits C and H. Biochemistry *44*, 15906-15914.

Finberg, K.E., Wagner, C.A., Bailey, M.A., Paunescu, T.G., Breton, S., Brown, D., Giebisch, G., Geibel, J.P., and Lifton, R.P. (2005). The B1-subunit of the H(+) ATPase is required for maximal urinary acidification. Proc Natl Acad Sci U S A *102*, 13616-13621.

Fire, A., Xu, S., Montgomery, M.K., Kostas, S.A., Driver, S.E., and Mello, C.C. (1998). Potent and specific genetic interference by double-stranded RNA in Caenorhabditis elegans. Nature *391*, 806-811.

Fischman, D.A., and Hay, E.D. (1962). Origin of osteoclasts from mononuclear leucocytes in regenerating newt limbs. Anat Rec *143*, 329-337.

Fisher, J.M., and Scheller, R.H. (1988). Prohormone processing and the secretory pathway. J Biol Chem *263*, 16515-16518.

Flannagan, R.S., Cosio, G., and Grinstein, S. (2009). Antimicrobial mechanisms of phagocytes and bacterial evasion strategies. Nat Rev Microbiol *7*, 355-366.

Forgac, M. (2007). Vacuolar ATPases: rotary proton pumps in physiology and pathophysiology. Nat Rev Mol Cell Biol *8*, 917-929.

Fournier, D., Luft, F.C., Bader, M., Ganten, D., and Andrade-Navarro, M.A. (2012). Emergence and evolution of the renin-angiotensin-aldosterone system. J Mol Med (Berl) *90*, 495-508.

Frankenberg, T., Kirschnek, S., Hacker, H., and Hacker, G. (2008). Phagocytosis-induced apoptosis of macrophages is linked to uptake, killing and degradation of bacteria. Eur J Immunol 38, 204-215.

Frattini, A., Orchard, P.J., Sobacchi, C., Giliani, S., Abinun, M., Mattsson, J.P., Keeling, D.J., Andersson, A.K., Wallbrandt, P., Zecca, L.*, et al.* (2000). Defects in TCIRG1 subunit of the vacuolar proton pump are responsible for a subset of human autosomal recessive osteopetrosis. Nat Genet *25*, 343-346.

Freundlich, M., Quiroz, Y., Zhang, Z., Zhang, Y., Bravo, Y., Weisinger, J.R., Li, Y.C., and Rodriguez-Iturbe, B. (2008). Suppression of renin-angiotensin gene expression in the kidney by paricalcitol. Kidney Int *74*, 1394-1402.

Gama Sosa, M.A., De Gasperi, R., and Elder, G.A. (2010). Animal transgenesis: an overview. Brain Struct Funct *214*, 91-109.

Gay, C.V., and Mueller, W.J. (1974). Carbonic anhydrase and osteoclasts: localization by labeled inhibitor autoradiography. Science *183*, 432-434.

Glass, D.A., 2nd, Bialek, P., Ahn, J.D., Starbuck, M., Patel, M.S., Clevers, H., Taketo, M.M., Long, F., McMahon, A.P., Lang, R.A., et al. (2005). Canonical Wnt signaling in differentiated osteoblasts controls osteoclast differentiation. Dev Cell 8, 751-764.

Glass, D.A., 2nd, and Karsenty, G. (2006). Canonical Wnt signaling in osteoblasts is required for osteoclast differentiation. Ann N Y Acad Sci 1068, 117-130.

Gonzalez, A.A., Luffman, C., Bourgeois, C.R., Vio, C.P., and Prieto, M.C. (2013). Angiotensin II-independent upregulation of cyclooxygenase-2 by activation of the (Pro)renin receptor in rat renal inner medullary cells. Hypertension *61*, 443-449.

Gordon, S., and Taylor, P.R. (2005). Monocyte and macrophage heterogeneity. Nat Rev Immunol *5*, 953-964.

Gossen, M., and Bujard, H. (1992). Tight control of gene expression in mammalian cells by tetracycline-responsive promoters. Proc Natl Acad Sci U S A *89*, 5547-5551.

Gossen, M., Freundlieb, S., Bender, G., Muller, G., Hillen, W., and Bujard, H. (1995). Transcriptional activation by tetracyclines in mammalian cells. Science *268*, 1766-1769.

Gowen, M., Lazner, F., Dodds, R., Kapadia, R., Feild, J., Tavaria, M., Bertoncello, I., Drake, F., Zavarselk, S., Tellis, I.*, et al.* (1999). Cathepsin K knockout mice develop osteopetrosis due to a deficit in matrix degradation but not demineralization. J Bone Miner Res *14*, 1654-1663.

Graham, L.A., Powell, B., and Stevens, T.H. (2000). Composition and assembly of the yeast vacuolar H(+)-ATPase complex. J Exp Biol *203*, 61-70.

Graham, L.A., Flannery, A.R., and Stevens, T.H. (2003). Structure and assembly of the yeast V-ATPase. J Bioenerg Biomembr *35*, 301-312.

Greco, C.M., Camera, M., Facchinetti, L., Brambilla, M., Pellegrino, S., Gelmi, M.L., Tremoli, E., Corsini, A., and Ferri, N. (2012). Chemotactic effect of prorenin on human aortic smooth muscle cells: a novel function of the (pro)renin receptor. Cardiovasc Res *95*, 366-374.

Gross, J.M., Perkins, B.D., Amsterdam, A., Egana, A., Darland, T., Matsui, J.I., Sciascia, S., Hopkins, N., and Dowling, J.E. (2005). Identification of zebrafish insertional mutants with defects in visual system development and function. Genetics *170*, 245-261.

Gruenberg, J., and van der Goot, F.G. (2006). Mechanisms of pathogen entry through the endosomal compartments. Nat Rev Mol Cell Biol *7*, 495-504.

Guillard, M., Dimopoulou, A., Fischer, B., Morava, E., Lefeber, D.J., Kornak, U., and Wevers, R.A. (2009). Vacuolar H+-ATPase meets glycosylation in patients with cutis laxa. Biochim Biophys Acta *1792*, 903-914.

Hatton, R., Stimpel, M., and Chambers, T.J. (1997). Angiotensin II is generated from angiotensin I by bone cells and stimulates osteoclastic bone resorption in vitro. J Endocrinol 152, 5-10.

Hayman, A.R., Jones, S.J., Boyde, A., Foster, D., Colledge, W.H., Carlton, M.B., Evans, M.J., and Cox, T.M. (1996). Mice lacking tartrate-resistant acid phosphatase (Acp 5) have disrupted endochondral ossification and mild osteopetrosis. Development *122*, 3151-3162.

Heaney, R.P., and Weaver, C.M. (2005). Newer perspectives on calcium nutrition and bone quality. J Am Coll Nutr *24*, 574S-581S.

Hermle, T., Saltukoglu, D., Grunewald, J., Walz, G., and Simons, M. (2010). Regulation of Frizzled-dependent planar polarity signaling by a V-ATPase subunit. Curr Biol *20*, 1269-1276.

Hermle, T., Guida, M.C., Beck, S., Helmstadter, S., and Simons, M. (2013). Drosophila ATP6AP2/VhaPRR functions both as a novel planar cell polarity core protein and a regulator of endosomal trafficking. EMBO J *32*, 245-259.

Hiesinger, P.R., Fayyazuddin, A., Mehta, S.Q., Rosenmund, T., Schulze, K.L., Zhai, R.G., Verstreken, P., Cao, Y., Zhou, Y., Kunz, J.*, et al.* (2005). The v-ATPase V0 subunit a1 is required for a late step in synaptic vesicle exocytosis in Drosophila. Cell *121*, 607-620.

Hirata, R., Umemoto, N., Ho, M.N., Ohya, Y., Stevens, T.H., and Anraku, Y. (1993). VMA12 is essential for assembly of the vacuolar H(+)-ATPase subunits onto the vacuolar membrane in Saccharomyces cerevisiae. J Biol Chem *268*, 961-967.

Hirose, T., Mori, N., Totsune, K., Morimoto, R., Maejima, T., Kawamura, T., Metoki, H., Asayama, K., Kikuya, M., Ohkubo, T.*, et al.* (2009a). Gene expression of (pro)renin receptor is upregulated in hearts and kidneys of rats with congestive heart failure. Peptides *30*, 2316-2322.

Hirose, T., Hashimoto, M., Totsune, K., Metoki, H., Asayama, K., Kikuya, M., Sugimoto, K., Katsuya, T., Ohkubo, T., Hashimoto, J.*, et al.* (2009b). Association of (pro)renin receptor gene polymorphism with blood pressure in Japanese men: the Ohasama study. Am J Hypertens *22*, 294-299.

Hirose, T., Mori, N., Totsune, K., Morimoto, R., Maejima, T., Kawamura, T., Metoki, H., Asayama, K., Kikuya, M., Ohkubo, T.*, et al.* (2010). Increased expression of (pro)renin receptor in the remnant kidneys of 5/6 nephrectomized rats. Regul Pept *159*, 93-99.

Hirose, T., Hashimoto, M., Totsune, K., Metoki, H., Hara, A., Satoh, M., Kikuya, M., Ohkubo, T., Asayama, K., Kondo, T.*, et al.* (2011). Association of (pro)renin receptor gene polymorphisms with lacunar infarction and left ventricular hypertrophy in Japanese women: the Ohasama study. Hypertens Res *34*, 530-535.

Horne-Badovinac, S., Lin, D., Waldron, S., Schwarz, M., Mbamalu, G., Pawson, T., Jan, Y., Stainier, D.Y., and Abdelilah-Seyfried, S. (2001). Positional cloning of heart and soul reveals multiple roles for PKC lambda in zebrafish organogenesis. Curr Biol *11*, 1492-1502.

Hsueh, W.A., Luetscher, J.A., Carlson, E.J., Grislis, G., Fraze, E., and McHargue, A. (1982). Changes in active and inactive renin throughout pregnancy. J Clin Endocrinol Metab *54*, 1010-1016.

Huang, J., and Siragy, H.M. (2009). Glucose promotes the production of interleukine-1beta and cyclooxygenase-2 in mesangial cells via enhanced (Pro)renin receptor expression. Endocrinology *150*, 5557-5565.

Huang, J., and Siragy, H.M. (2010). Regulation of (pro)renin receptor expression by glucose-induced mitogen-activated protein kinase, nuclear factor-kappaB, and activator protein-1 signaling pathways. Endocrinology *151*, 3317-3325.

Huang, J., Matavelli, L.C., and Siragy, H.M. (2011). Renal (pro)renin receptor contributes to development of diabetic kidney disease through transforming growth factor-beta1-connective tissue growth factor signalling cascade. Clin Exp Pharmacol Physiol *38*, 215-221.

Huang, Y., Wongamorntham, S., Kasting, J., McQuillan, D., Owens, R.T., Yu, L., Noble, N.A., and Border, W. (2006). Renin increases mesangial cell transforming growth factor-beta1 and matrix proteins through receptor-mediated, angiotensin II-independent mechanisms. Kidney Int *69*, 105-113.

Huang, Y., Noble, N.A., Zhang, J., Xu, C., and Border, W.A. (2007). Renin-stimulated TGF-beta1 expression is regulated by a mitogen-activated protein kinase in mesangial cells. Kidney Int *72*, 45-52.

Hume, D.A. (2011). Applications of myeloid-specific promoters in transgenic mice support in vivo imaging and functional genomics but do not support the concept of distinct macrophage and dendritic cell lineages or roles in immunity. J Leukoc Biol 89, 525-538.

Huotari, J., and Helenius, A. (2011). Endosome maturation. EMBO J *30*, 3481-3500.

Hurtado-Lorenzo, A., Skinner, M., El Annan, J., Futai, M., Sun-Wada, G.H., Bourgoin, S., Casanova, J., Wildeman, A., Bechoua, S., Ausiello, D.A.*, et al.* (2006). V-ATPase interacts with ARNO and Arf6 in early endosomes and regulates the protein degradative pathway. Nat Cell Biol *8*, 124-136.

Huss, M., and Wieczorek, H. (2009). Inhibitors of V-ATPases: old and new players. J Exp Biol *212*, 341-346.

Ichihara, A., Hayashi, M., Kaneshiro, Y., Suzuki, F., Nakagawa, T., Tada, Y., Koura, Y., Nishiyama, A., Okada, H., Uddin, M.N.*, et al.* (2004). Inhibition of diabetic nephropathy by a decoy peptide corresponding to the "handle" region for nonproteolytic activation of prorenin. J Clin Invest *114*, 1128-1135.

Ichihara, A., Suzuki, F., Nakagawa, T., Kaneshiro, Y., Takemitsu, T., Sakoda, M., Nabi, A.H., Nishiyama, A., Sugaya, T., Hayashi, M.*, et al.* (2006a). Prorenin receptor blockade inhibits development of glomerulosclerosis in diabetic angiotensin II type 1a receptor-deficient mice. J Am Soc Nephrol *17*, 1950-1961.

Ichihara, A., Kaneshiro, Y., Takemitsu, T., Sakoda, M., Suzuki, F., Nakagawa, T., Nishiyama, A., Inagami, T., and Hayashi, M. (2006b). Nonproteolytic activation of prorenin contributes to development of cardiac fibrosis in genetic hypertension. Hypertension *47*, 894-900.

Inoue, H., Noumi, T., Nagata, M., Murakami, H., and Kanazawa, H. (1999). Targeted disruption of the gene encoding the proteolipid subunit of mouse vacuolar H(+)-ATPase leads to early embryonic lethality. Biochim Biophys Acta *1413*, 130-138.

Ito, Y., Teitelbaum, S.L., Zou, W., Zheng, Y., Johnson, J.F., Chappel, J., Ross, F.P., and Zhao, H. (2010). Cdc42 regulates bone modeling and remodeling in mice by modulating RANKL/M-CSF signaling and osteoclast polarization. J Clin Invest 120, 1981-1993.

Jacome-Galarza, C.E., Lee, S.K., Lorenzo, J.A., and Aguila, H.L. (2013). Identification, characterization, and isolation of a common progenitor for osteoclasts, macrophages, and dendritic cells from murine bone marrow and periphery. J Bone Miner Res *28*, 1203-1213.

Jacquin, C., Gran, D.E., Lee, S.K., Lorenzo, J.A., and Aguila, H.L. (2006). Identification of multiple osteoclast precursor populations in murine bone marrow. J Bone Miner Res *21*, 67-77.

Jee, W.S., and Nolan, P.D. (1963). Origin of Osteoclasts from the Fusion of Phagocytes. Nature *200*, 225-226.

Jenuwein, T. (2002). Molecular biology. An RNA-guided pathway for the epigenome. Science *297*, 2215-2218.

Kanda, A., Noda, K., Saito, W., and Ishida, S. (2012). (Pro)renin receptor is associated with angiogenic activity in proliferative diabetic retinopathy. Diabetologia *55*, 3104-3113.

Kanda, A., Noda, K., Yuki, K., Ozawa, Y., Furukawa, T., Ichihara, A., and Ishida, S. (2013). Atp6ap2/(pro)renin receptor interacts with Par3 as a cell polarity determinant required for laminar formation during retinal development in mice. J Neurosci *33*, 19341-19351.

Kaneshiro, Y., Ichihara, A., Takemitsu, T., Sakoda, M., Suzuki, F., Nakagawa, T., Hayashi, M., and Inagami, T. (2006). Increased expression of cyclooxygenase-2 in the renal cortex of human prorenin receptor gene-transgenic rats. Kidney Int *70*, 641-646.

Kaneshiro, Y., Ichihara, A., Sakoda, M., Takemitsu, T., Nabi, A.H., Uddin, M.N., Nakagawa, T., Nishiyama, A., Suzuki, F., Inagami, T.*, et al.* (2007). Slowly progressive, angiotensin II-independent glomerulosclerosis in human (pro)renin receptor-transgenic rats. J Am Soc Nephrol *18*, 1789-1795.

Karet, F.E., Finberg, K.E., Nelson, R.D., Nayir, A., Mocan, H., Sanjad, S.A., Rodriguez-Soriano, J., Santos, F., Cremers, C.W., Di Pietro, A.*, et al.* (1999). Mutations in the gene encoding B1 subunit of H+-ATPase cause renal tubular acidosis with sensorineural deafness. Nat Genet *21*, 84-90.

Karlsson, C., Thornemo, M., Henriksson, H.B., and Lindahl, A. (2009). Identification of a stem cell niche in the zone of Ranvier within the knee joint. J Anat 215, 355-363.

Kaschina, E., Scholz, H., Steckelings, U.M., Sommerfeld, M., Kemnitz, U.R., Artuc, M., Schmidt, S., and Unger, T. (2009). Transition from atherosclerosis to aortic aneurysm in humans coincides with an increased expression of RAS components. Atherosclerosis *205*, 396-403.

Kenner, L., Hoebertz, A., Beil, F.T., Keon, N., Karreth, F., Eferl, R., Scheuch, H., Szremska, A., Amling, M., Schorpp-Kistner, M., et al. (2004). Mice lacking JunB are osteopenic due to cell-autonomous osteoblast and osteoclast defects. J Cell Biol 164, 613-623.

Kettner, C., Bertl, A., Obermeyer, G., Slayman, C., and Bihler, H. (2003). Electrophysiological analysis of the yeast V-type proton pump: variable coupling ratio and proton shunt. Biophys J *85*, 3730-3738.

Kim, H.J., Zhao, H., Kitaura, H., Bhattacharyya, S., Brewer, J.A., Muglia, L.J., Ross, F.P., and Teitelbaum, S.L. (2006). Glucocorticoids suppress bone formation via the osteoclast. J Clin Invest 116, 2152-2160.

Kim, K., Lee, S.H., Ha Kim, J., Choi, Y., and Kim, N. (2008). NFATc1 induces osteoclast fusion via up-regulation of Atp6v0d2 and the dendritic cell-specific transmembrane protein (DC-STAMP). Mol Endocrinol *22*, 176-185.

Kinchen, J.M., and Ravichandran, K.S. (2008). Phagosome maturation: going through the acid test. Nat Rev Mol Cell Biol *9*, 781-795.

Kinouchi, K., Ichihara, A., Sano, M., Sun-Wada, G.H., Wada, Y., Kurauchi-Mito, A., Bokuda, K., Narita, T., Oshima, Y., Sakoda, M.*, et al.* (2010). The (pro)renin receptor/ATP6AP2 is essential for vacuolar H+-ATPase assembly in murine cardiomyocytes. Circ Res *107*, 30-34.

Kissing, S., Hermsen, C., Repnik, U., Nesset, C.K., von Bargen, K., Griffiths, G., Ichihara, A., Lee, B.S., Schwake, M., De Brabander, J., et al. (2015). Vacuolar ATPase in phagosome-lysosome fusion. J Biol Chem 290, 14166-14180.

Kodama, H., Yamasaki, A., Nose, M., Niida, S., Ohgame, Y., Abe, M., Kumegawa, M., and Suda, T. (1991). Congenital osteoclast deficiency in osteopetrotic (op/op) mice is cured by injections of macrophage colony-stimulating factor. J Exp Med *173*, 269-272.

Kogianni, G., and Noble, B.S. (2007). The biology of osteocytes. Curr Osteoporos Rep *5*, 81-86.

Koike, C., Nishida, A., Akimoto, K., Nakaya, M.A., Noda, T., Ohno, S., and Furukawa, T. (2005). Function of atypical protein kinase C lambda in differentiating photoreceptors is required for proper lamination of mouse retina. J Neurosci *25*, 10290-10298.

Kornak, U., Schulz, A., Friedrich, W., Uhlhaas, S., Kremens, B., Voit, T., Hasan, C., Bode, U., Jentsch, T.J., and Kubisch, C. (2000). Mutations in the a3 subunit of the vacuolar H(+)-ATPase cause infantile malignant osteopetrosis. Hum Mol Genet *9*, 2059-2063.

Kornak, U., Kasper, D., Bosl, M.R., Kaiser, E., Schweizer, M., Schulz, A., Friedrich, W., Delling, G., and Jentsch, T.J. (2001). Loss of the ClC-7 chloride channel leads to osteopetrosis in mice and man. Cell *104*, 205-215.

Kornak, U., Reynders, E., Dimopoulou, A., van Reeuwijk, J., Fischer, B., Rajab, A., Budde, B., Nurnberg, P., Foulquier, F., Lefeber, D.*, et al.* (2008). Impaired glycosylation and cutis laxa caused by mutations in the vesicular H+-ATPase subunit ATP6V0A2. Nat Genet *40*, 32-34.

Korvatska, O., Strand, N.S., Berndt, J.D., Strovas, T., Chen, D.H., Leverenz, J.B., Kiianitsa, K., Mata, I.F., Karakoc, E., Greenup, J.L.*, et al.* (2013). Altered splicing of ATP6AP2 causes X-linked parkinsonism with spasticity (XPDS). Hum Mol Genet *22*, 3259-3268.

Kotnik, K., Popova, E., Todiras, M., Mori, M.A., Alenina, N., Seibler, J., and Bader, M. (2009). Inducible transgenic rat model for diabetes mellitus based on shRNA-mediated gene knockdown. PLoS One *4*, e5124.

Krebs, C., Hamming, I., Sadaghiani, S., Steinmetz, O.M., Meyer-Schwesinger, C., Fehr, S., Stahl, R.A., Garrelds, I.M., Danser, A.H., van Goor, H.*, et al.* (2007). Antihypertensive therapy upregulates renin and (pro)renin receptor in the clipped kidney of Goldblatt hypertensive rats. Kidney Int *72*, 725-730.

Krebs, C., Weber, M., Steinmetz, O., Meyer-Schwesinger, C., Stahl, R., Danser, A.H., Garrelds, I., van Goor, H., Nguyen, G., Muller, D.*, et al.* (2008). Effect of (pro)renin receptor inhibition by a decoy peptide on renal damage in the clipped kidney of Goldblatt rats. Kidney Int *74*, 823-824.

Kronenberg, H.M. (2003). Developmental regulation of the growth plate. Nature *423*, 332-336.

Krop, M., de Bruyn, J.H., Derkx, F.H., and Danser, A.H. (2008a). Renin and prorenin disappearance in humans post-nephrectomy: evidence for binding? Front Biosci *13*, 3931-3939.

Krop, M., and Danser, A.H. (2008b). Circulating versus tissue renin-angiotensin system: on the origin of (pro)renin. Curr Hypertens Rep *10*, 112-118.

Krop, M., Lu, X., Danser, A.H., and Meima, M.E. (2013). The (pro)renin receptor. A decade of research: what have we learned? Pflugers Arch *465*, 87-97.

Kukita, T., Wada, N., Kukita, A., Kakimoto, T., Sandra, F., Toh, K., Nagata, K., Iijima, T., Horiuchi, M., Matsusaki, H.*, et al.* (2004). RANKL-induced DC-STAMP is essential for osteoclastogenesis. J Exp Med *200*, 941-946.

Kumar, L.D., and Clarke, A.R. (2007). Gene manipulation through the use of small interfering RNA (siRNA): from in vitro to in vivo applications. Adv Drug Deliv Rev *59*, 87-100.

Kurauchi-Mito, A., Ichihara, A., Bokuda, K., Sakoda, M., Kinouchi, K., Yaguchi, T., Yamada, T., Sun-Wada, G.H., Wada, Y., and Itoh, H. (2014). Significant roles of the (pro)renin receptor in integrity of vascular smooth muscle cells. Hypertens Res 37, 830-835.

Lacey, D.L., Timms, E., Tan, H.L., Kelley, M.J., Dunstan, C.R., Burgess, T., Elliott, R., Colombero, A., Elliott, G., Scully, S.*, et al.* (1998). Osteoprotegerin ligand is a cytokine that regulates osteoclast differentiation and activation. Cell *93*, 165-176.

Laitala-Leinonen, T., Lowik, C., Papapoulos, S., and Vaananen, H.K. (1999). Inhibition of intravacuolar acidification by antisense RNA decreases osteoclast differentiation and bone resorption in vitro. J Cell Sci *112 (Pt 21)*, 3657-3666.

Laitala, T., and Vaananen, H.K. (1994). Inhibition of bone resorption in vitro by antisense RNA and DNA molecules targeted against carbonic anhydrase II or two subunits of vacuolar H(+)-ATPase. J Clin Invest *93*, 2311-2318.

Lamothe, B., Lai, Y., Xie, M., Schneider, M.D., and Darnay, B.G. (2013). TAK1 is essential for osteoclast differentiation and is an important modulator of cell death by apoptosis and necroptosis. Mol Cell Biol 33, 582-595.

Langenskiold, A. (1998). Role of the ossification groove of Ranvier in normal and pathologic bone growth: a review. J Pediatr Orthop 18, 173-177.

Lavin, Y., Mortha, A., Rahman, A., and Merad, M. (2015). Regulation of macrophage development and function in peripheral tissues. Nat Rev Immunol 15, 731-744.

Leckie, B.J., and Bottrill, A.R. (2011). A specific binding site for the prorenin propart peptide Arg10-Arg20 does not occur on human endothelial cells. J Renin Angiotensin Aldosterone Syst *12*, 36-41.

Lee, N.K. (2010). Molecular understanding of osteoclast differentiation and physiology. Endocrinol Metab 25, 264-269.

Lee, S.H., Rho, J., Jeong, D., Sul, J.Y., Kim, T., Kim, N., Kang, J.S., Miyamoto, T., Suda, T., Lee, S.K.*, et al.* (2006). v-ATPase V0 subunit d2-deficient mice exhibit impaired osteoclast fusion and increased bone formation. Nat Med *12*, 1403-1409.

Lerner, U.H. (2000). Osteoclast formation and resorption. Matrix Biol *19*, 107-120.

Levine, B., Mizushima, N., and Virgin, H.W. (2011). Autophagy in immunity and inflammation. Nature *469*, 323-335.

L'Huillier, N., Sharp, M. G. F., Dunbar, D. R. and Mullins, J. J. (2005) On the relationship between the renin receptor and the vacuolar proton ATPase membrane sector associated protein (M8-9). In The Local Cardiac Renin Angiotensin-Aldosterone System (Frolich, E. D. and Re, R. N., eds), pp. 17–34, Springer, New York.

Li, C.Y., Jepsen, K.J., Majeska, R.J., Zhang, J., Ni, R., Gelb, B.D., and Schaffler, M.B. (2006). Mice lacking cathepsin K maintain bone remodeling but develop bone fragility despite high bone mass. J Bone Miner Res *21*, 865-875.

Li, J., Sarosi, I., Yan, X.Q., Morony, S., Capparelli, C., Tan, H.L., McCabe, S., Elliott, R., Scully, S., Van, G.*, et al.* (2000). RANK is the intrinsic hematopoietic cell surface receptor that controls osteoclastogenesis and regulation of bone mass and calcium metabolism. Proc Natl Acad Sci U S A *97*, 1566-1571.

Li, P., Schwarz, E.M., O'Keefe, R.J., Ma, L., Looney, R.J., Ritchlin, C.T., Boyce, B.F., and Xing, L. (2004). Systemic tumor necrosis factor alpha mediates an increase in peripheral CD11bhigh osteoclast precursors in tumor necrosis factor alpha-transgenic mice. Arthritis Rheum *50*, 265-276.

Li, W., Sullivan, M.N., Zhang, S., Worker, C.J., Xiong, Z., Speth, R.C., and Feng, Y. (2015). Intracerebroventricular infusion of the (Pro)renin receptor antagonist PRO20 attenuates deoxycorticosterone acetate-salt-induced hypertension. Hypertension *65*, 352-361.

Li, Y.P., Chen, W., Liang, Y., Li, E., and Stashenko, P. (1999). Atp6i-deficient mice exhibit severe osteopetrosis due to loss of osteoclast-mediated extracellular acidification. Nat Genet *23*, 447-451.

Liegeois, S., Benedetto, A., Garnier, J.M., Schwab, Y., and Labouesse, M. (2006). The V0-ATPase mediates apical secretion of exosomes containing Hedgehog-related proteins in Caenorhabditis elegans. J Cell Biol *173*, 949-961.

Liu, G., Hitomi, H., Hosomi, N., Shibayama, Y., Nakano, D., Kiyomoto, H., Ma, H., Yamaji, Y., Kohno, M., Ichihara, A., *et al.* (2011). Prorenin induces vascular smooth muscle cell proliferation and hypertrophy via epidermal growth factor receptor-mediated extracellular signal-regulated kinase and Akt activation pathway. J Hypertens *29*, 696-705.

Liu, Q., Kane, P.M., Newman, P.R., and Forgac, M. (1996). Site-directed mutagenesis of the yeast V-ATPase B subunit (Vma2p). J Biol Chem *271*, 2018-2022.

Liu, Q., Leng, X.H., Newman, P.R., Vasilyeva, E., Kane, P.M., and Forgac, M. (1997). Site-directed mutagenesis of the yeast V-ATPase A subunit. J Biol Chem *272*, 11750-11756.

Livak, K.J., and Schmittgen, T.D. (2001). Analysis of relative gene expression data using real-time quantitative PCR and the 2(-Delta Delta C(T)) Method. Methods *25*, 402-408.

Lotinun, S., Kiviranta, R., Matsubara, T., Alzate, J.A., Neff, L., Luth, A., Koskivirta, I., Kleuser, B., Vacher, J., Vuorio, E., et al. (2013). Osteoclast-specific cathepsin K deletion stimulates S1P-dependent bone formation. J Clin Invest 123, 666-681.

Lu, M., Holliday, L.S., Zhang, L., Dunn, W.A., Jr., and Gluck, S.L. (2001). Interaction between aldolase and vacuolar H+-ATPase: evidence for direct coupling of glycolysis to the ATP-hydrolyzing proton pump. J Biol Chem *276*, 30407-30413.

Lu, X., Garrelds, I.M., Wagner, C.A., Danser, A.H., and Meima, M.E. (2013). (Pro)renin receptor is required for prorenin-dependent and -independent regulation of vacuolar H(+)-ATPase activity in MDCK.C11 collecting duct cells. Am J Physiol Renal Physiol *305*, F417-425.

Ludwig, J., Kerscher, S., Brandt, U., Pfeiffer, K., Getlawi, F., Apps, D.K., and Schagger, H. (1998). Identification and characterization of a novel 9.2-kDa membrane sector-associated protein of vacuolar proton-ATPase from chromaffin granules. J Biol Chem *273*, 10939-10947.

Luetscher, J.A., Kraemer, F.B., Wilson, D.M., Schwartz, H.C., and Bryer-Ash, M. (1985). Increased plasma inactive renin in diabetes mellitus. A marker of microvascular complications. N Engl J Med *312*, 1412-1417.

Lumbers, E.R. (1971). Activation of renin in human amniotic fluid by low pH. Enzymologia *40*, 329-336.

Mackie, E.J., Tatarczuch, L., and Mirams, M. (2011). The skeleton: a multi-functional complex organ: the growth plate chondrocyte and endochondral ossification. J Endocrinol *211*, 109-121.

MacRae, I.J., and Doudna, J.A. (2007). Ribonuclease revisited: structural insights into ribonuclease III family enzymes. Curr Opin Struct Biol *17*, 138-145.

Maeda, K., Kobayashi, Y., Udagawa, N., Uehara, S., Ishihara, A., Mizoguchi, T., Kikuchi, Y., Takada, I., Kato, S., Kani, S., et al. (2012). Wnt5a-Ror2 signaling between osteoblast-lineage cells and osteoclast precursors enhances osteoclastogenesis. Nat Med 18, 405-412.

Mahmud, H., Sillje, H.H., Cannon, M.V., van Gilst, W.H., and de Boer, R.A. (2012). Regulation of the (pro)renin-renin receptor in cardiac remodelling. J Cell Mol Med *16*, 722-729.

Mahmud, H., Candido, W.M., van Genne, L., Vreeswijk-Baudoin, I., Yu, H., van de Sluis, B., van Deursen, J., van Gilst, W.H., Sillje, H.H., and de Boer, R.A. (2014). Cardiac function and architecture are maintained in a model of cardiorestricted overexpression of the prorenin-renin receptor. PLoS One *9*, e89929.

Malicki, J., Jo, H., and Pujic, Z. (2003). Zebrafish N-cadherin, encoded by the glass onion locus, plays an essential role in retinal patterning. Dev Biol *259*, 95-108.

Malkus, P., Graham, L.A., Stevens, T.H., and Schekman, R. (2004). Role of Vma21p in assembly and transport of the yeast vacuolar ATPase. Mol Biol Cell *15*, 5075-5091.

Margolis, D.S., Szivek, J.A., Lai, L.W., and Lien, Y.H. (2008). Phenotypic characteristics of bone in carbonic anhydrase II-deficient mice. Calcif Tissue Int *82*, 66-76.

Marshansky, V., and Futai, M. (2008). The V-type H+-ATPase in vesicular trafficking: targeting, regulation and function. Curr Opin Cell Biol *20*, 415-426.

Marshansky, V., Rubinstein, J.L., and Gruber, G. (2014). Eukaryotic V-ATPase: novel structural findings and functional insights. Biochim Biophys Acta *1837*, 857-879.

Maruyama, N., Segawa, T., Kinoshita, N., and Ichihara, A. (2013). Novel sandwich ELISA for detecting the human soluble (pro)renin receptor. Front Biosci (Elite Ed) *5*, 583-590.

Masai, I., Lele, Z., Yamaguchi, M., Komori, A., Nakata, A., Nishiwaki, Y., Wada, H., Tanaka, H., Nojima, Y., Hammerschmidt, M*., et al.* (2003). N-cadherin mediates retinal lamination, maintenance of forebrain compartments and patterning of retinal neurites. Development *130*, 2479-2494.

Masland, R.H. (2001). The fundamental plan of the retina. Nat Neurosci *4*, 877-886.

Matavelli, L.C., Huang, J., and Siragy, H.M. (2010). (Pro)renin receptor contributes to diabetic nephropathy by enhancing renal inflammation. Clin Exp Pharmacol Physiol *37*, 277-282.

Matzke, M., Matzke, A.J., and Kooter, J.M. (2001). RNA: guiding gene silencing. Science *293*, 1080-1083.

Maxfield, F.R., and McGraw, T.E. (2004). Endocytic recycling. Nat Rev Mol Cell Biol *5*, 121-132.

Maxson, M.E., and Grinstein, S. (2014). The vacuolar-type H(+)-ATPase at a glance - more than a proton pump. J Cell Sci *127*, 4987-4993.

McHugh, K.P., Hodivala-Dilke, K., Zheng, M.H., Namba, N., Lam, J., Novack, D., Feng, X., Ross, F.P., Hynes, R.O., and Teitelbaum, S.L. (2000). Mice lacking beta3 integrins are osteosclerotic because of dysfunctional osteoclasts. J Clin Invest *105*, 433-440.

Melnyk, R.A., Tam, J., Boie, Y., Kennedy, B.P., and Percival, M.D. (2009). Renin and prorenin activate pathways implicated in organ damage in human mesangial cells independent of angiotensin II production. Am J Nephrol *30*, 232-243.

Mercure, C., Prescott, G., Lacombe, M.J., Silversides, D.W., and Reudelhuber, T.L. (2009). Chronic increases in circulating prorenin are not associated with renal or cardiac pathologies. Hypertension *53*, 1062-1069.

Mercure, C., Lacombe, M.J., Khazaie, K., and Reudelhuber, T.L. (2010). Cathepsin B is not the processing enzyme for mouse prorenin. Am J Physiol Regul Integr Comp Physiol *298*, R1212-1216.

Merkulova, M., Bakulina, A., Thaker, Y.R., Gruber, G., and Marshansky, V. (2010). Specific motifs of the V-ATPase a2-subunit isoform interact with catalytic and regulatory domains of ARNO. Biochim Biophys Acta *1797*, 1398-1409.

Miura, G.I., Froelick, G.J., Marsh, D.J., Stark, K.L., and Palmiter, R.D. (2003). The d subunit of the vacuolar ATPase (Atp6d) is essential for embryonic development. Transgenic Res *12*, 131-133.

Miyauchi, Y., Ninomiya, K., Miyamoto, H., Sakamoto, A., Iwasaki, R., Hoshi, H., Miyamoto, K., Hao, W., Yoshida, S., Morioka, H., et al. (2010). The Blimp1-Bcl6 axis is critical to regulate osteoclast differentiation and bone homeostasis. J Exp Med 207, 751-762.

Mizushima, N. (2007). Autophagy: process and function. Genes Dev *21*, 2861-2873.

Montes, E., Ruiz, V., Checa, M., Maldonado, V., Melendez-Zajgla, J., Montano, M., Ordonez-Razo, R., Cisneros, J., Garcia-de-Alba, C., Pardo, A*., et al.* (2012). Renin is an angiotensin-independent profibrotic mediator: role in pulmonary fibrosis. Eur Respir J *39*, 141-148.

Morel, N., Dedieu, J.C., and Philippe, J.M. (2003). Specific sorting of the a1 isoform of the V-H+ATPase a subunit to nerve terminals where it associates with both synaptic vesicles and the presynaptic plasma membrane. J Cell Sci *116*, 4751-4762.

Mosser, D.M., and Edwards, J.P. (2008). Exploring the full spectrum of macrophage activation. Nat Rev Immunol *8*, 958-969.

Moverare-Skrtic, S., Henning, P., Liu, X., Nagano, K., Saito, H., Borjesson, A.E., Sjogren, K., Windahl, S.H., Farman, H., Kindlund, B., et al. (2014). Osteoblast-derived WNT16 represses osteoclastogenesis and prevents cortical bone fragility fractures. Nat Med 20, 1279-1288.

Muench, S.P., Huss, M., Song, C.F., Phillips, C., Wieczorek, H., Trinick, J., and Harrison, M.A. (2009). Cryo-electron microscopy of the vacuolar ATPase motor reveals its mechanical and regulatory complexity. J Mol Biol *386*, 989-999.

Mulari, M., Vaaraniemi, J., and Vaananen, H.K. (2003). Intracellular membrane trafficking in bone resorbing osteoclasts. Microsc Res Tech *61*, 496-503.

Muller, D.N., Fischli, W., Clozel, J.P., Hilgers, K.F., Bohlender, J., Menard, J., Busjahn, A., Ganten, D., and Luft, F.C. (1998). Local angiotensin II generation in the rat heart: role of renin uptake. Circ Res *82*, 13-20.

Muller, D.N., Klanke, B., Feldt, S., Cordasic, N., Hartner, A., Schmieder, R.E., Luft, F.C., and Hilgers, K.F. (2008). (Pro)renin receptor peptide inhibitor "handle-region" peptide does not affect hypertensive nephrosclerosis in Goldblatt rats. Hypertension *51*, 676-681.

Mummery-Widmer, J.L., Yamazaki, M., Stoeger, T., Novatchkova, M., Bhalerao, S., Chen, D., Dietzl, G., Dickson, B.J., and Knoblich, J.A. (2009). Genome-wide analysis of Notch signalling in Drosophila by transgenic RNAi. Nature *458*, 987-992.

Muto, A., Mizoguchi, T., Udagawa, N., Ito, S., Kawahara, I., Abiko, Y., Arai, A., Harada, S., Kobayashi, Y., Nakamichi, Y.*, et al.* (2011). Lineage-committed osteoclast precursors circulate in blood and settle down into bone. J Bone Miner Res *26*, 2978-2990.

Nabi, A.H., Kageshima, A., Uddin, M.N., Nakagawa, T., Park, E.Y., and Suzuki, F. (2006). Binding properties of rat prorenin and renin to the recombinant rat renin/prorenin receptor prepared by a baculovirus expression system. Int J Mol Med *18*, 483-488.

Nakamura, T., Imai, Y., Matsumoto, T., Sato, S., Takeuchi, K., Igarashi, K., Harada, Y., Azuma, Y., Krust, A., Yamamoto, Y., et al. (2007). Estrogen prevents bone loss via estrogen receptor alpha and induction of Fas ligand in osteoclasts. Cell 130, 811-823.

Nakashima, T., Hayashi, M., Fukunaga, T., Kurata, K., Oh-Hora, M., Feng, J.Q., Bonewald, L.F., Kodama, T., Wutz, A., Wagner, E.F.*, et al.* (2011). Evidence for osteocyte regulation of bone homeostasis through RANKL expression. Nat Med *17*, 1231-1234.

Narducci, P., Bortul, R., Bareggi, R., and Nicolin, V. (2010). Clathrin-dependent endocytosis of membrane-bound RANKL in differentiated osteoclasts. Eur J Histochem 54, e6.

Nelson, N., and Harvey, W.R. (1999). Vacuolar and plasma membrane proton-adenosinetriphosphatases. Physiol Rev *79*, 361-385.

Nesbitt, S.A., and Horton, M.A. (1997). Trafficking of matrix collagens through bone-resorbing osteoclasts. Science *276*, 266-269.

Nguyen, G., Delarue, F., Berrou, J., Rondeau, E., and Sraer, J.D. (1996). Specific receptor binding of renin on human mesangial cells in culture increases plasminogen activator inhibitor-1 antigen. Kidney Int *50*, 1897-1903.

Nguyen, G., Bouzhir, L., Delarue, F., Rondeau, E., and Sraer, J.D. (1998). [Evidence of a renin receptor on human mesangial cells: effects on PAI1 and cGMP]. Nephrologie *19*, 411-416.

Nguyen, G., Delarue, F., Burckle, C., Bouzhir, L., Giller, T., and Sraer, J.D. (2002). Pivotal role of the renin/prorenin receptor in angiotensin II production and cellular responses to renin. J Clin Invest *109*, 1417-1427.

Nguyen, G., and Contrepas, A. (2008). Physiology and pharmacology of the (pro)renin receptor. Curr Opin Pharmacol *8*, 127-132.

Niehrs, C. (2012). The complex world of WNT receptor signalling. Nat Rev Mol Cell Biol *13*, 767-779.

Nishi, T., and Forgac, M. (2000). Molecular cloning and expression of three isoforms of the 100-kDa a subunit of the mouse vacuolar proton-translocating ATPase. J Biol Chem *275*, 6824-6830.

Niwa, H., Yamamura, K., and Miyazaki, J. (1991). Efficient selection for high-expression transfectants with a novel eukaryotic vector. Gene *108*, 193-199.

Nomiyama, H., Egami, K., Wada, N., Tou, K., Horiuchi, M., Matsusaki, H., Miura, R., Yoshie, O., and Kukita, T. (2005). Identification of genes differentially expressed in osteoclast-like cells. J Interferon Cytokine Res *25*, 227-231.

Novinec, M., and Lenarcic, B. (2013). Cathepsin K: a unique collagenolytic cysteine peptidase. Biol Chem 394, 1163-1179.

Nuckels, R.J., Ng, A., Darland, T., and Gross, J.M. (2009). The vacuolar-ATPase complex regulates retinoblast proliferation and survival, photoreceptor morphogenesis, and pigmentation in the zebrafish eye. Invest Ophthalmol Vis Sci *50*, 893-905.

Ohira, M., Smardon, A.M., Charsky, C.M., Liu, J., Tarsio, M., and Kane, P.M. (2006). The E and G subunits of the yeast V-ATPase interact tightly and are both present at more than one copy per V1 complex. J Biol Chem *281*, 22752-22760.

Oshima, Y., Kinouchi, K., Ichihara, A., Sakoda, M., Kurauchi-Mito, A., Bokuda, K., Narita, T., Kurosawa, H., Sun-Wada, G.H., Wada, Y.*, et al.* (2011). Prorenin receptor is essential for normal podocyte structure and function. J Am Soc Nephrol *22*, 2203-2212.

Ott, C., Schneider, M.P., Delles, C., Schlaich, M.P., Hilgers, K.F., and Schmieder, R.E. (2011). Association of (pro)renin receptor gene polymorphism with blood pressure in Caucasian men. Pharmacogenet Genomics *21*, 347-349.

Palecanda, A., and Kobzik, L. (2001). Receptors for unopsonized particles: the role of alveolar macrophage scavenger receptors. Curr Mol Med 1, 589-595.

Pan, F., Liu, X.G., Guo, Y.F., Chen, Y., Dong, S.S., Qiu, C., Zhang, Z.X., Zhou, Q., Yang, T.L., Guo, Y., et al. (2010). The regulation-of-autophagy pathway may influence Chinese stature variation: evidence from elder adults. J Hum Genet *55*, 441-447.

Parfitt, A.M. (2002). Targeted and nontargeted bone remodeling: relationship to basic multicellular unit origination and progression. Bone *30*, 5-7.

Pereira, L.G., Arnoni, C.P., Maquigussa, E., Cristovam, P.C., Dreyfuss, J., and Boim, M.A. (2012). (Pro)renin receptor: another member of the system controlled by angiotensin II? J Renin Angiotensin Aldosterone Syst *13*, 1-10.

Peri, F., and Nusslein-Volhard, C. (2008). Live imaging of neuronal degradation by microglia reveals a role for v0-ATPase a1 in phagosomal fusion in vivo. Cell *133*, 916-927.

Peters, B., Grisk, O., Becher, B., Wanka, H., Kuttler, B., Ludemann, J., Lorenz, G., Rettig, R., Mullins, J.J., and Peters, J. (2008). Dose-dependent titration of prorenin and blood pressure in Cyp1a1ren-2 transgenic rats: absence of prorenin-induced glomerulosclerosis. J Hypertens *26*, 102-109.

Peters, J., Schluter, T., Riegel, T., Peters, B.S., Beineke, A., Maschke, U., Hosten, N., Mullins, J.J., and Rettig, R. (2009). Lack of cardiac fibrosis in a new model of high prorenin hyperaldosteronism. Am J Physiol Heart Circ Physiol *297*, H1845-1852.

Pietrement, C., Sun-Wada, G.H., Silva, N.D., McKee, M., Marshansky, V., Brown, D., Futai, M., and Breton, S. (2006). Distinct expression patterns of different subunit isoforms of the V-ATPase in the rat epididymis. Biol Reprod *74*, 185-194.

Piton, A., Redin, C., and Mandel, J.L. (2013). XLID-causing mutations and associated genes challenged in light of data from large-scale human exome sequencing. Am J Hum Genet *93*, 368-383.

Podolska, K., and Svoboda, P. (2011). Targeting genes in living mammals by RNA interference. Brief Funct Genomics *10*, 238-247.

Poorkaj, P., Raskind, W.H., Leverenz, J.B., Matsushita, M., Zabetian, C.P., Samii, A., Kim, S., Gazi, N., Nutt, J.G., Wolff, J.*, et al.* (2010). A novel X-linked four-repeat tauopathy with Parkinsonism and spasticity. Mov Disord *25*, 1409-1417.

Prescott, G., Silversides, D.W., and Reudelhuber, T.L. (2002). Tissue activity of circulating prorenin. Am J Hypertens *15*, 280-285.

Qi, B., Cong, Q., Li, P., Ma, G., Guo, X., Yeh, J., Xie, M., Schneider, M.D., Liu, H., and Li, B. (2014). Ablation of Tak1 in osteoclast progenitor leads to defects in skeletal growth and bone remodeling in mice. Sci Rep 4, 7158.

Qin, A., Cheng, T.S., Pavlos, N.J., Lin, Z., Dai, K.R., and Zheng, M.H. (2012). V-ATPases in osteoclasts: structure, function and potential inhibitors of bone resorption. Int J Biochem Cell Biol *44*, 1422-1435.

Qing, H., Ardeshirpour, L., Pajevic, P.D., Dusevich, V., Jahn, K., Kato, S., Wysolmerski, J., and Bonewald, L.F. (2012). Demonstration of osteocytic perilacunar/canalicular remodeling in mice during lactation. J Bone Miner Res 27, 1018-1029.

Rademaker, M.T., Yandle, T.G., Ellmers, L.J., Charles, C.J., Nicholls, M.G., and Richards, A.M. (2012). Hemodynamic, hormonal, and renal effects of (pro)renin receptor blockade in experimental heart failure. Circ Heart Fail *5*, 645-652.

Ramser, J., Abidi, F.E., Burckle, C.A., Lenski, C., Toriello, H., Wen, G., Lubs, H.A., Engert, S., Stevenson, R.E., Meindl, A., *et al.* (2005). A unique exonic splice enhancer mutation in a family with X-linked mental retardation and epilepsy points to a novel role of the renin receptor. Hum Mol Genet *14*, 1019-1027.

Rantakokko, J., Aro, H.T., Savontaus, M., and Vuorio, E. (1996). Mouse cathepsin K: cDNA cloning and predominant expression of the gene in osteoclasts, and in some hypertrophying chondrocytes during mouse development. FEBS Lett 393, 307-313.

Reudelhuber, T.L., Ramla, D., Chiu, L., Mercure, C., and Seidah, N.G. (1994). Proteolytic processing of human prorenin in renal and non-renal tissues. Kidney Int *46*, 1522-1524.

Riediger, F., Quack, I., Qadri, F., Hartleben, B., Park, J.K., Potthoff, S.A., Sohn, D., Sihn, G., Rousselle, A., Fokuhl, V., *et al.* (2011). Prorenin receptor is essential for podocyte autophagy and survival. J Am Soc Nephrol *22*, 2193-2202.

Robling, A.G., Niziolek, P.J., Baldridge, L.A., Condon, K.W., Allen, M.R., Alam, I., Mantila, S.M., Gluhak-Heinrich, J., Bellido, T.M., Harris, S.E., *et al.* (2008). Mechanical stimulation of bone in vivo reduces osteocyte expression of Sost/sclerostin. J Biol Chem *283*, 5866-5875.

Rodriguez, J.I., Delgado, E., and Paniagua, R. (1985). Changes in young rat radius following excision of the perichondrial ring. Calcif Tissue Int 37, 677-683.

Rosen, H.N., Moses, A.C., Garber, J., Iloputaife, I.D., Ross, D.S., Lee, S.L., and Greenspan, S.L. (2000). Serum CTX: a new marker of bone resorption that shows treatment effect more often than other markers because of low coefficient of variability and large changes with bisphosphonate therapy. Calcif Tissue Int *66*, 100-103.

Rosendahl, A., Niemann, G., Lange, S., Ahadzadeh, E., Krebs, C., Contrepas, A., van Goor, H., Wiech, T., Bader, M., Schwake, M., *et al.* (2014). Increased expression of (pro)renin receptor does not cause hypertension or cardiac and renal fibrosis in mice. Lab Invest *94*, 863-872.

Ross, F.P. (2006). M-CSF, c-Fms, and signaling in osteoclasts and their precursors. Ann N Y Acad Sci *1068*, 110-116.

Rousselle, A., Sihn, G., Rotteveel, M., and Bader, M. (2014). (Pro)renin receptor and V-ATPase: from Drosophila to humans. Clin Sci (Lond) *126*, 529-536.

Saftig, P., Hunziker, E., Wehmeyer, O., Jones, S., Boyde, A., Rommerskirch, W., Moritz, J.D., Schu, P., and von Figura, K. (1998). Impaired osteoclastic bone resorption leads to osteopetrosis in cathepsin-K-deficient mice. Proc Natl Acad Sci U S A *95*, 13453-13458.

Saftig, P., and Klumperman, J. (2009). Lysosome biogenesis and lysosomal membrane proteins: trafficking meets function. Nat Rev Mol Cell Biol *10*, 623-635.

Sakoda, M., Ichihara, A., Kaneshiro, Y., Takemitsu, T., Nakazato, Y., Nabi, A.H., Nakagawa, T., Suzuki, F., Inagami, T., and Itoh, H. (2007). (Pro)renin receptor-mediated activation of mitogen-activated protein kinases in human vascular smooth muscle cells. Hypertens Res *30*, 1139-1146.

Saris, J.J., Derkx, F.H., Lamers, J.M., Saxena, P.R., Schalekamp, M.A., and Danser, A.H. (2001a). Cardiomyocytes bind and activate native human prorenin : role of soluble mannose 6-phosphate receptors. Hypertension *37*, 710-715.

Saris, J.J., Derkx, F.H., De Bruin, R.J., Dekkers, D.H., Lamers, J.M., Saxena, P.R., Schalekamp, M.A., and Jan Danser, A.H. (2001b). High-affinity prorenin binding to cardiac man-6-P/IGF-II receptors precedes proteolytic activation to renin. Am J Physiol Heart Circ Physiol *280*, H1706-1715.

Saris, J.J., van den Eijnden, M.M., Lamers, J.M., Saxena, P.R., Schalekamp, M.A., and Danser, A.H. (2002). Prorenin-induced myocyte proliferation: no role for intracellular angiotensin II. Hypertension *39*, 573-577.

Saris, J.J., t Hoen, P.A., Garrelds, I.M., Dekkers, D.H., den Dunnen, J.T., Lamers, J.M., and Jan Danser, A.H. (2006). Prorenin induces intracellular signaling in cardiomyocytes independently of angiotensin II. Hypertension *48*, 564-571.

Satofuka, S., Ichihara, A., Nagai, N., Yamashiro, K., Koto, T., Shinoda, H., Noda, K., Ozawa, Y., Inoue, M., Tsubota, K., *et al.* (2006). Suppression of ocular inflammation in endotoxin-induced uveitis by inhibiting nonproteolytic activation of prorenin. Invest Ophthalmol Vis Sci *47*, 2686-2692.

Satofuka, S., Ichihara, A., Nagai, N., Koto, T., Shinoda, H., Noda, K., Ozawa, Y., Inoue, M., Tsubota, K., Itoh, H., *et al.* (2007). Role of nonproteolytically activated prorenin in pathologic, but not physiologic, retinal neovascularization. Invest Ophthalmol Vis Sci *48*, 422-429.

Satofuka, S., Ichihara, A., Nagai, N., Noda, K., Ozawa, Y., Fukamizu, A., Tsubota, K., Itoh, H., Oike, Y., and Ishida, S. (2008). (Pro)renin receptor promotes choroidal neovascularization by activating its signal transduction and tissue renin-angiotensin system. Am J Pathol *173*, 1911-1918.

Satofuka, S., Ichihara, A., Nagai, N., Noda, K., Ozawa, Y., Fukamizu, A., Tsubota, K., Itoh, H., Oike, Y., and Ishida, S. (2009). (Pro)renin receptor-mediated signal transduction and tissue renin-angiotensin system contribute to diabetes-induced retinal inflammation. Diabetes *58*, 1625-1633.

Schefe, J.H., Menk, M., Reinemund, J., Effertz, K., Hobbs, R.M., Pandolfi, P.P., Ruiz, P., Unger, T., and Funke-Kaiser, H. (2006). A novel signal transduction cascade involving direct physical interaction of the renin/prorenin receptor with the transcription factor promyelocytic zinc finger protein. Circ Res *99*, 1355-1366.

Schefe, J.H., Neumann, C., Goebel, M., Danser, J., Kirsch, S., Gust, R., Kintscher, U., Unger, T., and Funke-Kaiser, H. (2008). Prorenin engages the (pro)renin receptor like renin and both ligand activities are unopposed by aliskiren. J Hypertens *26*, 1787-1794.

Schlesinger, P.H., Blair, H.C., Teitelbaum, S.L., and Edwards, J.C. (1997). Characterization of the osteoclast ruffled border chloride channel and its role in bone resorption. J Biol Chem *272*, 18636-18643.

Schmitz, C., Gotthardt, M., Hinderlich, S., Leheste, J.R., Gross, V., Vorum, H., Christensen, E.I., Luft, F.C., Takahashi, S., and Willnow, T.E. (2000). Normal blood pressure and plasma renin activity in mice lacking the renin-binding protein, a cellular renin inhibitor. J Biol Chem *275*, 15357-15362.

Schoonderwoert, V.T., and Martens, G.J. (2001). Proton pumping in the secretory pathway. J Membr Biol *182*, 159-169.

Schoonderwoert, V.T., and Martens, G.J. (2002). Targeted disruption of the mouse gene encoding the V-ATPase accessory subunit Ac45. Mol Membr Biol *19*, 67-71.

Scimeca, J.C., Franchi, A., Trojani, C., Parrinello, H., Grosgeorge, J., Robert, C., Jaillon, O., Poirier, C., Gaudray, P., and Carle, G.F. (2000). The gene encoding the mouse homologue of the human osteoclast-specific 116-kDa V-ATPase subunit bears a deletion in osteosclerotic (oc/oc) mutants. Bone *26*, 207-213.

Scott, E.W., Simon, M.C., Anastasi, J., and Singh, H. (1994). Requirement of transcription factor PU.1 in the development of multiple hematopoietic lineages. Science *265*, 1573-1577.

Sealey, J.E., Moon, C., Laragh, J.H., and Alderman, M. (1976). Plasma prorenin: cryoactivation and relationship to renin substrate in normal subjects. Am J Med *61*, 731-738.

Sealey, J.E., Wilson, M., Morganti, A.A., Zervoudakis, I., and Laragh, J.H. (1982). Changes in active and inactive renin throughout normal pregnancy. Clin Exp Hypertens A *4*, 2373-2384.

Seaman, M.N. (2012). The retromer complex - endosomal protein recycling and beyond. J Cell Sci 125, 4693-4702.

Seibler, J., Kleinridders, A., Kuter-Luks, B., Niehaves, S., Bruning, J.C., and Schwenk, F. (2007). Reversible gene knockdown in mice using a tight, inducible shRNA expression system. Nucleic Acids Res *35*, e54.

Sennoune, S.R., Bakunts, K., Martinez, G.M., Chua-Tuan, J.L., Kebir, Y., Attaya, M.N., and Martinez-Zaguilan, R. (2004). Vacuolar H+-ATPase in human breast cancer cells with distinct metastatic potential: distribution and functional activity. Am J Physiol Cell Physiol *286*, C1443-1452.

Shim, M.S., and Kwon, Y.J. (2010). Efficient and targeted delivery of siRNA in vivo. FEBS J *277*, 4814-4827.

Shimizu, H., Nakagami, H., Osako, M.K., Hanayama, R., Kunugiza, Y., Kizawa, T., Tomita, T., Yoshikawa, H., Ogihara, T., and Morishita, R. (2008). Angiotensin II accelerates osteoporosis by activating osteoclasts. FASEB J 22, 2465-2475.

Sihn, G., Rousselle, A., Vilianovitch, L., Burckle, C., and Bader, M. (2010). Physiology of the (pro)renin receptor: Wnt of change? Kidney Int *78*, 246-256.

Sihn, G., Burckle, C., Rousselle, A., Reimer, T., and Bader, M. (2013). (Pro)renin receptor: subcellular localizations and functions. Front Biosci (Elite Ed) *5*, 500-508.

Simonet, W.S., Lacey, D.L., Dunstan, C.R., Kelley, M., Chang, M.S., Luthy, R., Nguyen, H.Q., Wooden, S., Bennett, L., Boone, T.*, et al.* (1997). Osteoprotegerin: a novel secreted protein involved in the regulation of bone density. Cell *89*, 309-319.

Siragy, H.M., and Huang, J. (2008). Renal (pro)renin receptor upregulation in diabetic rats through enhanced angiotensin AT1 receptor and NADPH oxidase activity. Exp Physiol *93*, 709-714.

Skinner, S.L., Cran, E.J., Gibson, R., Taylor, R., Walters, W.A., and Catt, K.J. (1975). Angiotensins I and II, active and inactive renin, renin substrate, renin activity, and angiotensinase in human liquor amnii and plasma. Am J Obstet Gynecol *121*, 626-630.

Sly, W.S., Hewett-Emmett, D., Whyte, M.P., Yu, Y.S., and Tashian, R.E. (1983). Carbonic anhydrase II deficiency identified as the primary defect in the autosomal recessive syndrome of osteopetrosis with renal tubular acidosis and cerebral calcification. Proc Natl Acad Sci U S A *80*, 2752-2756.

Smith, A.N., Skaug, J., Choate, K.A., Nayir, A., Bakkaloglu, A., Ozen, S., Hulton, S.A., Sanjad, S.A., Al-Sabban, E.A., Lifton, R.P.*, et al.* (2000). Mutations in ATP6N1B, encoding a new kidney vacuolar proton pump 116-kD subunit, cause recessive distal renal tubular acidosis with preserved hearing. Nat Genet *26*, 71-75.

Sobacchi, C., Schulz, A., Coxon, F.P., Villa, A., and Helfrich, M.H. (2013). Osteopetrosis: genetics, treatment and new insights into osteoclast function. Nat Rev Endocrinol 9, 522-536.

Stankovic, A.R., Fisher, N.D., and Hollenberg, N.K. (2006). Prorenin and angiotensin-dependent renal vasoconstriction in type 1 and type 2 diabetes. J Am Soc Nephrol *17*, 3293-3299.

Stark, Z., and Savarirayan, R. (2009). Osteopetrosis. Orphanet J Rare Dis *4*, 5.

Steinman, R.M., Mellman, I.S., Muller, W.A., and Cohn, Z.A. (1983). Endocytosis and the recycling of plasma membrane. J Cell Biol 96, 1-27.

Stieger, K., Belbellaa, B., Le Guiner, C., Moullier, P., and Rolling, F. (2009). In vivo gene regulation using tetracycline-regulatable systems. Adv Drug Deliv Rev 61, 527-541.

Stover, E.H., Borthwick, K.J., Bavalia, C., Eady, N., Fritz, D.M., Rungroj, N., Giersch, A.B., Morton, C.C., Axon, P.R., Akil, I., et al. (2002). Novel ATP6V1B1 and ATP6V0A4 mutations in autosomal recessive distal renal tubular acidosis with new evidence for hearing loss. J Med Genet 39, 796-803.

Stuart, L.M., and Ezekowitz, R.A. (2005). Phagocytosis: elegant complexity. Immunity 22, 539-550.

Su, A.I., Wiltshire, T., Batalov, S., Lapp, H., Ching, K.A., Block, D., Zhang, J., Soden, R., Hayakawa, M., Kreiman, G., et al. (2004). A gene atlas of the mouse and human protein-encoding transcriptomes. Proc Natl Acad Sci U S A 101, 6062-6067.

Su, Y., Zhou, A., Al-Lamki, R.S., and Karet, F.E. (2003). The a-subunit of the V-type H+-ATPase interacts with phosphofructokinase-1 in humans. J Biol Chem 278, 20013-20018.

Suda, T., Takahashi, N., Udagawa, N., Jimi, E., Gillespie, M.T., and Martin, T.J. (1999). Modulation of osteoclast differentiation and function by the new members of the tumor necrosis factor receptor and ligand families. Endocr Rev 20, 345-357.

Sun-Wada, G., Murata, Y., Yamamoto, A., Kanazawa, H., Wada, Y., and Futai, M. (2000). Acidic endomembrane organelles are required for mouse postimplantation development. Dev Biol 228, 315-325.

Sun-Wada, G.H., Toyomura, T., Murata, Y., Yamamoto, A., Futai, M., and Wada, Y. (2006). The a3 isoform of V-ATPase regulates insulin secretion from pancreatic beta-cells. J Cell Sci 119, 4531-4540.

Sundquist, K., Lakkakorpi, P., Wallmark, B., and Vaananen, K. (1990). Inhibition of osteoclast proton transport by bafilomycin A1 abolishes bone resorption. Biochem Biophys Res Commun 168, 309-313.

Susani, L., Pangrazio, A., Sobacchi, C., Taranta, A., Mortier, G., Savarirayan, R., Villa, A., Orchard, P., Vezzoni, P., Albertini, A., et al. (2004). TCIRG1-dependent recessive osteopetrosis: mutation analysis, functional identification of the splicing defects, and in vitro rescue by U1 snRNA. Hum Mutat 24, 225-235.

Susic, D., Zhou, X., Frohlich, E.D., Lippton, H., and Knight, M. (2008). Cardiovascular effects of prorenin blockade in genetically spontaneously hypertensive rats on normal and high-salt diet. Am J Physiol Heart Circ Physiol 295, H1117-H1121.

Suzuki, A., and Ohno, S. (2006). The PAR-aPKC system: lessons in polarity. J Cell Sci 119, 979-987.

Suzuki, F., Hayakawa, M., Nakagawa, T., Nasir, U.M., Ebihara, A., Iwasawa, A., Ishida, Y., Nakamura, Y., and Murakami, K. (2003). Human prorenin has "gate and handle" regions for its non-proteolytic activation. J Biol Chem 278, 22217-22222.

Swaroop, A., Kim, D., and Forrest, D. (2010). Transcriptional regulation of photoreceptor development and homeostasis in the mammalian retina. Nat Rev Neurosci 11, 563-576.

Tada, M., Takahashi, S., Miyano, M., and Miyake, Y. (1992). Tissue-specific regulation of renin-binding protein gene expression in rats. J Biochem 112, 175-182.

Taichman, R.S. (2005). Blood and bone: two tissues whose fates are intertwined to create the hematopoietic stem-cell niche. Blood 105, 2631-2639.

Takahashi, H., Ichihara, A., Kaneshiro, Y., Inomata, K., Sakoda, M., Takemitsu, T., Nishiyama, A., and Itoh, H. (2007). Regression of nephropathy developed in diabetes by (Pro)renin receptor blockade. J Am Soc Nephrol 18, 2054-2061.

Takahashi, K., Yamamoto, H., Hirose, T., Hiraishi, K., Shoji, I., Shibasaki, A., Kato, I., Kaneko, K., Sasano, H., Satoh, F., et al. (2010). Expression of (pro)renin receptor in human kidneys with end-stage kidney disease due to diabetic nephropathy. Peptides 31, 1405-1408.

Takahashi, N., Akatsu, T., Udagawa, N., Sasaki, T., Yamaguchi, A., Moseley, J.M., Martin, T.J., and Suda, T. (1988). Osteoblastic cells are involved in osteoclast formation. Endocrinology 123, 2600-2602.

Takahashi, S., Ohsawa, T., Miura, R., and Miyake, Y. (1983). Purification of high molecular weight (HMW) renin from porcine kidney and direct evidence that the HMW renin is a complex of renin with renin binding protein (RnBP). J Biochem 93, 265-274.

Takahashi, S., Inoue, H., and Miyake, Y. (1992). The human gene for renin-binding protein. J Biol Chem 267, 13007-13013.

Takamori, S., Holt, M., Stenius, K., Lemke, E.A., Gronborg, M., Riedel, D., Urlaub, H., Schenck, S., Brugger, B., Ringler, P., et al. (2006). Molecular anatomy of a trafficking organelle. Cell 127, 831-846.

Takeshita, S., Fumoto, T., Matsuoka, K., Park, K.A., Aburatani, H., Kato, S., Ito, M., and Ikeda, K. (2013). Osteoclast-secreted CTHRC1 in the coupling of bone resorption to formation. J Clin Invest 123, 3914-3924.

Tamargo, J., Caballero, R., and Delpón, E. (2015). The Renin-Angiotensin System and Bone. Clin Rev Bone Min Metab 13, 125-148.

Tang, Y., Wu, X., Lei, W., Pang, L., Wan, C., Shi, Z., Zhao, L., Nagy, T.R., Peng, X., Hu, J., et al. (2009). TGF-beta1-induced migration of bone mesenchymal stem cells couples bone resorption with formation. Nat Med 15, 757-765.

Taranta, A., Migliaccio, S., Recchia, I., Caniglia, M., Luciani, M., De Rossi, G., Dionisi-Vici, C., Pinto, R.M., Francalanci, P., Boldrini, R., et al. (2003). Genotype-phenotype relationship in human ATP6i-dependent autosomal recessive osteopetrosis. Am J Pathol 162, 57-68.

Teitelbaum, S.L. (2000). Bone resorption by osteoclasts. Science 289, 1504-1508.

Teitelbaum, S.L., and Ross, F.P. (2003). Genetic regulation of osteoclast development and function. Nat Rev Genet 4, 638-649.

Thomason, J., Reyes, M., Allen, S.R., Jones, R.O., Beeram, M.R., Kuehl, T.J., Suzuki, F., and Uddin, M.N. (2015). Elevation of (Pro)Renin and (Pro)Renin Receptor in Preeclampsia. Am J Hypertens.

Tinkler, S.M., Linder, J.E., Williams, D.M., and Johnson, N.W. (1981). Formation of osteoclasts from blood monocytes during 1 alpha-OH Vit D-stimulated bone resorption in mice. J Anat 133, 389-396.

Toei, M., Saum, R., and Forgac, M. (2010). Regulation and isoform function of the V-ATPases. Biochemistry 49, 4715-4723.

Tondravi, M.M., McKercher, S.R., Anderson, K., Erdmann, J.M., Quiroz, M., Maki, R., and Teitelbaum, S.L. (1997). Osteopetrosis in mice lacking haematopoietic transcription factor PU.1. Nature 386, 81-84.

Torigoe, T., Izumi, H., Ishiguchi, H., Uramoto, H., Murakami, T., Ise, T., Yoshida, Y., Tanabe, M., Nomoto, M., Itoh, H., et al. (2002). Enhanced expression of the human vacuolar H+-ATPase c subunit gene (ATP6L) in response to anticancer agents. J Biol Chem 277, 36534-36543.

Toyomura, T., Murata, Y., Yamamoto, A., Oka, T., Sun-Wada, G.H., Wada, Y., and Futai, M. (2003). From lysosomes to the plasma membrane: localization of vacuolar-type H+ -ATPase with the a3 isoform during osteoclast differentiation. J Biol Chem 278, 22023-22030.

Tsuji-Takechi, K., Negishi-Koga, T., Sumiya, E., Kukita, A., Kato, S., Maeda, T., Pandolfi, P.P., Moriyama, K., and Takayanagi, H. (2012). Stage-specific functions of leukemia/lymphoma-related factor (LRF) in the transcriptional control of osteoclast development. Proc Natl Acad Sci U S A 109, 2561-2566.

Twigger, S.N., Nie, J., Ruotti, V., Yu, J., Chen, D., Li, D., Mathis, J., Narayanasamy, V., Gopinath, G.R., Pasko, D., et al. (2004). Integrative genomics: in silico coupling of rat physiology and complex traits with mouse and human data. Genome Res 14, 651-660.

Udagawa, N., Takahashi, N., Akatsu, T., Tanaka, H., Sasaki, T., Nishihara, T., Koga, T., Martin, T.J., and Suda, T. (1990). Origin of osteoclasts: mature monocytes and macrophages are capable of differentiating into osteoclasts under a suitable microenvironment prepared by bone marrow-derived stromal cells. Proc Natl Acad Sci U S A 87, 7260-7264.

Underhill, D.M., and Goodridge, H.S. (2012). Information processing during phagocytosis. Nat Rev Immunol 12, 492-502.

Uraoka, M., Ikeda, K., Nakagawa, Y., Koide, M., Akakabe, Y., Nakano-Kurimoto, R., Takahashi, T., Matoba, S., Yamada, H., Okigaki, M., et al. (2009). Prorenin induces ERK activation in endothelial cells to enhance neovascularization independently of the renin-angiotensin system. Biochem Biophys Res Commun 390, 1202-1207.

Vaananen, H.K., and Horton, M. (1995). The osteoclast clear zone is a specialized cell-extracellular matrix adhesion structure. J Cell Sci 108 (Pt 8), 2729-2732.

van den Eijnden, M.M., Saris, J.J., de Bruin, R.J., de Wit, E., Sluiter, W., Reudelhuber, T.L., Schalekamp, M.A., Derkx, F.H., and Danser, A.H. (2001). Prorenin accumulation and activation in human endothelial cells: importance of mannose 6-phosphate receptors. Arterioscler Thromb Vasc Biol 21, 911-916.

van Kesteren, C.A., Danser, A.H., Derkx, F.H., Dekkers, D.H., Lamers, J.M., Saxena, P.R., and Schalekamp, M.A. (1997). Mannose 6-phosphate receptor-mediated internalization and activation of prorenin by cardiac cells. Hypertension 30, 1389-1396.

van Kesteren, C.A., Saris, J.J., Dekkers, D.H., Lamers, J.M., Saxena, P.R., Schalekamp, M.A., and Danser, A.H. (1999). Cultured neonatal rat cardiac myocytes and fibroblasts do not synthesize renin or angiotensinogen: evidence for stretch-induced cardiomyocyte hypertrophy independent of angiotensin II. Cardiovasc Res 43, 148-156.

Veniant, M., Menard, J., Bruneval, P., Morley, S., Gonzales, M.F., and Mullins, J. (1996). Vascular damage without hypertension in transgenic rats expressing prorenin exclusively in the liver. J Clin Invest 98, 1966-1970.

Venzke, D., Domgall, I., Kocher, T., Fethiere, J., Fischer, S., and Bottcher, B. (2005). Elucidation of the stator organization in the V-ATPase of Neurospora crassa. J Mol Biol 349, 659-669.

Vitavska, O., Wieczorek, H., and Merzendorfer, H. (2003). A novel role for subunit C in mediating binding of the H+-V-ATPase to the actin cytoskeleton. J Biol Chem 278, 18499-18505.

Wagner, C.A., Finberg, K.E., Breton, S., Marshansky, V., Brown, D., and Geibel, J.P. (2004). Renal vacuolar H+-ATPase. Physiol Rev 84, 1263-1314.

Walker, D.G. (1972). Congenital osteopetrosis in mice cured by parabiotic union with normal siblings. Endocrinology 91, 916-920.

Walker, D.G. (1973). Osteopetrosis cured by temporary parabiosis. Science 180, 875.

Walker, D.G. (1975). Control of bone resorption by hematopoietic tissue. The induction and reversal of congenital osteopetrosis in mice through use of bone marrow and splenic transplants. J Exp Med 142, 651-663.

Wang, H., Kesinger, J.W., Zhou, Q., Wren, J.D., Martin, G., Turner, S., Tang, Y., Frank, M.B., and Centola, M. (2008). Identification and characterization of zebrafish ocular formation genes. Genome 51, 222-235.

Wei, X., and Malicki, J. (2002). nagie oko, encoding a MAGUK-family protein, is essential for cellular patterning of the retina. Nat Genet 31, 150-157.

Wei, X., Cheng, Y., Luo, Y., Shi, X., Nelson, S., and Hyde, D.R. (2004). The zebrafish Pard3 ortholog is required for separation of the eye fields and retinal lamination. Dev Biol 269, 286-301.

Wei, W., Zeve, D., Suh, J.M., Wang, X., Du, Y., Zerwekh, J.E., Dechow, P.C., Graff, J.M., and Wan, Y. (2011). Biphasic and dosage-dependent regulation of osteoclastogenesis by beta-catenin. Mol Cell Biol 31, 4706-4719.

Wiktor-Jedrzejczak, W., Bartocci, A., Ferrante, A.W., Jr., Ahmed-Ansari, A., Sell, K.W., Pollard, J.W., and Stanley, E.R. (1990). Total absence of colony-stimulating factor 1 in the macrophage-deficient osteopetrotic (op/op) mouse. Proc Natl Acad Sci U S A 87, 4828-4832.

Wiktor-Jedrzejczak, W., Urbanowska, E., Aukerman, S.L., Pollard, J.W., Stanley, E.R., Ralph, P., Ansari, A.A., Sell, K.W., and Szperl, M. (1991). Correction by CSF-1 of defects in the osteopetrotic op/op mouse suggests local, developmental, and humoral requirements for this growth factor. Exp Hematol 19, 1049-1054.

Wilkinson-Berka, J.L., Heine, R., Tan, G., Cooper, M.E., Hatzopoulos, K.M., Fletcher, E.L., Binger, K.J., Campbell, D.J., and Miller, A.G. (2010). RILLKKMPSV influences the vasculature, neurons and glia, and (pro)renin receptor expression in the retina. Hypertension 55, 1454-1460.

Wilson, R.C., and Doudna, J.A. (2013). Molecular mechanisms of RNA interference. Annu Rev Biophys 42, 217-239.

Xa, L.K., Lacombe, M.J., Mercure, C., Lazure, C., and Reudelhuber, T.L. (2014). General lysosomal hydrolysis can process prorenin accurately. Am J Physiol Regul Integr Comp Physiol 307, R505-513.

Xia, W.F., Tang, F.L., Xiong, L., Xiong, S., Jung, J.U., Lee, D.H., Li, X.S., Feng, X., Mei, L., and Xiong, W.C. (2013). Vps35 loss promotes hyperresorptive osteoclastogenesis and osteoporosis via sustained RANKL signaling. J Cell Biol 200, 821-837.

Xian, L., Wu, X., Pang, L., Lou, M., Rosen, C.J., Qiu, T., Crane, J., Frassica, F., Zhang, L., Rodriguez, J.P., et al. (2012). Matrix IGF-1 maintains bone mass by activation of mTOR in mesenchymal stem cells. Nat Med 18, 1095-1101.

Xiong, J., Onal, M., Jilka, R.L., Weinstein, R.S., Manolagas, S.C., and O'Brien, C.A. (2011). Matrix-embedded cells control osteoclast formation. Nat Med 17, 1235-1241.

Xu, T., Vasilyeva, E., and Forgac, M. (1999). Subunit interactions in the clathrin-coated vesicle vacuolar (H(+))-ATPase complex. J Biol Chem 274, 28909-28915.

Xu, T., and Forgac, M. (2000). Subunit D (Vma8p) of the yeast vacuolar H+-ATPase plays a role in coupling of proton transport and ATP hydrolysis. J Biol Chem 275, 22075-22081.

Yagi, M., Miyamoto, T., Sawatani, Y., Iwamoto, K., Hosogane, N., Fujita, N., Morita, K., Ninomiya, K., Suzuki, T., Miyamoto, K., et al. (2005). DC-STAMP is essential for cell-cell fusion in osteoclasts and foreign body giant cells. J Exp Med 202, 345-351.

Yamamoto, H., Komekado, H., and Kikuchi, A. (2006). Caveolin is necessary for Wnt-3a-dependent internalization of LRP6 and accumulation of beta-catenin. Dev Cell 11, 213-223.

Yang, D.Q., Feng, S., Chen, W., Zhao, H., Paulson, C., and Li, Y.P. (2012). V-ATPase subunit ATP6AP1 (Ac45) regulates osteoclast differentiation, extracellular acidification, lysosomal trafficking, and protease exocytosis in osteoclast-mediated bone resorption. J Bone Miner Res 27, 1695-1707.

Yang, W., Wang, J., Moore, D.C., Liang, H., Dooner, M., Wu, Q., Terek, R., Chen, Q., Ehrlich, M.G., Quesenberry, P.J., et al. (2013). Ptpn11 deletion in a novel progenitor causes metachondromatosis by inducing hedgehog signalling. Nature 499, 491-495.

Yao, Z., Li, P., Zhang, Q., Schwarz, E.M., Keng, P., Arbini, A., Boyce, B.F., and Xing, L. (2006). Tumor necrosis factor-alpha increases circulating osteoclast precursor numbers by promoting their proliferation and differentiation in the bone marrow through up-regulation of c-Fms expression. J Biol Chem 281, 11846-11855.

Yasuda, H., Shima, N., Nakagawa, N., Yamaguchi, K., Kinosaki, M., Mochizuki, S., Tomoyasu, A., Yano, K., Goto, M., Murakami, A., et al. (1998). Osteoclast differentiation factor is a ligand for osteoprotegerin/osteoclastogenesis-inhibitory factor and is identical to TRANCE/RANKL. Proc Natl Acad Sci U S A 95, 3597-3602.

Yi, R., Qin, Y., Macara, I.G., and Cullen, B.R. (2003). Exportin-5 mediates the nuclear export of pre-microRNAs and short hairpin RNAs. Genes Dev 17, 3011-3016.

Yoshida, H., Hayashi, S., Kunisada, T., Ogawa, M., Nishikawa, S., Okamura, H., Sudo, T., and Shultz, L.D. (1990). The murine mutation osteopetrosis is in the coding region of the macrophage colony stimulating factor gene. Nature 345, 442-444.

Yoshikawa, A., Aizaki, Y., Kusano, K., Kishi, F., Susumu, T., Iida, S., Ishiura, S., Nishimura, S., Shichiri, M., and Senbonmatsu, T. (2011). The (pro)renin receptor is cleaved by ADAM19 in the Golgi leading to its secretion into extracellular space. Hypertens Res 34, 599-605.

Yu, B., Chang, J., Liu, Y., Li, J., Kevork, K., Al-Hezaimi, K., Graves, D.T., Park, N.H., and Wang, C.Y. (2014). Wnt4 signaling prevents skeletal aging and inflammation by inhibiting nuclear factor-kappaB. Nat Med 20, 1009-1017.

Zhang, J., Noble, N.A., Border, W.A., Owens, R.T., and Huang, Y. (2008). Receptor-dependent prorenin activation and induction of PAI-1 expression in vascular smooth muscle cells. Am J Physiol Endocrinol Metab 295, E810-819.

Zhang, J., Wu, J., Gu, C., Noble, N.A., Border, W.A., and Huang, Y. (2012). Receptor-mediated nonproteolytic activation of prorenin and induction of TGF-beta1 and PAI-1 expression in renal mesangial cells. Am J Physiol Renal Physiol 303, F11-20.

Zhang, L., Guo, Y.F., Liu, Y.Z., Liu, Y.J., Xiong, D.H., Liu, X.G., Wang, L., Yang, T.L., Lei, S.F., Guo, Y., et al. (2010). Pathway-based genome-wide association analysis identified the importance of regulation-of-autophagy pathway for ultradistal radius BMD. J Bone Miner Res 25, 1572-1580.

Zhang, Y., Gao, X., and Michael Garavito, R. (2011). Structural analysis of the intracellular domain of (pro)renin receptor fused to maltose-binding protein. Biochem Biophys Res Commun 407, 674-679.

Zoncu, R., Bar-Peled, L., Efeyan, A., Wang, S., Sancak, Y., and Sabatini, D.M. (2011). mTORC1 senses lysosomal amino acids through an inside-out mechanism that requires the vacuolar H(+)-ATPase. Science 334, 678-683.

APPENDIX

ABBREVIATIONS, SYMBOLS AND UNITS

Table 22: Abbreviations

α-MEM	α-Minimum Essential Medium
ACE	Angiotensin converting enzyme
ADAM	A disintegrin and metalloprotease
AF647	Alexa Fluor 647
Ang	Angiotensin
AOG	Angiotensinogen
AP	Adaptor protein
APS	Ammonium persulfate
aPKC	Atypical protein kinase C
AT1	Angiotensin type 1 receptor
AT2	Angiotensin type 2 receptor
ATG	Autophagy protein
ATP6ap 1/2	V-ATPase associated protein ½
β-mercapto	2-Mercaptoethanol
Baf	Bafilomycin
BCA	Bicinchoninic acid
BD	Basolateral domain
BL	Body length
BM	Bone marrow
BMU	Basic multicellular unit
BSA	Bovine serum albumin
BV	Bone volume
BW	Body weight
CAII	Carbonic anhydrase II
CAPER	Endoplasmic reticulum localized type I transmembrane adaptator precursor C
CCLN7	Chloride channel 7
CD	Cluster of differentiation
cDNA	Complementary DANN
cKO	Conditional knock-out
Cort.Th.	Cortical thickness
COX2	Cyclooxygenase 2
Cre	Cre recombinase
CSF-1	Colony-stimulating factor 1
CSF-1R	Colony-stimulating factor 1 receptor
CTHRC1	Collagen triple helix repeat containing 1

Ctrl	Control
CtsK	Cathepsin K
CtsKcKO	Mice with CtsK-Cre-mediated (P)RR deletion
CTX-I	Cross Linked C-Telopeptide of Type I Collagen
D	Day
DAPI	4’,6-Diamidino-2-phenylindole
DC-STAMP	Dendritic cell-specific transmembrane protein
DEPC	Diethylpyrocarbonate
DMEM	Dulbecco's modified Eagle's medium with high glucose
DMEM-HG	Dulbecco's modified Eagle's medium
DMSO	Dimethyl sulfoxide
DNA	Deoxyribonucleic acid
DNase	Deoxyribonuclease
dNTP	Deoxyribonucleotide
Dox	Doxycycline
dPRR	*Drosophila* homolog of prorenin receptor
dsRBD	Double-stranded RNA-binding domain
dsRNA	Double-stranded RNA
DTT	1,4-Dithiothreitol
dUTP	Deoxyuridine triphosphate
E-Cad	E-Cadherin
EDTA	Ethylenediaminetetraacetic acid (EDTA)
EEA1	Early endosome antigen 1
EGFP	Enhanced green fluorescent protein
EGTA	Ethylene glycol tetraacetic acid (EGTA)
ELISA	Enzyme-linked immunosorbent assay
ER	Endoplasmic reticulum
ESCRT	Endosomal-sorting complex required for transport
FACS	Flow cytometry
FBS	Fetal bovine serum
Fmi	Flamingo
FSD	Functional secretory domain
fw	Forward
Fz	Frizzled
GAPDH	Glyceraldehyde-3-phosphate dehydrogenase
GFP	Green fluorescent protein
Glu	Glutamine
HBSS	Hank's balanced salt solution
HCT	Hematocrit
HE	Hematoxylin and eosin
HEK293	Human embryonic kidney cells
Het	Heterozygous
HGB	Hemoglobin
HOPS	Homotypic protein sorting
HPRT	Hypoxanthin-phosphoribosyl-transferase
HRP	Handle region peptide

HSC	Hematopoietic stem cell
IGF-1	Insulin-like growth factor 1
IHC	Immunohistochemistry
JGA	Juxtaglomerular apparatus
LAMP	Lysosomal-associated membrane protein
LB	Lysogeny broth
LBPA	Lysobiphosphatidic acid
LRP6	Low-density lipoprotein receptor-related protein 6
LS	Lysosensor
LT	Lysotracker
LysM	Lyzosyme M
LysMcKO	Mice with LysM-Cre-mediated (P)RR deletion
MAPK	Mitogen-activated protein kinase
M-CSF	Macrophage colony-stimulating factor
M-CSFR	Macrophage colony-stimulating factor receptor
MDC	Max Delbrück Center
MHC-II	Major histocompatibility complex II
µCT	Microcomputed tomography
MITF	Microphtalmia-associated transcription factor
M-MLV	Moloney Murine Leukemia Virus
MMA	Methyl methacrylate
MMPs	Matrix metalloproteinases
mRNA	Messenger RNA
mTORC1	Mammalian target of rapamycin complex 1
MVBs	Multi-vesicular bodies
NFATc1	Nuclear factor of activated T-cells cytoplasmic 1
NF-κB	Nuclear factor κB
op/op	Osteopetrotic mice
OPG	Osteoprotegerin
pA	Polyadenylation site
PAGE	Polyacrylamide gel electrophoresis
PAI-1	Plasminogen-activator inhibitor-1
PAR3	Partitioning defective 3 homolog
PBS	Phosphate buffered saline
PBS-Tr	Phosphate buffered saline with triton
PCP	Planar cell polarity
PCR	Polymerase chain reaction
PFA	Paraformaldehyde
PI(3)P	Phosphatidylinositol-3-phosphate
PL	Penis length
PLT	Platelets
PLZF	Promyelotic leukemia zinc finger
pn	*Pekin*
PPE	Prorenin-processing enzyme
(P)RR	(Pro)renin receptor
P/S	Penicillin and streptomycin
PTGS	Post-transcriptional gene silencing

pUb	Ubiquitin C promoter
Pv	P-value
PVDF	Polyvinylidene difluoride
PW	Penis weight
qPCR	Quantitative PCR
RANK	Receptor activator of NF-κB
RANKL	Receptor activator of NF-κB ligand
RAS	Renin-angiotensin system
RB	Ruffled border
RBC	Red blood cells
rec	Recombinant
RH	Random hexamer
RILP	Rab-interacting lysosomal protein
RISC	RNA-induced silencing complex
RNAi	RNA interfence
RNase	Ribonuclease
RnBP	Renin-binding protein
ROI	Region of interest
RT	Reverse transcription
rtTA	Reverse tetracycline-controlled transactivator
rv	Reverse
S1P	Sphingosin-1 phosphate
SD rat	Sprague Dawley rat
SDS	Sodium dodecylsulfate
sh rat	Transgenic rat
shRNA	Short hairpin RNA
siRNA	Short interfering RNA
s(P)RR	Soluble (P)RR
SW	Spleen weight
SZ	Sealing zone
TAE	Tris-acetate-EDTA
Tb.N.	Trabecular number
Tb.Sp.	Trabecular separation
Tb.Th.	Trabecular thickness
TBP	TATA-binding protein
TBS	Tris-buffered saline
TBS-T	Tris-buffered saline-triton
TE	Tris-EDTA
TEMED	Tetramethylethylendiamine
Tet	Tetracycline
TetO	Tet operator
TetR	Tet repressor
Tf	Transferrin
TGF-β	Transforming growth factor-β
TNF	Tumor necrosis factor
TRAF6	TNF receptor-associated factor 6
TRAP	Tartrate-resistant acid phosphatase

Tris	Tris(hydroxymethyl)aminomethane
tTA	Tetracycline-controlled transactivator
TV	Total volume
UV	Ultraviolet
V-ATPase	Vacuolar-ATPase proton pump
Vha	Vacuolar-type H+-ATPase
VhaPRR	Vacuolar-type H+-ATPase prorenin receptor
VMA	Vacuolar membrane ATPase activity
VPS	Vacuolar sorting protein
WB	Western blot
WBC	White blood cells
XLMR	X-linked mental retardation
XPDS	X-linked Parkinsonism with spasticity
YFP	Yellow fluorescent protein

Table 23: Symbols and units

°C	Degree Celsius
%	Percent
A	Ampere
AU	Arbitrary unit
bp	Base pair
g	Gramm
cm	Centimeter
dl	Deciliter
kg	Kilogramm
kV	Kilovolt
l	Liter
M	Molar
mg	Milligramm
min	Minute
ml	Milliliter
mm	Millimeter
mM	Millimolar
ms	Millisecond
ng	Nanogramm
nm	Nanometer
rpm	Rotations per minute
sec	Second
V	Volt
v/v	volume/volume
x g	Relative centrifugal force
µA	Microampere
µg	Microgramm
µl	Microliter
µm	Micrometer
µM	Micromolar

APPENDIX

LIST OF FIGURES

LIST OF TABLES

APPENDIX

Material and methods

Appendix

SELBSTSTÄNDIGKEITSERKLÄRUNG

IV APPENDIX

Ich versichere hiermit, die vorliegende Dissertation mit dem Titel „Role of the (Pro)renin Receptor [(P)RR/ATP6ap2] in Osteoclast and Macrophage Physiology“ selbständig verfasst und nur die angegebenen Hilfsmittel und Hilfen in Anspruch genommen zu haben. Abbildungen, die anderen Quellen unverändert entnommen oder diesen entlehnt wurden, sind mit der Quellenangabe gekennzeichnet.

Ich versichere, dass ich mich nicht anderweitig um einen Doktorgrad beworben habe oder einen entsprechenden Doktortitel besitze.

Die Promotionsordnung der Mathematisch-Naturwissenschaftlichen Fakultät I der Humboldt-Universität zu Berlin vom 27. Juni 2012 habe ich gelesen und akzeptiert.

Anthony Rousselle Berlin, März 2016

V APPENDIX

PUBLICATIONS

1. **Rousselle A**, Sihn G, Rotteveel M, Bader M. (Pro)renin receptor and V-ATPase: from *Drosophila* to humans. *Clinical Science*, 2014, 126: 529-536.

2. **Rousselle A**, Qadri F, Leukel L, Yilmaz R, Fontaine JF, Sihn G, Bader M, Ahluwalia A, Duchene J. CXCL5 limits macrophage foam cell formation in atherosclerosis. *JCI*, 2013; 123(3):1343-47.

3. Beis D, Duchene J, **Rousselle A**, Grohmann M, Qadri F, Bader M, Alenina N. Peripheral effects of central serotonin in a mouse model for sub-sickness behavior. *Brain, Behavior & Immunity***.** 2013; 29: S1-S24 (Abstract).

4. Sihn G, Burckle C, **Rousselle A**, Reimer T, Bader M. (Pro)renin receptor: subcellular localizations and functions. *Front Biosci* (Elite Ed.), 2013; 5:500-8.

5. Riediger F, Quack I, Qadri F, Hartleben B, Park JK, Potthoff SA, Sohn D, Sihn G, **Rousselle A**, Fokuhl V, Maschke U, Purfürst B, Schneider W, Rump LC, Luft FC, Dechend R, Bader M, Huber TB, Nguyen G, Muller DN. Prorenin receptor is essential for podocyte autophagy and survival. *J Am Soc Nephrol*. 2011; 22(12):2193-202.

6. Gayard M, Guilluy C, **Rousselle A**, Viollet B, Henrion D, Pacaud P, Loirand G, Rolli-Derkinderen M. AMPK alpha 1-induced RhoA phosphorylation mediates vasoprotective effects of estradiol. *Arterio Thromb Vasc Biol*., 2011; 31(11):2634-42.

7. Sihn G, **Rousselle A**, Vilianovitch L, Burckle C, Bader M. Physiology of the (pro)renin receptor: Wnt of change? *Kidney Int*., 2010; 78(3):246-56.

VI APPENDIX

SCIENTIFIC MEETINGS

1. **17th Annual Meeting of the European Council for Cardiovascular Research (ECCR)**, *October* 2013, La Colle sur Loup, Nice, France.
Rousselle A, Duchene J, Qadri F, Rotteveel M, Kornak U, Bader M and Sihn G. Deletion of (pro)renin receptor in osteoclasts is associated with growth retardation and bone abnormalities (poster).

2. German-French Symposium 2012 "Frontiers of Cardiovascular Research: From Basic Concepts to Novel Approaches in Therapy and Prevention", October 2012, Berlin, Germany. **Rousselle A**, Qadri F, Leukel L, Yilmaz R, Fontaine JF, Sihn G, Bader M, Ahluwalia A, Duchene J. CXCL5 limits macrophage foam cell formation in atherosclerosis (poster).

3. (P)RR international meeting 2012, December 2012, Berlin, Germany.
Rousselle A, Sihn G and Bader M. (Pro)renin receptor function in retina, bone and macrophages using animal models with depleted gene expression (talk).

4. P2R Symposium 2011, December 2011, Paris, France.
Rousselle A. New genetic models tothe functions of the (pro)renin receptor (talk).

5. P2R Symposium 2010, December 2010, Paris, France.
Rousselle A. Role of the (pro)renin receptor in bone physiology (talk).

6. P2R Symposium 2009, December 2009, Paris, France.
Rousselle A. The (pro)renin receptor: is it all about intracellular and vesicle trafficking? (talk).